Efficient Radio Resource Management in Integrated Terrestrial and Non-Terrestrial Networks

BY

DENISE JOANITAH BIRABWA

A thesis submitted for the degree of
Doctor of Philosophy
in the Department of Electrical Engineering,
Faculty of Engineering and the Built Environment, University of Cape Town
August 2023

Supervisor: Dr. Daniel Ramotsoela
Co-Supervisor: Mr. Neco Ventura

Declaration

I DENISE JOANITAH BIRABWA, assert and proclaim that the research presented in this thesis report titled, "Efficient Radio Resource Management in Integrated Terrestrial and Non-Terrestrial Networks" is my own work, both in conception and execution, except where acknowledged, and that it has not been and will not be submitted to any other university or institution of higher learning for the award of a degree or diploma.

Name
DENISE JOANITAH BIRABWA

Signature

_____

Date
29 August 2023

Dedication

To my mother, Ms. Grace Lwanga, who has sacrificed a lot to educate her children, I am who I am because of you.

To my siblings Allan Mbaziira and Lisa Namiiro, and my sister-in-law Mrs. Joanitor Mbaziira, who are a major support system in my life.

To my son Harvey Kizito Nsereko, who brightens my world.

Acknowledgements

I am grateful to the Almighty God, who has seen me through many obstacles in this Ph.D. journey. I called on your name at my point of need, and you answered, may your name be forever glorified. Great appreciation goes to my supervisors, Dr. Daniel Ramotsoela and Mr. Neco Ventura (RIP) who accepted to supervise this research work in my second year of study; for the advice, motivation, guidance, and support, I am genuinely grateful. I cannot forget to thank the Head of the Department, Prof. Fred Nicolls, for his support and understanding during the difficult time I had to change a supervisor. I acknowledge financial support from the Kyambogo University staff development fund, Uganda, and the International and Refugee Students Scholarship at the University of Cape Town, South Africa; many thanks.

I am profoundly grateful to my friends who have immensely supported me in the Ph.D. journey. Dr. Sunday Oladayo Oladejo, you were going through a rough patch yourself, but that did not change your beautiful heart, thank you for the guidance and support. Dr. Winnie Nakimuli, how did you never tire of listening to my trials and tribulations? Thank you. Dr. Kibalya Godfrey Mirondo, you made the problematic reviews of my journal papers understandable; thank you. To my dearest friend and brother, Mbiika Ceriano (RIP), I started the Ph.D. journey because of you. Your sickness and subsequent passing was a dark

period during this journey, but you are now in a better place, continue to rest in peace, brother. To Dr. Niwareeba Roland, your persistence in times of challenges motivated me not to give up; thank you for sharing these with me. Natalia Dambe, you were a housemate sent from the heavens. Kizito Nicholas, thank you for the hiking expeditions and tours around Western Cape; these always helped me unwind and relax. My fellowship group, the Emeralds, thank you, ladies, for standing with me in prayer and supplication; God has been kind. To the Communications Research Group (CRG), University of Cape Town, thank you for the valuable feedback and helpful suggestions during my research activities; I wish you all the best in your endeavours.

Finally, I am sincerely grateful to my family. My dearest mother, thank you for your support and guidance; your prayers, motivation, and encouragement have enabled me to reach this far with my thesis work. My dearest brother Allan and your wife Joanitor, thank you for looking after my dearest son in my absence; knowing he was in safe hands enabled me to concentrate on my studies. My baby sister Lisa, thank you for always being a call away. My uncles, aunties, grandparents, and cousins, thank you for your prayers and for asking that 'bad' question, 'When are you finishing your Ph.D.?'. With such questions, there was no room for failure!

Contents

Abstract

The beyond 5G (B5G) networks are envisaged to provide terra bps data rates and ubiquitous and unlimited wireless coverage. However, the terrestrial deployment of 5G networks poses a limitation in achieving a truly ubiquitous and seamlessly connected network. To this end, it has been proposed to integrate terrestrial networks (TNs) with non-terrestrial networks (NTNs), such as satellite communications, high-altitude platforms and low-altitude platforms. NTNs are characterised by wide coverage and less vulnerability to physical attacks and natural disasters, and hence, will complement TNs in providing ubiquitous wireless connectivity and enhanced broadband services to unserved and underserved areas. In addition, NTNs will provide network resilience to physical attacks and natural disasters, improve the quality of service (QoS) for overloaded TNs, and enhance service continuity for moving platforms. Consequently, the B5G network will be an integrated terrestrial and non-terrestrial network (ITNTN) consisting of multiple radio access networks (RANs) coexisting to provide radio access to multi-mode user equipment. This thesis addresses the problem of efficient user association and resource allocation in the ITNTN.

The RANs in the ITNTN have different capabilities and limitations in meeting the envisioned B5G contrasting user requirements such as throughput, latency, and mobility.

Therefore, determining an optimal association and resource allocation scheme that maps the heterogeneous users to the appropriate RANs while at the same time maximising resource utilisation, and providing the required user QoS, is rigorous and complex. Besides, such co-existence of the different RANs implies an increase in the number of wireless access nodes and thus raises a justifiable concern over the drastic increase in energy consumption and carbon emission expected to ensue. Accordingly, there is a need to develop efficient radio resource management (RRM) algorithms for the ITNTN that consider not only the heterogeneity in user QoS requirements but also the uniqueness of the different RANs in meeting these demands.

To this end, this research aims at developing efficient RRM schemes that achieve a spectrum-efficient and energy-efficient ITNTN while minimising mobility-induced handoffs. RRM takes the form of user association and resource allocation in this work. First, the research formulates the user association and resource allocation problem in the ITNTN as a multi-objective optimisation problem (MOOP) that jointly maximises the total data rate of the ITNTN while minimising the probability of mobility-induced handoffs. The problem is subjected to constraints on the resource budget and minimum user QoS requirements in terms of data rate. Moreover, the problem is formulated to allow differentiated service provisioning and priority-based user association and resource allocation, thus prioritising mission-critical users' service provisioning. The weighted sum method is adopted to simplify and transform the MOOP into a single-objective optimisation problem (SOOP). The SOOP's complexity is reduced by decomposing it into two sub-problems: the user association sub-problem and the resource distribution sub-problem. A service-aware greedy heuristic algorithm is proposed

to solve the user association sub-problem and its performance compared to the service-unaware scheme. Simulation results reveal that the service-aware algorithm achieves higher overall network spectrum efficiency (SE), user acceptance ratio (AR), and lower handoff probability. Furthermore, the resource distribution sub-problem is reformulated into a water-filling problem and solved utilising CVXPY, consequently analysing the effect of distributing the unallocated basic bandwidth units to the associated users.

Second, since the greedy heuristic solution to the user association sub-problem does not ordinarily produce an optimal solution, the work further proposes a polynomial-time solution based on the genetic algorithm (GA). The performance of the GA is evaluated by comparing it to the ILP solution, the greedy heuristic solution, and the random user association (RUA) algorithm. Simulation results reveal that the GA outperforms all algorithms in terms of SE and user acceptance ratio. Moreover, the GA achieves a handoff probability of zero, unlike the RUA algorithm.

Third, the proposed greedy heuristic and GA solutions to the user association sub-problem utilise a central node that requires nearly-complete information, which may not be available in real-time. Therefore, this research further proposes a centralised training and distributed execution multi-agent duelling double deep Q network (MA3DQN) solution that facilitates real-time decision-making. Each user collects the channel state and access node loading information in this approach and makes an association decision that considers its quality of service requirements. This section of the thesis further adopts the effective capacity theorem to guarantee the delay QoS requirements for mission-critical users. The MA3DQN's performance is validated through comparison with the GA, the ILP solution, a heuristic

approximation-based solution, the greedy approach, and the RUA algorithm. Moreover, the multi-agent deep Q network (MADQN) solution is also simulated as an additional benchmark algorithm. Simulation results reveal that as the number of users in the network increases, the acquired data rate of the MA3DQN is within 0.48% and 0.42% of that achieved by the GA and ILP, respectively, and outperforms all other algorithms. Notably, the proposed MA3DQN algorithm presents the best running time, attaining a gain of 99.9% over the GA algorithm, which performs the poorest among the algorithms characterised by polynomial worst-case time complexity. Besides, the MA3DQN approach maintains a handoff probability of zero, unlike the approximation-based, and RUA solutions.

Lastly, the thesis presents a weighted sum SOOP that maximises the energy efficiency (EE) of the ITNTN while simultaneously minimising the mobility-induced handoff probability. The formulated problem is a non-convex and mixed integer non-linear programming problem whose complexity is reduced through decomposition into two sub-problems: the user association and resource allocation (UARA) problem and the power allocation (PA) problem. The equivalent UARA problem maximises the total network data rate and minimises the mobility-induced handoffs, thus can be solved by the GA or the MA3DQN already discussed. On the other hand, the PA problem is a fractional programming problem (FPP) that is simplified through transformation into a weighted sum SOOP and solved using the particle swarm optimisation (PSO) approach. Simulation results reveal that depending on the value of the weighting factor in the SOOP, the particle swarm optimisation power allocation (PSOPA) algorithm either minimises power consumption, thereby maximising the EE of the ITNTN, or maximises the total network data rate. When the power consumption is

minimised, the PSOPA outperforms the equal power allocation (EPA) technique in EE. On the other hand, when the achieved network data rate is maximised, the PSOPA's achieved data rate approaches the upper bound set by the EPA algorithm.

Unlike many recent proposals in the literature on user association and resource allocation in the ITNTN, the algorithms proposed in this thesis consider the heterogeneity in user traffic types. Moreover, the capabilities and limitations of the different networks in meeting the contrasting user demands are considered. For instance, to the best of our knowledge, no work in literature prioritises the wide coverage non-terrestrial networks over terrestrial networks for long-distance and highly mobile applications. Such a consideration reduces the handoff rate, ultimately reducing the probability of handoff failure, delays, and communication overheads.

List of Abbreviations

3D	Three Dimension
3GPP	Third Generation Partnership Project
4G	Fourth-Generation of Mobile Networks
5G	Fifth-Generation of Mobile Networks
6G	Sixth-Generation of Mobile Networks
AI	Artificial Intelligence
AN	Access Node
AP	Access Point
AR	Acceptance Ratio
B5G	Beyond 5G
BBU	Basic Bandwidth Unit
big-O	big-Omicron
BnB	Branch and Bound
BS	Base Station
CAC	Call Admission Control
CDMA	Code Division Multiple Access
CPU	Central Processing Unit
CSI	Channel State Information
CU	Centralised Unit
D2D	Device to Device
DDN	Deep Neural Network
DDQL	Double Deep Q Learning
DDQN	Double Deep Q Network
DL	Downlink
DQL	Deep Q Learning
DQN	Deep Q Network
DRL	Deep Reinforcement Learning
DU	Distributed Unit
EE	Energy Efficiency
ELPC	Extremely Low-Power Communications
eMBB	enhanced Mobile BroadBand
eNB	evolve Node-B
EPA	Equal Power Allocation

EU	European Union
euRLLC	enhanced ultra-Reliable and Low-Latency Communications
FDMA	Frequency Division Multiple Access
feMBB	further enhanced Mobile BroadBand
FPP	Fractional Programming Problem
GA	Genetic Algorithm
GAP	Generalized Assignment Problem
GEO	Geostationary Earth Orbit
gNB	Next Generation Node B
gNB-CU	Next Generation Node B - Centralised Unit
gNB-DU	Next Generation Node B - Distributed Unit
GW	Gateway
HAP	High Altitude Platform
IAL	Inter-Aerial Link
IEEE	Institute of Electrical and Electronics Engineers
ILP	Integer Linear Programming
IoT	Internet of Things
IP	Internet Protocol
ISL	Inter-Satellite Link
ITNTN	Integrated Terrestrial and Non-Terrestrial Network
LAP	Low Altitude Platform
LDHMC	Long-Distance and High-Mobility Communication
LEO	Low Earth Orbit
LoS	Line of Sight
LP	Linear Programming
LTE	Long Term Evolution
MA3DQN	Multi-Agent Duelling Double Deep Q network
MAC	Medium Access Control
MADQN	Multi-Agent Deep Q network
MANET	Mobile Ad hoc Network
MBS	Macro Base Station
MDP	Markov Decision Process
MEO	Medium Earth Orbit
MIMO	Multiple Input Multiple Output
MINLP	Mixed Integer Non-Linear Programming
mMTC	Massive Machine-Type Communications
mmWave	Millimetre Wave
MOOP	Multi-Objective Optimisation Problem
NFV	Network Function Virtualization
NG	Next Generation
NGC	Next Generation Core network
NGc	Next Generation control plane
NGu	Next Generation user plane
NLoS	Non Line of Sight

NN	Neural Network
NP	Non-deterministic Polynomial-time
NR	New Radio
NS-3	Network Simulator 3
NTN	Non-Terrestrial Network
OFDM	Orthogonal Frequency Division Multiplexing
OFDMA	Orthogonal Frequency Division Multiple Access
OPEX	Operational Expenditure
PA	Power Allocation
PDCP	Packet Data Convergence Control
PRB	Physical Resource Block
PSO	Particle Swarm Optimisation
PSOPA	Particle Swarm Optimisation Power Allocation
QoE	Quality of Experience
QoS	Quality of Service
RAN	Radio Access Network
RAT	Radio Access Technology
RF	Radio Frequency
RL	Reinforcement Learning
RLC	Radio Link Control
RN	Relay Node
RRC	Radio Resource Control
RRM	Radio Resource Management
RSSI	Received Signal Strength Indicator
RTT	Round Trip Time
RUA	Random User Association
SAGIN	Space Air Ground Integrated Network
SatComs	Satellite Communications
SDN	Software Defined Network
SE	Spectrum Efficiency
SINR	Signal to Interference plus Noise Ratio
SNR	Signal to Noise Ratio
SOOP	Single-Objective Optimisation Problem
SPAN	Switch Port Analyser
SWAP	Size, Weight, And Power
TDMA	Time Division Multiple Access
TN	Terrestrial Network
TTI	Transmission Time Interval
UARA	User Association and Resource Allocation
UAV	Unmanned Aerial Vehicle
UDN	Ultra-Dense Network
UE	User Equipment
umMTC	ultra-massive Machine-Type Communications

uRLLC	ultra-Reliable and Low-Latency Communications
V2V	Vehicle-to-Vehicle
V2X	Vehicle-to-Everything
VANET	Vehicular Ad hoc Network
WiFi	Wireless Fidelity
WiMAX	Worldwide Interoperability for Microwave Access
WLAN	Wireless Local Area Networks

List of Tables

List of Figures

Chapter 1

Introduction

1.1 Introduction

Ongoing research on the sixth-generation (6G) of mobile networks reveals that 5G networks may not meet the user requirements of 2030 and beyond, owing to emerging applications such as holographic type communications, fully automated driving, and space travel [2, 3]. These applications will impose stringent requirements that include a peak data rate greater than 1 Tb/s and a delay less than 1 ms, which 5G clearly can not provide [3, 4, 5]. Furthermore, the three use cases defined for 5G, that is, enhanced mobile broadband (eMBB), ultra-reliable and low-latency communications (uRLLC), and massive machine-type communications (mMTC), do not effectively represent all the different service scenarios envisaged in the beyond 5G (B5G) networks [3, 4]. For example, other use cases like long-distance and high-mobility communications and low-power communications have been defined in [3]. Consequently, considerable research is directed towards finding enabling

solutions required for the next generation of wireless networks to meet the envisaged demanding user requirements [3, 4, 5, 6, 7].

The integration of terrestrial networks (TNs) such as 5G with non-terrestrial networks (NTNs) has been proposed as one of the key enabling features for 6G [3, 4, 5]. The considered NTNs are the satellite communications (SatComs) and the unmanned aerial vehicles (UAVs) [1]. The UAVs can be categorised into high altitude platforms (HAPs) and low altitude platforms (LAPs) [8]. Given their unique attributes of wide coverage, less vulnerability to physical attacks and natural disasters, and fast deployment of the UAVs, the NTNs will complement the terrestrial network (TN) in meeting 6G's stringent requirements and facilitating ubiquitous and reliable broadband coverage [3, 4, 5]. Moreover, massive investment in space privatization coupled with recent advances in manufacturing and launching processes have greatly reduced economic and technical constraints that inhibited the deployment and integration of SatComs with TNs. Due to the significant reduction in satellite size, multiple satellites can be transported using a single launcher, greatly reducing the launching cost [9]. Consequently, several private companies such as Amazon, Telesat, OneWeb, and SpaceX have deployed several low earth orbit (LEO) and medium earth orbit (MEO) constellations to deliver high throughput broadband services with low latency [10]. An instance of this deployment is the other 3 billion (O3b) MEO constellation of 20 satellites placed at an altitude of 8063 km in the circular orbit [10, 11]. The goal of the O3b constellation network is to deliver internet access to 3 billion people in Africa, Asia, and South America [11]. The Iridium system is another constellation of 66 LEO satellites at a height of about 780 km designed to provide data and voice services to the entire globe [11].

Accordingly, the future airborne communication network will consist of many constellations of satellites in different orbits connected by inter and intra-satellite links and providing relatively inexpensive telecommunications services. Consequently, the role of NTNs in the integration with TNs has been widely recognized [1], and in particular, the communication resilience and service continuity use case identified to meet the needs of users during scenarios when the TN is overloaded [12, 13].

Similar to [14] and [15], this research adopts a scenario in which there exists a large number of users, and hence, the TN access nodes (ANs) cannot adequately support all the arriving traffic. Such a scenario necessitates dynamic association of the users to not only the TN but also the available non-terrestrial network (NTN) ANs, to meet the different user demands. Therefore, this usage scenario implies the coexistence of multiple radio access networks (RANs) deployed in the form of TNs, LAPs, HAPs, and SatComs, as depicted in Fig. 1.1. These RANs are very diverse, with different capabilities and limitations. Similarly, various user applications have contrasting quality of service (QoS) requirements in terms of throughput, latency, mobility, etc. Determining an optimal association and resource allocation scheme that maps the heterogeneous users to the appropriate RANs while at the same time maximising resource utilisation, and providing the required user QoS, is not only rigorous but complex [15]. Therefore, this research addresses the user association and resource allocation problem in the integrated terrestrial and non-terrestrial network (ITNTN). The resulting user association and radio resource allocation algorithms consider the different use cases envisioned in 6G, ultimately optimising their radio resource allocation and prioritisation.

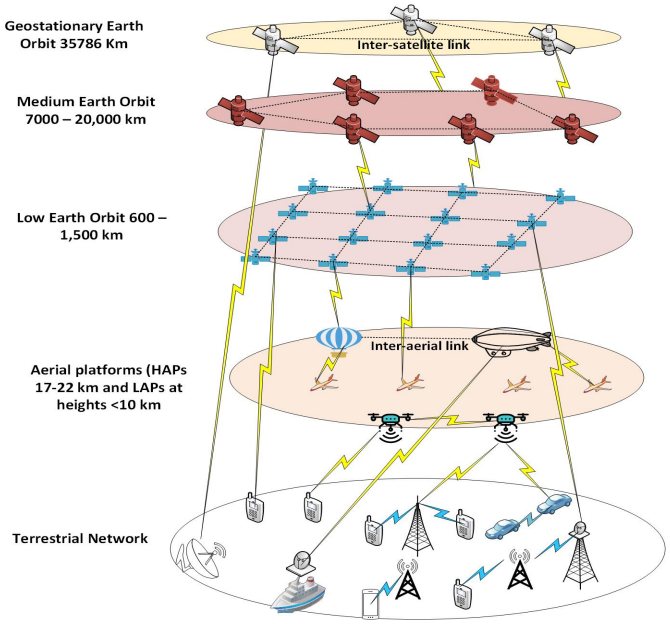

Figure 1.1: Layered architecture of the integrated terrestrial and non-terrestrial network.

1.2 Research background

Over the years, the explosive demand for high-speed wireless access has increasingly strained the TN, especially in highly populated urban areas. To counter the massive demand, technologies such as ultra-dense networks (UDNs), device-to-device (D2D) communications, and Millimetre Wave (mmWave) communications have been proposed as the nexus of B5G networks [8, 16]. While these technologies have shown great potential in increasing the capacity of wireless networks, they are faced with limitations [8, 16]. For instance, UDNs are limited by frequent handoff, interference, and backhaul challenges. On the other hand, D2D communication is faced with implementation complexity in terms of frequency planning and resource allocation. Similarly, mmWave communication is severely affected by blockage, such as buildings, and suffers from high propagation loss, rendering it a small-cell technology.

The use of NTNs as Base Stations (BSs) is envisioned to offer a solution to some of the above challenges and complement the TN in providing high-capacity wireless access in rural areas and hotspots [12]. After all, the broad coverage of the NTNs will provide access to hard-to-reach and under-served areas and facilitate continuity of service for high-speed users [1], thus limiting the frequency of handoff. Also, a considerable amount of research has elaborated the applicability of NTNs, especially satellites, in providing supplementary backhaul links to TNs [17, 18, 14]. Besides, given that the NTNs are located at altitudes above the ground, these can easily achieve line of sight (LoS) communication with ground users and thus facilitate high-capacity wireless access using mmWave communication, provided that high gain antennas are used to reduce attenuation due to long propagation distances [12].

While most research on the integration of NTNs with TNs focused on using the satellite for backhaul, this research will focus on integrating the satellite with the TNs, HAPs, and LAPs for fronthaul radio access. We argue that in a scenario of many users whose traffic can hardly be supported by the terrestrial BSs, all available access nodes, including the SatComs, should be able to provide radio access and thus satisfy the QoS requirements of different users. A few recent research has also addressed the use of SatComs for radio access in the integrated network [19, 20, 21], but these works did not expound on how to meet the needs of different use-cases, i.e., eMBB, uRLLC, etc. Furthermore, to the best of our knowledge, none of the literature has addressed the prioritisation of the wider coverage NTNs for long-distance and highly mobile users to reduce call drops that result from a high number

of handoffs. Moreover, most of the work does not consider joint RAN resource management of all four networks: the TN, HAPs, LAPs, and SatComs.

1.3 Research motivation

In future wireless networks, space communication is envisaged to complement the ground TNs in providing broadband wireless connectivity [22]. Indeed, UAVs have been found to offer several applications, ranging from use as aerial BSs to acting as cellular-connected user equipment (UE) [8]. Unlike the fixed TN access nodes, UAVs are mobile and can flexibly be deployed for radio access during periods of traffic peaks and emergency scenarios [23]. Besides, technological progress in solar cells, batteries, and aeronautics have motivated companies such as Airbus [24] and Google [25] to invest heavily in HAPs. In addition, recent times have witnessed the massive deployment of Low Earth Orbit (LEO) satellite constellation, including 2,622 One Web satellites and 1,584 Starling satellites [26]. Moreover, feasibility studies on radio access through the NTNs have been successfully undertaken by the Third Generation Partnership Project (3GPP) [1, 27]. Consequently, the B5G networks are expected to comprise the TNs, LAPs, HAPs, and SatComs, integrated to provide 3D wireless connectivity [26].

Motivated by these trends, this research seeks to study the problem of user association and radio resource allocation in the ITNTN, consisting of many users generating traffic that the TN ANs can not entirely support, for example, in an urban area during a carnival event. Such a usage scenario necessitates the deployment of NTNs to decongest and support the TN RAN in providing radio access to the different users. The question that arises then is how to

map the contrasting user demands to the heterogeneous RANs to maximise radio resource utilisation and the number of admitted users. At the same time, the mapping should meet the requirements of the different entities, including the users' QoS and the access nodes' resource and power budgets.

1.4 Problem statement

In 6G networks, multiple RANs, including the SatComs, LAPs, HAPs, and TNs, will co-exist [28]. These networks have different characteristics and constraints. For example, satellite communication is endowed with wide coverage but limited by long propagation delays and weak received signal strength. The LAPs are characterised by fast and low-cost deployment yet are constrained by the number of available channels. Therefore, their usage should be prioritised for traffic whose QoS requirements may not be met satisfactorily by the other available RANs [11]. Along the same lines, the TN is endowed with a rich pool of resources that enable it to achieve higher throughput and lower latency than the NTNs. However, even with such a large pool of resources, the TN will not be able to support the massive wireless network demand envisaged in the years 2030 and beyond [2]. Moreover, the TN BSs are characterised by a small cell radius that results in an increased number of handoffs experienced by mobile users [11].

Simultaneously, the UE in such a network will be multi-mode, embedded with multiple RAN interfaces, thus able to access any of the RANs mentioned above [29]. However, different user applications are characterised by exceedingly divergent QoS requirements and scenarios. Typical user scenarios envisaged to be supported by 6G include further enhanced mobile

broadband (feMBB), enhanced ultra-reliable and low-latency communications (euRLLC), ultra-massive machine-type communications (umMTC), long-distance and high-mobility communication (LDHMC), and extremely low-power communications (ELPC) [3]. To take a case in point, SatComs is more appropriate than the TN for the LDHMC service group due to its wide coverage, which reduces the number of handoffs, consequently decreasing the associated delays and signalling overheads and thus increasing the QoS for such applications. On the contrary, its long propagation delay makes it unsuitable for direct connectivity of the mission-critical euRLLC service group.

Furthermore, it is plausible that feMBB and umMTC use cases whose QoS requirements could have been met by SatComs use up available resources in other RANs. In such a scenario, the resources for the mission-critical euRLLC service group, which the available resources in SatComs cannot support, will be reduced. Consequently, euRLLC calls will be blocked regardless of existing SatComs resources, leading to inefficient utilisation of resources which ultimately reduces the spectrum efficiency (SE) of the ITNTN.

Ultimately, there is a need to map the different service groups to the appropriate RAN to ensure efficient resource utilisation and thus maximise the SE of the ITNTN, making the association problem non-trivial. The typical user association and resource allocation algorithms for the TN are based on putting traffic where there is available bandwidth [30] and are thus not optimised to suit the different networks' peculiarities in the ITNTN. For instance, regardless of how much bandwidth is available at the SatComs access node, euRLLC traffic cannot be scheduled through it. Moreover, in literature, the widely employed user association schemes are based on maximum received signal to interference plus noise ratio

(SINR). However, the RANs in the ITNTN have resource blocks of different bandwidths, thus, a RAN may have a higher SINR, but because of a smaller sized resource block, it achieves less data rate than another RAN with a bigger sized resource block. Therefore, an association based on maximum SINR does not guarantee maximum data rate in the ITNTN, thereby leading to a lower SE. Consequently, in the current user association and resource allocation algorithms, the networks' different capabilities and characteristics are not harnessed in an optimised manner, resulting in inefficient utilisation of the joint network resources, leading to the SE problem. Besides, integrating NTNs with TNs introduces an energy efficiency (EE) problem that must also be addressed. The ITNTN will be an ultra-wide communication network consisting of many ubiquitous nodes that will increase the total energy consumption and carbon emissions [31]. Therefore, it is imperative to develop EE algorithms for the ITNTN that will lead to a green and energy-saving communication network.

From the foregoing, this research intends to fill the gap in the literature on the development of efficient algorithms and schemes for radio resource management in the ITNTN, given diverse users. In particular, the study addresses the problem of efficient user association and resource allocation in the ITNTN by developing algorithms that maximise the SE and EE of the network while ensuring QoS provisioning to the different users. The users are differentiated according to their use case, as either feMBB, euRLLC, or LDHMC. Moreover, the work prioritises using RANs with the largest cell radius for service provisioning mobile LDHMC users, with the goal of minimising mobility-induced handoffs.

Also, provisioning the mission-critical euRLLC service group is prioritised over other service groups to avoid its denial of service, which could be catastrophic.

Consequently, the user association and resource allocation problem in the ITNTN is a non-linear combinatorial and non-convex problem that is NP-hard with no efficient polynomial-time solution. Exact solutions like the branch and bound that return a global optimal solution to such problems exist. Still, these are characterised by a computational complexity that increases exponentially with the network's dimension. To this end, this research is dedicated to finding near-optimal but polynomial-time solutions to the user association and resource allocation problem in the ITNTN. Moreover, the study investigates the use of reinforcement learning (RL) to facilitate real-time user association decision-making, a desirable attribute for 6G scenarios characterised by delay-sensitive applications.

1.5 Research questions

In addressing the aforementioned problem, this research seeks to answer some questions, including but not limited to the following:

i) *How can users with contrasting QoS requirements be associated with RANs having different capabilities and limitations?*

ii) *How can the ITNTN resources be allocated to users in a manner that maximises the SE of the ITNTN while simultaneously minimising the mobility-induced handoffs and guaranteeing users' QoS requirements?*

iii) *How can the EE of the ITNTN be maximised while at the same time meeting the user's QoS demands, ensuring efficiency in resource utilisation, and minimising mobility-induced handoffs?*

iv) *How can efficient user association and resource allocation in the ITNTN be achieved intelligently using the RL technique?*

1.6 Hypothesis/Research objectives

1.6.1 Hypothesis

It is hypothesized that integrating TN with NTNs will lead to communication resilience and service continuity during traffic peaks in TNs, thereby increasing network availability, capacity and throughput.

1.6.2 Research objectives

This research aims to develop and validate efficient radio resource management algorithms for the ITNTN that will maximise the network's spectrum and energy efficiency while minimising mobility-induced handoffs and ensuring user QoS provisioning. The objectives of the research include the following:

i) To carry out an extensive literature review on radio resource management (RRM) in the ITNTN, identifying and addressing limitations in the existing solutions.

ii) To develop a robust user association and resource allocation scheme that maximises the SE of the ITNTN by maximising the total network data rate while minimising the probability of mobility-induced handoff, subject to constraints on user QoS requirements, access node resource, and power budgets.

iii) To develop an intelligent user association and resource allocation scheme based on RL that facilitates real-time RRM in the ITNTN.

iv) To develop an energy-efficient RRM scheme for the ITNTN that also minimises the probability of mobility-induced handoff and ensures user QoS provisioning while assuring that the radio and power resources of the access nodes are not exceeded.

v) To implement the aforementioned proposed algorithms using Python.

vi) To evaluate and analyse the performance of the proposed algorithms against suitable performance metrics and existing solutions.

1.7 Research methodology

The methodology used for this research follows a step-wise procedure depicted by Fig. 1.2 and described in [32] as:

i) Recognize the problem: This step is undertaken to review and understand radio resource management in the ITNTN and identify gaps in the proposed solutions.

ii) Define the problem: This step details the system model and assumptions considered for this research following the steps highlighted below:

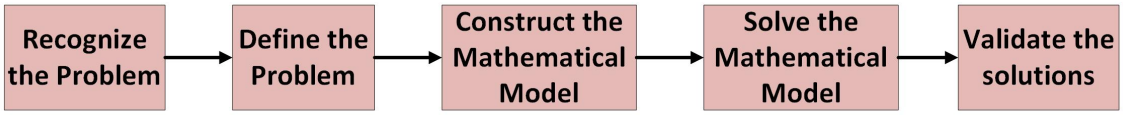

Figure 1.2: Research methodology.

a) Definition of the general model: This involves describing the deployment scenario in which the characteristics of the different users, RANs, and access nodes are defined.

b) Definition of the mobility, channel, and signal quality models: The users' movement patterns are defined in this step. Moreover, the path loss, channel gain, and the received SINR from the access nodes to the UE are computed. From these computations, the data rate achieved by a user is calculated.

iii) Construct the Mathematical Model: A mathematical model is a simplified representation of the actual problem. This step comprises four main activities:

a) Clearly defining the requirements of the different entities, such as users and access nodes of the ITNTN. Such a definition aids proper decision-making, such that users' needs are satisfied while considering the power and resource budgets of the access nodes.

b) Identifying the decision variables used to define the decisions to be made in the user association and resource allocation problem. Such decision variables include the access node and resource unit decision variables.

c) Defining the problem constraints in terms of decision variables. Constraints provide rules that ensure limits and restrictions are satisfied. For instance, all users have a minimum QoS, and access nodes have maximum resource and power budgets.

d) Defining the objective functions. An objective function assigns a value and measures the quality of the alternatives to choose from to yield the best result. In this research, the objective functions are multi-objective optimisation problems that: i) Maximise the total network data rate (thereby maximising the network SE) while minimising the probability of mobility-induced handoffs and ii) Maximise the EE of the ITNTN while also minimising the mobility-induced handoff probability.

iv) Solving the Mathematical Model: Given that the problem is non-convex and combinatorial, it is NP-hard with no efficient polynomial-time solution. Many hand-crafted algorithms for solving combinatorial problems are sub-optimal, costly to compute, and mathematically not well defined due to the complex nature of the problems [33]. Nonetheless, exact algorithms such as branch and bound exist that return a global optimal solution for such problems. However, given that these algorithms are based on searching all the different possible solutions in the search space, they have a high time complexity that is inefficient for provisioning users, especially the delay-sensitive applications in wireless networks. On the other hand, it has been shown in the literature that meta-heuristic approaches, such as the genetic algorithm, can find near-optimal solutions to resource allocation problems in polynomial time [34, 35]. The meta-heuristics have lower computational complexity and require less computational resources, thus making them more efficient for 6G networks than the exact solutions. In the same manner, once the training is done, machine learning approaches can find near-optimal solutions to combinatorial optimisation problems at significantly reduced running times compared to exact solutions, and meta-heuristics [36]. Consequently, this

research investigates and compares the solutions to the user association and resource allocation problem in the ITNTNs obtained by meta-heuristics and machine learning, particularly RL.

v) Validating Solutions: The solutions will be evaluated against suitable performance metrics and existing solutions.

1.8 Research contributions

This thesis addresses the problem of user association and resource allocation in the ITNTN. The considered usage scenario is such that many users whose traffic cannot be supported entirely by the TN RAN exist, necessitating radio access through the NTN RANs as well. The RANs in the considered ITNTN have different attributes in meeting the envisioned heterogeneous user demands in the B5G network. Consequently, mapping users to the appropriate RAN while ensuring efficient spectrum and energy utilisation is not trivial. In solving this problem, contributions have been made to peer-reviewed conferences and journal publications, as highlighted later in this subsection. The novel contributions of this research are therefore summarised as follows:

i) Formulation of a user association and resource allocation scheme for an ITNTN comprising the TN, LAP, HAP, and SatComs RANs. This scheme considers the heterogeneity in user demands and the different RANs' uniqueness in meeting these demands. Resource allocation is priority-based, so the mission-critical euRLLC service group can be prioritised over the other service groups to avoid its denial of service,

which could lead to catastrophic events. Moreover, given the long propagation delays experienced by the SatComs RAN, the scheme ensures that the mission-critical users are not associated with the SatComs RAN of the ITNTN. Furthermore, since large cell radii characterise the NTNs compared with the TN BSs, they are prioritised to serve the mobile LDHMC service group to minimise the probability of mobility-induced handoffs.

Consequently, the user association and resource allocation problem is formulated as a multi-objective optimisation problem (MOOP) that jointly maximises the total data rate of the ITNTN and minimises the mobility-induced handoff probability. The problem is subjected to constraints on the resource budget and minimum user QoS requirements. The complexity of the formulated MOOP is reduced by adopting the weighted sum method to transform the MOOP into a single-objective optimisation problem (SOOP), which is a weighted sum of the total network data rate and the handoff reduction functions. However, the SOOP is combinatorial and thus NP-hard. The complexity of the SOOP is reduced by decomposing it into two sub-problems: a) the user association sub-problem that associates users to appropriate ANs and further allocates them the minimum resources required to meet their QoS requirements. b) The resource distribution phase that allocates the unallocated resources, if any, after the user association phase.

ii) Development of a service-aware greedy algorithm to solve the user association sub-problem and demonstrate the relevance of differentiated service provisioning and consideration of the RANs' different capabilities and limitations in resource management of the ITNTN. Furthermore, reformulation of the resource distribution sub-problem into

a water-filling problem, which is solved utilising CVXPY, a Python-embedded modelling language used to solve convex optimisation problems. Part of this work, particularly the greedy algorithm resulted in the publication of the conference paper [37].

iii) Development of a near-optimal but polynomial time solution based on the genetic algorithm (GA) to solve the user association sub-problem in i) above. The problem is encoded into a sequence of chromosomes with genes representing the user association solutions. Service group-dependent fitness functions are formulated to determine the near-optimal user association and resource allocation solution. Concurrently, the Gurobi solver is used to determine the user association sub-problem via integer linear programming (ILP). However, the worst-case time complexity of the ILP solution is exponential, justifying the use of the proposed polynomial-time GA. Therefore, the performance of the GA is validated through comparison with the ILP solution and two other solutions, the heuristic greedy algorithm in ii) above and the random user association (RUA) algorithm. Moreover, the GA solution is used to show that a set of Pareto optimal solutions exists in solving the MOOP formulated in i) as a weighted sum SOOP. This work culminated in the publication of a journal paper in IEEE Access [38].

iv) Development of a latency-aware multi-agent deep reinforcement learning (DRL) solution to the user association sub-problem in i). While the GA solution proposed in iii) determines near-optimal solutions in polynomial time, it lacks the intelligence that facilitates real-time decision-making, a desirable attribute for B5G networks, especially those serving mission-critical users. Therefore, a multi-agent solution based on a double

deep Q network with duelling architecture is proposed to determine solutions on the fly. The solution defines each user's state, action, and reward function. Moreover, to reduce the computational complexity and memory required during training, the work adopts the centralised training but distributed execution approach. The distributed execution enables real-time decision-making without users needing to know other users' channel state information in the network. Moreover, the effective capacity theorem is also adopted to guarantee the delay QoS requirements for mission-critical users. The performance of the proposed multi-agent duelling double deep Q network (MA3DQN) algorithm is validated using performance metrics such as the achieved total network data rate, user acceptance ratio, probability of handoff, and execution time. The performance of the MA3DQN algorithm is compared to the GA, the ILP solution, the greedy algorithm, the RUA algorithm, an approximation-based heuristic algorithm proposed by [39], and a simulated multi-agent deep Q network algorithm. This work resulted in a journal paper [40] publication in Computer Networks, Elsevier.

v) Development of an energy-efficient user association and resource allocation algorithm for the ITNTN. In i), the constant power allocation strategy is assumed to tame the problem complexity: hence, i) focuses on achieving a spectrum-efficient network. However, to address the EE of the ITNTN, the user association and resource allocation problem is formulated as a weighted sum SOOP that maximises the global EE of the ITNTN while simultaneously minimising the probability of mobility-induced handoff. Maximising EE in the SOOP presents a mixed integer non-linear fractional programming problem, making the computation of the formulated SOOP complex. The complexity of the

SOOP is reduced through decomposition into two sub-problems: the user association and resource allocation (UARA) problem and the power allocation (PA) problem. The equivalent UARA problem focuses on user association and resource allocation by fixing the resource block transmit power, consequently maximising the total network data rate and minimising the mobility-induced handoff probability. The PA problem then allocates power to the different resource blocks allocated to the users such that the users' QoS in terms of data rate or delay bound rate is satisfied while maximising the EE of the ITNTN. The PA problem is a fractional programming problem (FPP) that is simplified through transformation into a weighted sum SOOP. We show that a set of Pareto optimal solutions exists when the PA FPP is solved as a weighted sum SOOP.

Since the UARA problem is similar to the SOOP in i), it can be solved by any of the algorithms proposed in ii)-iv). On the other hand, the PA problem is solved using the particle swarm optimisation (PSO) algorithm due to its simplicity in implementation, high efficiency, and fast convergence. The performance of the particle swarm optimisation power allocation (PSOPA) algorithm is compared to the equal power allocation (EPA) strategy to validate the EE performance. This work culminated in publishing a conference paper [41].

The complete list of the publications associated with the contributions described above is presented as follows:

- **Journal papers**

[J.1] D. J. Birabwa, D. Ramotsoela, and N. Ventura, "Service-aware user association and resource allocation in integrated terrestrial and non-terrestrial networks: A genetic algorithm approach," IEEE Access, vol. 10, pp. 104337-104357, 2022.

[J.2] D. J. Birabwa, D. Ramotsoela, and N. Ventura, "Multi-agent deep reinforcement learning for user association and resource allocation in integrated terrestrial and non-terrestrial networks," Computer Networks, p. 109827, 2023.

- **Conference papers**

[C.1] D. J. Birabwa, D. Ramotsoela, and N. Ventura, "Slice-aware user association and resource allocation in integrated terrestrial and non-terrestrial networks," in Proc. Southern Afr. Telecommun. Netw. Appl. Conf. (SATNAC), 2021, pp. 44-49.

[C.2] D. J. Birabwa, D. Ramotsoela, N. Ventura, "Energy-efficient user association and resource allocation in integrated terrestrial and non-terrestrial networks," in Proc. Southern Africa Telecommunication Networks and Applications Conference (SATNAC), 2022, pp. 249–254.

1.9 Research scope

This thesis is dedicated to developing efficient radio resource management algorithms for a network comprising the integration of TNs such as 5G and NTNs that include the LAPs, HAPs, and SatComs. The algorithms enhance radio resource utilisation by ensuring users having heterogeneous demands are associated with the appropriate RANs that maximise the total network data rate, thereby maximising the SE of the network. Moreover, the

algorithms utilise the NTNs' attribute of large coverage cells to minimise the number of handoffs experienced by mobile users. The scope of the research is limited to resource management in the access network, focusing on the downlink transmission since the downlink traffic constitutes a large portion of the network traffic [42].

The UE considered in this work are limited to the multimode usage scenario and, as such, can only connect to a single RAN for a particular call/session at a time. Therefore, the use of multi-homed devices that allow simultaneous transmission of data through multiple access networks is out of the scope of this work and can be investigated in future work. Moreover, the UAVs are considered quasi-stationary, with an assumption that their placement has already been optimised to cater to the usage scenario at hand that involves many users, say in an urban area during a carnival or sports event. Investigation of a scenario in which UAVs move to keep up with spatially changing traffic can be addressed in future work. The simulations in this work are carried out using the Python programming language, but these could also be implemented using NS-3 or OpNet network simulators, or on a test bed in future research.

1.10 Thesis organisation

The remainder of the thesis is organised as depicted in Fig. 1.3 and described as follows:

Chapter 2 describes the ITNTN architecture and further elaborates on the different architectures proposed by 3GPP for NTN radio access. Also, the chapter gives the related projects concerning the integration of TNs with NTNs. Moreover, it discusses the concept of RRM, focussing on RRM frameworks, RAN selection considerations in heterogeneous

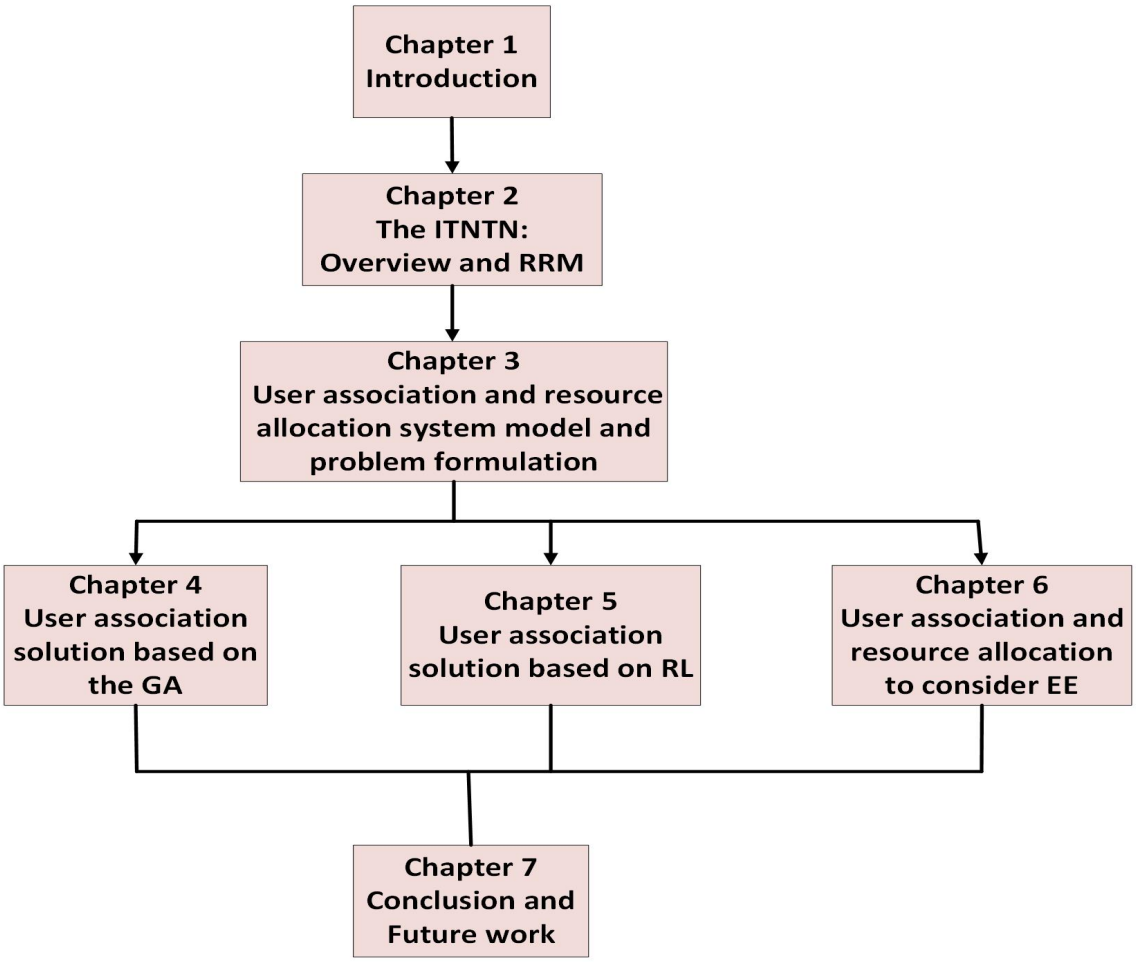

Figure 1.3: Thesis organisation.

networks, and a comprehensive literature review on RRM in the ITNTN.

Chapter 3 presents the proposed service-aware user association and resource allocation system model and problem formulation. In particular, the system model discusses the ITNTN deployment scenario, user mobility model, channel model, and signal quality model. Based on the system model, the user association and resource allocation problem is formulated as a MOOP maximising the total network data rate while minimising the probability of mobility-induced handoff. The complexity of the MOOP is then reduced

by adopting the weighted sum method, which transforms the MOOP into a SOOP. The complexity of the SOOP problem is reduced by decomposing it into two sub-problems: the user association sub-problem followed by the optional resource distribution sub-problem. A service-aware greedy heuristic algorithm is proposed to solve the user association sub-problem, and simulations are carried out to validate the relevance of differentiated service provisioning in the ITNTN. Moreover, the resource distribution problem is reformulated as a water-filling problem and consequently solved utilising CVXPY.

Chapter 4 presents the GA user association and resource allocation solution to the user association sub-problem formulated in Chapter 3. The GA solution is compared to the ILP solution, the greedy algorithm, and the RUA algorithm.

Chapter 5 investigates the use of RL to solve the user association sub-problem formulated in Chapter 3. A centralised learning but distributed execution MA3DQN algorithm is proposed, and its performance is evaluated through comparison with the GA, the ILP, the greedy, RUA, approximation-based, and the multi-agent DQN algorithms.

Chapter 6 presents an energy-efficient user association and resource allocation problem for the ITNTN. The problem is formulated as a SOOP that maximises the global network EE while minimising the probability of mobility-induced handoff. The SOOP is decomposed into two problems: the user association and resource allocation (UARA) problem and the power allocation (PA) problem. The UARA problem is similar to that described in Chapter 3 and thus can be solved by any of the algorithms described in Chapters 3-5. The PA problem, on the other hand, is solved using the particle swarm optimisation meta-heuristic algorithm.

Chapter 7 winds up the thesis report with the conclusion and possible areas for future work.

Chapter 2

Literature Review

This chapter first introduces a reader to the ITNTN architecture and further discusses the RAN architectures proposed by the 3GPP for the NTNs. Moreover, it elaborates on related projects concerning integrating TNs with the NTNs. The chapter then discusses the state-of-the-art RRM in heterogeneous networks, describing the different RRM frameworks and design considerations for RAN selection. It then gives a comprehensive literature review on RRM for the ITNTN, clearly detailing the recognised research gaps.

2.1 Introduction

The integration of TNs with NTNs has been widely viewed as one of the enabling features of 6G wireless networks [4, 3, 5, 6, 7]. The considered NTNs are the satellites, the HAPs, and the LAPs. Such integration is motivated by considerable investments in satellites by companies such as SpaceX, OneWeb, and Telesat [10], and in HAPs by Airbus and Google [24, 25]. Moreover, the 3GPP successfully investigated the use of the NTNs for wireless radio

access [1, 27]. Consequently, the future wireless networks will be an ITNTN comprising of the TN, the satellite, the HAPs, and the LAPs, all providing radio access to multi-mode UE, as depicted by Fig. 1.1.

On the other hand, the B5G networks are also anticipated to support different service groups characterised by contrasting QoS requirements such as throughput, latency, reliability, and mobility [3]. The different RANs in the ITNTN are characterised by divergent capabilities and limitations toward meeting the demands of the envisaged heterogeneous users. For instance, the satellite has the most extensive coverage area making it the most suitable RAN to serve long-distance and highly mobile users with limited need for handoff. On the other hand, its long propagation delay limits its usage for delay-sensitive mission-critical applications. The TN RAN is characterised by a large pool of resources that result in high throughput and lower latency. Yet, even these resources will not be sufficient to meet the high demand envisaged in the years 2030 and beyond [2]. Besides, the TN is limited by coverage per base station (BS), resulting in increased handoffs for mobile users. Accordingly, to reduce the mobility-induced handoffs and the associated handoff signalling overhead, delays, and probability of handoff failure, it is more suitable to use the NTNs characterised by larger cell radii for service provisioning mobile users, consequently improving their QoS. The LAPs and HAPs, on the other hand, are limited by the available number of channels. Thus their access should be prioritised for users whose QoS requirements can not be satisfied by other available RANs [11].

From the foregoing, it is clear that the different RANs in the ITNTN have divergent strengths and weaknesses in supporting users with contrasting demands, necessitating

efficient RRM schemes that consider the RANs' peculiarities in meeting the diverse user QoS requirements, an issue that this thesis addresses. Consequently, this chapter of the thesis describes the concept of RRM, giving a detailed literature review on RRM in the ITNTN and the recognised research gaps. However, before digging into RRM in the ITNTN, a reader needs to first understand the architecture of the ITNTN, the NTN RAN architectures as proposed by the 3GPP, the role of NTNs in the envisioned ITNTN, and the related projects as regards the integration, all described in the following sections.

2.2 General architecture of the ITNTN

The ITNTN architecture consists of a layered and 3-dimensional integration of SatComs, aerial platforms (LAPs and HAPs), and the TN as illustrated in Fig. 1.1. This section describes the different layers of the ITNTN.

2.2.1 Satellite communications (SatComs)

SatComs consists of the Geostationary Earth Orbit (GEO), MEO, and LEO satellites located at altitudes of 35,786 km, 7,000 – 20,000 km, and 600 – 1,500 km respectively [1]. The satellites in the different orbits are interconnected by very high throughput inter-satellite links (ISLs) that will enable direct packet routing through space using either radio frequency (RF) or optical frequencies [1, 10, 43].

Satellites have the broadest geographical coverage and, as such, are suitable for providing communication services to moving platforms like aircraft and high-speed trains with little

need for handoffs. On the other hand, SatComs suffers from long propagation delays that limit its application for direct connectivity of the euRLLC delay-sensitive services. For instance, the worst-case one-way delay from the UE to the gNB considering the transparent and regenerative (discussed in Section 2.3) GEO satellites is 272.375 ms and 135.286 ms, respectively, as reported by 3GPP in [1]. Propagation delays for LEO and MEO depend on the satellite's altitude above the earth's surface; moreover, increasing the altitude by 1000 km increases the one-way delay by 20 ms for a single hop [11]. This latency is way beyond the envisaged 1 ms latency provision for delay-sensitive applications in B5G. Hence, SatComs is not an efficient access network for such services, yet it enhances the capacity for the feMBB and provides the needed ubiquitous connectivity for the LDHMC service group as highlighted by the different use cases described in [44]. However, it should be noted that SatComs can support the euRLLC service group by leveraging its broadcast and multicast features. Content can be broadcast and cached at the network edge or the terminals, thus enabling the envisaged 1 ms delay and 99.999% reliability of the euRLLC service group [44].

The GEO satellites have the broadest coverage, with only three needed to cover the globe, excluding polar regions [9, 45]. They travel eastwards at the same rotational speed as the earth in a circular orbit with zero inclination and have a 24-hour view of a particular area. Since GEO satellites appear stationary to the earth, they have the advantage that line-of-sight (LoS) communication can easily be achieved to/from ground antennas without the need to track the satellite's motion. This is particularly useful in applications requiring a large number of ground antennas. For instance, such a feature can lead to considerable savings in ground equipment needed at relay nodes discussed in Section 2.3. GEO satellites are,

however, faced with the highest latency and propagation losses that lead to a comparatively weak received signal.

MEO satellites have a smaller coverage area than the GEO satellites. They have a rotational period of 5 – 12 hours and a visibility period of about 2 – 4 hours [9]. They are smaller than GEO satellites and hence less expensive to launch. On the other hand, the LEO satellites are at the lowest altitude from the earth's surface and, as such, have the smallest coverage area traded off for lower propagation delays and propagation path loss. LEO satellites are the smallest compared to GEO and MEO satellites and are thus the least expensive to build and launch. A satellite in LEO takes approximately 100 minutes to rotate around the earth and is visible for about 15 minutes from a particular point on earth [9]. Consequently, many LEO satellites are needed to provide uninterrupted connectivity.

2.2.2 High altitude platforms (HAPs)

HAPs are repeaters flying at an altitude of 17 – 22 km in the stratosphere [46, 47]. Such an altitude is above the civilian airspace, which does not go beyond 15 km above the earth's surface and is not affected by strong winds implying that minimum effort is required to compensate for unpredicted movements caused by the wind.

Several studies and projects on HAPs were carried out in the 1990s and 2000s. Still, most could not continue due to limited technological progress in the fields of solar cells, batteries, and aeronautics, coupled with limitations in regulations, reliability, and safety. However, recent technological advancements have returned interest in HAPs portrayed by several companies investing in their development to provide telecommunication services. An

example is the Google LOON project that operated between 2011 and 2021, using a network of interconnected solar-powered balloons located at altitudes between 18 – 25 km in the stratosphere [25]. These balloons had onboard LTE eNBs capable of providing broadband services to unserved and underserved areas around the world. Aquila is another project that was run by Facebook from 2014 to 2018 [48]. The main objective was to build a fleet of solar-powered aircraft flying at an altitude of about 18 km to provide internet access to people in under-connected regions. Zephyr is another solar-powered unmanned aircraft built by Airbus operating in the stratosphere at about 21 km above the earth's surface [24]. StratoBus is an autonomous HAP airship built by Thales Alenia Space to fly at an altitude of about 20 km. It is envisaged to perform several missions such as surveillance, navigation, observation, and telecommunications. The total lifespan of the airship is about five years [49].

HAPs can be classified as aerostatic and aerodynamic [47]. The aerostatic HAPs are in the form of balloons or airships and utilise the concept of buoyancy to stay aloft in the air. The need to compensate for thin air in the lower stratosphere leads to huge aerostatic HAPs, often 100m and over in length. The Balloons are usually unpowered, designed to stay still in space, while airships are powered using solar panels mounted on their surfaces and are quasi-stationary with onboard electric motors and propellers for station keeping [46]. The aerodynamic HAP, on the other hand, is based on the principle of dynamic forces that result from moving through the air. It is an aircraft that has to stay in a forward motion to keep aloft. It requires a wide wingspan to obtain sufficient lift against the air density in the altitudes of around 20 km [47]. Such a wingspan leads to a radius of motion of about 2 km

above the coverage area [50]. Aerodynamic aircraft is characterised by being lightweight, resulting in low payload capacity, and the need for constant motion leads to high operation costs.

Compared to satellites, HAPs have a stronger received signal, lower latency, and reduced implementation, deployment, and launch costs. Also, they can fly to a given area in response to temporal or spatial traffic demands. This makes them suitable for emergency response services and traffic offloading from a congested BS due to circumstances such as events like the Olympics. Compared to the TN, HAPs require a much lower number of BSs to serve the same area. For example, 16 HAPs with an elevation angle of 10° are needed to cover the entire Japan while Greece needs 8 HAPs [46, 47], compared to the multitudes of BSs forming backhaul links to the core network that are required using the TN. Given the wide coverage of up to 200 km radius provided by a single HAP, the end-to-end delay for transmissions greater than 20 km is less than that experienced in the TNs [50]. HAPs have a propagation RTT (Round Trip Time) of 1.5 ms, and since any point within the 200 km radius can be reached by a single hop, the delay is independent of distance from the transmitter to the receiver. However, using the TN to cover the same area necessitates transmission through multiple nodes with a processing delay of about 1 – 5 ms per node, significantly increasing the RTT for large distances [50]. Moreover, HAPs quickly provide efficient coverage to users in areas where it is challenging to deploy TNs and continuous service to high-speed vehicles.

While HAPs offer many advantages, they have a smaller coverage area than satellites, and the need for refuelling reduces their service provision time. Hence to benefit from the

numerous advantages highlighted, it is imperative to use HAPs in cooperation with SatComs and TNs to provide ubiquitous and continuous broadband communication.

HAPs are envisaged to serve many applications, including but not limited to broadcast/multicast, surveillance, navigation, remote sensing, and provision of high-capacity access and backhaul links to UEs and gNBs, thus reducing the traffic burden on the TN.

2.2.3 Low altitude platforms (LAPs)

LAPs have received considerable attention from academia and industry. Compared to the other networks of the ITNTN, LAPs have the lowest cost and are characterised by fast and easy deployment [51, 23, 46]. This attribute makes them suitable for providing communication services for emergency response and acting as aerial BSs for direct UE connectivity and traffic offloading during duration-limited events such as festivals and sports events. They are relatively small and light and operate at low altitudes, not exceeding 10 km above the earth's surface [51]. Their low altitude implies reduced propagation losses with the ability to establish a clear line of sight with the transmitters and receivers [23].

LAPs are of two types; the fixed-wing LAP that has to maintain continuous motion at very high speeds up to 120 km/h to remain aloft, and the rotary-wing LAPs that can remain stationary in the air [23]. Fixed-wing LAPs are capable of lifting load as heavy as 100 kg while rotary-wing LAPs lift load in the range of 10 – 50 kg [50]. The application determines the type of LAP to use; for example, a rotary-wing LAP would be preferred to complement the TNs in providing high data rate wireless access during stadium events.

Given their advantages, LAPs suffer from several constraints such as size, weight, and power (SWAP) that limit their communication capabilities and flight duration [23, 46]. This implies two things; on the one hand, they have limited channels and thus can not simultaneously provide wireless access to many users in their coverage. On the other hand, the LAP links may experience an outage due to energy drainage, and if they are operating as a multi-LAP network, this will lead to frequent changes in the network topology as old links are removed, and new ones are added. Moreover, since LAPs are at a low altitude, they suffer from interference from other LAP aerial BSs, terrestrial BS, and UEs [52].

2.2.4 Terrestrial network (TN)

The terrestrial layer includes fixed and mobile users using different radio access technologies (RATs) such as 5G, 4G, and Wireless Fidelity (WiFi) to access heterogeneous networks consisting of macro-, micro-, pico- and femtocells. This layer supports different communication paradigms developed in recent times, such as device-to-device (D2D), vehicle-to-vehicle (V2V), and vehicle-to-everything (V2X) communications. As illustrated in Fig. 1.1, the user equipment, including cell phones and vehicles, are multi-radio terminals capable of connecting to various access technologies, including satellite and aerial platforms. The 5G and beyond core is envisioned to support seamless integration between terrestrial and non-terrestrial networks.

Table 2.1 depicts a summary showing the attributes of the different networks that constitute the ITNTN.

Table 2.1: Comparison of the different networks comprising the ITNTN.

Platform	Classification	Key features	Advantages	Disadvantages
Satellite	GEO	• Altitude: 35,786 km • Same rotational speed as the earth • Zero inclination • Circular orbit • 24-hour view	• Largest coverage area • LoS communication easily achieved with GEO since UEs do not need to track satellite's motion • Broadcast/multicast capabilities	• Longest propagation delay. GEO have about 270 ms one-way delay, MEO about 110 ms and LEO less than 40 ms • Very high path loss hence the weakest received signal strength • A constellation of satellites needed for continuous service in LEO and MEO • High mobility of MEO and LEO leads to significant Doppler shifts • Most expensive to implement and launch, especially the GEO
	MEO	• Altitude: 7000 – 20,000 km • Rotational period of 5 – 12 hours • Visibility period of about 2 – 4 hours		
	LEO	• Altitude: 600 –1500 km • Rotational period of about 100 minutes • Visibility period of about 15 minutes		
HAPs unmanned repeaters flying at an altitude in the range of 17–22 km in the stratosphere	Balloon	• Usually unpowered • Stationary	• Stronger received signal than the SatComs • Lower latency than SatComs • Relatively fast and low cost in terms of implementation, deployment, and launching • Capable to fly to a given area in response to spatial and temporal traffic demands • Requires fewer BSs than TN for the same area • Lower end-to-end delay than TN for coverage area greater than 20 km	• Smaller coverage area than SatComs • Needs refuelling hence reduced service provision time
	Airship	• Powered using solar panels • Quasi-stationary		
	Aircraft	• Have to stay in forward motion to keep aloft in the air. • Fly in a circular path of radius $\approx$ 2 km		
LAPs Small, light fuelled unmanned airplanes operated at low altitudes of less than 10 km above the earth's surface	Fixed-wing	• Moves at high speeds up to 120 km/h • Capable of lifting heavy load up to 100 kg	• Lowest cost • Easiest and fastest deployment • Reduced propagation losses with the ability to establish clear LoS • Lower latency than HAPs	• Limited by SWAP, hence have lowest capacity and flight duration • Low altitude implies interference from other UAV aerial BSs, terrestrial BSs, and UEs • Mobility leads to Doppler shift
	Rotary-wing	• Can remain stationary in air • Lift load in the range of 10 – 50 kg		
Terrestrial Networks	Cellular (2G, 3G, 4G, 5G)	• Is a heterogeneous network consisting of macro-, micro-, pico-, and femtocells • Users access the radio network using multiple RATs	• Lowest latency • Rich resources • High throughput	• Limited coverage • Vulnerable to disaster • Difficult to deploy in certain areas like mountainous areas • Financial costs may outweigh the gain when used in sparsely populated and rural areas
	WLAN			
	WiMAX			
	Ad Hoc (MANET, VANET, SPAN)			

2.3 NTN radio access network architecture

The access network architecture for the NTN proposed by 3GPP [1] is based on whether the space/aerial payload is transparent or regenerative and whether the link from the UE

to the space/aerial platform is direct or indirect through a relay node (RN) as illustrated in Fig. 2.1. A transparent payload performs as a relay, with its function being frequency filtering, frequency conversion from uplink to downlink, and signal amplification. On the other hand, a regenerative payload performs the functions of a transparent payload and also implements demodulation/decoding, switching, routing, and coding/modulation. Such a payload is considered a next-generation node B (gNB) as it performs the functions of a base station.

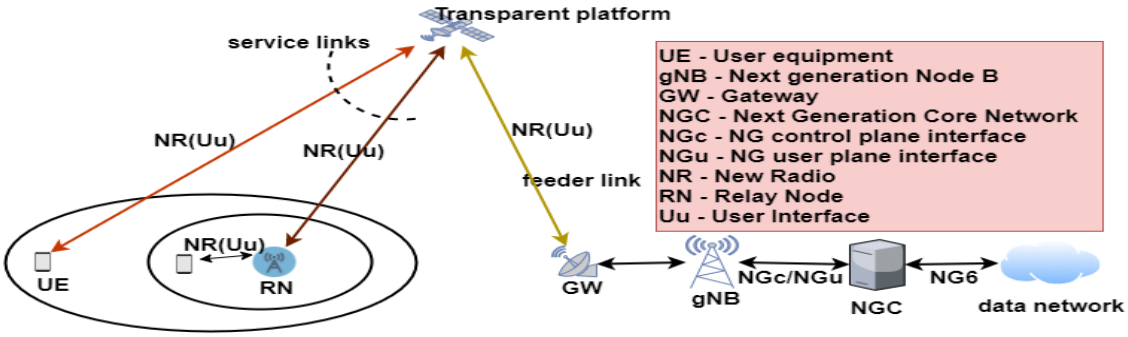

(a) Transparent payload has no gNB. Two scenarios: A) UE connected directly to the space/aerial platform and B) UE connected to the space/aerial platform through the RN.

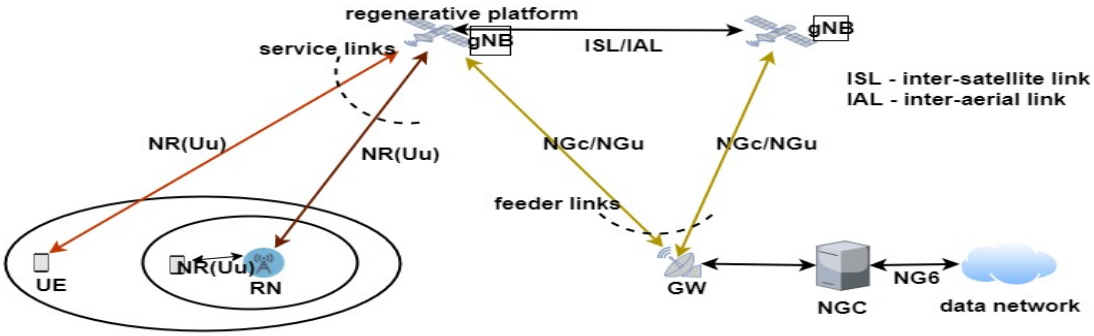

(b) Regenerative payload consists of gNB. Two scenarios: C) UE connected directly to the space/aerial platform and D) UE connected to the space/aerial platform through the RN.

Figure 2.1: NTN radio access network architecture.

The type of gNB functions performed by a regenerative payload is limited by the available power and mass of the payload. Consequently, the regenerative RAN architecture is further classified into two types [1]: i) the regenerative architecture with gNB-DU processed load, and ii) the regenerative architecture with gNB processed load. The gNB-DU processed load architecture splits the gNB into the centralised unit (CU) that runs the RRC and PDCP layers of the LTE protocol stack, and the distributed unit (DU) responsible for the RLC, MAC, and parts of the physical layer. The gNB-DU is thus the payload while the gNB-CU is located at the GW of Fig. 2.1(b). On the other hand, the regenerative architecture with gNB processed load does not split the gNB functions.

The radio link from the UE or the RN to the space/aerial transponder is called a service link, while that from the transponder to the gateways (GWs) is called the feeder link. As shown in Fig. 2.1, the service link uses the New Radio (NR) interface, while the interface of the feeder link depends on whether the transponder is transparent or regenerative, with the former using the NR interface and the latter using the NG (Next Generation) interface. The NG interface supports the separation of the user plane from the control plane to give the NG control plane (NGc) and the NG user plane (NGu) interfaces. The NR and NG interfaces maintain their definitions, principles, and functionality as described in [53], but will have different RF characteristics that consider the space/aerial platform link constraints.

Based on the definitions above, there are four different architectural scenarios; A and B are illustrated in Fig. 2.1(a) while C and D are described in Fig. 2.1(b). In scenario A, a UE connects directly to a transparent payload; in B, the connection is through an RN. Scenario C considers direct connectivity from a UE to a regenerative payload, and D depicts

the connectivity going through an RN. Table 2.2 summarizes the four different NTN RAN architectural scenarios.

Without loss of generality, the work in this thesis is based on the assumption that the NTN access nodes are regenerative, and users can connect to them directly. This assumption is because the work considers a usage scenario of many users whose traffic the TN, including the relay nodes, can not entirely support. Thus, it necessitates the UE to be able to directly connect to all ANs, including the NTNs, which should have the capacity to act as gNBs, and support the TN. Therefore, scenario C is considered in this work.

Table 2.2: Non-terrestrial network RAN scenarios. [1]

NTN architecture scenario	**NTN Terminal**	**Space or Aerial Platform**	**NTN Gateway**
A: access network serves UEs via transparent space/aerial platforms	UE	Transparent, with a Remote Radio Head that relays Uu radio interface signals. Performs frequency filtering, conversion, and amplification	gNB
B: access network serves Relay Node via transparent space/aerial platforms	Relay Node	Transparent, with a Remote Radio Head that relays Uu radio interface signals	gNB
C: access network serves UEs via a regenerative space/aerial platform that has a gNB onboard	UE	gNB or relay node that performs frequency filtering, conversion, amplification, demodulation/ decoding, switch and/or routing, coding and modulation	Router interfacing to core network
D: access network serves Relay Node via a regenerative space/aerial platform that has a gNB onboard	Relay Node	gNB or relay node that performs frequency filtering, conversion, amplification, demodulation/ decoding, switch and/or routing, coding and modulation	Router interfacing to core network

2.4 Role of non-terrestrial networks in the integrated network

NTNs are characterised by wide coverage, less vulnerability to physical attacks and natural disasters, broadcast and multicast features and hence can be used to complement the TN by enhancing or providing [1, 10, 43, 54]:

- Ubiquitous broadband coverage: NTNs will expand the TN coverage to unserved, difficult-to-reach, and under-served areas. Moreover, the widely spread-out IoT devices are envisioned to be connected to the network through NTNs.

- Capacity: NTNs will provide alternative radio access and backhaul links to offload excess traffic during peak hours or scenarios of an unexpected surge in traffic within a specific area. For instance, UAVs can easily and quickly be deployed as aerial BSs to support the terrestrial gNBs through traffic offloading and on-demand high data rate wireless access during events such as sports and festivities.

- Service reliability: NTNs will ensure continuity in service provisioning to IoT devices and moving platforms such as high-speed trains, air crafts, and vessels on high seas following the provision of a large footprint with no need for frequent handoffs.

- Network availability and resilience: NTNs will provide alternative radio access and backhaul links that will provide service in cases of faults and outages of the terrestrial network due to physical attacks and natural disasters.

- Network scalability: Through the broadcast and multicast features, NTNs, mainly the SatComs, will be used to offload the terrestrial backhaul network by broadcasting highly viewed data content to the edges of the terrestrial network.

2.5 Related projects

Several projects have been funded to realize the integration of NTNs with TN. This section briefly highlights some of these projects.

- Satellite and Terrestrial Network for 5G (Sat5G): This is a European Union Horizon 2020 (EU H2020) project that defines optimal satellite-based backhaul and traffic offloading solutions to support the eMBB 5G service group [44, 55]. It defines four main use cases in which SatComs can complement the terrestrial network, these being [44]: i) Delivery and offloading of multimedia content and MEC virtual network function software to the edge of the network. ii) 5G fixed backhaul to provide 5G services, especially to areas faced with the difficult deployment of TNs. iii) 5G to premises providing 5G broadband access to under-served areas/premises using hybrid terrestrial-satellite connections. iv) 5G moving platform backhaul that provides 5G access to moving platforms such as aircraft, trains, and vessels.

- VIrtualized hybrid satellite-TerrestriAl systems for resilient and fLexible future networks (VITAL): VITAL is another EU H2020 project that ran from 2015 to 2017. The project aimed to bring NFV into the satellite domain and leverage SDN to efficiently manage and optimise the operation of the hybrid terrestrial and satellite

network [56]. NFV was meant to enable operators to virtualize the satellite network and offer it to third-party operators or service providers as an Infrastructure as a Service (IaaS). SDN provides a unified control plane to efficiently manage the TN-NTN hybrid network's operation. This project focused on three application scenarios; satellite virtual network operator services, satellite backhauling, and hybrid terrestrial-satellite service delivery.

- Demonstrator for Satellite Terrestrial Integration in the 5G Context (SATis5): The SATis5 is a European Space Agency (ESA) project whose aim is to build a proof of concept test-bed that will deploy, evaluate, and showcase the benefits of satellite integration with terrestrial networks [57]. The project focuses on the eMBB and mMTC service groups and mainly looks at the backhaul satellite use case. [58] demonstrates one of the project's test beds in which an edge node with packet core functionality can connect to a central core network through either the satellite or terrestrial backhaul.

- Shared Access Terrestrial-Satellite Backhaul Network enabled by Smart Antennas (SANSA): SANSA is an EU H2020 project aimed at enhancing mobile network capacity and resilience by proposing spectrum efficient self-organising hybrid terrestrial-satellite backhaul network [59]. The SANSA use cases include [60]: i) Offering resilience through backup satellite backhaul links used when terrestrial links fail. ii) Provision of offloading capability via satellite to avoid terrestrial link congestion. iii) Possibility of low-cost new node deployment on the fly. iv) Content delivery network integration. v) Remote cell connectivity.

- NETwork of Stratospheric Platforms for Traffic Monitoring, Environmental Surveillance and Broadband Services (HeliNET): The HeliNET project was funded by the EC's 5th framework program. It ran from January 2000 up to March 2003 with deliverables including developing a scale-size plane HAP that can provide broadband communication, environmental monitoring, and remote sensing [61, 62].

- Communications from Aerial Platform Networks Delivering Broadband Communications for All (CAPANINA): CAPANINA was a continuation of the HeliNET project, funded by the EC's 6th framework program from November 2003 to January 2007. The project aimed at investigating and validating the use of HAPs in delivering broadband backhaul to hard-to-reach areas and high-speed trains moving up to 300km/h with onboard WiFi access points [63].

Most of the projects discussed above focus on providing either a backup or parallel space/aerial backhaul link similar to scenario B discussed in Section 2.3. Moreover, they do not consider the integration of all the RANs that constitute the ITNTN, i.e., the TNs, LAPs, HAPs, and SatComs; hence, they do not consider their different peculiarities in meeting contrasting user QoS requirements. On the contrary, the work proposed in this thesis considers a multi-mode UE capable of direct connectivity to either the terrestrial or NTN access node acting as a gNB, as shown in scenario C of Fig. 2.1(b). Consequently, multiple links from the wireless network will be available to the UEs, including terrestrial links, satellite links, and aerial links, as illustrated in Fig. 1.1. As already highlighted is Section 2.1, these different RANs are characterised with various constraints and capabilities towards meeting the diversified requirements of the 6G user groups. The challenge then is

how to efficiently map users having heterogeneous QoS demands to the appropriate RAN of the ITNTN. Hence, radio resource management algorithms and schemes play a vital role in the realisation of the ITNTN.

2.6 Radio resource management (RRM) in the ITNTN

RRM ensures efficient resource allocation and QoS provisioning given multi-class traffic with diverse requirements in the presence of different network constraints and parameters such as path loss, limited spectrum, fading, and thermal noise [9]. The purpose of RRM, therefore, is to either maximise certain performance parameters such as network throughput, bandwidth utilisation, and achieved revenue or minimise other parameters like end-to-end delay, delay jitter, and packet loss, subject to certain constraints such as minimum achieved data rate of a user, maximum available power at the AN, maximum call dropping (or blocking) probability or (and) minimum signal-to-noise ratio [9, 64].

2.6.1 RRM frameworks

RRM can be grouped into three sections, namely [64]:

i) Frequency/time/space resource allocation: This category comprises functions like channel allocation, scheduling, beam and bandwidth allocation, transmission, and coding rate control [9]. Frequency resources are in the form of sub-channels, and time resources are in the form of timeslots. In contrast, space resource allocation is a form of frequency reuse to achieve spatial separation using MIMO and beamforming techniques.

Frequency and time resources can be used concurrently. For instance, the physical resource block (PRB) defined by 3GPP for 5G NR interface [53]. The PRB represents the smallest time-frequency resource unit allocated to a user. It occupies one timeslot of 0.5 ms, consisting of 7 OFDM symbols and 12 sub-carriers, each with a bandwidth size depending on the chosen sub-carrier spacing. Unlike LTE which had only one possible sub-carrier spacing of 15 kHz, the 5G NR introduces scalable numerology that allows sub-carrier bandwidth/spacing to vary ranging from 15 kHz and 480 kHz according to $\Delta f = 2^{\mu}, \mu = 0, 1, 2, 3, 4, 5$ [65]. Since the different RANs in the ITNTN may use different resources, we shall use the basic bandwidth unit (BBU) to represent a unit of radio resources [66] in this work. Therefore, no matter the radio resource used in any RAN of the ITNTN, the system capacity will be represented in terms of bandwidth.

ii) Power allocation and control: Power allocation and control are critical, especially in interference-limited networks like code division multiple access (CDMA), where users use the same frequency for signal transmission [67]. The total network interference always limits the number of users admitted in such networks, and as such, power control is necessary to increase network capacity [67]. Moreover, economic and environmental factors limit an access node's transmit power since an increase in energy consumption increases operator expenditure and greenhouse emissions. Besides, power control has been effectively used to solve the near-far problem experienced by users located at varying distances from the BS and concurrently transmitting on the same frequency [68]. Without power control, the nearby UE overshadows signal transmissions from the far UE, reducing the equivalent network capacity.

iii) Call admission control (CAC) and handover: CAC is used to either grant or deny access of new calls to the network. CAC controls congestion of the network and all its associated effects, such as an increase in packet loss, end-to-end delay, delay jitter, handoff failure rate, and service degradation of existing users. This is achieved by restricting access of new calls to the network depending on resource availability and loading conditions. If available resources satisfy the QoS requirements of a new call without degrading the QoS of existing calls, then the call is admitted, otherwise, it is rejected.

This thesis focuses mainly on user association/scheduling, channel allocation, and power allocation. Chapters 3, 4 and 5 are focussed on user association and resource allocation in terms of BBUs, while Chapter 6 associates users to the appropriate network and allocates them both BBUs and power. As the ITNTN consists of RANs that could be managed independently, the works in literature, however, prove that the radio resources of the different RANs of the ITNTN can best be managed jointly [69, 14, 70, 19, 71, 20, 15]. Following the benefits of joint resource management, as highlighted in the next section, resource management for the different RANs of the ITNTN will be carried out jointly in this work.

2.6.2 Benefits of joint resource management

Joint management of the different RAN radio resources in the ITNTN presents benefits highlighted in this section:

i) Overall QoS enhancement: NTNs provide additional radio resources that complement the TNs in providing broadband access, especially during traffic peaks. Moreover, since an NTN access node offers wider coverage than the TN BS, NTNs guarantee

continuity and reliability in service provisioning of highly mobile applications through reduced handoffs. Therefore, joint management will ensure a user's association with the appropriate RAN, depending on the user's requirements.

ii) Efficient resource allocation and utilisation: The TN is endowed with a rich pool of resources resulting in high data rates and low latency compared to the NTNs, especially the SatComs. Therefore, many users would prefer to associate with the TN, even when the NTNs can meet their QoS requirements. However, user demands are expected to rise beyond what the TN can sustain. Moreover, the HAPs and UAVs that have a comparably low latency as the TN are limited by capacity [50]. Therefore, joint resource management of the ITNTN is needed to ensure efficient resource allocation and utilisation, dependent on RANs' capabilities, limitations, loading, and user QoS requirements.

iii) Interference management: Two types of interference will exist in the ITNTN: cross-tier and co-tier. Cross-tier interference occurs between different tiers, for instance, the downlink (DL) of a TN UE experiences cross-tier interference from the HAP, UAV, and SatComs DL transmissions. On the other hand, co-tier interference occurs within a tier, for example, when a TN DL is subjected to interference from other TN BSs. Joint resource management facilitates total network capacity maximisation subject to SINR constraints. Moreover, it aids appropriate power allocation and control schemes that mitigate interference.

iv) User fairness management: The RANs in the ITNTN have different capabilities and attributes. To ensure fairness in QoS provided to the various users accessing the ITNTN through different RANs, joint management of resources is necessary. Each user in the network should be guaranteed at least the minimum QoS, irrespective of the RAN used.

v) Enhanced network resilience: Joint management of resources will enable NTNs to automatically provide backup access links in case of faults or outages of the TN due to natural disasters and physical attacks.

2.6.3 RAN selection in heterogeneous networks

In a heterogeneous network such as the ITNTN, RRM schemes are required to select the best-suited RAN that supports the QoS requirements of incoming new and handover calls. Users can connect to any of the available RANs and freely roam from one to another using either multi-mode or multi-homed devices embedded with multiple RAN interfaces. Multi-mode UEs can only connect to a single RAN for a particular call/session at a time. Switching to another RAN for such devices implies that the ongoing call must first be broken. On the other hand, multi-homed terminals can change in-between networks for a single call (IP mobility) and are also capable of transmitting data from a single session through multiple access networks (multi-homing) [72]. Nonetheless, multi-mode and multi-homed UEs in a multi-access network must be connected to the most appropriate RAN anywhere and anytime.

The critical questions to ask in the design of RAN selection algorithms are: i) Who makes the RAN selection decision? and ii) Which criteria or attributes are used in the RAN selection process? This section is dedicated to answering these questions.

2.6.3.1 RAN selection decision maker

The decision to associate a user to a particular RAN node deemed the most appropriate among many alternatives is either user-centric [73, 74, 75, 76, 77] or network-centric [78, 79].

In the user-centric approach, the UE selects the best RAN based on several criteria such as received signal strength, user preferences, potential power consumption, user service subscriber profile, and capability of RAN to support the ongoing applications [80]. While the user-centric approaches provide customized individual performance with less overheads, knowledge of network conditions is unknown, resulting in inefficiency. To enhance their performance, they are assisted by the network [74, 75, 76]; the so-called user-centric network-assisted algorithms. In these algorithms, the network shares its conditions, such as network load, price, available bandwidth, and latency, with the UE, which then makes a final network selection decision taking into account the network parameters, measured link conditions, user preferences, and service requirements. Along the same lines, 3GPP defined the network access network discovery and selection function (ANDSF) [81], whose purpose is to avail UEs with access discovery information and operator-based policies necessary for RAN selection in a multi-access environment. An example of such policies is the inter-system mobility policy used by a multi-mode UE to decide when inter-system mobility is allowed or restricted and to select the most preferred access network to access the evolved packet core. The

UE, therefore, makes the final RAN selection decision based on its link measurements, user preferences, and network policies. Artificial Intelligence (AI) has also been introduced in user-centric approaches [77]. The UE is equipped with intelligence to learn and predict time-varying network and link conditions, thus customizing network selection based on its requirements.

The above two user-centric approaches yield sub-optimal global performance, which can be improved through network-centric strategies. These schemes foster efficient management of the scarce and limited radio resources of the available RANs. Consequently, the network decides the RAN to serve a UE based on parameters such as network load, BS coverage area, user's subscription profile, mobility, and signal strength indicator. Network-centric approaches can be distributed across BSs or may utilise a central entity that manages network selection decisions across several cells or RATs [82]. Though they may reduce user QoE given that user preference is usually not a priority, network-centric approaches result in optimal performance since they maintain a global view of the network conditions.

In this thesis, Chapters 3, 4 and 6 utilise a network-centric approach for user association and resource allocation in the ITNTN. In contrast, Chapter 5 introduces AI in the user association process to enable user-centric network-assisted real-time decision-making. Table 2.3 summarizes the characteristics of user-centric, user-centric network-assisted, and network-centric decision-making schemes.

Table 2.3: Network selection decision making schemes.

Scheme		Characteristics	Advantages	Disadvantages
User-centric		UE makes network selection decision	• User satisfaction • Low overheads	No knowledge of network conditions leading to: • Load imbalance thus inefficient utilisation of resources • Increased call blocking and dropping probability • Successful connection not guaranteed, the selected network may prefer to serve more valuable users
User-centric network assisted		UE makes decision assisted by information broadcasted by the network	• Better decision making than user-centric, taking into account network conditions, hence more efficient resource utilisation • User satisfaction	• Increased overhead • Possibility of network masking their conditions as they are interested in making more revenue • Successful connection not guaranteed as the selected network may prefer to serve more valuable users
Network-centric	Centralised	Central entity in the network manages network selection decision	• Efficient control of limited and scarce network resources and load balancing	• Complex and requires higher signalling and computation overheads • Increased response time and delay • User preference not a priority hence the possibility of reduced user QoE.
	Distributed	Network selection distributed at the BSs with direct interfaces between BSs		

2.6.3.2 RAN selection decision criteria

Traditionally, RAN selection is based on received signal strength or signal to noise ratio (SNR) threshold and hysteresis values as described in [82]. The authors looked at network selection in integrated WiFi and LTE networks. Because users naturally prefer to connect to the cheapest network, provided it offers reliable communication, the UEs continuously monitor the SNR of signalling messages received from neighbouring WiFi access points. Once the SNR exceeds a predefined threshold, the UE steers traffic through the WiFi RAN, otherwise, the LTE network is used.

These algorithms are, however, inefficient in a multi-access network. They do not factor in users' preferences, application requirements, and network conditions such as loading, leading to a high probability of incorrect decisions. Network selection in a multi-access network is a multi-criteria decision problem that must consider the inherent heterogeneity of available RANs, service applications, and user preferences. It necessitates the formulation of a utility function $u(j, C, \upsilon)$ that expresses the capability of a RAN j in satisfying the QoS requirements of the service group υ given a set C of different considerations/criteria. The objective of the network selection algorithm, therefore, is to either maximise or minimise the utility function subject to certain conditions as illustrated by

$$\max \quad u(j, C, s) \tag{2.1}$$

$$\text{subject to} \quad j \in A(C, \upsilon),$$

where $A(C, \upsilon)$ is the set of RANs available to serve a service group υ call/session request given a set C of different criteria. The solution to (2.1) is the best RAN that satisfies the user's QoS requirements [83]. Fig. 2.2 illustrates the network selection decision-making process.

The different criteria to consider in RAN selection in a multi-access environment can be classified into four main categories [84] as illustrated by Fig. 2.2:

- Network based: This category includes parameters that describe the wireless network characteristics such as network load, pricing scheme, monetary cost, security, coverage, available bandwidth, and received signal strength indicator.

- Application requirements: This includes parameters related to QoS requirements of the diverse user applications, expressed through performance metrics such as expected minimum data rates, maximum delay, maximum jitter, maximum allowable bit error rate, and packet loss. For the network to satisfy contrasting QoS requirements from different applications, traffic is classified into service groups, with each comprising user requests with the same QoS needs.

- User preferences: Different users have different preferences. One may put more emphasis on the cost of the service, while another is concerned about a high-quality application. For example, a real-time user may select a network with high data rates to achieve high service quality. In the same way, a non-real-time user may opt for a network with high data rates to reduce service delivery time. Metrics used to factor in user preference are service price, battery power consumption, security level, and data rates [85].

- Device-based criteria: UEs have different capabilities in terms of mobility, capacity, CPU, battery power, and supported interfaces. Some can only connect to one RAN at a time for a session, while others can distribute a session's traffic to multiple RANs.

The criteria used for network selection in this thesis fall into all four categories described above. The problem formulated in Chapter 3 and the corresponding solutions consider network-based criteria by taking into account the access nodes' available resources and cell coverage. Moreover, application requirements are also considered by guaranteeing the minimum required data rate for data-intensive applications and ensuring the minimum data

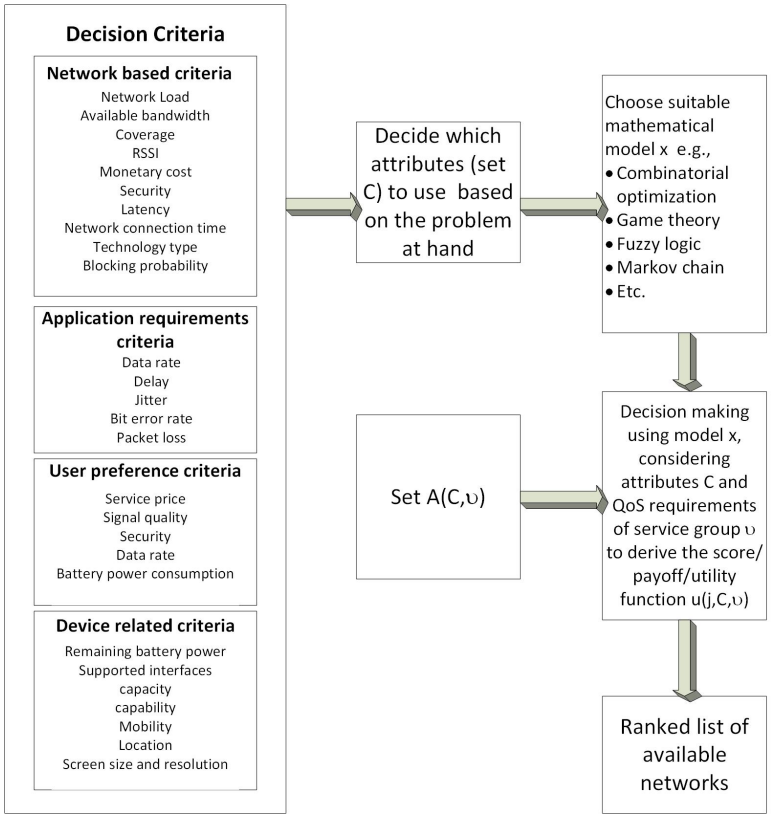

Figure 2.2: Network selection decision making process.

rate that guarantees a specified bound on the delay violation probability is satisfied for the delay-sensitive users. Also, user preference is addressed since the objective of the static users, as will be seen in Chapters 3 – 6, will be to maximise their data rate. In contrast, mobile users will prioritise minimising the probability of handoff. Concerning device-based criteria, this work considers only multi-mode UE; thus, the devices can only connect to one access node at a time.

2.6.4 Literature review on RRM for the ITNTN

This thesis considers the user association and resource allocation problem in the ITNTN, which several works have recently addressed. This section describes the related work and gives the research gap this thesis seeks to address.

2.6.4.1 Related work

The authors in [69] propose a user association and resource allocation problem that maximises the overall sum rate of an integrated terrestrial and UAV RAN with macro BSs and satellite backhaul links. The authors supplement this work in [14] by considering the limited life endurance of UAVs and the energy consumption costs of the access nodes. However, the work did not consider the satellite as an access node but as a backhaul link. Neither were HAPs considered in this integration. Therefore, the authors did not consider the idea of having space (satellite), and aerial (LAPs and HAPs) nodes complement the TN in providing radio access to users. Moreover, the work did not account for how the different user requirements were to be met.

In [70], the authors propose a load-balancing algorithm for an integrated terrestrial and satellite network. They define the radio resource utilisation ratio as a metric measuring each cell's load status and group traffic into delay-sensitive and delay-tolerant. Traffic from an overloaded terrestrial cell is offloaded first to neighbouring terrestrial cells and then to the satellite cell. Only delay-tolerant traffic is offloaded to the satellite network. However, for 6G networks to have an effective and efficient resource allocation scheme, traffic can not only be classified into two but in different use cases that effectively capture all future network

demands. Moreover, this work associates users to the non-terrestrial network only when the terrestrial network is overloaded. Besides, the authors did not consider other NTNs, such as LAPs and HAPs, nor did they consider power constraints.

In [19], the authors jointly optimise resource allocation, user association of both access and backhaul links, and HAPs' locations to maximise users' throughput in an integrated satellite, airborne and terrestrial network. These authors neither considered the heterogeneous user QoS requirements nor the different limitations of the networks in the integration. The authors in [71] propose a joint algorithm that optimises resource allocation and user association to a terrestrial macro base station (MBS) and multiple UAVs mounted BSs using in-band wireless backhaul. However, the authors only consider UAVs and TNs in their analysis and do not account for the provisioning of the different use-case QoS requirements.

The authors in [20] propose an algorithm that maximises the energy efficiency of an integrated satellite/terrestrial cache-enabled RAN. The LEO satellites and terrestrial APs provide users with content distribution and retrieval services, thereby offloading such traffic from the MBS. The work does not consider the implementation of an integrated terrestrial-aerial-space RAN. Neither does it address QoS provisioning to different use cases, as it considers only one service: content distribution. In [15], the authors propose an optimisation problem that maximises the network capacity while ensuring QoS in terms of minimised interference between many users in an integrated terrestrial and satellite network. The work fails to distinguish users according to their different QoS requirements, such as data rates

and does not guarantee that these QoS demands are satisfied. Besides, it assumes that all the available networks can support all different users.

The authors in [86] maximised the minimum ergodic achievable rate of a user-UAV link. This work optimises only the UAV RAN and not the entire integrated terrestrial-satellite-UAV RAN. Besides, the work did not incorporate QoS provisioning of the different use cases. The authors in [21] first optimise multi-beam dynamic radio resource allocation for LEO-ground downlinks and after optimise dynamic resource allocation for HAP-ground downlinks when LEO satellites and HAPs share the same spectrum. This work does not consider joint resource management of the different tiers, as it optimises the resource allocation of each tier separately. The authors in [17] propose a traffic offloading scheme that takes into account the heterogeneity of user demands. The optimisation algorithm first maximises the eMBB use-case data rate, subjected to stringent outage probability for the uRLLC use-case. The algorithm then maximises the emBB traffic offloaded from the TN access node to the SatComs backhaul while the uRLLC traffic is channelled through the TN backhaul. This work does not consider using SatComs directly for radio access, nor does it incorporate the UAVs in the radio resource management.

The authors in [87] proposed a network selection scheme for integrated terrestrial and drone cell networks that maximised proportional fairness of data rates across all users under coarse correlated equilibrium and minimum data rate constraints. However, this work did not consider service-differentiated provisioning and only integrated the UAV and MBS networks. The authors in [88] propose an algorithm that jointly optimises network selection, transmit power of aerial and vessel-enabled BSs, and aerial BS position in the

hybrid satellite-UAV-terrestrial maritime network. The network utilises the satellite and terrestrial BSs for backhaul. While the work guarantees the user QoS in terms of data rate, it does not address differentiated service provisioning. It thus does not investigate the peculiarities faced by the different networks in meeting the contrasting demands of users. In [89], the authors propose a content service-oriented resource allocation scheme for a space-air-ground integrated network (SAGIN). They utilise a three-sided matching algorithm to determine the optimal matching between users, content sources, and the space-air-ground network facilities. However, this work does not consider the strengths and limitations of the different networks in the SAGIN towards meeting the heterogeneous user demands, nor does it analyse differentiated service provisioning.

Machine learning approaches have also been adopted to introduce intelligence and thus facilitate automation in solving optimisation problems in the ITNTN. The authors in [90] elaborate on how machine learning can solve four main problems in the ITNTN: resource management, attack detection, security authentication, and target recognition and location. Furthermore, in [91], the authors study the challenges of resource optimisation in the ITNTN due to the heterogeneity of the integrated network. They propose a traffic control solution based on convolutional neural networks that optimises path combinations for the satellite communication system. However, both references [90] and [91] do not consider user association issues, which the current thesis addresses.

On the other hand, the work in [92] utilises ensembling DNNs to optimise the user association in the integrated space-HAPs-ground networks. In [93], the authors propose a multi-armed bandit approach that maximises user fairness while minimising the loading at

the base stations in the integrated satellite-UAVs-ground network. The upper confidence bound approach is utilised to optimise UAVs' joint 3D trajectory design and resource allocation. The authors in [94] propose a user association and power control multi-agent scheme based on a multi-agent deep deterministic policy gradient approach aimed at maximising the total energy efficiency of the system. The authors supplement this work in [95] by developing a deployment method of local cache pools to achieve lower time delay and energy efficiency in the terrestrial-satellite network.

The authors in [96] propose a centralised learning and distributed execution DRL algorithm for NTNs. In the proposed scheme, users are associated with NTN BSs in a manner that enhances the long-term system throughput and minimises handoffs. The authors in [97] formulate a joint computation offloading and resource allocation problem in a mobile edge computing (MEC) enabled integrated aerial-terrestrial vehicular network. The problem is solved by utilising a multi-agent double DQL solution. Similarly, in [98], the authors propose a DRL scheme for resource allocation of vehicular networks served by NTNs. In the scheme, both the satellite and ground vehicles act as agents that collaborate to determine the resource allocation decisions.

In [99], the authors propose a distributed relative value iteration approach that schedules user uplink transmission through an aerial or a terrestrial BS to minimise the long-term average user transmit power. In [100], the authors propose a network control and resource allocation problem for massive IoT in the space-terrestrial integrated network. The problem is solved using deep actor-critic RL. The authors in [101] investigate a joint user association, channel allocation, and transmission power control problem in a UAV network

with constrained backhaul links. The problem is formulated to maximise the system utility, which depends on the downlink data rate and transmission cost in terms of the UAV's energy and backhaul bandwidth needs. Multi-agent hybrid DRL algorithm is utilised to solve the problem. All the works in [92, 93, 94, 95, 96, 97, 98, 99, 100, 101] do not consider the integration of all the four RANs in the ITNTN. Moreover, they do not account for user QoS provisioning according to heterogeneous service groups nor examine the uniqueness of the different RANs in the ITNTN in meeting the contrasting user requirements.

2.6.4.2 Research gaps

To the best of our knowledge, the main gaps in the state-of-the-art literature that this thesis has addressed are:

i) The integration of all four networks, the TN, LAPs, HAPs, and the SatComs, to provide radio access to multi-mode users. This thesis seeks to find efficient dynamic radio access user association and resource allocation schemes for an ITNTN comprising the TN, LAP, HAP, and SatComs access nodes. It thus investigates scenario C discussed in Section 2.3, in which a multi-mode user equipment can access the network through the TN and all NTN access nodes.

ii) Consideration of the heterogeneity in user QoS requirements in the user association and resource allocation framework for the ITNTN. This thesis leverages differentiated service provisioning, a salient feature of 5G that allows the classification of various user services into different service groups (use-cases), with each service group comprising services of related attributes and priorities [102, 103]. This work considers three service groups:

feMBB, euRLLC, and LDHMC. The feMBB service group comprises data-intensive users demanding multimedia content and services such as high-definition and ultra-high definition video streaming. On the other hand, the euRLLC consists of mission-critical services requiring high availability, reliability, and low latency, such as remote surgery, autonomous vehicles, and factory automation. Lastly, the LDHMC use case consists of highly mobile applications requiring reliable connectivity and high data rates. Moreover, the user association and resource allocation schemes proposed in this work are priority-aware and, as such, associate and serve users according to the priorities of their service groups. In this work, the euRLLC users are prioritised over other users to avoid their denial of service, which could be catastrophic. However, the priority can also be based on other factors, such as the use case that yields more revenue to the operator.

iii) Consideration of the unique features and limitations of the different RANs of the ITNTN in meeting the contrasting user requirements. Since the RANs in the ITNTN are characterised by different strengths and limitations towards meeting the heterogeneous user QoS demands, user association and resource allocation algorithms should be cognizant of these peculiarities. To this end, unlike the works in literature, this thesis prioritises the association of mobile users to access nodes with the largest cell radius to minimise mobility-induced handoffs and thus provide reliable connectivity for the mobile LDHMC service group. Also, since the SatComs is characterised by long propagation delays, access to this RAN by the mission-critical euRLLC users is restricted.

iv) Finally, the use of AI to associate users in real-time to the appropriate RANs of the ITNTN in a manner that harnesses the different RAN characteristics in an optimised way to meet the QoS requirements of divergent service groups efficiently.

Subsequently, Chapter 3 formulates a user association and resource allocation problem that addresses the identified gaps i)–iii), while Chapters 4 and 5 give the solutions to this problem, with Chapter 5 focusing mainly on the AI solution that addresses gap iv). Since the problem defined in Chapter 3 focuses on achieving a spectrum-efficient network, this problem is reformulated in Chapter 6 to achieve an energy-efficient network while still addressing the gaps i)–iii) identified in the existing literature.

2.7 Chapter summary

The integration of the TN with NTNs has been envisioned to enhance wireless coverage and capacity and increase network availability and reliability. This chapter described the ITNTN architecture and elaborated on the different architectural scenarios for radio access using the NTNs. In addition, the role of the NTNs in the integration was elucidated, and a couple of projects carried out over the years to realize the integration of the TN with NTNs were described. Furthermore, the need for efficient RRM algorithms to map users having different requirements to the heterogeneous RANs of the ITNTN was recognized, and the different RRM frameworks and network selection considerations were discussed. As this thesis focuses on the user association and resource allocation aspect of RRM, a detailed literature review

on the same concerning the ITNTN was given, and the gaps that the thesis seeks to address were identified.

Chapter 3

A Novel Service-Aware User Association and Resource Allocation System Model and Problem Formulation

Integrating the TNs with NTNs to provide radio access as anticipated in the B5G networks calls for efficient user association and resource allocation (UARA) strategies. In this chapter, we present the deployment scenario of the ITNTN, the user mobility, channel and signal quality models, and assumptions considered in this thesis. Based on this scenario, a UARA problem is formulated and consequently solved as two sub-problems: the user association and resource distribution sub-problems.

3.1 Introduction

The B5G networks are anticipated to support different service groups characterised by contrasting QoS requirements. According to [3], the service groups envisioned to be supported by 6G include ultra-massive machine-type communications (umMTC), further enhanced mobile broadband (feMBB), enhanced ultra-reliable and low-latency communications (euRLLC), long-distance and high-mobility communication (LDHMC), and extremely low power communications (ELPC).

The different RANs in the ITNTN are characterised by divergent strengths and limitations toward meeting the demands of the envisaged heterogeneous users, necessitating efficient radio resource management schemes. Consequently, this chapter addresses the UARA problem, focusing on efficiently mapping users with diverse QoS requirements to the appropriate RAN of the ITNTN. In particular, and similar to [14, 15], the work considers the usage scenario in which there exists a large number of users whose traffic cannot be entirely supported by the TN RAN, for example, in an urban area during a carnival event. Such a usage scenario necessitates the deployment of NTNs to decongest and support the TN RAN in providing radio access to the different users. Three service groups are considered: the data-intensive feMBB, the delay-sensitive euRLLC, and the mobile LDHMC service groups. The UE in this integrated network is regarded as a multi-radio terminal that can access either the terrestrial access network or the space/airborne communication networks, including the SatComs, HAPs, and LAPs. Without loss of generality, the NTN access nodes (ANs) are assumed to be regenerative, and users can connect to them directly.

The UARA problem is formulated as a multi-objective optimisation problem (MOOP), maximising the total network data rate while simultaneously prioritising large coverage NTNs over the TNs for service provisioning of the mobile LDHMC service group to minimise mobility-induced handoff probability. The MOOP is constrained to a limited resource budget and user QoS requirements. Moreover, given that denial of service to the euRLLC service group may result in catastrophic events, the optimisation problem is priority-aware, such that service provisioning of this service group over others can be prioritised. However, the priority can also be based on other factors, such as the use case that yields more revenue to the operator. Besides, since long propagation delays characterise the SatComs ANs, the problem limits access of the euRLLC users to these ANs. The MOOP is simplified and transformed into a weighted sum single-objective optimisation problem (SOOP). However, the SOOP is combinatorial, making it NP-hard, and thus, it is exponentially complex and mathematically intractable to obtain its optimum solution.

The complexity of the SOOP is reduced by decomposing it into two sub-problems: i) the user association sub-problem that associates users to appropriate ANs and further allocates them the minimum resources required to meet their QoS requirements, ii) the resource distribution phase that allocates the unallocated resources, if any, after the user association phase. The resource distribution phase is carried out to further improve the total network data rate. However, this phase is optional since once a user receives enough resources to satisfy its QoS requirements, allocating more resources may translate into spending unnecessary power [104].

A service-aware greedy algorithm is proposed to solve the problem in the user association phase. Moreover, to demonstrate the relevance of differentiated service provisioning and consideration of the RANs' different capabilities and limitations in resource management of the ITNTN, the performance of the proposed service-aware algorithm is compared with the service-unaware algorithm. The service-unaware algorithm does not consider the: i) heterogeneity in user traffic types and ii) uniqueness in the capabilities and limitations of the ITNTN RANs.

3.2 System model

This section describes the deployment scenario, mobility model, channel model, signal quality model, and assumptions considered in this work. The notations used to define the problem are presented in Table 3.1.

3.2.1 Deployment scenario

A downlink transmission of an integrated communication network consisting of four RANs, namely, the MBS, LAP, HAP, and the LEO SatComs, as depicted in Fig. 3.1, is considered. An AN in the MBS RAN is indexed as $b \in \mathcal{B}$ while that in the LAP RAN is denoted as $l \in \mathcal{L}$. Similarly, a HAP AN is represented as $h \in \mathcal{H}$ while the SatComs AN is indexed as $s \in \mathcal{S}$. A RAN in the ITNTN is denoted by $j \in \{\mathcal{B}, \mathcal{L}, \mathcal{H}, \mathcal{S}\}$, while an AN in the j-th RAN is represented by n_j. Similar to [105, 106, 107, 108], this work is premised on the assumption that each UAV AN $n_j \in \{l, h\}$ is stationary or quasi-stationary with negligible mobility.

Table 3.1: Notations defined in Chapter 3.

Symbol	Description
b, l, h, s	MBS, LAP, HAP, SatComs AN
$\mathcal{B}, \mathcal{L}, \mathcal{H}, \mathcal{S}$	Set of ANs in the MBS, LAP, HAP, SatComs RAN
j, n_j	A RAN, AN in the j-th RAN
$\mathcal{U}$	The set of users in the ITNTN
$\upsilon, \mathcal{E}, \mathcal{R}, \mathcal{D}$	A use-case, feMBB, euRLLC, LDHMC use-case
$\mathcal{U}_{\mathcal{E}}, \mathcal{U}_{\mathcal{R}}, \mathcal{U}_{\mathcal{D}}$	Set of users demanding $\mathcal{E}, \mathcal{R}$, and $\mathcal{D}$, respectively
$u, u_{\mathcal{E}}, u_{\mathcal{R}}, u_{\mathcal{D}}$	User, An feMBB, euRLLC, LDHMC user
$\mathcal{W}_j$	Set of basic bandwidth unit (BBU) owned by RAN j
w_j	A BBU owned by RAN j
$\mathcal{T}_{w_j}, \Phi_{n_j}$	Bandwidth of a BBU w_j, bandwidth of an AN n_j
$\mathcal{N}$	Set of all ANs in the ITNTN
$z_{n_j}, R_{n_j}, (x_{n_j}, y_{n_j})$	Altitude, cell radius, ground coordinates of n_j
(x_u, y_u)	User u coordinates
$d_{n_j,u}, \theta_{n_j,u}$	Distance, elevation angle from user u to AN n_j
h_{n_j}, τ_{n_j}	MBS height, loss due to shadow fading
$PL_{n_j,u,w_j}, \Gamma_{n_j,u,w_j}$ $\mathcal{C}_{n_j,u,w_j}$	Path loss, channel gain, data rate, of a user u using BBU w_j of AN n_j
$\gamma_{n_j,u_q,w_j}, P_{n_j,u_q,w_j}$	SINR, transmit power of a user u_q using BBU w_j of AN n_j
$f_{n_j,w_j}, \beta_{n_j,u_q,w_j}$	Carrier frequency, small-scale fast fading
$Prob^{LoS}_{n_j,u}, Prob^{NLoS}_{n_j,u}$	LoS probability, NLoS probability
x, y	Environmental constants used for UAV path loss model
$PL^{LoS}_{n_j,u,w_j}, PL^{NLoS}_{n_j,u,w_j}$	LoS path loss, NLoS path loss
$\eta_{LoS}, \ \eta_{NLoS}$	Additional loss in a UAV LoS, NLoS propagation
CL, PL^k, PL^e, PL^y	Loss due to clutter, atmospheric gases, scintillation, building entry.
$\mu_{n_j,u}, \omega_{n_j,u,w_j}, \pi_{n_j,u}, nb^{u_\upsilon}_{n_j}$	User association variable, resource allocation variable, coverage index, minimum required number of BBUs
$\delta_1, \delta_2, \delta$	Normalisation factors
$\mathcal{C}^{\upsilon}_{min}, R_{max}$	Service group υ minimum data rate, the largest possible cell radius in the ITNTN
$\rho_{u_\upsilon}, \alpha$	User priority factor, objective function trade-off factor
$\mathcal{U}_{served}$	A set of served users
$\mathcal{U}_{associated}$	A set of users for which $\mu_{n_j,u} = 1$

Immobility of UAVs is assumed to avoid disconnections due to the UAV AN moving out of coverage of already connected users, some of whom could be mission-critical. Consequently,

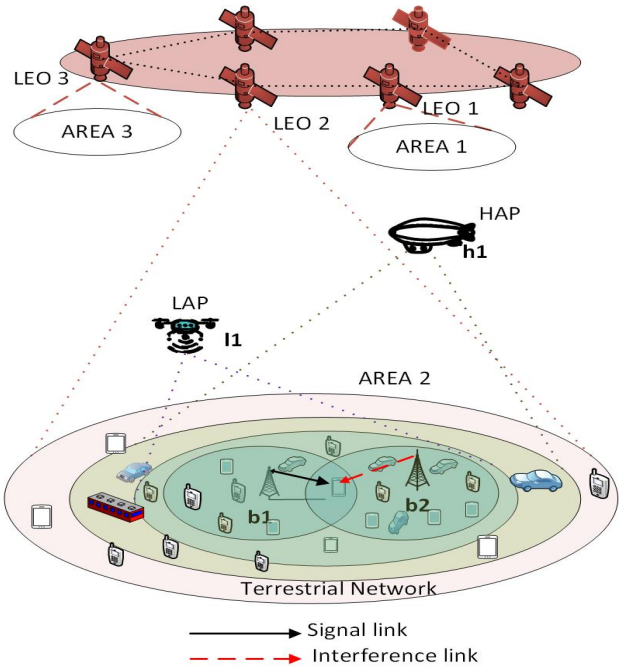

Figure 3.1: System model.

we assume to use the rotary-wing LAPs and balloon or airship HAPs that can remain quasi-stationary [23, 47]. Moreover, we assume that the placement of the UAV ANs has already been optimised to cater to the usage scenario in which there is a large number of users, say in an urban area, during a carnival event.

The system provides downlink communications to a set of users $\mathcal{U} = \{1, 2, 3, \ldots, |\mathcal{U}|\}$ and supports three use-cases namely: feMBB, euRLLC, and LDHMC, denoted by $\mathcal{E}$, $\mathcal{R}$, and $\mathcal{D}$ respectively, such that $v \in \{\mathcal{E}, \mathcal{R}, \mathcal{D}\}$. Users demanding use-cases $\mathcal{E}$, $\mathcal{R}$, and $\mathcal{D}$ are grouped in sets denoted by $\mathcal{U}_{\mathcal{E}}$, $\mathcal{U}_{\mathcal{R}}$, and $\mathcal{U}_{\mathcal{D}}$ respectively, such that, $u_{\mathcal{E}} \in \mathcal{U}_{\mathcal{E}}$, $u_{\mathcal{R}} \in \mathcal{U}_{\mathcal{R}}$, $u_{\mathcal{D}} \in \mathcal{U}_{\mathcal{D}}$, $\mathcal{U} = \mathcal{U}_{\mathcal{E}} \cup \mathcal{U}_{\mathcal{R}} \cup \mathcal{U}_{\mathcal{D}}$ and $\mathcal{U}_{\mathcal{E}} \cap \mathcal{U}_{\mathcal{R}} \cap \mathcal{U}_{\mathcal{D}} = \emptyset$. Without loss of generality, the $\mathcal{U}_{\mathcal{E}}$ and $\mathcal{U}_{\mathcal{R}}$ users are assumed to be static while the $\mathcal{U}_{\mathcal{D}}$ users are mobile. An example of a static use-case belonging to the $\mathcal{U}_{\mathcal{R}}$ service group is remote surgery within a hospital or private clinic in the considered urban area. Also, a user $u \in \mathcal{U}$ is assumed to be embedded

with multiple RAN interfaces and thus can access any of the available RAN $j \in \{\mathcal{B}, \mathcal{L}, \mathcal{H}, \mathcal{S}\}$ within its coverage.

Since the different RANs in the ITNTN may have different multiple access schemes such as OFDMA, TDMA, and FDMA, the BBU is used to represent the unit of radio resources as was done in [66]. Therefore, no matter what access technique is used, the system capacity is represented in terms of bandwidth. Furthermore, spatial multiplexing involving multiple-users multiple-input single-output (MU-MISO) or multiple-users multiple-input multiple-output (MU-MIMO) is out of the scope of this work and can be considered in future work. Therefore, as was done by [35], the AN and UE are both considered to have a single antenna, with the AN transmitting data via different BBUs to the intended connected users. Similar to [42], this work assumes shared spectrum mode, such that all ANs that belong to the same RAN j own the same set $\mathcal{W}_j$ of BBUs. A BBU $w_j \in \mathcal{W}_j$ has a bandwidth denoted by $\mathcal{T}_{w_j}$, while the bandwidth of an AN $n_j \in \mathcal{N}$ where $\mathcal{N} = \{\mathcal{B} \cup \mathcal{L} \cup \mathcal{H} \cup \mathcal{S}\}$ is represented as Φ_{n_j}.

Furthermore, as was done by [19], we make the following assumptions: i) A user $u \in \mathcal{U}$ can associate with at most one AN. ii) For simplicity, the different RANs use frequencies sparsely separated from each other, thus have no cross-tier interference. iii) Intra-cell interference on the downlink between users associated with the same AN is negligible, as it can be effectively controlled through multiple access techniques. iv) Co-tier interference exists, where a user receives signals from different ANs in the same RAN. This interference is added to the thermal noise in the SINR expression.

The system model used for the LEO SatComs RAN is adopted from [20]. A LEO satellite follows a specific pattern in which it periodically serves one area followed by another. Consequently, in this work, we assume that each non-overlapping area depicted in Fig. 3.1 is served by one LEO satellite for a given time. Hence, a user in a given location can access only one satellite at any given time. As an illustration, let us consider each LEO satellite's view time of any given area to be t. Then if LEO 2 starts to view area 2 at time t_1, this view continues until a time $t_1 + t$, after which service provisioning of area 2 is handed over to LEO 1, which views from $t_1 + t$ until $t_1 + 2t$. Handover from one satellite to another is assumed to be managed by the Network Control Center [20]. This handover process is out of scope and thus shall not be considered in this work. As the entire considered terrestrial area is under coverage by a single satellite during its service period, the satellite guarantees seamless coverage of the terrestrial RAN, irrespective of its mobility. Moreover, in practice, thousands of LEO satellites are deployed, for example, in the Starlink project, implying that a particular area can be covered by multiple LEO satellites simultaneously [109, 18]. Therefore, the mobility model of the satellite shall not be considered in this work.

3.2.2 User mobility model

Due to its simplicity and analytical tractability, the random walk mobility model [110] is used to imitate the LDHMC users' movement patterns. In each new transmission interval t, a user $u_{\mathcal{D}} \in \mathcal{U}_{\mathcal{D}}$ chooses a direction $\theta^t_{u_{\mathcal{D}}} \in [0 \;\; 2\pi]$ that is randomly and uniformly distributed. In the same manner, the user's speed $V^t_{u_{\mathcal{D}}} \in [V_{min} \;\; V_{max}]$ is randomly assigned following a uniform distribution, with V_{min} and V_{max} being the minimum and maximum velocity respectively,

that a user can have. Considering the user's location in time interval t as $(x_{u_{\mathcal{D}}}(t), y_{u_{\mathcal{D}}}(t))$, then the location $(x_{u_{\mathcal{D}}}(t+1), y_{u_{\mathcal{D}}}(t+1))$ in interval $t+1$ is given by

$$\begin{aligned} x_{u_{\mathcal{D}}}(t+1) &= x_{u_{\mathcal{D}}}(t) + \frac{V^t_{u_{\mathcal{D}}}}{V_{max}} \times D_{max} \times \cos\theta^t_{u_{\mathcal{D}}}, \\ y_{u_{\mathcal{D}}}(t+1) &= y_{u_{\mathcal{D}}}(t) + \frac{V^t_{u_{\mathcal{D}}}}{V_{max}} \times D_{max} \times \sin\theta^t_{u_{\mathcal{D}}}, \end{aligned} \tag{3.1}$$

where D_{max} is the maximum distance that can be moved by a user in a given flight interval. We consider LDHMC users to move within the LEO satellite coverage area, assumed to be 5 km, such that they are reflected off the boundary of the circular region.

3.2.3 Channel model

The ground location of any AN $n_j \in \{\mathcal{B} \cup \mathcal{L} \cup \mathcal{H} \cup \mathcal{S}\}$ is represented by $g_{n_j} = \{[x_{n_j}, y_{n_j}]^T \in \mathbb{R}^2\}$. In this case, for the NTN ANs, g_{n_j} is their projection on the ground. On the other hand, the coordinate of a user $u \in \mathcal{U}$ is given by $g_u = \{[x_u, y_u]^T \in \mathbb{R}^2 | u \in \mathcal{U}\}$. Consequently, the distance $d_{n_j,u}$ from an AN $n_j \in \{\mathcal{B} \cup \mathcal{L} \cup \mathcal{H} \cup \mathcal{S}\}$ to a user u can be calculated using

$$d_{n_j,u} = \sqrt{\|g_u - g_{n_j}\|_2^2 + z_{n_j}^2} \quad \forall j \in \{\mathcal{B}, \mathcal{L}, \mathcal{H}, \mathcal{S}\}, \ \forall u \in \mathcal{U}, \tag{3.2}$$

where z_{n_j} is the height of the AN and $\|.\|_2$ is the 2-norm operator. Path loss modelling is divided into three categories: i) MBS TN, ii) UAV, i.e., HAPs and LAPs, and iii) SatComs.

3.2.3.1 MBS terrestrial network path loss model

The path loss of a user $u \in \mathcal{U}$ using a BBU $w_j \in \mathcal{W}_j | j \in \mathcal{B}$ to communicate with an urban MBS $n_j \in \mathcal{B}$ that is located a distance $d_{n_j,u}$ metres away is given by [111]

$$PL_{n_j,u,w_j} = 40(1 - 4 \times 10^{-3} h_{n_j}) \log_{10}\left(\frac{d_{n_j,u}}{1000}\right) - 18 \log_{10} h_{n_j} + 21 \log_{10} f_{n_j,w_j} + 80 + \tau_{n_j,u}$$
$$\forall\, j \in \mathcal{B}, \quad \forall\, i \in \mathcal{U}. \tag{3.3}$$

The term h_{n_j} represents the MBS height in metres, f_{n_j,w_j} is the carrier frequency in MHz, and $\tau_{n_j,u}$ is the path loss due to shadow fading, assumed to be a Gaussian random variable with zero mean and σ standard deviation in dB. $\tau_{n_j,u}$ can be expressed as $\tau_{n_j,u} = \log_{10}(F_{n_j,u})$ where $F_{n_j,u}$ is the log-normal shadow fading path loss between the user u and AN n_j [111].

3.2.3.2 UAV path loss model

The path loss from a UAV AN $n_j \in \{\mathcal{L} \cup \mathcal{H}\}$ to a user $u \in \mathcal{U}$ is modelled according to [112]. In this model, the probability that a user u has a LoS link from a UAV AN $n_j \in \{\mathcal{L} \cup \mathcal{H}\}$ is given by

$$Prob^{LoS}_{n_j,u} = \frac{1}{1 + x \exp(-y(\theta_{n_j,u} - x))} \quad \forall n_j \in \{\mathcal{L} \cup \mathcal{H}\}. \tag{3.4}$$

The constants x and y are dependent on the environment while the elevation angle $\theta_{n_j,u}$ is given by $\frac{180}{\pi} \arctan(\frac{z_{n_j}}{\|g_u - g_{n_j}\|_2})$. The signal from the UAV AN propagates through free space until it reaches the environment on earth, where it undergoes additional loss due to shadowing, scattering, and reflections caused by buildings, foliage, etc. Consequently, the

path loss from the UAV AN $n_j \in \{\mathcal{L} \cup \mathcal{H}\}$ and a user u located at distance $d_{_{n_j,u}}$ is given by

$$PL_{_{n_j,u,w_j}} = \begin{cases} PL^{LoS}_{_{n_j,u,w_j}} = 20\log_{10} d_{_{n_j,u}} + 20\log_{10} f_{_{n_j,w_j}} \\ -27.55 + \eta_{LoS}\ , \qquad \text{LoS scenario} \\ \\ PL^{NLoS}_{_{n_j,u,w_j}} = 20\log_{10} d_{_{n_j,u}} + 20\log_{10} f_{_{n_j,w_j}} \\ -27.55 + \eta_{NLoS} \quad \text{NLoS scenario,} \end{cases} \tag{3.5}$$

where $d_{_{n_j,u}}$ is the distance in metres computed using (3.2), $f_{_{n_j,w_j}}$ is carrier frequency in MHz, and η_{LoS} or η_{NLoS} is the additional loss experienced in LoS or NLoS propagation respectively. The additional loss η_{LoS} or η_{NLoS} has a Gaussian distribution [112]. The equivalent path loss is then given by [71]

$$PL^{equiv}_{n_j,u,w_j} = Prob^{LoS}_{n_j,u} * PL^{LoS}_{_{n_j,u,w_j}} + Prob^{NLoS}_{n_j,u} * PL^{NLoS}_{_{n_j,u,w_j}}, \tag{3.6}$$

where $Prob^{NLoS}_{n_j,u} = 1 - Prob^{LoS}_{n_j,u}$ is the probability that a user experiences a NLoS link.

3.2.3.3 SatComs path loss model

Assuming clear sky conditions, the path loss between an AN $n_j \in \{\mathcal{S}\}$ and a user u at a distance $d_{_{n_j,u}}$ from the node, is given by [1]

$$\begin{aligned} PL_{n_j,u,w_j} = 20\log_{10} d_{_{n_j,u}} \ + \ 20\log_{10} f_{_{n_j,w_j}} \ - \ 27.55 \ + \ \tau_{n_j} \\ + CL \ + \ PL^k \ + \ PL^e \ + \ PL^y, \ \ \forall\, n_j \in \mathcal{S}. \end{aligned} \tag{3.7}$$

The frequency f_{n_j,w_j} is in MHz, while the range $d_{n_j,u}$ in metres and can be determined using (3.2). On the other hand, τ_{n_j} in (3.7) depicts the loss due to shadow fading, while CL gives the clutter loss resulting from reflections and scattering caused by surrounding buildings and objects on the ground. τ_{n_j} and CL depend on whether the propagation is LoS or NLoS. The terms PL^k, PL^e, and PL^y represent attenuation due to atmospheric gases, ionospheric or tropospheric scintillation, and building entry loss. The equivalent path loss is determined using (3.6) whereby the LoS probability $P_{n_j,i}^{LoS}$ which depends on the elevation angle and UE environment, is obtained from Table 6.6.1-1 in [1].

3.2.4 Signal quality model

Using the results from the preceding sections 3.2.3.1 to 3.2.3.3, the linear channel gain due to large-scale fading effects of path loss and shadowing from an AN $n_j \in \mathcal{N}$ and user u, communicating via a BBU w_j is given by [111]

$$\Gamma_{n_j,u,w_j} = 10^{-\frac{PL_{n_j,u,w_j}}{10}}. \tag{3.8}$$

A question that can arise is how the ANs obtain the channel state information (CSI). In practice, for time division duplex systems, the ANs can exploit reciprocity between downlink and uplink channels to estimate the downlink channel [113, 114]. In comparison, for the frequency division duplex systems, weaker reciprocity often exists in the uplink and downlink frequencies [113, 114]. Consequently, the CSI at the ANs for these systems can be obtained as feedback from the UE [113, 114]. Several works in literature are dedicated to reducing the

amount of CSI feedback in the frequency division duplex systems [114, 115], but this is out of the scope of this work. The obtained CSI feedback from UEs suffers high latency for ANs at high altitudes, like the SatComs, hence, this CSI is usually outdated [116]. Therefore, for such RANs, CSI can be obtained using the widely used training data-based CSI estimation techniques [117, 118, 119]. However, due to the complexities involved in simulating the CSI feedback and estimation techniques, this work assumes that the large-scale CSI is available at the ANs as was done in [111, 19, 35, 86]. Therefore, the corresponding channel gain can be calculated using (3.8).

The SINR ratio experienced by the user u using BBU w_j of AN n_j is then determined using [35, 120]

$$\gamma_{n_j,u_q,w_j} = \begin{cases} \dfrac{P_{n_j,u_q,w_j}\ \Gamma_{n_j,u_q,w_j}}{\sigma^2 \quad + \sum\limits_{\substack{f_j \in \mathcal{N} \\ f_j \neq n_j}} P_{f_j,u_q,w_j}\ \Gamma_{f_j,u_q,w_j}} & \forall u_q \in \{\mathcal{U}_\mathcal{E} \cup \mathcal{U}_\mathcal{R}\},\ \forall j \in \{\mathcal{B},\mathcal{L},\mathcal{H},\mathcal{S}\} \text{ static user} \\ \dfrac{P_{n_j,u_q,w_j}\ \Gamma_{n_j,u_q,w_j}|\beta_{n_j,u_q,w_j}|^2}{\sigma^2 \quad + \sum\limits_{\substack{f_j \in \mathcal{N} \\ f_j \neq n_j}} P_{f_j,u_q,w_j}\ \Gamma_{f_j,u_q,w_j}\ |\beta_{f_j,u_q,w_j}|^2} & \forall u_q \in \mathcal{U}_\mathcal{D},\ \forall j \in \{\mathcal{B},\mathcal{L},\mathcal{H},\mathcal{S}\} \text{ mobile user.} \end{cases} \tag{3.9}$$

The terms β_{n_j,u_q,w_j} and β_{f_j,u_q,w_j} denote the small-scale fast fading component that accounts for the mobility of a user and is assumed to be independent and identically distributed (i.i.d.) as $\mathcal{CN}(0,1)$ [121]. P_{n_j,u_q,w_j} is the transmit power from an AN n_j to a user u_q using BBU w_j while P_{f_j,u_q,w_j} depicts the co-tier interference from any other AN f_j in the j-th RAN reaching the same user u_q. Like [122], the interference calculation is based on the worst-case scenario, in which all ANs are transmitting at any given instant. This is a reasonable assumption

since this work assumes a usage scenario involving many users, thus, it is highly likely that all ANs may have data for transmission.

Similar to [123], [124], and [125], and in a bid to reduce complexity, this chapter and corresponding solutions in Chapters 4 and 5 shall not optimise power allocation. Therefore, the transmit power P_{n_j,u_q,w_j} in these chapters is assumed to be fixed and uniformly allocated to all ANs' BBUs. The power P_{n_j,u_q,w_j} is given as $P_{n_j}^{thres}/|\mathcal{W}_j|$, where $P_{n_j}^{thres}$ is the maximum available power at the AN n_j and $|.|$ represents the cardinality of the set. Power optimisation is considered in Chapter 6 to ensure an energy-efficient network.

The maximum data rate that can be achieved by a user $u \in \mathcal{U}$ on the BBU w_j of AN n_j is then given by the Shannon capacity as

$$\mathcal{C}_{n_j,u,w_j} = \mathcal{T}_{w_j} \log_2(1 + \gamma_{n_j,u,w_j}), \tag{3.10}$$

where $\mathcal{T}_{w_j}$ is the bandwidth for BBU $w_j \in \mathcal{W}_j$.

3.2.5 Access association and resource allocation

In this work, a user can associate with at most one AN of the ITNTN within coverage. Hence, a binary decision variable $\mu_{n_j,u} \in \{0,1\}$ is defined to specify whether the user $u \in \mathcal{U}$ is associated with the AN $n_j \in \mathcal{N}$ of the j-th RAN. $\mu_{n_j,u} \in \{0,1\}$ is defined as

$$\mu_{n_j,u} = \begin{cases} 1, & \text{if user } u \text{ is associated with AN } n_j \\ 0, & \text{otherwise.} \end{cases} \tag{3.11}$$

Moreover, in the scenario depicted by Fig. 3.1, a user $u \in \mathcal{U}$ can only associate with ANs in whose coverage the user lies. Therefore, we define a binary index $\pi_{n_j,u}$ that indicates whether a user u is within AN n_j's coverage. If the distance between a user u's location (x_u, y_u) and the ground location of the AN n_j (x_{n_j}, y_{n_j}) is less than the AN's cell radius R_{n_j}, then $\pi_{n_j,u} = 1$, otherwise, $\pi_{n_j,u} = 0$, as illustrated by

$$\pi_{n_j,u} = \begin{cases} 1, & if \ \sqrt{(x_u - x_{n_j})^2 + (y_u - y_{n_j})^2} \leqslant R_{n_j} \\ 0, & \text{otherwise.} \end{cases} \tag{3.12}$$

Also, a binary resource allocation decision variable $\omega_{n_j,u,w_j} \in \{0, 1\}$ is defined as

$$\omega_{n_j,u,w_j} = \begin{cases} 1, & \text{if BBU } w_j \text{ of AN } n_j \text{ is allocated to the user } u \\ 0, & \text{otherwise,} \end{cases} \tag{3.13}$$

to specify whether the BBU $w_j \in \mathcal{W}_j$ of AN n_j is allocated to the user u.

Therefore, for a user to be served by at most one AN that is within coverage, the following conditions must be satisfied:

$$\mu_{n_j,u} \leq \pi_{n_j,u}, \quad \forall \ n_j \in \mathcal{N}, \quad \forall \ u \in \mathcal{U} \tag{3.14}$$

$$\sum_{n_j \in \{\mathcal{B} \ \cup \ \mathcal{L} \ \cup \ \mathcal{H}\}} \pi_{n_j,u} \ \mu_{n_j,u} \ \omega_{n_j,u,w_j} \leqslant 1, \quad \forall \ u_{\mathcal{R}} \in \mathcal{U}_{\mathcal{R}} \tag{3.15}$$

$$\sum_{n_j \in \{\mathcal{S}\}} \pi_{n_j,u} \ \mu_{n_j,u} \ \omega_{n_j,u,w_j} = 0, \quad \forall \ u_{\mathcal{R}} \in \mathcal{U}_{\mathcal{R}} \tag{3.16}$$

$$\sum_{n_j \in \mathcal{N}} \pi_{n_j,u}\ \mu_{n_j,u}\ \omega_{n_j,u,w_j} \leqslant 1, \quad \forall\ u_{\mathcal{D}} \in \mathcal{U}_{\mathcal{D}},\ u_{\mathcal{E}} \in \mathcal{U}_{\mathcal{E}} \tag{3.17}$$

(3.14) allows a user to associate with ANs in whose coverage the user lies. In constraint (3.15), the mission-critical users $\mathcal{U}_{\mathcal{R}}$ can be served by at most one AN of either the TN, LAP, or HAP RANs. Since satellite communication is constrained with long propagation delays, (3.16) ensures that the $\mathcal{U}_{\mathcal{R}}$ users are not served by the satellite RAN. Constraint (3.17), on the other hand, allows a user belonging to either $\mathcal{U}_{\mathcal{D}}$ or $\mathcal{U}_{\mathcal{E}}$, to access at most one of any of the available ANs. To mitigate the intra-cell interference between users associated with the same AN n_j, we assume that for each AN, the BBU w_j can be used by at most one user and thus define the constraint

$$\sum_{u \in \mathcal{U}} \pi_{n_j,u}\ \mu_{n_j,u}\ \omega_{n_j,u,w_j} \leqslant 1, \quad \forall\ n_j \in \mathcal{N}, \quad \forall w_j \in \mathcal{W}_j. \tag{3.18}$$

3.2.6 Downlink data rate

The maximum data rate $\mathcal{C}_{n_j,u,w_j}$ that can be achieved by a user $u \in \mathcal{U}$ associated with AN n_j and using BBU w_j was defined by (3.10). Therefore, the total network sum rate is then given by

$$\Omega = \sum_{n_j \in \mathcal{N}} \sum_{u \in \mathcal{U}} \sum_{w_j \in \mathcal{W}_j} \rho_{u_\upsilon}\ \mu_{n_j,u}\ \omega_{n_j,u,w_j}\ \mathcal{C}_{n_j,u,w_j}, \tag{3.19}$$

where $\rho_{u_\upsilon} \in [0,1]$ is a weighting factor for a user $u \in \mathcal{U}$ demanding a given service belonging to service group $\upsilon \in \{\mathcal{E}, \mathcal{R}, \mathcal{D}\}$. ρ_{u_υ} prioritises service provisioning of users based on the service they demand. This work prioritises the service group $\mathcal{R}$ over $\mathcal{D}$ and $\mathcal{E}$, given that denial of service to the $\mathcal{U}_{\mathcal{R}}$ users could result in catastrophic events.

In determining to allocate a user $u \in \mathcal{U}$ resources of AN n_j, the node's radio resource capacity must not be exceeded, hence:

$$\sum_{u \in \mathcal{U}} \sum_{w_j \in \mathcal{W}_j} \pi_{n_j,u}\ \mu_{n_j,u}\ \omega_{n_j,u,w_j}\ \mathcal{T}_{w_j} \leq \Phi_{n_j}, \quad \forall\ n_j \in \mathcal{N}, \tag{3.20}$$

where Φ_{n_j} is n_j's total bandwidth. Moreover, for any served user belonging to the service group $\upsilon \in \{\mathcal{E}, \mathcal{R}, \mathcal{D}\}$, its minimum requested data rate $\mathcal{C}^{\upsilon}_{min}$ must be guaranteed. Thus we define the constraint:

$$\sum_{n_j \in \mathcal{N}} \sum_{w_j \in \mathcal{W}_j} \pi_{n_j,u}\ \mu_{n_j,u}\ \omega_{n_j,u,w_j}\ \mathcal{C}_{n_j,u,w_j} \geqslant \mathcal{C}^{\upsilon}_{min}, \quad \forall\ u \in \mathcal{U}_{served}, \quad \forall\ \upsilon \in \{\mathcal{E}, \mathcal{R}, \mathcal{D}\}, \tag{3.21}$$

where $\mathcal{U}_{served}$ is the set of served users.

3.2.7 Handoff reduction

This work maximises the overall system data rate while minimising mobility-induced handoff probability. We define the probability of handoff as the ratio of the number of users that experienced a handoff to the total number of mobile users during a given transmission time interval (TTI). To minimise the probability of handoff, the handoff reduction function

$$\Lambda = \sum_{n_j \in \mathcal{N}} \sum_{u \in \mathcal{U}} \sum_{w_j \in \mathcal{W}_j} \rho_{u_\upsilon}\ \mu_{n_j,u}\ \omega_{n_j,u,w_j}\ \frac{R_{n_j}}{R_{max}}, \tag{3.22}$$

is maximised in each TTI. The term R_{max} in (3.22) represents the largest cell radius in the ITNTN while R_{n_j} is n_j's cell radius. A mobile user traverses several small cells during an

ongoing call. Hence, the smaller the ANs' cell radii, the more the number of handoffs due to user mobility. In order to limit the mobility-induced handoff, we introduce the handoff reduction ratio $(R_{n_j}/R_{max}) \in (0, 1]$ in (3.22) to prioritise the association of mobile users to ANs with the largest cell radius. In this way, a maximum value of the ratio (R_{n_j}/R_{max}) implies a reduced number of handoffs since the mobile user will be associated with an available AN having the largest cell radius in each TTI, ultimately reducing the probability of handoff.

3.3 Problem formulation

In this section, the UARA problem is formulated as a MOOP that maximises the total system data rate while at the same time minimising the probability of mobility-induced handoff. The probability of handoff is minimised by maximising the association of mobile users to ANs with a large cell radius. ρ_{u_v} in (3.19) and (3.22) can be used to prioritise the service group $\mathcal{R}$ users over other users. The MOOP is formulated as

$$\max_{(\mu,\ \omega)\ \in\ \Delta} \quad \{\Omega, \Lambda\}, \tag{3.23}$$

where Δ is the set consisting of all feasible UARA solutions satisfying the following constraints

$$\text{C1: } \mu_{_{n_j,u}} \leq \pi_{_{n_j,u}}, \quad \forall\ n_j \in \mathcal{N}, \quad \forall\ u \in \mathcal{U} \tag{3.23a}$$

$$\text{C2:} \sum_{n_j \in \{\mathcal{B} \cup \mathcal{L} \cup \mathcal{H}\}} \pi_{n_j,u}\ \mu_{n_j,u}\ \omega_{n_j,u,w_j} \leqslant 1, \quad \forall\ u_{\mathcal{R}} \in \mathcal{U}_{\mathcal{R}} \tag{3.23b}$$

$$\text{C3:} \sum_{n_j \in \{\mathcal{S}\}} \pi_{n_j,u}\ \mu_{n_j,u}\ \omega_{n_j,u,w_j} = 0, \quad \forall\ u_{\mathcal{R}} \in \mathcal{U}_{\mathcal{R}} \tag{3.23c}$$

$$\text{C4:} \sum_{n_j \in \mathcal{N}} \pi_{n_j,u}\ \mu_{n_j,u}\ \omega_{n_j,u,w_j} \leqslant 1, \ \forall\ u_{\mathcal{E}} \in \mathcal{U}_{\mathcal{E}}, \ \forall\ u_{\mathcal{D}} \in \mathcal{U}_{\mathcal{D}} \tag{3.23d}$$

$$\text{C5:} \sum_{n_j \in \mathcal{N}} \sum_{w_j \in \mathcal{W}_j} \pi_{n_j,u}\ \mu_{n_j,u}\ \omega_{n_j,u,w_j} \mathcal{C}_{n_j,u,w_j} \geqslant \mathcal{C}^{\upsilon}_{min}, \ \forall u \in \mathcal{U}_{served}, \ \forall\ \upsilon \in \{\mathcal{E}, \mathcal{R}, \mathcal{D}\} \tag{3.23e}$$

$$\text{C6:} \sum_{u \in \mathcal{U}} \sum_{w_j \in \mathcal{W}_j} \pi_{n_j,u}\ \mu_{n_j,u}\ \omega_{n_j,u,w_j} \mathcal{T}_{w_j} \leq \Phi_{n_j}, \quad \forall\ n_j \in \mathcal{N} \tag{3.23f}$$

$$\text{C7:} \sum_{u \in \mathcal{U}} \pi_{n_j,u}\ \mu_{n_j,u}\ \omega_{n_j,u,w_j} \leqslant 1, \ \forall\ n_j \in \mathcal{N}, \ \forall w_j \in \mathcal{W}_j \tag{3.23g}$$

$$\text{C8: } \mu_{n_j,u} = \{0,1\},\ \omega_{n_j,u,w_j} = \{0,1\}, \ \forall\ j \in \{\mathcal{B}, \mathcal{H}, \mathcal{L}, \mathcal{S}\}, \ \forall\ n_j \in \mathcal{N}, \ \forall\ w_j \in \mathcal{W}_j, \ \forall\ u \in \mathcal{U}. \tag{3.23h}$$

In constraint C1, the user can only associate with an AN in whose coverage the user lies. In contrast, the constraints C2, C3, and C4 allow a user to be served by, at most, one AN that can meet the QoS requirements of the user. C5 ensures that a served user receives at least its minimum required data rate, while in C6, the maximum AN resource budget cannot be exceeded. In C7, a BBU can be allocated to at most one user, while C8 ensures that the UARA variables are binary.

To solve the MOOP in (3.23), the concept of Pareto optimality as defined in [126] is utilised, and this states that:

Definition 1: A point $\Delta_0 \in \Delta$ is said to be Pareto optimal if and only if there is no other point $\Delta_1 \in \Delta$ such that $\Omega(\Delta_1) \geq \Omega(\Delta_0)$, $\Lambda(\Delta_1) \geq \Lambda(\Delta_0)$ and at least one Ω or Λ has been strictly improved.

In simple terms, a point is Pareto Optimal if there is no other point that can improve both Ω and Λ simultaneously. The set of all Pareto optimal points gives an optimal trade-off between Ω and Λ by providing the maximum value of Ω for any given value of Λ and vice versa. The weighted sum method can provide a complete set of Pareto optimal solutions to the MOOP in (3.23). Therefore, similar to [127, 128, 129] and owing to its simplicity and low computational complexity, the weighted sum method is adopted to transform the MOOP in (3.23) into a SOOP, which is a weighted sum of the two objective functions as shown below:

$$\max_{\mu_{n_j,u},\, \omega_{n_j,u,w_j}} \quad \alpha\ \delta_1\ \Omega + (1-\alpha)\ \delta_2\ \Lambda \tag{3.24}$$

$$\text{s.t.} \quad (3.23a), (3.23b), (3.23c), (3.23d), (3.23e), (3.23f), (3.23g), (3.23h).$$

The terms δ_1 and δ_2 in (3.24) are normalisation factors associated with Ω and Λ, respectively, introduced to put the two functions on the same scale. Normalisation of Ω can be achieved by dividing it by the maximum possible data rate that can be achieved in the network. Therefore, δ_1 is given by

$$\delta_1 = \frac{1}{\sum_{n_j=1}^{|\mathcal{N}|} \sum_{w_j=1}^{|\mathcal{W}_j|} \max\ \mathcal{C}_{n_j,u,w_j}}. \tag{3.25}$$

On the other hand, the handoff reduction ratio $(R_{n_j}/R_{max}) \in (0, 1]$ in the term Λ defined in (3.22) makes the function Λ unitless. However, the summation of the term $\rho_{u_v}\ \mu_{n_j,u}\ \omega_{n_j,u,w_j}$ over all BBUs allocated to the different users connected to the different ANs as seen in (3.22)

leads to a value greater than 1. Therefore, to normalise this result, δ_2 is given by

$$\delta_2 = \frac{1}{|\mathcal{U}_{\mathcal{D}}|}. \tag{3.26}$$

α in (3.24) provides a trade-off between data rate maximisation and mobility-induced handoff minimisation for mobile users. This parameter is particularly useful since the ANs that maximise data rate may not necessarily minimise handoff, and hence is used to define the importance of the two objective functions. It is important to note that for static users, i.e., the euRLLC and feMBB service groups, α is one since these users do not experience mobility-induced handoff. On the other hand, when the values of α are varied in the range [0,1] for the mobile users, the set of all Pareto optimal points to the MOOP in (3.23) can be obtained [130]. However, in this work, we consider the priority of the mobile LDHMC service group to be handoff minimisation, and as such, we set α to 0 for these users. Nonetheless, the impact of α on data rate maximisation and handoff probability minimisation for mobile users is analysed in the next chapter.

3.4 SOOP simplification

The problem defined in (3.24) is combinatorial in the UARA variables, and as such, finding the optimum solution is exponentially complex and mathematically intractable. Similar to [39, 104, 131] and in a bid to reduce the problem complexity, the problem is subdivided into two phases: the user association phase solving sub-problem **P1** and the resource distribution phase that solves sub-problem **P2**.

In the user association phase, the resource allocation variables are fixed. However, it is essential to note that the number of BBUs allocated to a user cannot be set to any arbitrary value since the QoS constraint C5 in (3.23e) must be satisfied. Therefore, to ensure that the QoS constraint is not violated in the user association phase, the equation

$$nb_{n_j}^{u_\upsilon} = \left\lceil \frac{\mathcal{C}_{min}^{\upsilon}}{\mathcal{C}_{n_j,u,w_j}} \right\rceil, \ \forall \upsilon \in \{\mathcal{E}, \mathcal{R}, \mathcal{D}\}, \forall u \in \mathcal{U}_{associated}, \forall n_j \in \mathcal{N}, \tag{3.27}$$

must be satisfied for an associated user $u \in \mathcal{U}_{associated}$, where $\mathcal{U}_{associated}$ is the set of users for which $\mu_{n_j,u} = 1$.

We assume $\mathcal{C}_{min}^{\upsilon}$ to be the requested data rate of a user belonging to service group $\upsilon \in \{\mathcal{R}, \mathcal{D}, \mathcal{E}\}$. In (3.27), $nb_{n_j}^{u_\upsilon}$ represents the minimum number of BBUs that an AN n_j should allocate the user u to meet its data rate QoS, while $\lceil \cdot \rceil$ is the ceiling operator. Suffice it to note that since we are dealing with a scenario in which many users exist in the network, fixing the allocated BBUs to a minimum that meets a user's QoS requirement ensures fairness among users in the network as it avoids users experiencing good channels from using up all the resources in a bid to maximise the network data rate. Replacing C5 in (3.23e) by (3.27) fixes the number of BBUs that AN n_j allocates the user u (if the user is associated), and as such transforms the problem (3.24) into finding only the Boolean user association variables $\mu_{n_j,u}$.

The second phase then uses the known user association variables to distribute the remaining BBUs of each AN, thus increasing the users' data rate and consequently maximising the total network data rate. However, this phase is optional since allocating more

resources than the users need to meet their QoS requirements implies spending unnecessary power [104]. In this work, to keep the system model simple and mathematically tractable, we consider the ANs' channels flat.

3.4.1 User association phase

The equivalent utility function can be defined in terms of the minimum number of BBUs allocated to the users as:

$$\chi = \alpha\ \delta_1 \sum_{n_j \in \mathcal{N}} \sum_{u \in \mathcal{U}} \rho_{u_\upsilon}\ \mu_{n_j,u}\ nb_{n_j}^{u_\upsilon}\ \mathcal{C}_{n_j,u,w_j} \quad + \quad (1-\alpha)\ \delta_2 \sum_{n_j \in \mathcal{N}} \sum_{u \in \mathcal{U}} \rho_{u_\upsilon}\ \mu_{n_j,u}\ \frac{R_{n_j}}{R_{max}}. \tag{3.28}$$

$nb_{n_j}^{u_\upsilon}\ \mathcal{C}_{n_j,u,w_j}$ in (3.28) is a constant for a given user u associated to a given AN n_j, since $nb_{n_j}^{u_\upsilon}$ is a constant. The equivalent user association optimisation problem **P1** that maximises the utility function χ while ensuring that the user QoS is satisfied and the AN resource budget is not exceeded is illustrated below:

P1

$$\max_{\mu_{n_j,u}} \quad \chi \tag{3.29}$$

s.t.

C1: $\mu_{n_j,u} \leq \pi_{n_j,u}, \quad \forall\ n_j \in \mathcal{N}, \quad \forall\ u \in \mathcal{U}$

C2: $\sum_{n_j \in \{\mathcal{B}\ \cup\ \mathcal{L}\ \cup\ \mathcal{H}\}} \pi_{n_j,u}\ \mu_{n_j,u} \quad \leqslant \quad 1, \quad \forall\ u_{\mathcal{R}} \in \mathcal{U}_{\mathcal{R}}$

C3: $\sum_{n_j \in \{\mathcal{S}\}} \pi_{n_j,u}\ \mu_{n_j,u} \quad = \quad 0, \quad \forall\ u_{\mathcal{R}} \in \mathcal{U}_{\mathcal{R}}$

$$\text{C4:} \sum_{n_j \in \mathcal{N}} \pi_{n_j,u}\ \mu_{n_j,u} \quad \leqslant \quad 1, \quad \forall\ u_{\mathcal{D}} \in \mathcal{U}_{\mathcal{D}},\ u_{\mathcal{E}} \in \mathcal{U}_{\mathcal{E}}$$

$$\text{C5:}\ nb_{n_j}^{u_\upsilon} = \left\lceil \frac{\mathcal{C}_{min}^{\upsilon}}{\mathcal{C}_{n_j,u,w_j}} \right\rceil, \quad \forall\ \upsilon \in \{\mathcal{R}, \mathcal{E}, \mathcal{D}\}, \quad \forall u \in \mathcal{U}_{associated}$$

$$\text{C6:} \sum_{u \in \mathcal{U}} \pi_{n_j,u}\ \mu_{n_j,u}\ nb_{n_j}^{u_\upsilon}\ \mathcal{T}_{w_j} \leq \Phi_{n_j}, \quad \forall\ n_j \in \mathcal{N}$$

$$\text{C7:}\ \mu_{n_j,u} = \{0, 1\}, \quad \forall\ u \in \mathcal{U}\ \ \forall\ j \in \{\mathcal{B}, \mathcal{H}, \mathcal{L}, \mathcal{S}\}, \quad \forall\ n_j \in \mathcal{N}$$

The operator $\lceil \cdot \rceil$ in C5 of (3.29) ensures that a BBU is allocated to at most one user. The optimisation problem **P1** in (3.29) is a $(0, 1)$ integer linear programming (ILP) problem which is one of Karp's 21 NP-complete problems [132]. Exact algorithms such as branch and bound (BnB) exist that return a global optimal solution for such problems. However, these techniques require an exponential upper bound time complexity that varies in tandem with the network dimension. Consequently, in Section 3.5, we propose a heuristic service-aware greedy algorithm to problem **P1**, characterised by polynomial-time complexity.

3.4.2 BBU distribution phase

After the user association phase is completed, some ANs may still have extra BBUs that have not been allocated to the users. The essence of the resource distribution phase is to distribute these BBUs among the associated users to increase the total network data rate. Let $\mathcal{U}_{n_j}$ define the set of users associated by **P1** to the AN n_j, that is,

$$\mathcal{U}_{n_j} = \{u \mid \mu_{n_j,u} = 1\} \quad \forall n_j \in \mathcal{N}. \tag{3.30}$$

To maximise the total network data rate of the ITNTN, the following optimisation problem is defined at each AN n_j

P2

$$\max_{nb^{u}_{n_j}{}'} \quad \sum_{u \in \mathcal{U}_{n_j}} nb^{u}_{n_j} \, \mathcal{C}_{n_j,u,w_j} \tag{3.31}$$

s.t.

$$\text{C1: } \sum_{u \in \mathcal{U}_{n_j}} nb^{u}_{n_j} = Num^{BBU}_{n_j},$$

$$\text{C2: } nb^{u}_{n_j} = \overline{nb^{u}_{n_j}} + nb^{u}_{n_j}{}' \quad \forall u \in \mathcal{U}_{n_j},$$

$$\text{C3: } nb^{u}_{n_j}{}' \in \{1, 2, \ldots, (Num^{BBU}_{n_j} - 1)\}.$$

Note that the subscript υ on u in $nb^{u_\upsilon}_{n_j}$ has been dropped for brevity purposes. $\overline{nb^{u}_{n_j}}$ in (3.31) represents the number of already allocated BBUs to the user u by AN n_j satisfying the data rate QoS requirement. On the other hand, $nb^{u}_{n_j}{}'$ represents the number of BBUs that will be added to the user u after solving **P2**. Important to note is that **P2** is only solved when there exist unallocated BBUs at the AN after the association phase. Besides, this phase is optional as allocating more resources than required to satisfy user QoS requirements may translate into spending unnecessary power [104].

Problem **P2** can be convexified by letting the variables $nb^{u}_{n_j}{}'$ be continuous, and thus, the constraint C3 in (3.31) becomes $nb^{u}_{n_j}{}' \geqslant 0$. Since convex optimisation can be used to solve the classic water-filling problem, **P2** is then transformed into the water-filling structure given on page 245, example 5.2 of [133] by replacing the utility function ($nb^{u}_{n_j} \, \mathcal{C}_{n_j,u,w_j}$) with the

logarithmic function $\log\left((\overline{nb^{u}_{n_j}} + nb^{u}_{n_j}{}')\ \mathcal{C}_{n_j,u,w_j}\right)$. Therefore, rewriting **P2** in the equivalent water-filling structure yields:

P3

$$\min_{nb^{u}_{n_j}{}'} \quad \sum_{u\in\mathcal{U}_{n_j}} -\log\left((\overline{nb^{u}_{n_j}} + nb^{u}_{n_j}{}')\ \mathcal{C}_{n_j,u,w_j}\right) \tag{3.32}$$

s.t.

$$\text{C1: } \sum_{u\in\mathcal{U}_{n_j}} (\overline{nb^{u}_{n_j}} + nb^{u}_{n_j}{}') = Num^{BBU}_{n_j},$$

$$\text{C2: } nb^{u}_{n_j}{}' \geqslant 0.$$

Notice that in (3.32), the problem was transformed into a minimisation problem. This is because $\log(\cdot)$ is a concave function, and it can only be transformed into a convex function as $-\log(\cdot)$, and minimisation of a $-\log(\cdot)$ is equivalent to maximising $\log(\cdot)$. Problem **P3** is a convex optimisation problem we solve using CVXPY.

CVXPY is a Python-embedded modelling language for convex optimisation problems that automatically transforms a problem into a standard form and calls a solver to return the results. In the end, the optimal solution $nb^{u}_{n_j}{}'$ for user u is the solution to **P3** rounded to the closest integer value that is smaller than the solution produced by solving **P3**. Section 3.6.2 in the simulation results depicts the effect of distributing the unallocated BBUs on the total network data rate.

3.5 Novel service-aware greedy solution to problem P1

3.5.1 The proposed greedy algorithm

A service-aware greedy heuristic algorithm is developed to find a good, feasible solution with polynomial-time complexity for the UARA problem **P1**. Four factors are considered in the association process: i) the mission-critical service group $\mathcal{R}$ is prioritised, ii) users are prioritised depending on the number of ANs within their coverage, iii) a static user is associated with an available AN with the highest SINR, and iv) a mobile user is associated to an available AN with the broadest cell radius. Resource allocation is done concurrently with user association by ensuring that users are attached to ANs whose available number of BBUs, $Num_{n_j}^{BBU}$ is greater than the minimum number of BBUs $nb_{n_j}^{u_\upsilon}$ required by user u_υ belonging to service group $\upsilon \in \{\mathcal{R}, \mathcal{E}, \mathcal{D}\}$ as given in (3.27). The performance of the proposed service-aware algorithm is then compared with the service-unaware algorithm that does not consider the: i) heterogeneity in user traffic types and ii) uniqueness in the capabilities and limitations of the RANs.

The pseudo-code of the proposed service-aware greedy algorithm is given in Algorithm 1 and is based on the snapshot model [134]. Lines 3-8 of Algorithm 1 determine user u's path loss, channel gain, SINR, the achievable data rate on a single BBU w_j of AN n_j, and the required minimum number of BBUs and after that, store all ANs in whose coverage u lies in a set Cov^u. Line 9 sorts users in each service group to prioritise them according to the number of ANs within their coverage. Users in service group $\mathcal{R}$ are serviced in lines 11-31. Lines 32-46 associate and allocate resources to users in the $\mathcal{D}$ service group while prioritising access

to an AN with the largest cell radius. Users of service group $\mathcal{E}$ are provisioned through lines 47-49. Line 51 returns a list $Assoc^{u}_{n_j}$ containing the AN n_j serving user u, and the number of BBUs $nb^{u_v}_{n_j}$ allocated to the user. Fig. 3.2 illustrates the greedy algorithm process.

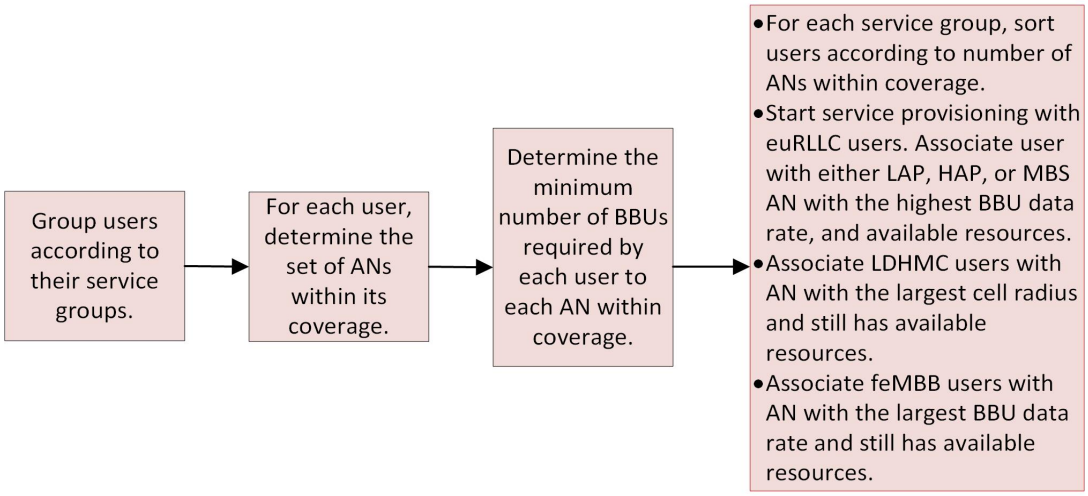

Figure 3.2: The greedy algorithm process.

3.5.2 Computational complexity of the greedy algorithm

The big Omicron (big-O) is employed to characterise the time complexity of all the solutions proposed in this thesis. The big-O is a mathematical notation that gives a measure of an algorithm's worst-case execution time or required memory in relation to the problem size. A detailed description of the big-O can be found in [135, 136].

The greedy algorithm first sorts the users according to the number of ANs within their coverage. The time complexity of this sorting procedure is $O(|\mathcal{U}| \log |\mathcal{U}|)$, where $|\mathcal{U}|$ represents the number of users in the ITNTN. The static users are associated with the appropriate AN based on maximum SINR, while the mobile ones consider the broadest cell radius. Consequently, each user must determine the SINR or cell radius of the

Algorithm 1 Service-Aware greedy user association and resource allocation algorithm

Input: f_{n_j}, $P_{n_j}^{thres}$, $Num_{n_j}^{BBU}$, z_{n_j}, $\mathcal{C}_{min}^{v}$, $\mathcal{T}_{w_j}$
Output: User association and resource allocation set, $Assoc_{n_j}^{u}$

procedure GREEDY USER ASSOCIATION AND RESOURCE ALLOCATION ALGORITHM
Initialise: $Assoc_{n_j}^{u} = \emptyset$
  for Each user $u \in \{\mathcal{U}_R, \mathcal{U}_E, \mathcal{U}_D\}$ **do**
    for Each AN $n_j \in \mathcal{N}$ **do**
      Calculate PL_{n_j,i,c_j}, Γ_{n_j,i,c_j}, γ_{n_j,u,w_j}, $\mathcal{C}_{n_j,u,w_j}$ and $nb_{n_j}^{u_v}$
      Add n_j to Cov^u if u is within n_j's coverage
    end for
  end for
  sort $\{\mathcal{U}_R, \mathcal{U}_E, \mathcal{U}_D\}$ according to $|Cov^u|$
  for Each user $u \in \{\mathcal{U}_R \cup \mathcal{U}_D \cup \mathcal{U}_E\}$ **do**
    if *user* $u \in \mathcal{U}_R$ **then**
      if $Cov^u == \emptyset$ **then**
        $\pi_{n_j,u}\mu_{n_j,u} = 0 \; \forall j \in \{\mathcal{B}, \mathcal{L}, \mathcal{H}, \mathcal{S}\}$
      else
        sort Cov^u according γ_{n_j,u,w_j}
        $\pi_{n_j,u}\mu_{n_j,u} = 0$
        for $n_j \in Cov^u$ **do**
          if $n_j \in \mathcal{S}$ **then**
            pass
          else
            if $Num_{n_j}^{BBU} < nb_{n_j}^{u_v}$ **then**
              pass
            else
              $\pi_{n_j,u}\mu_{n_j,u} = 1$
              Deduct $nb_{n_j}^{u_v}$ from $Num_{n_j}^{BBU}$
              Append $[u, n_j, nb_{n_j}^{u_v}]$ to $Assoc_{n_j}^{u}$
              break
            end if
          end if
        end for
      end if
    else if *user* $u \in \mathcal{U}_D$
      steps 12-14
      sort Cov^u according to cell radius
      $\pi_{n_j,u}\mu_{n_j,u} = 0$
      for $n_j \in Cov^u$ **do**
        if $Num_{n_j}^{BBU} < nb_{n_j}^{u_v}$ **then**
          pass
        else
          $\pi_{n_j,u}\mu_{n_j,u} = 1$
          Deduct $nb_{n_j}^{u_v}$ from $Num_{n_j}^{BBU}$
          Append $[u, n_j, nb_{n_j}^{u_v}]$ to $Assoc_{n_j}^{u}$
          break
        end if
      end for
    end if
    if $i \in \mathcal{U}_E$ **then**
      steps 12-17, 21-28, 29-31
    end if
  end for
  Return $Assoc_{n_j}^{u}$
end procedure

different ANs. The time complexity for this computation is of the order $O(|\mathcal{U}| \times |\mathcal{N}|)$ where $|\mathcal{N}|$ is the total number of ANs in the ITNTN. For each user, the SINR values or cell radius to the different ANs must be sorted such that if the AN with the highest SINR or broadest cell radius does not have sufficient resources to meet the user's QoS requirements, then the user is associated with the next best AN. The time complexity due to this sorting is $O(|\mathcal{N}| \log |\mathcal{N}| \times |\mathcal{U}|)$. Therefore, the overall complexity of the greedy algorithm is given as $O(|\mathcal{U}| \log |\mathcal{U}| + |\mathcal{U}| \times |\mathcal{N}| + |\mathcal{N}| \log |\mathcal{N}| \times |\mathcal{U}|)$ which can be reduced to $O(|\mathcal{U}| \times (\log |\mathcal{U}| + |\mathcal{N}| \log |\mathcal{N}|))$.

3.6 Results and performance evaluation

One of the leading research gaps highlighted in Chapter 2 was the need for RRM techniques for the ITNTN that consider the user QoS heterogeneity and the peculiarities faced by the different RANs in meeting these diverse user requirements. This section shows the significance of service-aware UARA in the ITNTN.

To evaluate the performance of the proposed service-aware greedy algorithm, we consider a circular radius of 4 km of an urban environment covered by the LEO satellite and the HAP. Within this region are 14 MBSs, and 3 LAPs, with each tier having a radius of 1 km and 2 km, respectively. Users and ANs are uniformly and randomly distributed. The parameters used in the simulation are given in Table 3.2 [19, 1, 111, 112].

The proposed service-aware algorithm is compared with the service-unaware algorithm, which associates users based on maximum SINR. Like the service-aware approach, the service-unaware approach prioritises users according to the number of ANs within their

Table 3.2: Simulation parameters and values.

Parameter	Value
$f_{n_\mathcal{B}}, f_{n_\mathcal{L}}, f_{n_\mathcal{H}}, f_{n_\mathcal{S}}$ (Frequencies)	[4, 2, 3, 5] GHz
$\mathcal{T}_{w_\mathcal{B}}, \mathcal{T}_{w_\mathcal{L}}, \mathcal{T}_{w_\mathcal{H}}, \mathcal{T}_{w_\mathcal{S}}$ (BBU bandwidth)	[0.18, 0.18, 1, 2] MHz
Number of BBUs for $[n_\mathcal{B}, n_\mathcal{L}, n_\mathcal{H}, n_\mathcal{S}]$	[50, 50, 100, 200]
$[P_{n_\mathcal{B}}^{thres}, P_{n_\mathcal{L}}^{thres}, P_{n_\mathcal{H}}^{thres}, P_{n_\mathcal{S}}^{thres}]$ (maximum power at ANs)	[40, 25, 100, 250] Watts
$x,\ y,\ \eta_{LoS},\ \eta_{NLoS}$	[10.39, 0.05, 1, 20]
Shadow fading $[\mathcal{B}, \mathcal{S}]$	[8, 4] dB
$[CL,\ PL^k,\ PL^y]$	[0, 0, 23 dB]
AN height $[z_{n_\mathcal{B}}, z_{n_\mathcal{L}}, z_{n_\mathcal{H}}, z_{n_\mathcal{S}}]$	[0.04, 2, 17, 600] km
Service group user ratio $[\lvert\mathcal{U}_\mathcal{E}\rvert : \lvert\mathcal{U}_\mathcal{R}\rvert : \lvert\mathcal{U}_\mathcal{D}\rvert]$	[0.6:0.3:0.1]
$\mathcal{C}_{min}^{\upsilon} \forall \upsilon \in [\mathcal{E}, \mathcal{R}, \mathcal{D}]$	[1000, 500, 1000] kbps
Noise spectral density	-174 dBm

coverage. However, it does not consider the heterogeneity in user QoS requirements and RAN capabilities in meeting these needs. Performance evaluation is based on three main metrics: the acceptance ratio (AR), the spectrum efficiency (SE), and the handoff probability. In this work, the user AR quantifies the ratio of served users to the total number of users in the network. On the other hand, the SE is the ratio of the overall system data rate to the total network bandwidth [137], while the probability of handoff is defined as the ratio of the number of users that experienced a handoff (and are thus served by another AN) to the total number of mobile users during a given TTI.

3.6.1 Comparison of service-aware versus service-unaware algorithms

In Fig. 3.3, the AR of mission-critical users is 1 for the service-aware scheme. On the other hand, the AR of mission-critical users is lower in the service-unaware algorithm and keeps reducing as the number of users increases. The 26% difference in performance arises

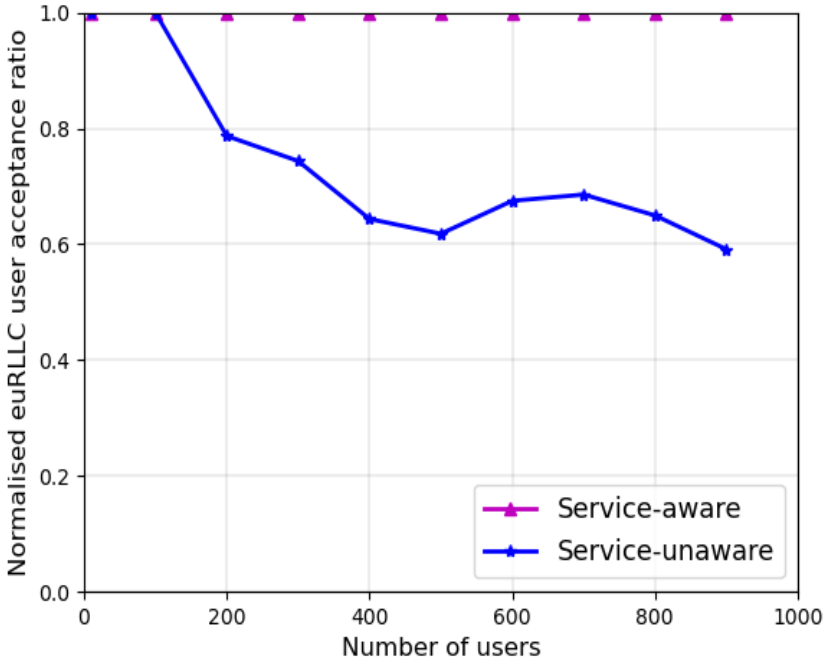

Figure 3.3: euRLLC AR; service-aware vs. service-unaware.

from the fact that the service-aware algorithm prioritises mission-critical users and associates them only with the RANs that meet their needs. In comparison, service-unaware does not distinguish users based on their QoS needs, nor does it consider the limitations of the different RANs in meeting these demands. This results in a reduced acceptance ratio of the $\mathcal{R}$ slice since these are not prioritised and are possibly associated with RANs that cannot meet their needs.

In Figs. 3.4 and 3.5, both algorithms have acceptance ratios of $\mathcal{E}$ and $\mathcal{D}$ at 100% for a smaller number of users when resources are still available. As the number of users increases, resources reduce, and hence the acceptance ratio decreases. The service-unaware algorithm performs better in this case since this did not prioritise mission-critical users. Therefore, slice $\mathcal{E}$ and $\mathcal{D}$ users were able to use up resources that are prioritised for slice $\mathcal{R}$ users in the service-aware algorithm. Moreover, as depicted by Fig. 3.6, the service-aware

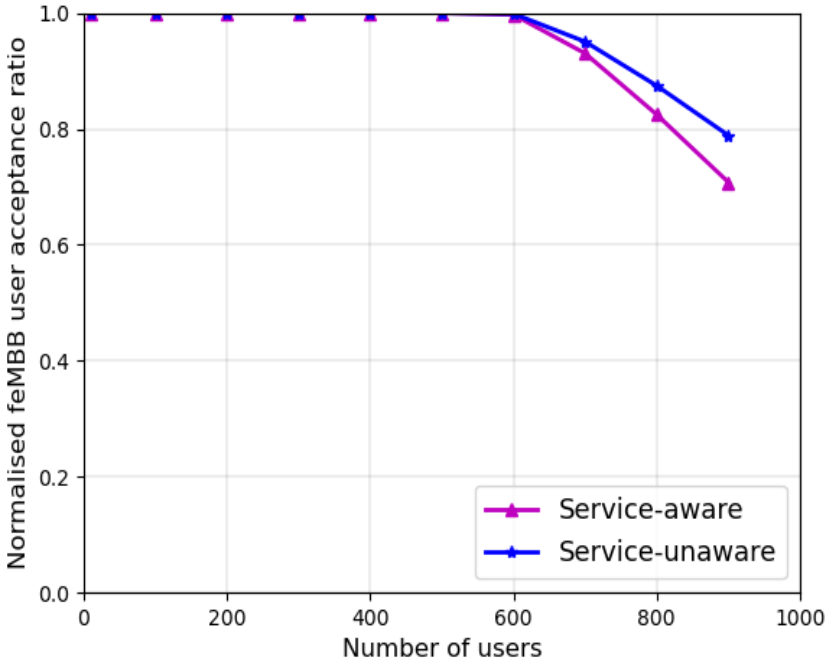

Figure 3.4: feMBB AR; service-aware vs. service-unaware.

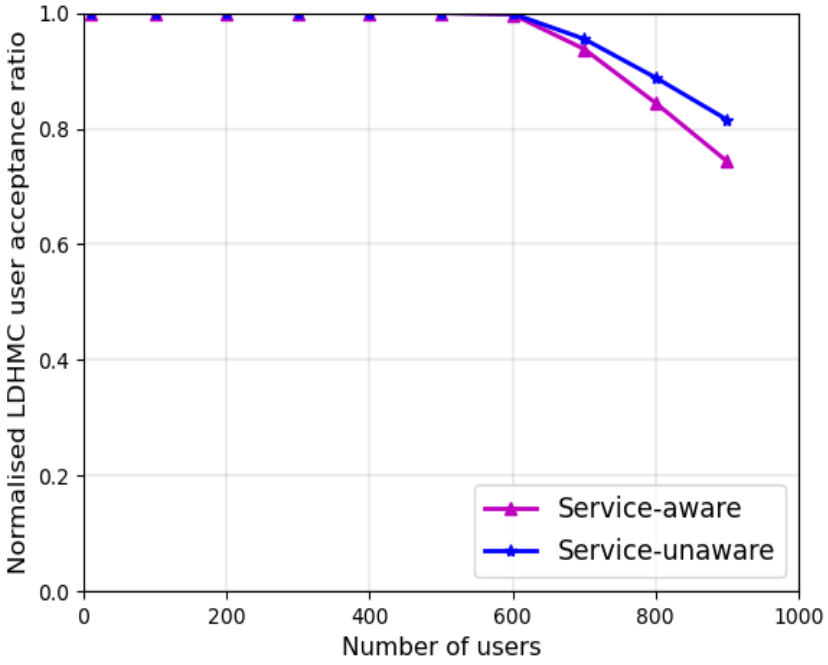

Figure 3.5: LDHMC AR; service-aware vs. service-unaware.

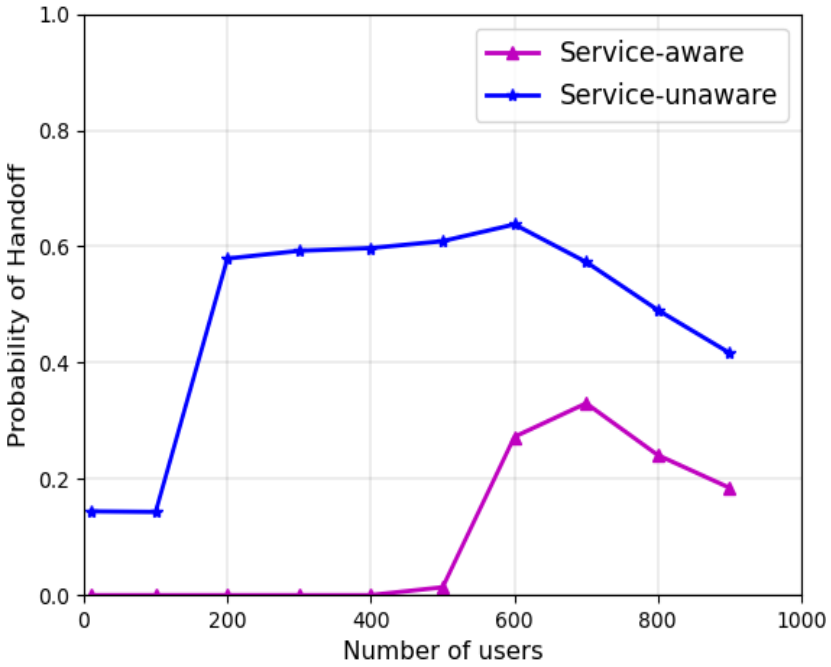

Figure 3.6: Probability of handoff; service-aware vs. service-unaware.

algorithm outperforms the service-unaware by 78% in terms of handoff probability. The service-aware algorithm prioritises using ANs with the broadest cell radius for access by mobile LDHMC users. It hence achieves a handoff probability of 0 up to 400 users. As the number of users increases beyond 400, the resources of the AN with the largest cell radius are depleted. Thus mobile users are forced to attach to ANs with smaller coverage, hence the rise in handoff probability for the service-aware algorithm. However, even at this point, the service-aware performs better as it still attaches the users to an AN with the broadest coverage among the available ANs. The worse performance of the service-unaware scheme is attributed to associating mobile users according to maximum SINR. Thus as the user moves, it keeps alternating between ANs depending on which has the maximum SINR. The handoff probability of both algorithms falls for a higher number of users beyond 700 since

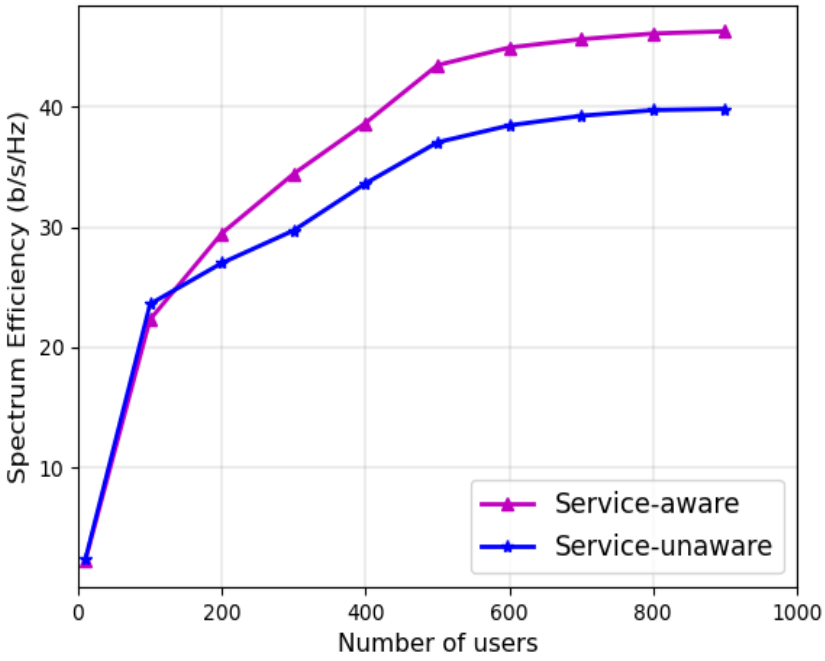

Figure 3.7: Spectrum efficiency; service-aware vs. service-unaware.

the number of served LDHMC users decreases as the number of users increases beyond what the network can sustain.

Figs. 3.7 and 3.8 show that even with the priorities subjected to the service-aware algorithm, its overall SE and user AR are better than the service-unaware algorithm. The average gain achieved by the service-aware algorithm over the service-unaware scheme is 12% and 9.8% in SE and user AR, respectively. Therefore, the service-aware algorithm prioritises mission-critical applications, whose rejection results in adverse consequences, prioritises the use of broader coverage NTNs for highly mobile users, thereby minimising the handoff probability, and at the same time, maximises the number of admitted users and the network SE.

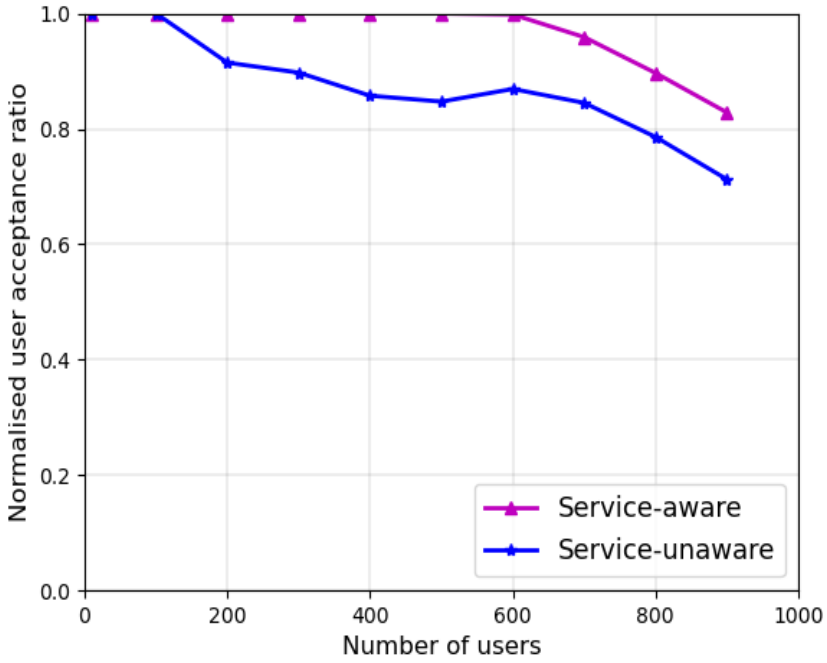

Figure 3.8: User acceptance ratio; service-aware vs. service-unaware.

3.6.2 Effect of the BBU distribution phase

Fig. 3.9 depicts the relationship between the user association and the BBU distribution phases. Since the user association phase allocates only the minimum required number of BBUs, it achieves a lower total network data rate. On the other hand, the BBU distribution phase not only allocates the minimum required BBUs during the association phase but also distributes any extra unallocated AN's BBUs according to the optimisation problem (3.32), thereby achieving a higher network data rate. As the number of users increases beyond what the available resources can support, both algorithms converge to a constant data rate. Moreover, even at this point of convergence, the BBU distribution phase slightly outperforms the user association phase since it ensures all BBUs of the AN are allocated to the users. In contrast, the latter can only allocate any unallocated BBUs if they meet an unassociated

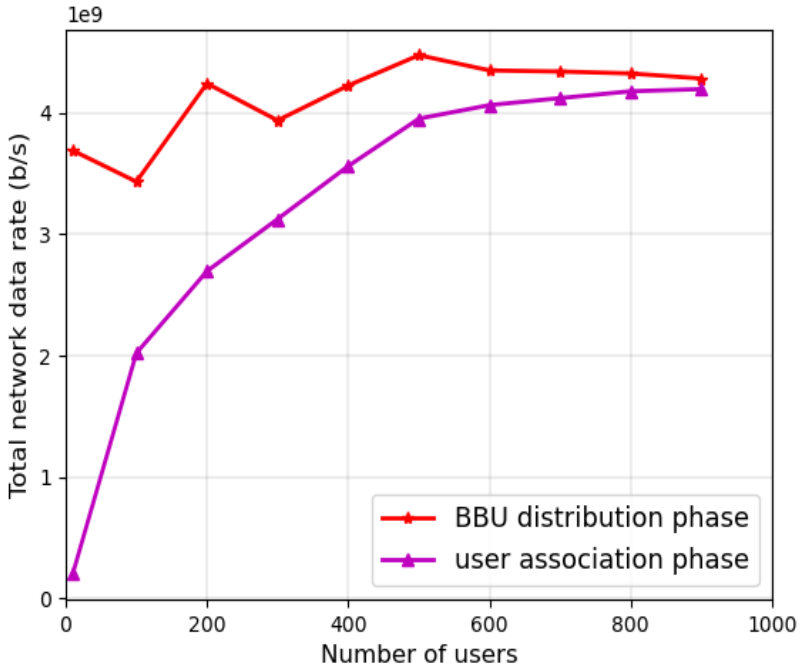

Figure 3.9: Effect of distributing the remaining BBUs after the user association phase.

user's requirements. Also, an oscillation in performance is observed for the BBU distribution phase. For instance, the data rate observed when the number of users is 10 is more than that observed for 100 users. This is because, for the same number of ANs serving these users, the number of extra unallocated BBUs is more for the 10 users. Since the extra BBUs are allocated to maximise the total network data rate, the BBU phase achieves a higher data rate for 10 than 100 users. The data rate increases for the 200 users, however, because the number of ANs that the users are associated with increases.

3.7 Chapter summary

This chapter formulated a user association and resource allocation problem in the ITNTN as a MOOP that maximised the total network data rate and minimised the mobility-induced handoff. Moreover, the mission-critical euRLLC service group provisioning was prioritised over other service groups. The MOOP was transformed into a weighted sum SOOP to reduce complexity. The SOOP was non-linear and combinatorial, making it NP-hard. In order to reduce its complexity, it was decomposed into two sub-problems: the user association sub-problem and the resource distribution sub-problem. The user association sub-problem associated users with appropriate ANs while ensuring they were allocated the minimum resources required to meet their QoS. The distribution phase then allocated the remaining unallocated resources of the AN. A service-aware greedy heuristic polynomial-time algorithm was proposed to solve the user association sub-problem, and results showed that it outperforms the service-unaware scheme in terms of spectrum efficiency, user acceptance ratio, and handoff probability, by 12%, 9.8%, and 78% on average, respectively. Also, the resource distribution problem was reformulated into the water-filling structure and solved using CVXPY. The simulation results showed the effect of the resource distribution phase.

While the proposed greedy heuristic algorithm can find a feasible solution to the user association sub-problem **P1** in polynomial-time, it ordinarily does not produce an optimal solution. Even so, it may give local optimal solutions that approximate the global optimal solution. Therefore, in the following chapter, the Gurobi solver is used to estimate an efficient solution to the user association problem via LP relaxation. Moreover, since the ILP

solution returned by the Gurobi solver is characterised by exponential time complexity, a meta-heuristic algorithm is proposed that gives a near-optimal solution in polynomial-time.

Chapter 4

User Association and Resource Allocation in the ITNTN: A Genetic Algorithm Approach

In Chapter 3, a user association problem **P1** that maximised the total network data rate while minimising the occurrence of mobility-induced handoffs in the ITNTN was formulated. The optimal solution to this problem can be determined using variants of the branch and bound algorithm. However, these solutions become intractable with a large number of variables. Therefore, this chapter presents a near-optimal but polynomial-time solution to **P1** based on the genetic algorithm (GA). Moreover, to validate the performance of the proposed GA, the solution to **P1** is determined via ILP using the Gurobi solver.

4.1 Introduction

To facilitate efficient RRM in the ITNTN, Chapter 3 formulated a UARA problem as a MOOP (3.23) that maximised the total network data rate and minimised the mobility-induced handoff. The MOOP was simplified into a weighted sum SOOP (3.24), which was combinatorial in the UARA variables and thus NP-hard. The SOOP's complexity was reduced by subdividing it into two sub-problems: i) the user association sub-problem **P1** in (3.29), that associated users to appropriate ANs and further allocated them the minimum resources required to meet their QoS requirements. ii) The resource distribution sub-problem **P2** defined in (3.31) that allocated the unallocated resources, if any, after the user association phase. **P2** was reformulated into the water-filling structure and solved using CVXPY, consequently showing the effect of distributing the unallocated BBUs. On the other hand, **P1** was solved using a polynomial time greedy heuristic algorithm. However, greedy solutions do not ordinarily produce optimal solutions. Therefore, this chapter is dedicated to determining an efficient solution to the user association sub-problem **P1**.

Problem **P1** is an ILP problem that is NP-complete. Available techniques for solving such problems can roughly be classified into two main categories, exact and heuristic approaches. Exact algorithms such as branch and bound, dynamic programming, and constraint programming, in particular the large class of ILP techniques including linear programming relaxation, branch-and-cut, cutting plane and column generation are guaranteed to obtain an optimal solution, but at the cost of increased computation time, especially for large dimension problems [138]. On the heuristic side, metaheuristics have proven to obtain near-optimal solutions to ILP problems in polynomial time. Therefore, metaheuristics sacrifice

the guarantee of getting optimal solutions for near-optimal solutions but generated in a significantly reduced amount of time. Moreover, they are simple to implement and, as such, have received a great deal of attention in the last 50 years. Metaheuristic algorithms include population-based schemes such as the GA, PSO, and other techniques like tabu search, simulated annealing, iterated local search, and ant colony optimisation. An interested reader is referred to [138] for a detailed introduction to metaheuristic algorithms.

Consequently, this chapter proposes a near-optimal but polynomial-time solution based on the GA to **P1**. The GA is a metaheuristic search algorithm that uses the theory of evolution and natural selection to solve optimisation problems. It is well suited for multi-objective and non-mathematical optimisation problems, efficiently and easily enforcing different constraints and searching over multiple sets of solutions in a large search space to return a near-optimal solution [139]. Given its ease of implementation and optimisation of discrete and continuous radio parameters, the GA is an excellent optimisation tool for radio resource management in the ITNTN. The performance of the proposed GA is compared to three other algorithms: the ILP solution determined via LP relaxation and branch and bound using the Gurobi solver, the greedy solution described in the previous chapter, and the random user association (RUA) solution. Table 4.1 presents the notations used in this chapter.

4.2 The user association sub-problem P1

For clarity, problem P1 is recalled in this section. The problem was formulated such that its objective function is a weighted sum of the total network data rate and the handoff reduction

Table 4.1: Notations defined in Chapter 4.

Symbol	Description
b, l, h, s	MBS, LAP, HAP, SatComs AN
$\mathcal{B}, \mathcal{L}, \mathcal{H}, \mathcal{S}$	Set of ANs in the MBS, LAP, HAP, SatComs RAN
j, n_j	A RAN, AN in the j-th RAN
$\mathcal{U}$	The set of users in the ITNTN
$\upsilon, \mathcal{E}, \mathcal{R}, \mathcal{D}$	A use-case, feMBB, euRLLC, LDHMC use-case
$\mathcal{U}_{\mathcal{E}}, \mathcal{U}_{\mathcal{R}}\mathcal{U}_{\mathcal{D}}$	Set of users demanding $\mathcal{E}, \mathcal{R}, \mathcal{D}$
$u, u_{\mathcal{E}}, u_{\mathcal{R}}, u_{\mathcal{D}}$	User, an feMBB, euRLLC, LDHMC user
$\mathcal{W}_j$	Set of BBUs owned by RAN j
w_j	A BBU owned by RAN j
$\mathcal{T}_{w_j}, \Phi_{n_j}$	Bandwidth of a BBU w_j, bandwidth of AN n_j
x, y	Environmental constants used for UAV path loss model
$\eta_{LoS},\ \eta_{NLoS}$	Additional loss in a UAV LoS, NLoS propagation
CL, PL^k, PL^e, PL^y	Loss due to clutter, atmospheric gases, scintillation, building entry.
$\mathcal{N}$	Set of all ANs in the ITNTN
z_{n_j}, R_{n_j}	Altitude and cell radius of n_j
$\mathcal{C}_{n_j,u,w_j}, nb_{n_j}^{u_\upsilon}$	Data rate of a user u using BBU w_j of AN n_j, minimum required number of BBUs
$\mu_{n_j,u}, R_{max}$	User association variable, the largest possible cell radius in the ITNTN
$\delta_1, \delta_2, \delta$	Normalisation factors
$\mathcal{C}_{min}^{\upsilon}, \pi_{n_j,u}$	Service group υ minimum data rate, coverage index
$\rho_{u_\upsilon}, \alpha$	User priority factor, objective function trade-off factor
$\xi_{u_\upsilon}, \xi_{u_{\mathcal{D}}}$	User penalty factors
M, G, P_c, P_m, E_r	Population size, number of iterations, cross over probability, mutation probability, elitism ratio
$\mu_k, \mu_{n_j,u}^k, x_{u,k}$	A k-th chromosome, a gene of the k-th chromosome indicating user u is associated with AN n_j, validity status of user u's gene in the k-th chromosome

function, as shown below:

$$\chi = \alpha\ \delta_1 \sum_{n_j \in \mathcal{N}} \sum_{u \in \mathcal{U}} \rho_{u_\upsilon}\ \mu_{n_j,u}\ nb_{n_j}^{u_\upsilon}\ \mathcal{C}_{n_j,u,w_j}\ \ +\ \ (1-\alpha)\ \delta_2 \sum_{n_j \in \mathcal{N}} \sum_{u \in \mathcal{U}} \rho_{u_\upsilon}\ \mu_{n_j,u}\ \frac{R_{n_j}}{R_{max}}. \quad (4.1)$$

The term $\mu_{n_j,u} \in \{0,1\}$ in (4.1) is a user association variable that is 1 when a user u is associated to the AN n_j, and 0 otherwise. On the other hand, $\rho_{u_\upsilon} \in [0,1]$ is a priority factor used to prioritise a user belonging to a certain service group $\upsilon \in \{\mathcal{R}, \mathcal{E}, \mathcal{D}\}$. In contrast, $nb_{n_j}^{u_\upsilon}$ is the minimum number of BBUs that the AN n_j allocates the user to meet the required QoS. $\mathcal{C}_{n_j,u,w_j}$ is the achievable data rate over a BBU w_j allocated to a user u by the AN n_j. R_{n_j} is the AN n_j's cell radius while R_{max} is the largest possible cell radius in the ITNTN. The terms δ_1 and δ_2 are for normalisation purposes to enable the addition of the two functions having different units while α provides a trade-off between data rate maximisation and mobility-induced handoff minimisation for mobile users.

The user association problem **P1** was therefore formulated to maximise the utility function as depicted below:

P1

$$\max_{\mu_{n_j,u}} \quad \chi \tag{4.2}$$

s.t.

C1: $\mu_{n_j,u} \leq \pi_{n_j,u}, \quad \forall\, n_j \in \mathcal{N}, \quad \forall\, u \in \mathcal{U}$

C2: $\sum_{n_j \in \{\mathcal{B} \cup \mathcal{L} \cup \mathcal{H}\}} \pi_{n_j,u}\ \mu_{n_j,u} \quad \leqslant \quad 1, \quad \forall\, u_\mathcal{R} \in \mathcal{U}_\mathcal{R}$

C3: $\sum_{n_j \in \{\mathcal{S}\}} \pi_{n_j,u}\ \mu_{n_j,u} \quad = \quad 0, \quad \forall\, u_\mathcal{R} \in \mathcal{U}_\mathcal{R}$

C4: $\sum_{n_j \in \mathcal{N}} \pi_{n_j,u}\ \mu_{n_j,u} \quad \leqslant \quad 1, \quad \forall\, u_\mathcal{D} \in \mathcal{U}_\mathcal{D},\ u_\mathcal{E} \in \mathcal{U}_\mathcal{E}$

C5: $nb_{n_j}^{u_\upsilon} = \left\lceil \dfrac{\mathcal{C}_{min}^{\upsilon}}{\mathcal{C}_{n_j,u,w_j}} \right\rceil, \quad \forall\, \upsilon \in \{\mathcal{R}, \mathcal{E}, \mathcal{D}\}, \quad \forall u \in \mathcal{U}_{associated}$

$$\text{C6:} \sum_{u \in \mathcal{U}} \pi_{n_j,u} \ \mu_{n_j,u} \ nb_{n_j}^{u_v} \ \mathcal{T}_{w_j} \leq \Phi_{n_j}, \quad \forall \ n_j \in \mathcal{N}$$

$$\text{C7:} \ \mu_{n_j,u} = \{0,1\}, \quad \forall \ u \in \mathcal{U} \ \ \forall \ j \in \{\mathcal{B}, \mathcal{H}, \mathcal{L}, \mathcal{S}\}, \quad \forall \ n_j \in \mathcal{N}$$

$\pi_{n_j,u}$ in (4.2) indicates whether the user u lies within the AN n_j's coverage. Therefore, constraint C1 in (4.2) ensures that a user associates with an AN in whose coverage the user lies. Constraints C2, C3, and C4 allow, at most, one available and capable AN to serve the user. In C5, a user is guaranteed the minimum number of BBUs necessary to satisfy the user's QoS, while C6 ensures that the AN's resource budget is not exceeded. Lastly, C7 ensures that the user association variable is binary.

Problem **P1** is an ILP problem that can be solved by off the shelf solvers using ILP. Therefore, in this chapter, the ILP solution to **P1** is determined by LP relaxation using the Gurobi solver. However, the worst-case computational complexity of the ILP solution increases exponentially with the network dimension, as will be demonstrated in Section 4.4. Consequently, the following section proposes a polynomial time solution based on the GA.

4.3 The proposed genetic algorithm (GA)

The proposed GA solution is described in this section, but first, a brief review of GA is elucidated.

4.3.1 A review of the GA

The GA is a search metaheuristic based on the principle of natural selection in which the fittest individuals of a population are selected to produce children of the next generation. The algorithm starts with generating an initial population of randomly generated solutions called chromosomes. Each chromosome is made up of genes, which are the decision variables of the optimisation problem.

A fitness function corresponding to the objective function is defined and used to measure the fitness of each chromosome in the population. Parents are selected from the population for reproduction based on their fitness values. In the crossover phase, the parents exchange genes, producing new chromosomes, otherwise called children. The crossover phase is governed by the probability of crossover P_c, which determines whether to consider a child or parent chromosome in the new population.

The mutation operator is used to randomly change one or more genes of the chromosomes to create diversity in the new population and prevent the GA from converging to a local optimum. The mutation depends on the probability of mutation P_m, with high values of P_m changing the algorithm to random search. After mutation, the elitism operator ensures that the best solutions/chromosomes in the old population are not lost through crossover and mutation. Therefore, depending on the elitism ratio E_r, a given fraction of the best chromosomes in the old population replace other chromosomes in the new population. The algorithm then terminates when the termination criteria are satisfied, and the chromosome with the best fitness value is the solution to the optimisation problem. There are several termination criteria used in literature [140], including: i) when a fixed number of generations

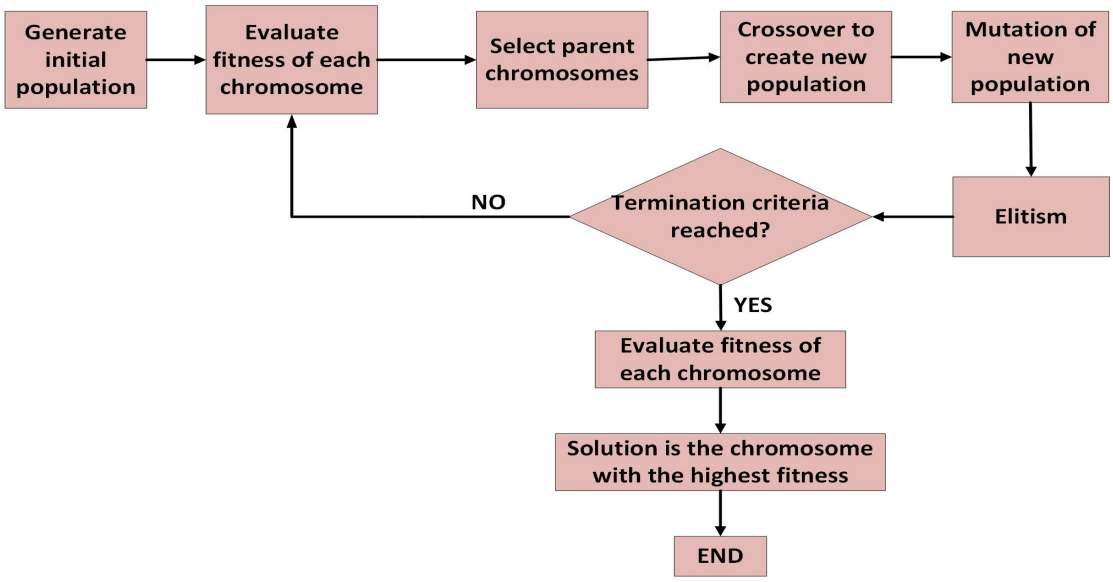

Figure 4.1: The GA process.

is reached, ii) when a certain fitness level is reached, and iii) when there is no improvement in the best fitness value. In this work, the termination criterion is either when there is no improvement in the best fitness value for a given number of consecutive iterations or when a fixed number of generations is reached. The GA process is illustrated in Fig. 4.1.

4.3.2 The proposed GA

A population set $\mathcal{M}$ consisting of M chromosomes is defined. A chromosome $\mu_k \in \mathcal{M}$ is defined as an $|\mathcal{U}|$ dimensional vector that represents a user association solution $\mu_k = (\mu^k_{n_j,1}, \mu^k_{n_j,2}, \ldots, \mu^k_{n_j,|\mathcal{U}|}) \in \mathbb{R}^{|\mathcal{U}|} \ \forall \ \mu_k \in \mathcal{M}, \ k \in \{1, 2, \ldots, M\}$, such that $\mu^k_{n_j,u} \in \{1, 2, \ldots, |\mathcal{N}|\} \ \forall \ u \in \mathcal{U}$. Recall that $\mathcal{U}$ represents the set of users in the ITNTN while $\mathcal{N}$ denotes the set of ANs.

In any given iteration, the fitness value of a gene $\mu^k_{n_j,u}$ of a chromosome μ_k, that represents the optimisation problem **P1**, is defined depending on the service group of user u.

4.3.2.1 Fitness value for an euRLLC or feMBB gene (Data rate maximisation fitness value)

Since an euRLLC user $u_{\mathcal{R}}$ or an feMBB user $u_{\mathcal{E}}$ is static, the objective for these service groups is to maximise the achieved total network data rate. The fitness value of a gene belonging to an $u_{\mathcal{R}}$ or $u_{\mathcal{E}}$ user is given by

$$\Theta_{\upsilon}(\mu^{k}_{n_j,u}) = x_{u,k}\left(\delta\ \mathcal{C}_{n_j,u,w_j}\right) \quad - \quad \xi_{u_{\upsilon}}(1 - x_{u,k}), \quad \forall\ u_{\mathcal{R}} \in \mathcal{U}_{\mathcal{R}}, \quad u_{\mathcal{E}} \in \mathcal{U}_{\mathcal{E}}, \quad \upsilon \in \{\mathcal{R}, \mathcal{E}\}, \tag{4.3}$$

where $\mathcal{C}_{n_j,u,w_j}$ is the data rate a user u can achieve over one BBU w_j of AN n_j, given by (3.10). δ is used to normalise the data rate $\mathcal{C}_{n_j,u,w_j}$. $x_{u,k} \in \{0, 1\}$ denotes the validity status of the gene $\mu^{k}_{n_j,u}$. $x_{u,k} = 1$ if the user u's association variable/gene $\mu^{k}_{n_j,u}$ is valid and 0 otherwise. A gene $\mu^{k}_{n_j,u}$ is valid if the AN n_j is within the coverage of user u, is capable of serving the user, and has sufficient resources to meet the QoS requirements of the user. $\xi_{u_{\upsilon}} \in [0, 1]$ is the penalty cost for not admitting a user of service group $\upsilon \in \{\mathcal{E}, \mathcal{R}\}$.

4.3.2.2 Fitness value for an LDHMC gene (Handoff minimisation fitness value)

The fitness value for users demanding the LDHMC service group $\mathcal{D}$ prioritises association to ANs with large cell radius to minimise handoff probability. Consequently, the fitness value for these users is expressed as

$$\Theta_{\mathcal{D}}(\mu^{k}_{n_j,u}) = x_{u,k}\ \frac{R_{n_j}}{R_{max}} \quad - \quad \xi_{u_{\mathcal{D}}}(1 - x_{u,k}),\ \forall\ u_{\mathcal{D}} \in \mathcal{U}_{\mathcal{D}}, \tag{4.4}$$

where $\xi_{u_{\mathcal{D}}}$ is a penalty for not admitting an $u_{\mathcal{D}}$ user, R_{n_j} is the cell radius of n_j, and R_{max} the largest possible cell radius in the ITNTN.

The penalties $\xi_{u_{\upsilon}}$ in (4.3) and $\xi_{u_{\mathcal{D}}}$ in (4.4) are varied depending on the priority of a given service group. We prioritise the euRLLC service group in this work since denial of its service may lead to catastrophic consequences. We also prioritise access to the NTN with a large coverage area for the mobile LDHMC use case to minimise the probability of handoff. Nonetheless, the priority can also be based on other factors, such as the use case that yields more revenue to the operator.

For any given gene $\mu^{k}_{n_j,u}$ of a chromosome μ_{k}, if $x_{u,k} = 1$, then the user u_{υ} where $\upsilon \in \{\mathcal{E}, \mathcal{R}, \mathcal{D}\}$ is allocated its minimum required number of BBUs $nb^{u_{\upsilon}}_{n_j}$ given by (3.27) in Chapter 3 and rewritten for clarity as

$$nb^{u_{\upsilon}}_{n_j} = \left\lceil \frac{\mathcal{C}^{\upsilon}_{min}}{\mathcal{C}_{n_j,u,w_j}} \right\rceil, \ \forall \upsilon \in \{\mathcal{E}, \mathcal{R}, \mathcal{D}\}, \forall u \in \mathcal{U}, \forall n_j \in \mathcal{N}, \tag{4.5}$$

else, the user is not allocated any resources. We assume that $\mathcal{C}^{\upsilon}_{min}$ is the data rate request from a user demanding a service in the service group $\upsilon \in \{\mathcal{R}, \mathcal{E}, \mathcal{D}\}$. The overall fitness value of the chromosome μ_{k} in any given iteration is the summation of all fitness values for the different genes in the chromosome given by:

$$\Theta(\mu_{k}) = \sum_{u \in \mathcal{U}} \Theta_{\upsilon}(\mu^{k}_{n_j,u}), \quad \forall \ \upsilon \in \{\mathcal{R}, \mathcal{E}, \mathcal{D}\}. \tag{4.6}$$

According to (4.6), all users in the network cooperate and contribute to the fitness value of the chromosome, ultimately leading to fairness between users since the goal is to admit as many users as possible to maximise the fitness value.

4.3.2.3 The GA pseudo-code

The pseudo-code of the proposed GA is given in Algorithm 2. The selection of parents in line 7 is achieved using the roulette wheel technique. In this technique, each chromosome in the population is assigned a probability P_{μ_k} of being selected, depicted by

$$P_{\mu_k} = \frac{\Theta(\mu_k)}{\sum_{\mu_k \in \mathcal{M}} \Theta(\mu_k)}, \tag{4.7}$$

that is proportional to its fitness value. The chromosomes with higher values of P_{μ_k} have higher chances of contributing to the creation of the next generation.

In lines 8–9, the two selected parents recombine through the crossover operator. In this work, the two-point crossover technique is used [140]. In this technique, two points are randomly selected on both parents, and genes are exchanged between them to create two different chromosomes, otherwise called children. For each created child, if a randomly generated number in the range $[0, 1]$ is less than P_c, the child is inserted into the new population, otherwise, the parent is. The new chromosomes are then mutated as per line 10 of Algorithm 2. For each gene in the chromosomes created in lines 8–9, if a random number in the range [0,1] is less than P_m, the gene is mutated by replacing it with a random gene $\mu^k_{n_j,u} \in \{1, 2, \ldots, |\mathcal{N}|\}$, otherwise, the gene is not mutated. Line 12 performs the elitism

process, which replaces E_r of the chromosomes in the new population with the same fraction of best-performing chromosomes in the old population. In line 15, if the fitness value of the best chromosome remains unchanged for a given number of consecutive iterations Q, the algorithm breaks out of the for loop and returns the best/optimal user association solution μ_k^*. Line 17 returns the optimal user association, which is the chromosome in the population with the best fitness value. This solution indicates which ANs the users should be associated with but does not give the number of BBUs that should be allocated to the users to meet their QoS requirements. Therefore, line 18 of Algorithm 2 inputs the optimal user association decision into Algorithm 3, and this returns a list $Assoc_{n_j}^u$ containing the AN n_j (which is the gene $\mu_{n_j,u}^k$) serving user u, and the number of BBUs $nb_{n_j}^{u_v}$ determined according to (4.5) that are allocated to the user.

4.3.2.4 Computational complexity of the proposed GA

Similar to Section 3.5.2, the computational complexity of the different algorithms discussed in this chapter is analysed using the big-O notation. The GA performs the selection, crossover, and mutation operators in each generation. Similar to many roulette wheel selection routines, a chromosome is selected for reproduction in this work using a search algorithm. Hence, the time complexity of the selection operator is of the order O(M) [141], where M is the population size. The time taken to execute the crossover is proportional to the population size M, hence its time complexity is bounded by O(M). On the other hand, mutation requires that a random number in the range [0,1] is generated for every gene of every chromosome. Therefore, the time complexity of mutation in any given generation is O($M \times |\mathcal{U}|$), where

Algorithm 2 Genetic algorithm for service-aware user association and resource allocation

Input: Size of population M, Number of genes $|\mathcal{U}|$, Number of iterations G, Number of consecutive iterations Q for stopping criterion, P_c, P_m, E_r, achievable data rate user statistics to the different ANs determined using (3.10)

Output: User association and resource allocation set, $Assoc^u_{n_j}$

procedure USER ASSOCIATION AND RESOURCE ALLOCATION
Generate the initial population set $\mathcal{M}$ containing M chromosomes each of length $|\mathcal{U}|$
Calculate the fitness value of each chromosome in $\mathcal{M}$ using (4.6)
    for $iteration = 1 : G$ **do**
        Create empty new population set $\mathcal{M}_{new}$
        for $w = 1 : M/2$ **do**
            Select two parents from $\mathcal{M}$ using the roulette wheel technique
            Carry out crossover on the two parents to create two children
            Insert either the children or parent chromosomes in $\mathcal{M}_{new}$ using P_c
            For each of the just inserted chromosomes in $\mathcal{M}_{new}$, carry out mutation based on P_m
        end for
        Carry out Elitism using E_r
        $\mathcal{M} = \mathcal{M}_{new}$
        Determine the fitness of each chromosome in $\mathcal{M}$
        Break the for loop if fitness value of best chromosome does not change for Q consecutive iterations
    end for
    return the user association solution μ^*_k
    Input μ^*_k in Algorithm 3 to determine the number of BBUs allocated to user u for each association decision $\mu^k_{n_j,u}$ in μ^*_k
    Return $Assoc^u_{n_j}$
end procedure

$|\mathcal{U}|$ is the number of genes in a chromosome, which also corresponds to the number of users in the ITNTN. Also, the summation of all genes' fitness values gives a chromosome's fitness value. Moreover, the SINR or cell radius to the different access nodes must be known to calculate the fitness values. Therefore, the time complexity due to the evaluation of fitness values of all chromosomes in a generation is $\mathrm{O}(M \times |\mathcal{U}| \times |\mathcal{N}|)$. The overall time complexity of the proposed GA is therefore given by $\mathrm{O}(G \times (M + M + M \times |\mathcal{U}| + M \times |\mathcal{U}| \times |\mathcal{N}|)) = \mathrm{O}(G \times M \times (2 + |\mathcal{U}| + |\mathcal{U}| \times |\mathcal{N}|))$, where G is the number of generations. This time complexity

Algorithm 3 Resource allocation algorithm

Input: Chromosome μ_k, access node available number of BBUs $Num_{n_j}^{BBU}$, achievable data rate user statistics to the different ANs determined using (3.10)
Output: User association and resource allocation set, $Assoc_{n_j}^{u}$

procedure RESOURCE ALLOCATION
Initialise: $Assoc_{n_j}^{u} = \emptyset$
  for Each gene $\mu_{n_j,u}^{k} \in \mu_k$ **do**
    $u = 1$
    Determine validity status $x_{u,k}$ of $\mu_{n_j,u}^{k}$
    if $x_{u,k} == 1$ **then**
      Allocate $nb_{n_j}^{u_v}$ BBUs to user u according to (4.5)
      Deduct $nb_{n_j}^{u_v}$ from $Num_{n_j}^{BBU}$
      Append $[u, \mu_{n_j,u}^{k}, nb_{n_j}^{u_v}]$ to $Assoc_{n_j}^{u}$
    else
      $nb_{n_j}^{u_v} = 0$
      Append $[u, \mu_{n_j,u}^{k}, nb_{n_j}^{u_v}]$ to $Assoc_{n_j}^{u}$
    end if
    $u = u + 1$
  end for
  Return $Assoc_{n_j}^{u}$
end procedure

can be reduced to $\mathrm{O}(G \times M \times |\mathcal{U}| \times |\mathcal{N}|)$. Consequently, the proposed GA has a polynomial time complexity of the order $\mathrm{O}(G \times M \times |\mathcal{U}| \times |\mathcal{N}|)$.

4.4 The ILP solution

The problem **P1** is an NP complete problem that can be solved using variants of the branch and bound algorithm. Therefore, we utilise the Gurobi solver to derive the ILP solution based on linear programming (LP) relaxation and branch and bound [142]. Since the decision variables are binary, the problem's search space has a size of two to the power of the number of binary variables. The number of association variables $\mu_{n_j,u}$ is $|\mathcal{U}| \times |\mathcal{N}|$. However, for a

given user u_v, the minimum number of BBUs $nb_{n_j}^{u_v}$ required to meet its QoS demands varies according to the AN the user is associated with. This implies that the user then has to also decide the AN to associate with based on the variable $nb_{n_j}^{u_v}$. Consequently, this gives an additional $|\mathcal{U}| \times |\mathcal{N}|$ decision variables, making the total number of variables $2 \times |\mathcal{U}| \times |\mathcal{N}|$. The computational complexity of the ILP solution is then given by $\mathrm{O}(2^{2\times|\mathcal{U}|\times|\mathcal{N}|})$. Hence, the worst-case computational complexity of the ILP solution varies exponentially with the number of users and the number of ANs in the network. Ultimately, this necessitates other efficient solutions to the problem that require a worst-case time complexity that is polynomial and not exponential, hence, the proposed GA.

4.5 The baseline and random user association (RUA) algorithms

The baseline and RUA schemes are also analysed as benchmark solutions. The baseline association also called the greedy algorithm in this work, associates static users with ANs based on maximum SINR. In contrast, mobile users are associated according to the largest cell radius. The description of the greedy algorithm, together with its pseudo code, is given in Section 3.5. The overall time complexity of the greedy algorithm is $\mathrm{O}(|\mathcal{U}| \times (\log|\mathcal{U}| + |\mathcal{N}|\log|\mathcal{N}|))$ as explained in Section 3.5.2. Since the accuracy of the proposed GA is dependent on the population size M and the number of generations G, which are usually greater than the number of access nodes $|\mathcal{N}|$, it is clear that the greedy algorithm has a much shorter worst-case running time than the proposed GA. However,

as the results will show in Section 4.6, the GA achieves a better performance regarding maximising the objective function in problem **P1**.

On the other hand, the RUA approach associates users randomly with any available AN. Such an algorithm has the shortest worst-case running time, which is proportional to the number of users. Hence, the time complexity of the RUA algorithm is given by $O(|\mathcal{U}|)$. Important to note is that, like the GA, both the greedy and RUA algorithms prioritise i) the euRLLC use-case and ii) the use of NTNs over the TNs for service provisioning of the mobile LDHMC users. The RUA algorithm associates mobile users randomly to any available NTN, and if these are not available, then the TN is considered.

4.6 Results and performance evaluation

In this section, the performance of the proposed GA is compared to the ILP solution estimated by the Gurobi solver, greedy, and RUA solutions. First, the main simulation parameters are presented, and after, the results and their discussion.

4.6.1 Simulation assumptions

We consider a circular urban region of 3 km radius that is within the coverage of a LEO satellite and a HAP AN and also contains 1 LAP AN and MBSs with a radius of 2 km and 1 km respectively. Fig. 4.2 is an example of the network deployment with 2 MBSs in the considered user distribution area. Users within the considered region are uniformly and randomly distributed. Table 4.2 [19, 1, 111, 112] gives the radio environment parameters

used to validate the proposed solution. Given that the performance of the GA is highly dependent on the probability of crossover P_c, probability of mutation P_m, and population size $\mathcal{M}$, the values of these parameters are determined before results analysis.

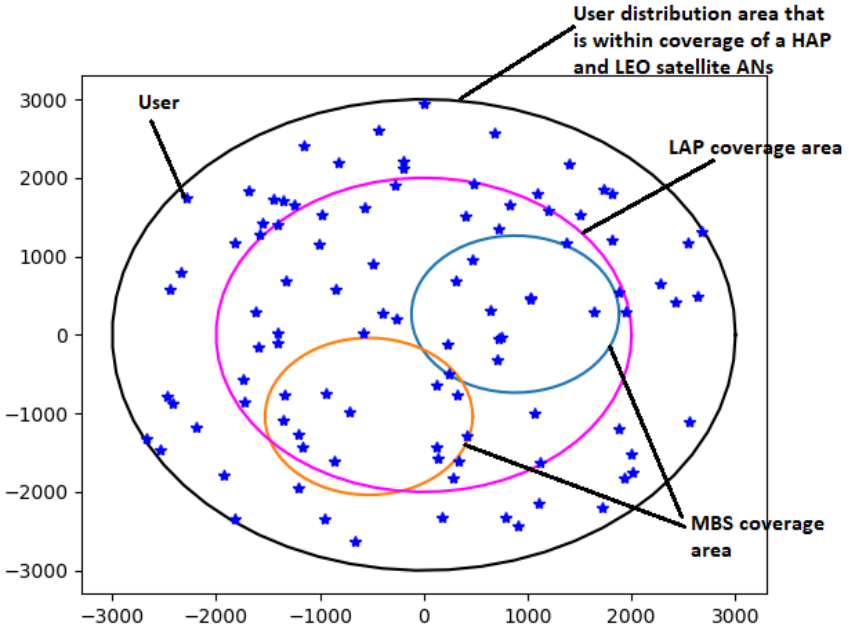

Figure 4.2: Network deployment.

Table 4.2: Simulation parameters and values.

Parameter	Value
$f_{n_\mathcal{B}}, f_{n_\mathcal{L}}, f_{n_\mathcal{H}}, f_{n_\mathcal{S}}$ (Frequencies)	[4, 2, 3, 5] GHz
$\mathcal{T}_{w_\mathcal{B}}, \mathcal{T}_{w_\mathcal{L}}, \mathcal{T}_{w_\mathcal{H}}, \mathcal{T}_{w_\mathcal{S}}$ (BBU bandwidth)	[0.18, 0.18, 1, 2] MHz
Number of BBUs for $[n_\mathcal{B}, n_\mathcal{L}, n_\mathcal{H}, n_\mathcal{S}]$	[10, 10, 20, 20]
$[P_{n_\mathcal{B}}^{thres}, P_{n_\mathcal{L}}^{thres}, P_{n_\mathcal{H}}^{thres}, P_{n_\mathcal{S}}^{thres}]$ (maximum power at ANs)	[8, 5, 20, 25] Watts
$x,\ y,\ \eta_{LoS},\ \eta_{NLoS}$	[10.39, 0.05, 1, 20]
Shadow fading $[\mathcal{B}, \mathcal{S}]$	[8, 4] dB
$[CL,\ PL^k,\ PL^y]$	[0, 0, 23 dB]
AN height $[z_{n_\mathcal{B}}, z_{n_\mathcal{L}}, z_{n_\mathcal{H}}, z_{n_\mathcal{S}}]$	[40 m, 2 km, 17 km, 600 km]
Service group user ratio $[\lvert\mathcal{U}_\mathcal{R}\rvert : \lvert\mathcal{U}_\mathcal{D}\rvert : \lvert\mathcal{U}_\mathcal{E}\rvert]$	[0.3:0.1:0.6]
$\mathcal{C}_{min}^{\upsilon}\upsilon \in [\mathcal{R}, \mathcal{D}, \mathcal{E}]$	[500, 1000, 1000] kbps
Noise spectral density	-174 dBm

4.6.2 GA parameter setting

The appropriate parameters used in the proposed GA solution are identified in this subsection. Fig. 4.3 shows the effect of P_c on the GA convergence. P_m, M and the number of users $|\mathcal{U}|$ are fixed at 0.1, 50, and 80, respectively, while P_c is varied from 0.2 to 1, with increments of 0.2. It is observed that the higher the value of P_c, the larger the fitness value, hence, the better the solution found by the GA is at satisfying the objective function. Since $P_c = 0.8$ performed well as per Fig. 4.3, it is chosen to be used in this work.

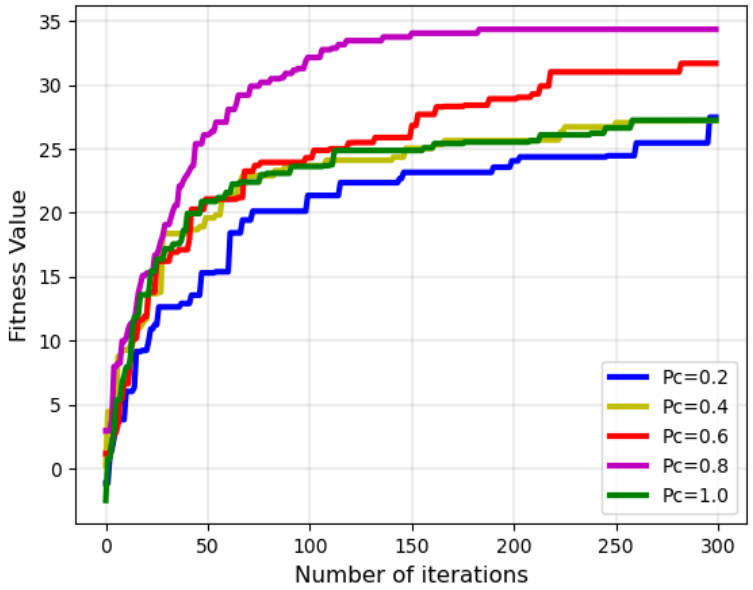

Figure 4.3: Effect of probability of crossover on GA convergence.

Next, the effect of P_m on convergence is analysed by setting $P_c = 0.8$, $M = 50$ and $|\mathcal{U}| = 80$. Fig. 4.4 shows that the higher the value of P_m, the worse the performance of the GA, as the algorithm is transformed into a random search. P_m is set to 0.1 since its fitness

value and convergence rate are much better than any other value of P_m, as shown in Fig. 4.4.

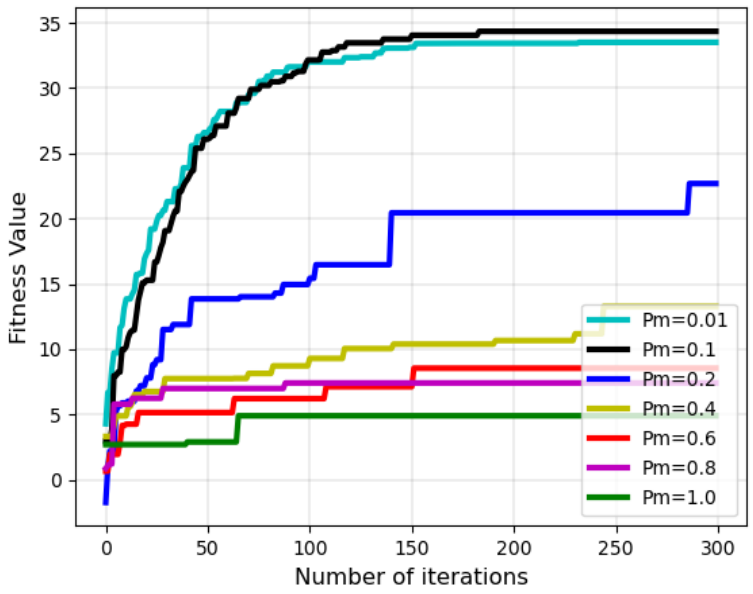

Figure 4.4: Effect of probability of mutation on GA convergence.

In Fig. 4.5, the effect of population size M on the GA convergence is analysed, with $P_c = 0.8$, $P_m = 0.1$ and $|\mathcal{U}| = 80$. The figure shows that convergence speed increases with the population size M. Also, we observe that convergence is achieved by the 200th iteration for all population sizes. In the following section, we set the population size M to 50 and the number of iterations G to 150. These parameters are chosen to strike a balance between the accuracy and computation complexity of the GA, as both increase with M and G. Table 4.3 gives the parameters used for the GA.

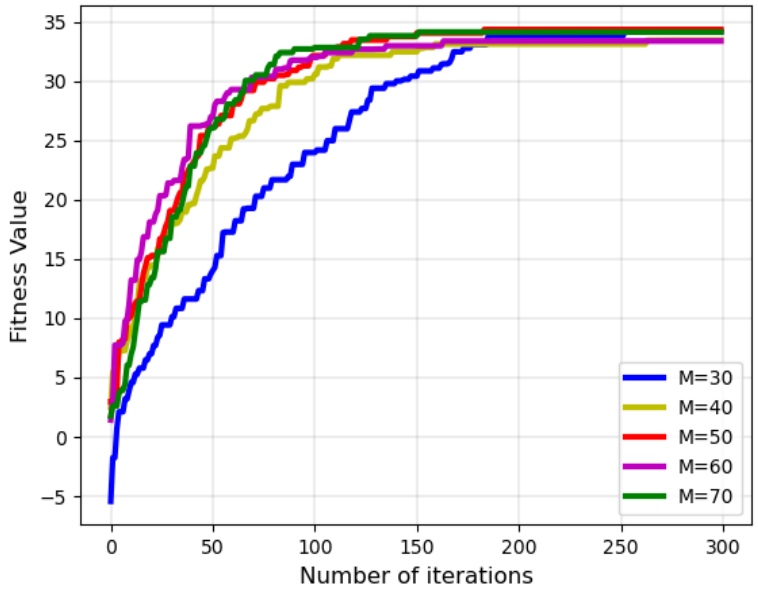

Figure 4.5: Effect of population size on GA convergence.

Table 4.3: GA parameters.

Parameter	Value
Probability of crossover P_c	0.8
Probability of mutation P_m	0.1
Population size M	50
Number of iterations G	150

4.6.3 Simulation results

To validate the performance of the proposed GA, we simulate the ILP solution based on the Gurobi solver of the problem **P1**. In addition, we compare the proposed GA with the greedy algorithm and the RUA scheme.

Performance evaluation is based on four main metrics: the user AR, the total network data rate as defined in (3.19), the SE, and the handoff probability. The user AR quantifies the ratio of served users to the total number of users in the network. On the other hand, the SE is the ratio of the overall system data rate to the total network bandwidth [137]. At

the same time, we define the probability of handoff as the ratio of the number of users that experienced a handoff (and are thus served by another AN) to the total number of mobile users during a given TTI.

4.6.3.1 Impact of trade-off factor α

This section first analyses the effect of the trade-off term α on data rate maximisation (objective 1) and handoff minimisation (objective 2) in (4.1). As α affects only mobile users, for this analysis, we consider 20 LDHMC users in a network comprising 5 ANs, i.e., 2 MBSs, 1 LAP, 1 HAP, and 1 SatComs AN.

Fig. 4.6 depicts that in solving the MOOP in (3.23) as a SOOP **P1** for varying values of α, a set of Pareto-optimal solutions exist. These solutions are generated using Algorithm 2 for values of α ranging from 0 to 1 with an increment size of approximately 0.0526. As Fig. 4.6 shows, the generated Pareto-optimal solutions form a Pareto-optimal front below which the region comprises suboptimal solutions and above which are infeasible solutions. From the figure, the points are concentrated at both ends of the curve. This shows that for the mobile users, α acts to either maximise data rate or minimise mobility-induced handoff. When the value of α is lower than 0.5, function two of (4.1) is maximised, which ultimately minimises the handoff probability, and as α increases beyond 0.5, then function one is maximised consequently maximising data rate. Figs. 4.7 and 4.8 further support this observation. In Fig. 4.7, the SE is low for low values of α, and a step to higher SE is observed at $\alpha \approx 0.5$. In the same manner, in Fig. 4.8, the probability of handoff is approximately 0 for $\alpha < 0.5$ when objective two is prioritised, and once α increases above 0.5, the handoff probability

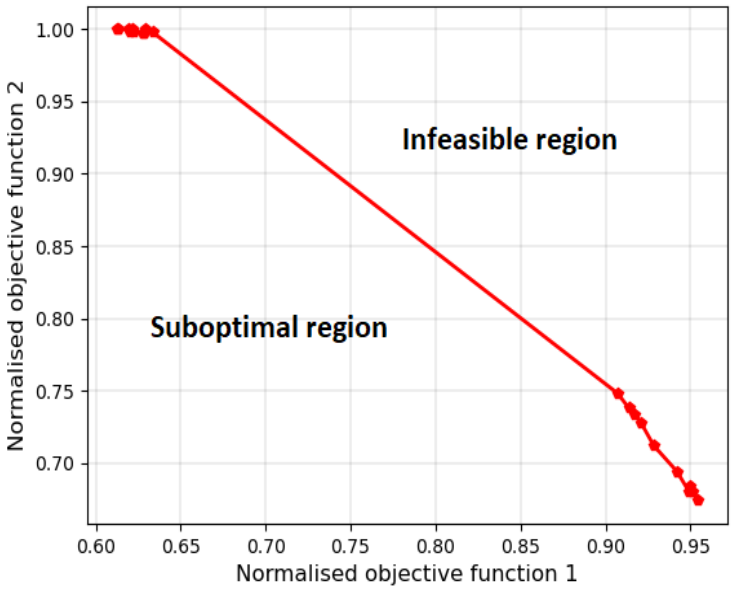

Figure 4.6: Pareto-optimal front of the MOOP in (3.23).

increases since the priority becomes data rate maximisation, and the nodes that maximise data rate are not necessarily the same as those that minimise mobility-induced handoff. The

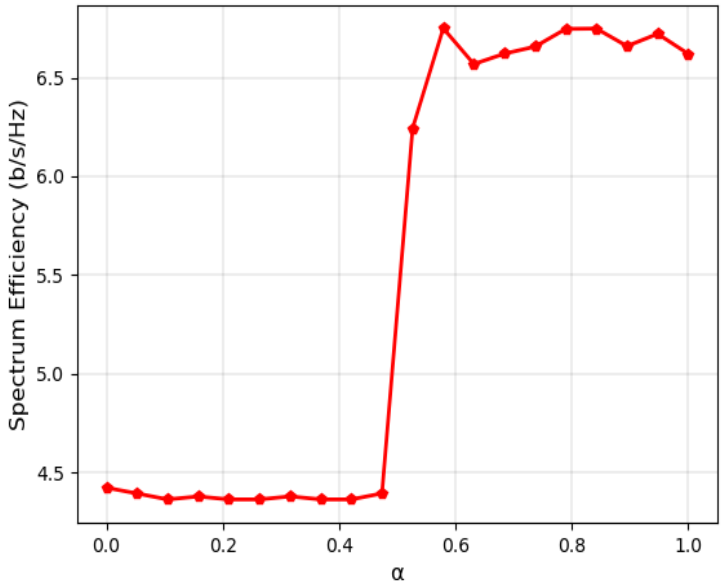

Figure 4.7: Spectrum efficiency with varying α.

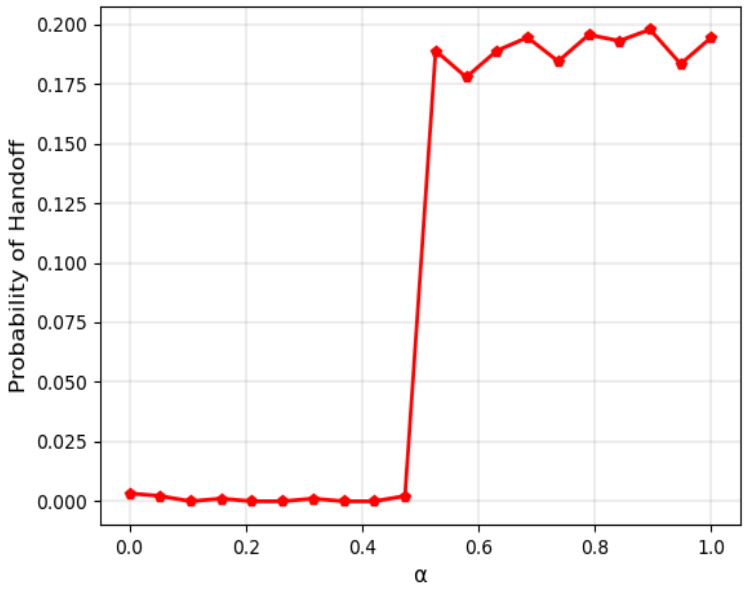

Figure 4.8: Probability of handoff with varying α.

instability observed in both Figs. 4.7 and 4.8 for $\alpha > 0.5$ is caused by motion of the users. The users keep moving at different velocities out and into coverage of different ANs resulting in unstable achieved total data rate and handoffs experienced. Since α either maximises the data rate or minimises the mobility-induced handoff, in all the following simulations, we assume that the objective of the mobile users is to minimise the handoff probability and, as such, set $\alpha = 0$ for the LDHMC service group.

4.6.3.2 Impact of user density

We then evaluate the proposed algorithm's performance while varying the number of users in the network. We maintain the number of ANs at 5, with 2 MBSs, 1 LAP, 1 HAP, and 1 SatComs AN.

In Fig. 4.9, we analyse the user AR performance of all algorithms. Generally, as the number of users in the network increases, the AR reduces due to resource scarcity. On average, the AR achieved by the GA, ILP, greedy, and RUA algorithms is 0.923, 0.912, 0.894, and 0.886, respectively. The proposed GA achieves a user AR that is better than the ILP, greedy, and RUA solutions by 1.2% 3.1% and 3.9%, respectively. The GA performs better than all algorithms because its fitness value is optimised to increase with the number of users admitted to the network. In contrast, the ILP, greedy, and RUA do not optimise user AR.

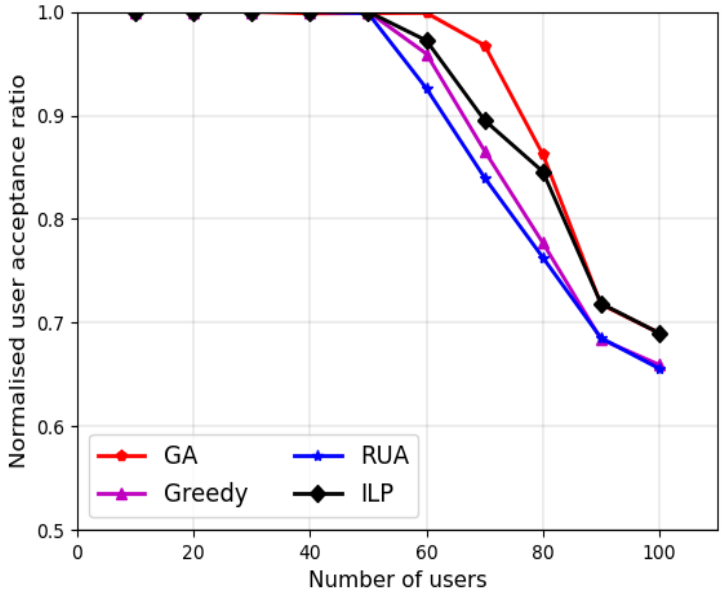

Figure 4.9: User acceptance ratio with varying number of users.

Figs. 4.10 and 4.11 depict the performance of the different algorithms with respect to the achieved total network data rate and spectrum efficiency, respectively. The two figures follow the same shape since the number of ANs is fixed, implying that the total system bandwidth is also fixed. As the number of users in the network increases, the total data rate increases,

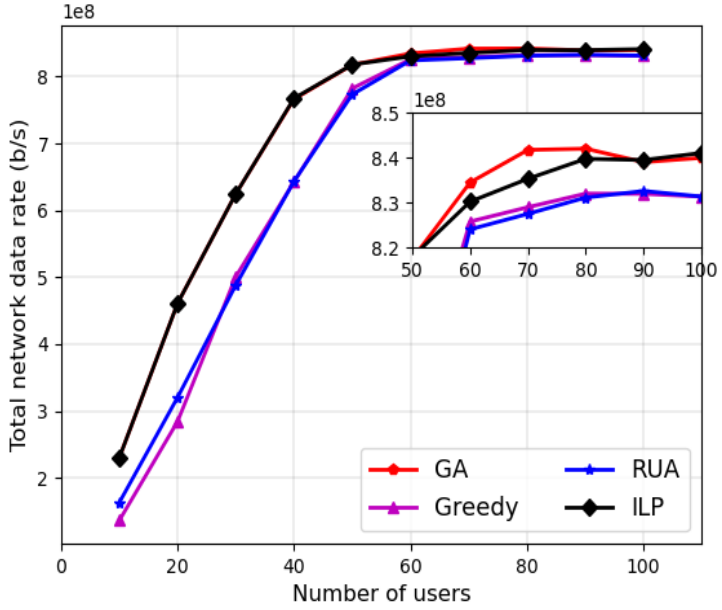

Figure 4.10: Total network data rate with varying number of users.

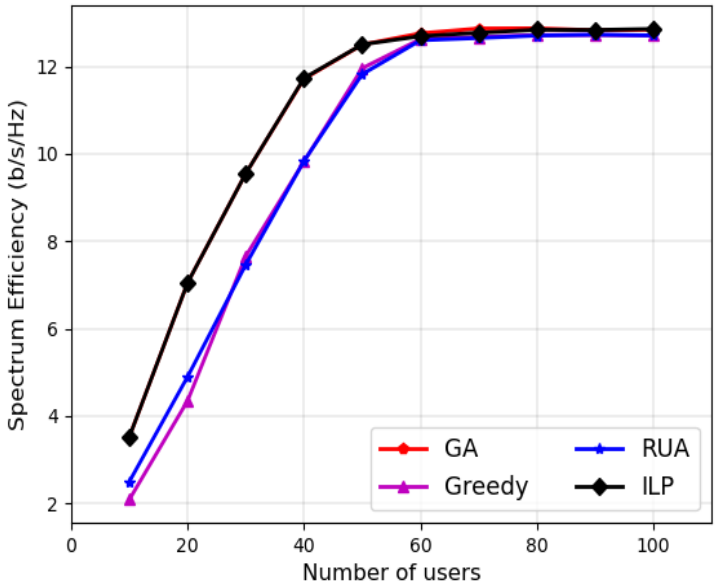

Figure 4.11: Spectrum efficiency with varying number of users.

thus increasing the achieved SE. However, at about 60 users and above, the achieved network data rate remains constant since the available resources become insufficient to meet the

QoS requirements of all users. Ultimately, all algorithms saturate, as the achieved total network data rate and resulting SE remain constant irrespective of the number of users in the network. The SE achieved on average by the GA, ILP, greedy, and RUA algorithms is 10.852, 10.836, 9.934, and 9.993 b/s/Hz respectively. The performance of the GA outperforms the ILP, greedy, and RUA algorithms by 0.14%, 8.45%, and 7.92% on average, respectively. It is important to note that the RANs in the ITNTN have BBUs of different bandwidths. Therefore, a RAN may have a higher SINR, but because of smaller-sized BBUs, it achieves less data rate than another RAN with bigger-sized BBUs. Thus, the greedy algorithm, whose association for static users is based on maximum SINR, does not guarantee maximum data rate in the ITNTN, thereby leading to a lower SE when compared to the proposed GA, whose value function is based on maximising the achieved data rate. The performance of the RUA algorithm is also lower than the GA, as this algorithm associates users randomly to any available capable RAN without regard for the achieved data rate. The excellent performance of both the GA and the ILP solutions is because both are based on maximising the data rate of the ITNTN.

In Fig. 4.12, the euRLLC user acceptance ratio performance is depicted. The euRLLC users are prioritised over other users for all four algorithms, as it is vital to mitigate call blocks for this use case. Consequently, a high AR is observed for all algorithms, with average values being 0.996, 0.997, 1, and 0.997 for GA, ILP, greedy, and RUA algorithms, respectively. The GA performs worse as this trades off euRLLC user acceptance for the feMBB users, as observed in Fig. 4.14. Hence, its better performance in total network data rate in Fig. 4.10 when compared to the ILP solution, whose priority factor in the SOOP **P1** forces it to

connect more euRLLC users who require less data rate than the feMBB users. Nonetheless, the GA's euRLLC AR performance is within an average of 0.14% of the ILP solution's euRLLC AR. The greedy algorithm performs the best in euRLCC user AR since it is hand-crafted to serve all euRLLC users without regard to the achieved total network data rate.

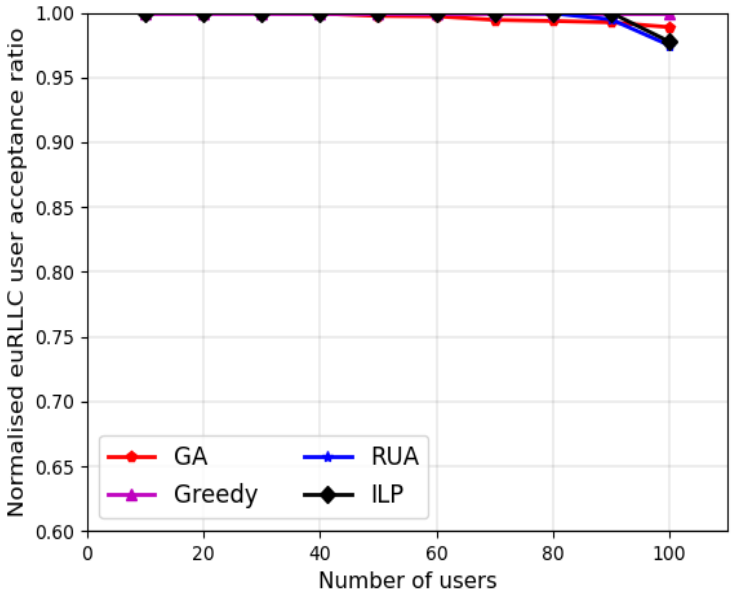

Figure 4.12: euRLLC acceptance ratio with varying number of users.

The large coverage NTNs were prioritised in all four algorithms to serve the mobile LDHMC service group. Therefore, as is depicted by Fig. 4.13, the AR for this service group is 1 for all algorithms and all numbers of users. This is because of available resources in the network to serve this service class. On the other hand, Fig. 4.14 shows the acceptance ratio of the feMBB use case. In this work, the priority of this use case is lower than other use cases, hence the steep decline in AR beyond 60 users when the resources in the network are

no longer enough to serve all users. The feMBB AR performance of the GA, ILP, greedy, and RUA algorithms is 0.87, 0.85, 0.82, and 0.81 on average, respectively.

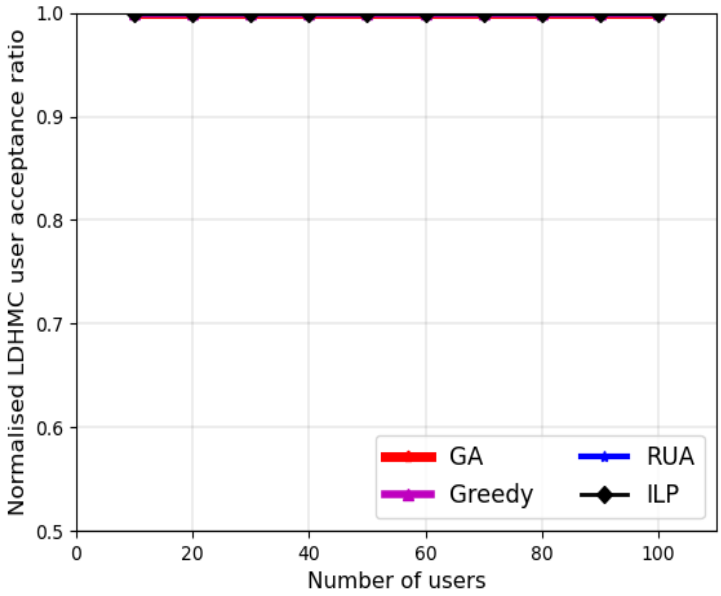

Figure 4.13: LDHMC acceptance ratio with varying number of users.

We analyse the handoff performance of all algorithms in Fig. 4.15. The GA, ILP, and greedy algorithms can associate the LDHMC mobile users to the ANs with the largest cell radius and thus achieve a handoff probability of 0 for all numbers of users in the network. Such a good performance is because the GA uses the fitness function to impose a high penalty for not associating mobile users to the RAN with the largest cell radius. Similarly, the ILP model is coded to maximise the handoff reduction function in **P1**. Along the same lines, the greedy heuristic algorithm is hand-crafted to prioritise using the RAN with the broadest cell radius for mobile users. On the other hand, the handoff probability for the RUA algorithm is worse by 48.5% on average, respectively. This is because in the RUA algorithm, the LDHMC user association randomly alternates between the NTN ANs, thus

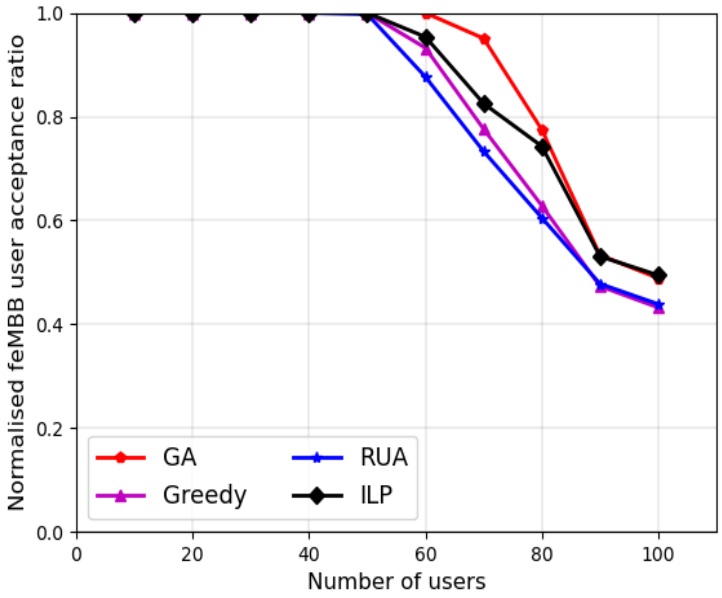

Figure 4.14: feMBB acceptance ratio with varying number of users.

achieving the highest handoff probability. This probability reduces with the number of users for the RUA algorithm because resources of smaller radius ANs are depleted, and users are now forced to associate with the large coverage cells.

4.6.3.3 Impact of access nodes density

Next, we analyse the impact of AN density on the four different algorithms. While ANs are deployed randomly, the placement of ANs that belong to the same tier is such that there is a limit to the amount of area that can be overlapped by different cells. Therefore, to enable the deployment of many MBSs in the considered region, the user distribution radius is increased to 4 km. This region is still within the coverage of 1 satellite and 1 HAP. We also deploy 1 LAP and vary the MBSs from 2 to 10 while maintaining the number of users at 80.

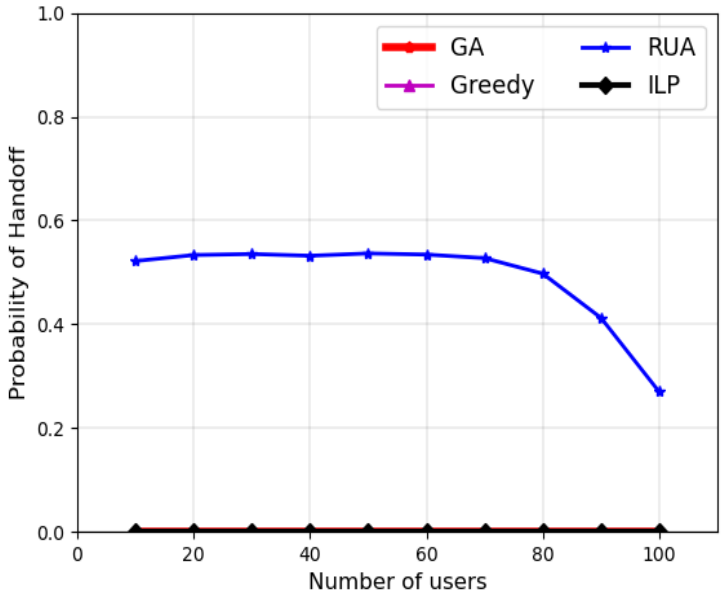

Figure 4.15: Probability of handoff with varying number of users.

Fig. 4.16 shows that the GA achieves the best total network data rate performance as the number of ANs in the network increases. On average, GA's performance outperforms the ILP, greedy, and RUA algorithms by 0.24%, 1.04% and 1.1%, respectively. The oscillatory behaviour of the achieved network data rate as the number of ANs increases is due to the random deployment of both ANs and users in each iteration during the simulation. A scenario can happen when users in certain cells have high path loss resulting into reduced data rate. The AR will increase since the number of ANs serving unserved users is increasing, as shown by Fig. 4.18, but it is possible for the data rate to reduce if majority of these users have high path loss to their associated ANs.

Fig. 4.17 depicts the SE achieved by all four algorithms. Generally, the SE decreases as the number of ANs increases because the rate of increase in data rate is less than the rate at which bandwidth increases. Consequently, the ratio of the total network data rate

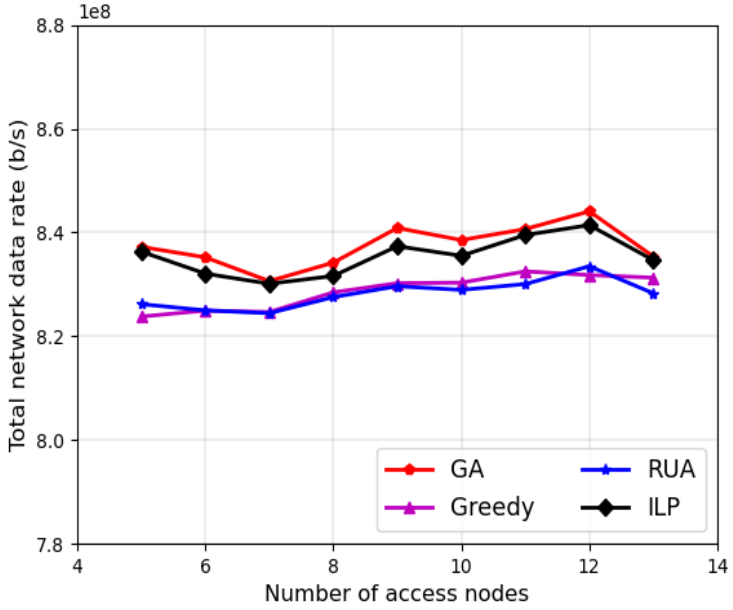

Figure 4.16: Total network data rate with varying number of access nodes.

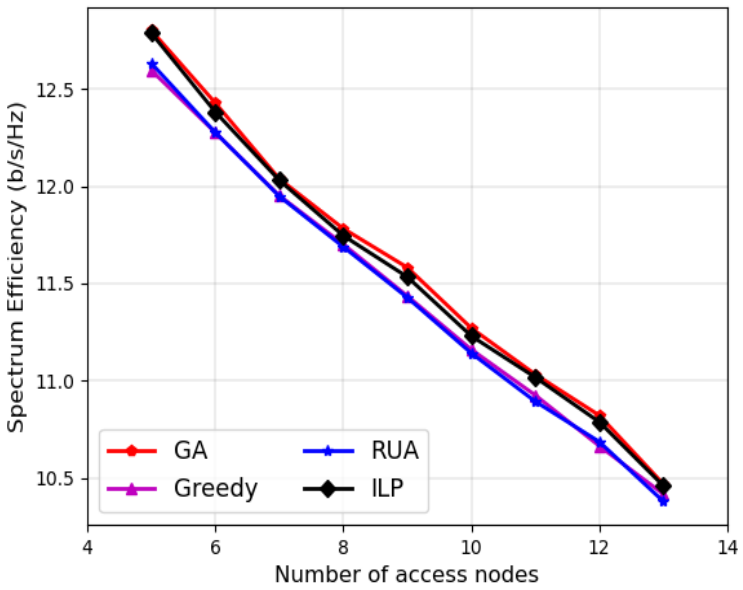

Figure 4.17: Spectrum efficiency with varying number of access nodes.

to total network bandwidth decreases as the number of access nodes increases. The GA still

outperforms the ILP, greedy, and RUA algorithms by 0.24%, 1.04%, and 1.1%, on average, respectively.

Fig. 4.18 shows that the average AR achieved by the GA, ILP, greedy, and RUA algorithms is 0.899, 0.866, 0.843, and 0.824, respectively. The GA outperforms the ILP, greedy, and RUA algorithms by 3.7%, 6.2%, and 8.3%, respectively. Since all users in the

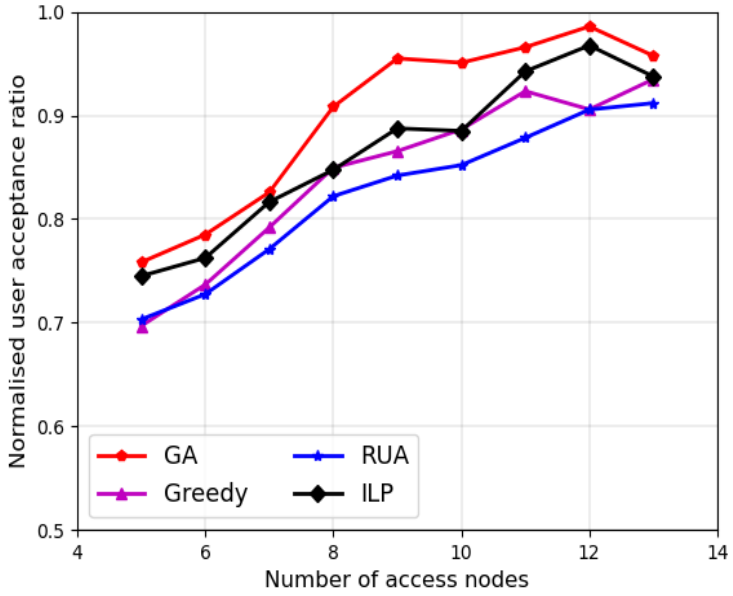

Figure 4.18: User acceptance ratio with varying number of access nodes.

network cooperatively contribute to the fitness value of the GA algorithm, this solution maximises the number of admitted users in the network. It hence achieves a higher user AR than all other algorithms. The greedy and RUA algorithms have poorer performance in terms of SE and AR since these lack the intelligence needed to maximise **P1**. The greedy algorithm associates static users based on maximum SINR, while the RUA approach does so randomly without regard for maximising the AR or achieved data rate. The ILP solution

also has a poorer AR performance than the GA since the objective function **P1** does not maximise user AR.

Moreover, Fig. 4.19 also shows that as the number of ANs in the network increases, the GA, ILP, and greedy solutions achieve superior performance in terms of handoff probability. Such high performance is attributed to the GA fitness function and the greedy algorithm formulated to associate mobile LDHMC with the AN with the largest cell radius in each TTI. Also, since maximising the handoff reduction function is part of the objectives of **P1**, the ILP solution associates the mobile users to the cell with the largest radius too. As such, the GA, ILP, and greedy algorithms achieve a handoff probability of 0. On the contrary the

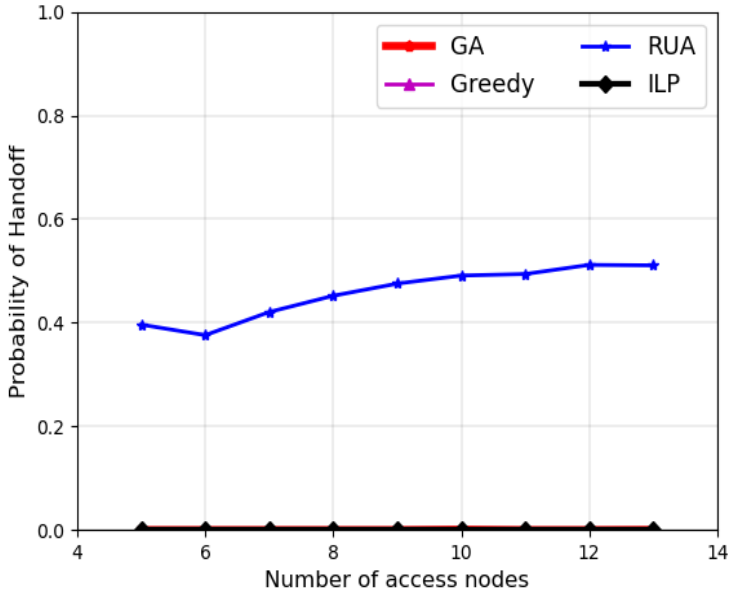

Figure 4.19: Probability of handoff with varying number of access nodes.

GA, ILP, and greedy algorithms perform better than the RUA approach regarding handoff probability by 51.8% on average. The poor performance of the RUA algorithm is attributed to the fact that a mobile user is associated with any NTN AN at random. Consequently,

the ANs chosen for the association by the RUA algorithm keep changing in each iteration. Since the GA achieves a handoff probability of 0 while maintaining the highest data rate performance, it is well suited for future scenarios characterised by highly mobile users for which increased handoff implies increased delays and a high probability of call drops due to handoff failure, consequently degrading the QoS of the users.

4.6.3.4 Impact of network overload

The previous simulations argue that the nodes with the broadest coverage should be prioritised to serve the LDHMC service group to reduce mobility-induced handoff. However, in this section, we analyse the performance of the proposed GA in a network experiencing overload conditions. To best evaluate this scenario, we decided to give the same priority to both the feMBB and LDHMC service groups to have a fair comparison in overloading conditions for both use cases. The euRLLC use case is still prioritised, and the simulation is performed considering 5 ANs, i.e., 2 MBS, 1 LAP, 1 HAP, and 1 Satcoms AN.

First, Fig. 4.20 shows that for all algorithms, there is a slight change in the SE as the number of users increases in the overloading conditions. In this condition, the limit on the number of users the network can support has already been reached, beyond which the network observes only a slight variation in SE. On average, the ILP solution outperforms the GA, greedy, and RUA algorithms by 0.6%, 1.65%, and 1.5%, respectively. We observe a decrease in performance of the GA when compared to the ILP solution during conditions of overload. This is attributed to the fact that the accuracy of the GA reduces for the same number of chromosomes and generations during conditions of overload. Nonetheless,

on average, the GA still outperforms the greedy and RUA algorithms by 0.7% and 0.54%, respectively.

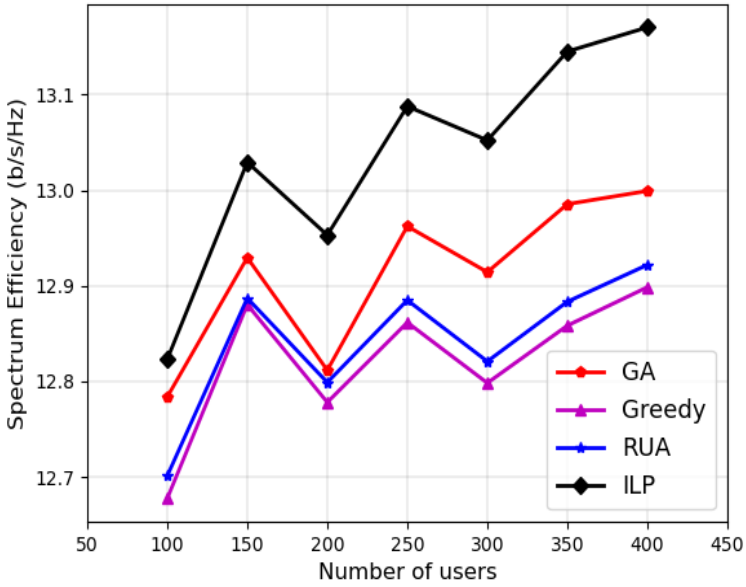

Figure 4.20: Spectrum efficiency with varying number of users.

Fig. 4.21 shows the AR of all algorithms in overloading conditions. In Fig. 4.21, the ILP solution outperforms the GA, greedy, and RUA algorithms in user AR by 1.3%, 3.3%, and 3.2%, on average, respectively, during overloading conditions. A slight reduction in user AR performance by the GA is observed when compared to the ILP solution for very high number of users. Nevertheless, the GA still outperforms the greedy and RUA algorithms. Similarly, the GA's handoff performance declines during overload conditions, as depicted by Fig. 4.22. The handoff performance of all algorithms decreases with increasing users since the ratio of the number of served LDHMC users to total LDHMC users reduces. Consequently, the ratio of the total number of users that experience a handoff during a given TTI to the total number of mobile users also decreases as the number of users increases. The performance of the GA

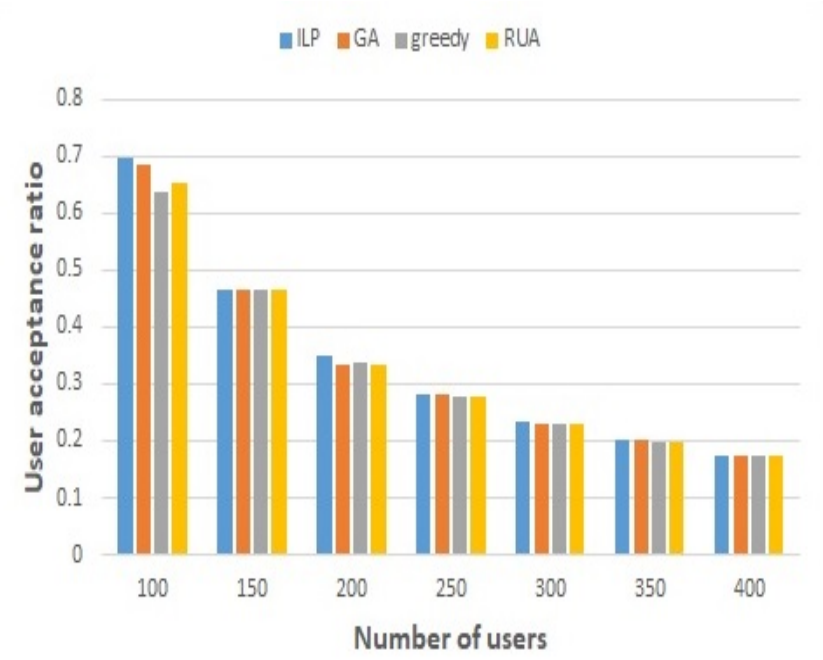

Figure 4.21: User AR under network overload conditions.

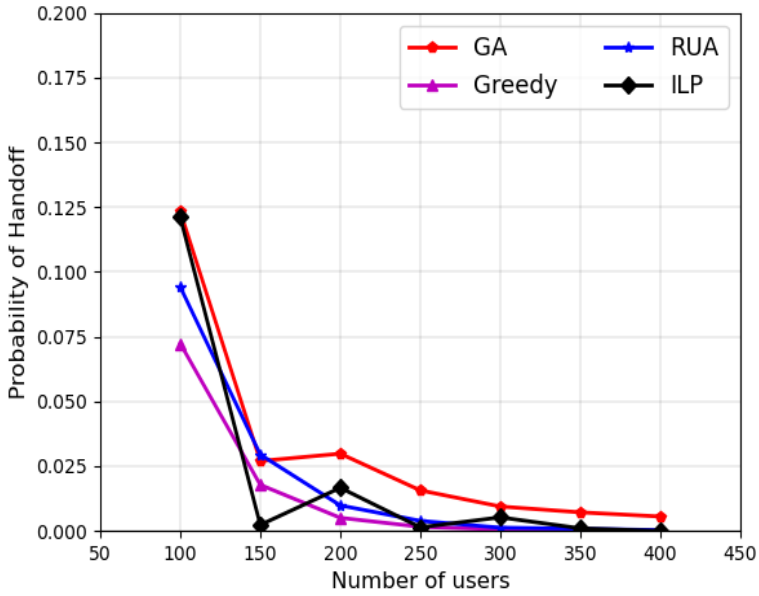

Figure 4.22: Mobility-induced handoff under network overload conditions.

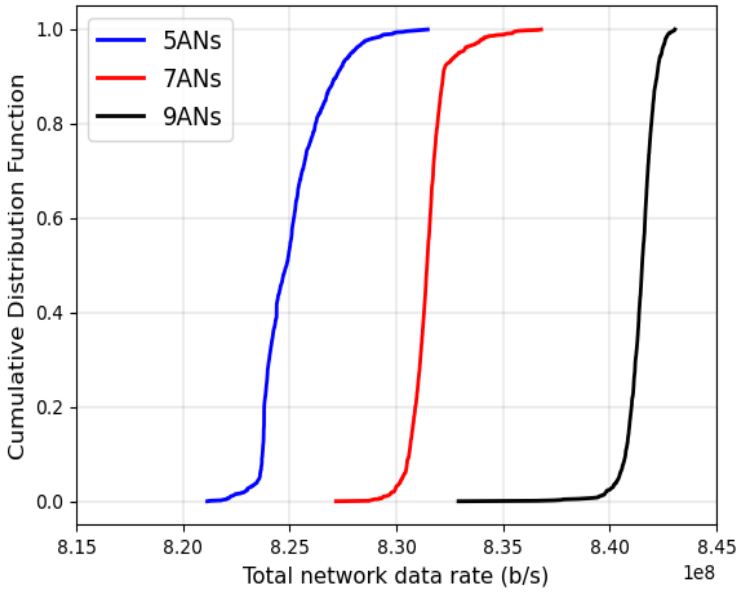

Figure 4.23: The CDF of the total network data rate using the GA.

in Figs. 4.20, 4.21, and 4.22 can be improved by increasing the number of chromosomes and generations during the simulation process. However, this increases the computation complexity as was elucidated in Section 4.3.2.4.

4.6.3.5 Cumulative Distribution Function (CDF) of the total network data rate

In this section, the CDF is used to provide an insight into the performance bounds of the proposed GA. The total network data rate performance is analysed over 1000 simulations for 80 users in a network consisting of 2 MBSs, 1 LAP, 1 HAP, and 1 satellite. Fig. 4.23 depicts the CDF for varying number of ANs in the network. The figure shows a steep rise of the CDF from 0 to 1 for all three considered number of ANs, indicating a small range within which all 1000 results fall. For instance, considering 7 ANs in the network, the figure shows the probability that a simulation will return data rate less than 8.3×10^8 b/s is almost zero

(about 0.02), while 99% of the simulations return a data rate that is less than 8.35×10^8 b/s. This gives an insight into the upper and lower bound performance, with the upper bound having a gain of about 0.6% over the lower value.

4.7 Chapter summary

This chapter presented a polynomial-time solution based on the GA to the user association sub-problem **P1**. In the GA solution, **P1** was encoded into a sequence of chromosomes, and service-dependent fitness functions were formulated to determine the near-optimal UARA solution. The simulation results showed that as the number of users in the network increased, the proposed GA achieved a user AR that was better than the ILP, greedy, and RUA solutions by 1.2%, 3.1% and 3.9%, respectively. Also, its SE performance outperformed the ILP, greedy, and RUA algorithms by 0.14% 8.45% and 7.92% on average, respectively. Moreover, the GA still presented a gain of 48.5% on average, over the RUA algorithm in terms of handoff probability.

The simulation results further revealed that for an increasing number of ANs, the proposed GA's SE outperforms the ILP, greedy and RUA schemes by 0.2%, 1.04% and 1.1% on average, respectively. Moreover, the GA outperformed the RUA algorithm in terms of handoff probability by 51.8% on average, and its user acceptance ratio outperformed the ILP, greedy and RUA algorithms on average by 3.7%, 6.2% and 8.3%, respectively. Results however showed a decline in performance of the GA during overload conditions. In these conditions, the GA performed worse than the ILP solution in terms of SE and AR, by 0.6%, and 1.3%, on average, respectively. Nonetheless, the GA outperformed the greedy and RUA

algorithms by 0.7% and 0.54% respectively in SE; and 2.07% and 1.65% respectively in terms of AR.

Chapter 5

Latency-Aware Multi-Agent Deep Reinforcement Learning for User Association and Resource Allocation in the ITNTN

This chapter investigates the use of reinforcement learning, particularly the double deep Q learning with duelling architecture, to solve the user association sub-problem **P1** defined in (3.29). Moreover, the centralised training and distributed execution framework is adopted to allow faster convergence and facilitate real-time decision-making. Furthermore, in addition to ensuring data rate QoS provisioning as done by the preceding chapters, this chapter also guarantees the delay QoS requirement for the mission-critical euRLLC service group.

5.1 Introduction

The user association sub-problem **P1**, formulated in Section 3.4.1, is a weighted sum SOOP that associates users to the appropriate ANs and further allocates the minimum resources required to meet their QoS requirements. The problem was formulated to be priority-aware, prioritising the euRLLC users to avoid their denial of service, which could be catastrophic. Moreover, to minimise the mobility-induced handoffs, the problem prioritised service provisioning of the LDHMC service group through ANs with the largest radii. Also, given the long propagation delays experienced by the satellite RAN, the optimisation problem ensured that the mission-critical users are not associated with the satellite RAN of the ITNTN.

The user association problem **P1** was observed to be an NP-complete problem and thus can be solved efficiently using variants of branch and bound algorithms. However, these require a worst-case time complexity that increases exponentially with the problem size, as was shown in Section 4.4. Near-optimal but polynomial-time solutions to NP-complete problems have been obtained in literature utilising various strategies such as meta-heuristics like the GA [143], PSO [144], and game theory [145]. As a matter of fact, Chapter 4 presented a near-optimal solution to **P1** based on the GA. However, these approaches utilise a central node that requires nearly complete information to derive the UARA solution. This information may not be available in real-time and, if available, is acquired at the expense of increased communication overheads [96]. Therefore, achieving efficient solutions without such complete information is challenging for these strategies. Besides, the metaheuristics that yield near-optimal solutions in polynomial time are still computationally complex since their

accuracy depends on parameters such as the population size and the number of generations for the GA case; thus, these algorithms are hard to execute in real time. Furthermore, given the dynamic environment of the ITNTN involving users having heterogeneous demands and RANs characterised by different peculiarities in meeting these needs, there is a need for more intelligent and flexible UARA techniques that can yield near-optimal solutions in real time.

Recently, the reinforcement learning (RL) technique has been found to provide the needed intelligence in determining efficient solutions for large-scale dynamic environments, especially wireless networks [146, 147, 148]. RL can perceive changes in such dynamic networks through interaction with the environment and making the appropriate decision. In dynamic network environments scenarios, model-free RL algorithms are often used in determining the optimal policy, primarily because they can infer decisions without prior knowledge about the system model and adapt to stochastic transitions in the system [149]. Given that Q-learning [150] is the simplest and most commonly used model-free RL algorithm, we adopt this technique to introduce intelligence and thus determine a near-optimal solution to the formulated SOOP **P1** defined in (3.29). However, the Q-learning based on the Q-table works well for a small-scale optimisation problem, yet the formulated UARA problem for the ITNTN is characterised by large state and action spaces. As such, finding the optimal policy through the Q-learning iterative process of computing and updating the Q-value table is challenging.

Making use of deep neural networks (DNNs), however, deep reinforcement learning (DRL) has shown great potential in resource management of large-scale wireless networks [146, 147, 148]. The starting point of DRL is the Deep Q-Learning (DQL) or Deep Q-Network (DQN) technique, but it is limited by the Q-value over-estimation problem [151]. We leverage the

double DQL (DDQL) algorithm proposed by [151] to solve the over-estimation issue such that optimal reward values can be obtained. Moreover, we further utilise the duelling architecture [152] that yields a more reliable Q-value for each action and thus improves the performance of DQN. Simulation results validate the higher performance of the duelling double DQN when compared to the DQN algorithm.

While it is possible to use the single agent RL to find the solution to **P1**, we agree with [153] that the single agent RL is insufficient in modelling systems with interrelated agents. In such a case, the single RL agent learns to make decisions while considering other agents as part of the environment, thereby not considering their impact on its decision and eliminating any possibilities of coordination among agents. Therefore, while using the duelling double DQN to solve the formulated problem **P1**, the centralised training and distributed execution framework is adopted, as was done by [147, 148, 123]. This framework considers a multi-agent system in which each user in the network acts as an agent. In every time step, all agents simultaneously take actions in a distributed manner and store their experiences in the replay memory. A central node then samples a batch of experiences from the replay memory, which it uses to train the centralised DQN model. After this, the new parameters are propagated to the different agents to update their copies of the DQN.

On the one hand, centralised training allows agents to learn together since they share parameters, leading to faster convergence [148]. Moreover, it also significantly reduces the computation and storage resources required for the training phase [148]. On the other hand, the distributed execution enables each user to infer a decision without knowledge of other users' CSI, facilitating real-time decision-making. Consequently, different from the

GA proposed in Chapter 4, this chapter presents a real-time solution to **P1** based on the centralised and distributed multi-agent duelling double deep Q network (MA3DQN) in which each user acts as an agent, required to determine the best AN for its service provisioning. Moreover, unlike the previous chapters, this chapter leverages the effective capacity theorem [154] to guarantee the delay QoS requirement for the mission-critical euRLLC service group. Furthermore, as was already discussed in Section 2.6.4.1, the works [92, 93, 94, 95, 96, 97, 98, 99, 100, 101] in the literature that focused on using RL to facilitate intelligence and real-time resource management in the ITNTN did not consider the integration of all the four RANs in the ITNTN. Also, they did not account for user QoS provisioning according to heterogeneous service groups nor examine the uniqueness of the different RANs in the ITNTN in meeting the contrasting user requirements, a gap that the proposed MA3DQN solution to **P1** addresses. The performance of the proposed MA3DQN solution is compared to six other algorithms: the GA and ILP solutions presented in Chapter 4, the greedy algorithm proposed in Chapter 3, the RUA algorithm, the approximation algorithm proposed by [39] to solve the generalised assignment problem (GAP), and the simulated multi-agent DQN (MADQN) algorithm. The notations used in this chapter are in Table 5.1.

5.2 System model

The system model used in this chapter is similar to that described in Section 3.2, but with minor changes that allow packetized traffic. Therefore, as was done by [155], link-layer packetized traffic is used to model data traffic arrivals at the transmission queue of an AN. Data packets that are destined to a user u_v belonging to service group $v \in \{\mathcal{R}, \mathcal{E}, \mathcal{D}\}$ arrive at

Table 5.1: Notations defined in Chapter 5.

Symbol	Description
b, l, h, s	MBS, LAP, HAP, satellite AN
$\mathcal{B}, \mathcal{L}, \mathcal{H}, \mathcal{S}$	Set of ANs in the MBS, LAP, HAP, satellite RAN
$j, n_j, \mathcal{U}$	A RAN, AN in the j-th RAN, the set of users in the ITNTN
$\upsilon, \mathcal{E}, \mathcal{R}, \mathcal{D}$	A service group, feMBB, euRLLC, LDHMC service group
$\mathcal{U}_{\mathcal{E}}, \mathcal{U}_{\mathcal{R}}, \mathcal{U}_{\mathcal{D}}$	Set of users demanding $\mathcal{E}, \mathcal{R}, \mathcal{D}$
$u, u_{\mathcal{E}}, u_{\mathcal{R}}, u_{\mathcal{D}}, u_{\upsilon}$	User, an feMBB, euRLLC, LDHMC user, user belonging to service group υ
$\mathcal{W}_j, w_j, R_{n_j}$	A set of BBUs owned by RAN j, a BBU owned by RAN j, n_j cell radius
$\mathcal{T}_{w_j}, \Phi_{n_j}, \mathcal{N}$	Bandwidth of the BBU w_j, AN n_j bandwidth, set of all ANs in the ITNTN
$\mathcal{C}_{n_j,u,w_j}$	Data rate of a user u using BBU w_j of AN n_j
$\mu_{n_j,u}, \pi^u_{n_j}$	User association variable, coverage index
δ *and* $\varphi_{u_{\upsilon}}, \varphi_{u_{\mathcal{D}}}$	Normalisation factor and penalty factors
$\lambda_{u_{\upsilon}}$, $\mathrm{L}_{u_{\upsilon}}, \mathrm{D}_{\max}, \varepsilon$	Average packet arrival rate, packet size, delay bound, delay bound violation probability
$nb^{u_{\upsilon}}_{n_j}$	Minimum number of BBUs allocated to user u belonging to service group υ by AN n_j
$\varphi, \vartheta_{u_{\mathcal{R}}}, \mathcal{C}^{min}_{u_{\mathcal{R}}}$	Effective capacity, QoS exponent, minimum delay bound rate
R_{max}	The largest possible cell radius in the ITNTN
S, A, P, R	State space, action space, transition probability, reward function
x^u_{t,n_j}	Association validity status of user u associated with AN n_j in time step t
s_t, a_t, r_t	State, action, and reward at time step t
$s^u_t, a^u_t, r^{u_{\upsilon}}_t$	State, action, and reward of agent u at time step t
$s^u, a^u, r^{u_{\upsilon}}$	State, action, and reward of agent u
s, a, r, s'	Current state, action taken at state s, reward obtained, next state
γ, α	Discount factor, learning rate
ξ^u_t, UV^u_t, LF^u_t	Coverage vector, achievable utility vector, loading status vector of user/agent u to different ANs in time step t
$\xi^u_{t,n_j}, UV^u_{t,n_j}, LF^u_{t,n_j}$	Coverage status, achievable utility value, loading status of agent u to AN n_j in time step t

the AN transmission queue periodically, following a Poisson process with an average arrival rate of $\lambda_{u_{\upsilon}}$ packets/s, each packet having a size $\mathrm{L}_{u_{\upsilon}}$ bits $\forall \upsilon \in \{\mathcal{R}, \mathcal{E}, \mathcal{D}\}$.

5.2.1 Delay QoS model

The Shannon capacity depicted by (3.10) does not consider the QoS delay requirement, which is critical for the euRLLC users. Given the stochastic behaviour of the mission-critical $\mathcal{U}_{\mathcal{R}}$ users, we employ the effective capacity theorem defined in [154] to guarantee their delay QoS, as was done by [35]. The effective capacity is used in this work because of its implementation simplicity, high accuracy, and ease in translating delay-bound QoS metrics into guarantees. Therefore, the effective capacity theorem determines the minimum achievable rate bounded by a specified latency violation probability. In this regard, considering an euRLL user $u_{\mathcal{R}}$, its effective capacity is given by [154]

$$\varphi(\vartheta_{u_{\mathcal{R}}}) = \lim_{t\to\infty} \frac{1}{t}\frac{1}{\vartheta_{u_{\mathcal{R}}}} \log \mathbb{E}\left[e^{\vartheta_{u_{\mathcal{R}}} Z^{t}_{\vartheta_{u_{\mathcal{R}}}}}\right], \tag{5.1}$$

where $\vartheta_{u_{\mathcal{R}}}$ is the QoS exponent, $Z^{t}_{\vartheta_{u_{\mathcal{R}}}}$ is the number of data packet arrivals of user $u_{\mathcal{R}}$ over the time interval $[0, 1)$ and $\mathbb{E}[\cdot]$ denotes the expectation operator.

Employing the definition of the moment generating function of a Poisson process over the time interval $[0, t)$, (5.1) is further derived as [156]

$$\varphi(\vartheta_{u_{\mathcal{R}}}) = \frac{\lambda_{u_{\mathcal{R}}}(e^{\vartheta_{u_{\mathcal{R}}}} - 1)}{\vartheta_{u_{\mathcal{R}}}}, \tag{5.2}$$

where $\lambda_{u_{\mathcal{R}}}$ packets/s is the average arrival rate of data packets arriving at an euRLLC user.

On the other hand, utilising the large deviation theory [154, 157], the probability that the downlink transmission delay $\mathrm{D}^{u_{\mathcal{R}}}_{n_j}$ of an euRLLC packet from AN n_j to user $u_{\mathcal{R}}$ exceeding

a delay bound $\mathrm{D}_{\max}$ is approximated as

$$Pr\{\mathrm{D}_{n_j}^{u_{\mathcal{R}}} \geqslant \mathrm{D}_{\max}\} \approx e^{-\vartheta_{u_{\mathcal{R}}} \lambda_{u_{\mathcal{R}}} \mathrm{D}_{\max}} \leqslant \varepsilon, \tag{5.3}$$

where ε is the delay bound violation probability threshold. The minimum achievable rate $\lambda_{u_{\mathcal{R}}}^{min}$ in packets/s can be obtained from (5.3) as

$$\lambda_{u_{\mathcal{R}}}^{min} = -\frac{\log_e \varepsilon}{\vartheta_{u_{\mathcal{R}}} \mathrm{D}_{\max}}. \tag{5.4}$$

According to the effective capacity theory [154], the delay bound violation probability can be guaranteed not to exceed the threshold ε in (5.3) only if $\lambda_{u_{\mathcal{R}}}^{min}$ is equal to the effective capacity $\varphi(\vartheta_{u_{\mathcal{R}}})$. Therefore, equating (5.4) to (5.2) and after carrying out some algebraic manipulation as illustrated in Appendix A, the minimum rate in bits/s that guarantees the bound on the delay violation probability can be expressed as

$$\mathcal{C}_{u_{\mathcal{R}}}^{min} = -\frac{\mathrm{L}_{u_{\mathcal{R}}} \log_e \varepsilon}{\mathrm{D}_{\max} \log_e \left(1 - \dfrac{\log_e \varepsilon}{\lambda_{u_{\mathcal{R}}} \mathrm{D}_{\max}}\right)}, \tag{5.5}$$

where $\mathrm{L}_{u_{\mathcal{R}}}$ is the euRLLC user's packet size.

5.3 Problem formulation

In this section, the optimisation problem **P1** formulated in Chapter 3 is recalled and updated to account for packetized traffic and the guarantee on delay QoS for the euRLLC service

group. The QoS requirement for the feMBB and LDHMC use cases is maintained as data rate. Recall that the objective function of problem **P1** was a weighted-sum SOOP comprising two functions, the achieved total network data rate and the network handoff reduction. For purposes of clarity, the objective function is rewritten below:

$$\chi = \alpha' \ \delta_1 \sum_{n_j \in \mathcal{N}} \sum_{u \in \mathcal{U}} \rho_{u_\upsilon} \ \mu_{n_j,u} \ nb_{n_j}^{u_\upsilon} \ \mathcal{C}_{n_j,u,w_j} \ + \ (1-\alpha') \ \delta_2 \ \sum_{n_j \in \mathcal{N}} \sum_{u \in \mathcal{U}} \rho_{u_\upsilon} \ \mu_{n_j,u} \ \frac{R_{n_j}}{R_{max}}, \quad (5.6)$$

where α' provides a trade-off between data rate maximisation and handoff reduction maximisation. δ_1 and δ_2 are normalisation factors while ρ_{u_υ} enables prioritisation of a user u belonging to any service group $\upsilon \in \{\mathcal{R}, \mathcal{E}, \mathcal{D}\}$. $\mu_{n_j,u}$ is a binary association factor that is 1 when the user u is associated to the AN n_j, and 0 otherwise. $nb_{n_j}^{u_\upsilon}$ is the minimum number of BBUs that AN n_j allocates to user u belonging to the service group υ to meet its QoS requirements. On the other hand, $\mathcal{C}_{n_j,u,w_j}$ is the data rate that the AN n_j allocates a user u over the BBU w_j. In contrast, R_{n_j} is n_j's cell radius while R_{max} is the largest cell radius in the ITNTN. Thus, taking into consideration packetized traffic and delay QoS requirements for mission-critical users, the formulated problem is then given as

P4:

$$\max_{\mu_{n_j,u}} \quad \chi \quad (5.7)$$

s.t.

C1: $\mu_{n_j,u} \leq \pi_{n_j,u}, \quad \forall \ n_j \in \mathcal{N}, \quad \forall \ u \in \mathcal{U}$

C2: $\sum_{n_j \in \{\mathcal{B} \ \cup \ \mathcal{L} \ \cup \ \mathcal{H}\}} \pi_{n_j,u} \ \mu_{n_j,u} \quad \leqslant \quad 1, \quad \forall \ u_{\mathcal{R}} \in \mathcal{U}_{\mathcal{R}}$

$$\text{C3:} \sum_{n_j \in \{\mathcal{S}\}} \pi_{n_j,u}\ \mu_{n_j,u} \quad = \quad 0, \quad \forall\ u_{\mathcal{R}} \in \mathcal{U}_{\mathcal{R}}$$

$$\text{C4:} \sum_{n_j \in \mathcal{N}} \pi_{n_j,u}\ \mu_{n_j,u} \quad \leqslant \quad 1, \quad \forall\ u_{\mathcal{D}} \in \mathcal{U}_{\mathcal{D}},\ u_{\mathcal{E}} \in \mathcal{U}_{\mathcal{E}}$$

$$\text{C5:}\ nb_{n_j}^{u_\upsilon} = \left\lceil \frac{\lambda_{u_\upsilon}\ \mathrm{L}_{u_\upsilon}}{\mathcal{C}_{n_j,u,w_j}} \right\rceil, \quad \forall\ \upsilon \in \{\mathcal{E}, \mathcal{D}\}, \quad \forall u_{\mathcal{E}} \in \mathcal{U}_{\mathcal{E}}^{assoc}, \quad \forall u_{\mathcal{D}} \in \mathcal{U}_{\mathcal{D}}^{assoc}$$

$$\text{C6:}\ nb_{n_j}^{u_{\mathcal{R}}} = \left\lceil \frac{\mathcal{C}_{u_{\mathcal{R}}}^{min}}{\mathcal{C}_{n_j,u,w_j}} \right\rceil, \quad \forall\ u_{\mathcal{R}} \in \mathcal{U}_{\mathcal{R}}^{assoc},$$

$$\text{C7:} \sum_{u \in \mathcal{U}} \pi_{n_j,u}\ \mu_{n_j,u}\ nb_{n_j}^{u_\upsilon}\ \mathcal{T}_{w_j} \leq \Phi_{n_j}, \quad \forall\ n_j \in \mathcal{N}$$

$$\text{C8:}\ \mu_{n_j,u} = \{0, 1\}, \quad \forall\ u \in \mathcal{U}\ \ \forall\ j \in \{\mathcal{B}, \mathcal{H}, \mathcal{L}, \mathcal{S}\}, \quad \forall\ n_j \in \mathcal{N}.$$

In constraint C1, $\pi_{n_j,u}$ represents a binary index that is 1 when the user lies in the AN's coverage and 0 otherwise. Therefore, C1 ensures that a user can only associate with an AN in whose coverage the user lies. In contrast, the constraints C2, C3, and C4 allow a user to be served by, at most, one AN that can meet the QoS requirements of the user. Constraint C5 ensures that a served feMBB or LDHMC user receives the minimum number of BBUs required to meet its data rate, while in C6, the minimum number of BBUs that guarantee the delay bound rate of an ueRLLC user is assured. The operator, $\lceil \cdot \rceil$ in C5 and C6, ensures that a BBU is allocated to at most one user. On the other hand, $\mathcal{U}_{\mathcal{E}}^{assoc}$, $\mathcal{U}_{\mathcal{D}}^{assoc}$, and $\mathcal{U}_{\mathcal{R}}^{assoc}$ in C5 and C6 define sets of associated users belonging to $\mathcal{E}$, $\mathcal{D}$, and $\mathcal{R}$, respectively, such that $\mathcal{U}_{\mathcal{E}}^{assoc} \cup \mathcal{U}_{\mathcal{D}}^{assoc} \cup \mathcal{U}_{\mathcal{R}}^{assoc} = \mathcal{U}_{associated}$, where $\mathcal{U}_{associated}$ is the set of users for which $\mu_{n_j,u} = 1$. C7 ensures that the AN's resource budget is not exceeded, while C8 assures that the user association variable is binary.

The optimisation problem **P4**, just like **P1**, is a $(0, 1)$ ILP problem. Chapter 4 demonstrated that an ILP solution to such a problem can be determined using LP relaxation and branch and bound via the Gurobi solver. However, it was seen that this solution has a computational complexity that increases exponentially with the network dimension and thus is inappropriate, especially in large-scale networks such as the ITNTN. Moreover, such high-time complexity is not well suited for 6G scenarios characterised by delay-sensitive applications. The GA solution was proposed in Chapter 4 to obtain a near-optimal solution in polynomial time for the optimisation problem **P1**. Still, this requires near-complete information by a central node to obtain the near-optimal solution. Such information may be unavailable in real-time and, if available, is acquired at the expense of increased communication overheads [96]. Besides, the GA solution is still computationally expensive, as its accuracy depends on parameters such as the number of generations and population size, which must be high to obtain a good solution. Thus, the GA does not give a real-time solution.

However, works in literature such as [123, 96] have demonstrated the capability of RL approaches in finding near-optimal solutions to combinatorial optimisation problems characterised by dynamic environments. Moreover, the intelligence obtained after training in the RL algorithms enables these schemes to make real-time decisions. Consequently, this chapter investigates using RL to solve the problem **P4**. In particular, the work embraces the centralised training and distributed execution framework to reduce the computation resources and memory required for training and allow real-time decision-making by the users without needing to know other users' information in the network.

5.4 The proposed reinforcement learning (RL) user association solution

The proposed multi-agent duelling double deep Q-learning solution to problem **P4** is described in this section, but first, a brief review of RL, including the Q-learning and DRL techniques, is expounded.

5.4.1 A review on Q-learning and deep reinforcement learning (DRL)

In a single-agent RL system, an agent interacts with an environment by taking actions to maximise some reward. Such a problem can be modeled as a Markov decision process (MDP) represented by a tuple (S, A, P, R). S represents the set of possible states of the environment, A denotes the action space, $P = P(s_{t+1} \mid s_t, a_t)$ is the transition probability from state s_t to s_{t+1} after executing action a_t, and $R = R(s_t, a_t)$ is the reward function [158]. According to Fig. 5.1, each time step t involves an agent observing the current state $s_t \in S$ of the environment and selecting an action $a_t \in A$ according to a policy $\pi(a_t \mid s_t)$. The agent executes the selected action, receives a reward $r_{t+1} = R(s_t, a_t)$ and then the environment transitions to a new state $s_{t+1} \in S$ with transition probability $P(s_{t+1} \mid s_t, a_t)$. The agent continues this process until the terminal state is reached, marking the end of an episode, after which the process is repeated in a new episode. The accumulated discounted reward

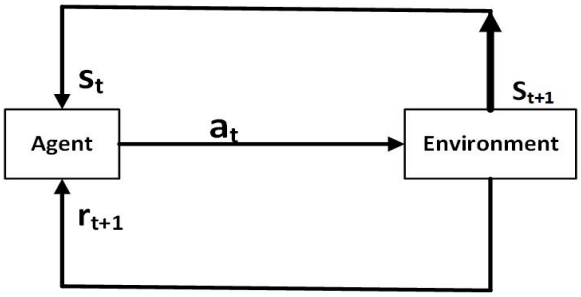

Figure 5.1: The agent–environment interaction in a Markov decision process.

in time step t is defined as [158]

$$G_t = \sum_{k=0}^{\infty} \gamma^k r_{t+k+1}, \tag{5.8}$$

where $\gamma \in [0, 1)$ is the discount factor used to determine the present value of future rewards. When $\gamma = 0$, the agent is only concerned about maximising immediate rewards, and as γ approaches 1, the agent becomes more far-sighted and considers future rewards more strongly. The agent's goal is to learn a policy $\pi : S \rightarrow A$ that maximises the expected accumulated discounted reward across any given episode. The Q-learning algorithm has been used extensively in scenarios involving dynamic network environments to determine this policy.

5.4.1.1 Q-learning

The Q-learning RL algorithm's policies are characterised by the state-action value function (Q-function/Q-value). The Q-function $Q^\pi(s, a)$ for the state-action pair (s, a) under policy π gives the fitness value of performing action a when the environment is in state s. In other words, $Q^\pi(s, a)$ is the expected return an agent accumulates when the environment starts from state s and the agent takes action a and thereafter follows the policy π. Mathematically,

the Q-function is defined as

$$Q^{\pi}(s,a) = \mathbb{E}\left(\sum_{k=0}^{\infty} \gamma^{k} r_{t+k+1} \mid s_t = s, a_t = a\right), \tag{5.9}$$

where $\mathbb{E}(\cdot)$ denotes the expectation operator. The optimal Q-function is then given by $Q^{*}(s,a) = \max_{\pi} Q^{\pi}(s,a)$. $Q^{*}(s,a)$ obeys the Bellman optimality equation given by [158]

$$Q^{*}(s,a) = \mathbb{E}\left(r_{t+1} + \gamma \max_{a'} Q^{*}(s_{t+1}, a') \mid s_t = s, a_t = a\right), \tag{5.10}$$

where a' is an action in the next state s_{t+1}. Once the optimal Q-function $Q^{*}(s,a)$ is known, the optimal policy π^{*} for any given state $s \in S$ is determined by simply selecting the action that gives the highest Q-function, that is,

$$\pi^{*}(s) = \operatorname*{argmax}_{a} \; Q^{*}(s,a). \tag{5.11}$$

Based on the agent's experience $< s, a, r, s' >$, where s is the current state, a is the action taken at state s, r is the reward obtained from the environment after executing action a at current state s, and s' is the next state, Q-learning updates $Q^{*}(s,a)$ recursively [158]. The update formula is given as

$$Q(s,a) \leftarrow Q(s,a) + \alpha \, [r + \gamma \max_{a'} Q(s',a') - Q(s,a)]. \tag{5.12}$$

The time index is dropped in (5.12) for simplicity. $\alpha \in [0, 1]$ is the learning rate used to determine how much newly acquired information overrides the old information. The term $r + \gamma \max_{a'} Q(s', a')$ in (5.12) is referred to as the target, while $Q(s, a)$ is the estimation. The Q-values for all possible state-action pairs are stored in a table referred to as the Q-table, such that $Q : S \times A \rightarrow \mathbb{R}$.

The exploitation versus exploration dilemma must be addressed when deciding which action to take for any state. During exploitation, the agent exploits the acquired knowledge to improve performance by taking the action with the highest Q-function. On the other hand, exploration allows the agent to take any random action to explore the environment and possibly get better performance than what is already known. Consequently, there is a need to consider the trade-off between exploitation and exploration during the action selection procedure. One simple but very efficient strategy is the ϵ-*greedy* decision policy. In the ϵ-*greedy* strategy, a random action is taken with probability $\epsilon \in (0, 1)$, while a greedy action is chosen with probability $1 - \epsilon$. ϵ is set to one at the beginning of the training period, and as the agent learns, it is decayed by a predefined rate until it is 0.1 and fixed after that [159].

5.4.1.2 Deep Q-learning (DQL)

Q-learning performs well for problems with small state and action spaces. However, as the state and action spaces increase, the iterative process for updating the different possible state-action pairs becomes computationally inefficient mainly because of two reasons [149]. First, the computational resources and time needed to traverse all the different state-action

pairs to update their Q-values become infeasible. Second, the amount of storage needed for the Q-table increases exponentially with the state and action spaces. Therefore, instead of storing a lookup table of Q-values, recent research has proposed using function approximators to estimate the Q-function. Since neural networks (NNs) can be used to approximate any function, [159] proposed the DQL (also known as DQN) framework that integrates Q-learning with multi-layer NNs (also called DNNs). In DQL, the agent's state s is the input to the DNN, which then predicts the Q-value $Q(s, a)$ for each possible action a in the given input state s. If the optimal Q-function $Q^*(s, a)$ is known, the obvious strategy is for the agent to choose the next action as that with the highest Q-value [153]. The DNN in DQN is characterised by a set of weights θ that are used to determine the Q-function. Consequently, the task of finding the optimal Q-function $Q^*(s, a)$ is essentially limited to searching the best θ, such that $Q(s, a; \theta) \approx Q^*(s, a)$ [123]. Simply utilising the DQN to estimate the Q-function often leads to learning instability. Two proposals have been applied to the DQN to limit the learning instability [160, 161]:

i) Instead of using one DQN to evaluate both the target and estimation in (5.12), two DQNs: the target $\overline{Q}(s, a; \overline{\theta})$ DQN and online $Q(s, a; \theta)$ DQN, having similar structure are utilised. More specifically, for any experience $< s, a, r, s' >$, the target DQN is used to estimate the target $r + \gamma \max_{a'} \overline{Q}(s', a'; \overline{\theta})$ while the online network calculates the estimation $Q(s, a; \theta)$. The weights of the online DQN network are updated in each time step to minimise the loss function defined by

$$Loss_{DQN}(\theta) = [y_{DQN} - Q(s, a; \theta)]^2, \tag{5.13}$$

where $y_{DQN} = r + \gamma \max_{a'} \overline{Q}(s', a'; \overline{\theta})$. On the other hand, the set of weights $\overline{\theta}$ of the target network are updated after every τ time steps and set to be equal to θ.

ii) In each time step, the experience $< s, a, r, s' >$ is stored in the experience memory D. Therefore, instead of using only the current experience $< s, a, r, s' >$ of each time step during the learning process, the online DQN is trained by a mini-batch B of experiences sampled randomly from D. This strategy, commonly known as the experience or memory replay, is used to reduce the correlation among training samples and, as such, ensure that the optimal policy is not driven to a local minima [160].

5.4.1.3 Double DQN (DDQN)

In DQN, the max operator in the target ($r + \gamma \max_{a'} \overline{Q}(s', a'; \overline{\theta})$) uses the same network to both select and evaluate an action. This leads to a maximisation bias problem, making the Q-value function overly optimistic [158]. To solve this problem and consequently improve performance, the DDQN [151] is proposed, in which the online network selects the next state best action, and the target network determines the Q-value of the selected action. Therefore, the loss function in DDQN is given by

$$Loss_{DDQN}(\theta) = [y_{DDQN} - Q(s, a; \theta)]^2, \tag{5.14}$$

where $y_{DDQN} = r + \gamma \, \overline{Q}(s', \text{argmax}_{a'} \; Q(s', a'; \theta); \overline{\theta})$.

5.4.1.4 The duelling architecture

In the DQN and DDQN, the DNN of either the online or target network determines the Q-value $Q(s,a)$, which represents the value of choosing action a while in state s. However, the duelling architecture proposed by [152] decouples the estimation of $Q(s,a)$ into two separate estimators: i) the state value function $V(s)$ that estimates how good it is for an agent to be in state s, and, ii) the advantage function $A(s,a)$ that gives the advantage of taking action a at state s. Therefore, in the duelling architecture, the last hidden layer of the DNN is split into two sub-networks to estimate $V(s)$ and $A(s,a)$ separately, as depicted by Fig. 5.2. The two streams $V(s)$ and $A(s,a)$ are combined through an aggregation layer to give the Q-function $Q(s,a)$. The aggregation layer combines $V(s)$ and $A(s,a)$ according to [152]:

$$Q(s,a;\theta,\alpha,\beta) = [V(s;\theta,\beta) + \left(A(s,a;\theta,\alpha) - \max_{a' \in A} A(s,a';\theta,\alpha)\right), \tag{5.15}$$

where θ are the mutual parameters for $V(s)$ and $A(s,a)$ while β and α are the unique parameters for determining $V(s)$ and $A(s,a)$ respectively. The duelling architecture leads to more reliable Q-values since it considers the state's value, thus improving performance.

5.4.2 The proposed multi-agent duelling double deep Q-network (MA3DQN) solution

The proposed MA3DQN solution to the problem in (5.7) is presented in this section. First, we present the multi-agent MDP formulation of the problem and later discuss the MA3DQN process.

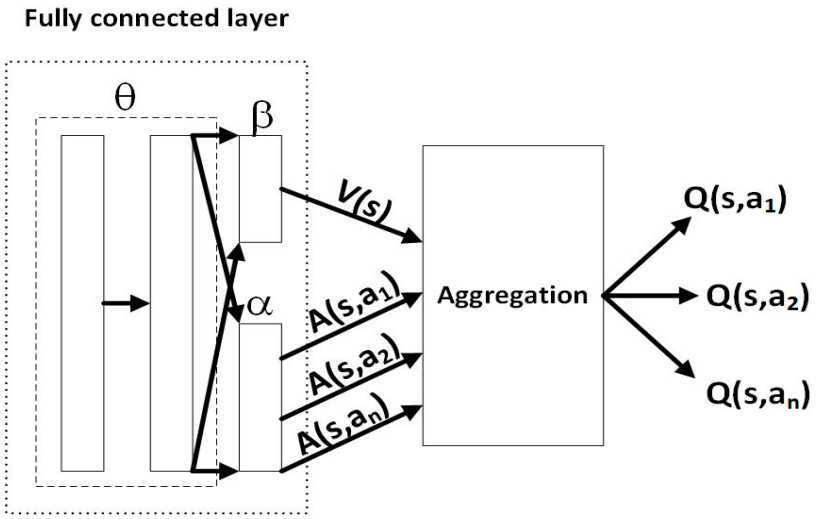

Figure 5.2: The duelling architecture.

5.4.2.1 The multi-agent MDP formulation

Similar to [148, 123], we propose a multi-agent RL solution in which each user u is an agent, observing a local state $s_t^u \in S^u$ of the environment, and taking an action $a_t^u \in A^u$ at time step t, with the objective of maximising its long-term accumulative reward. Since other agents' actions affect each agent's decision, the multi-agent RL is modeled as an extended MDP [162]. The three key components of the extended MDP model, i.e., state, action, and reward, are defined as follows.

i) State: The state of the environment as observed by agent u at time step t, s_t^u is defined by relevant features of both the agent and the environment that enable the agent to choose actions that lead to a high cumulative reward. Consequently, the state of each agent consists of four parts: i) The agent's service group $u_v \in \{\mathcal{E}, \mathcal{R}, \mathcal{D}\}$. This feature lets the agent know which ANs are incapable or suitable for service provisioning based on its service group. ii) An $\mid \mathcal{N} \mid$ dimensional vector ξ_t^u that represents the coverage status

of the agent u by the different ANs at time step t, i.e., $\xi_t^u = (\xi_{t,1}^u, \xi_{t,2}^u, \ldots, \xi_{t,|\mathcal{N}|}^u) \in \mathbb{R}^{|\mathcal{N}|}$. $\xi_{t,n_j}^u \in \{0,1\}\ \forall n_j \in \{1,2,\ldots,|\mathcal{N}|\}$ denotes the coverage status of AN n_j to the agent u in time step t. $\xi_{t,n_j}^u = 1$ if in time step t, the agent u is within the AN n_j's coverage, and it is 0 otherwise. iii) An $|\mathcal{N}|$ dimensional vector $UV_t^u = (UV_{t,1}^u, UV_{t,2}^u, \ldots, UV_{t,|\mathcal{N}|}^u) \in \mathbb{R}^{|\mathcal{N}|}$ with the entry UV_{t,n_j}^u being a function of the achievable utility of an agent u if served by AN n_j in time step t. For a static user, UV_{t,n_j}^u is the normalised data rate $\delta\mathcal{C}_{n_j,u,w_j}$ achieved on a single BBU. δ is used to normalise the data rate $\mathcal{C}_{n_j,u,w_j}$ given by (3.10). Since the RANs in the ITNTN have differently sized BBUs, the allocated data rate depends on both the SINR from the AN and the bandwidth of the AN's BBUs. As such, the achievable data rate on a single BBU is a relevant feature that can guide an agent to choose more rewarding actions. On the other hand, the value of UV_{t,n_j}^u for a mobile user is given by the handoff reduction ratio (R_{n_j}/R_{max}) in (5.6). With this feature, an agent can learn which ANs result in a high utility value and which yield a low one. iv) An $|\mathcal{N}|$ dimensional vector $LF_t^u = (LF_{t,1}^u, LF_{t,2}^u, \ldots, LF_{t,|\mathcal{N}|}^u) \in \mathbb{R}^{|\mathcal{N}|}$ that gives the loading factor of the different ANs as observed by the agent u in time step t. The entry LF_{t,n_j}^u in LF_t^u gives the number of available BBUs on the AN n_j observed by the agent u during the time step t. Thus, the state of the user u at time t is given as $s_t^u = \{u_v, \xi_t^u, UV_t^u, LF_t^u\}$.

A question that can arise is how an agent obtains the information in the observed state. We assume that the ANs are indexed, with each AN having a copy of the index vector $[1,2,\ldots,|\mathcal{N}|]$, such that $n_j \in [1,2,\ldots,|\mathcal{N}|]$. Once a user completes the channel measurement of AN n_j, it is within the AN's coverage; hence, the entry corresponding

to n_j in the vector ξ_t^u is set to 1; otherwise, it is set to 0. Also, utilising the unique pilot signals that are constantly broadcast by ANs [131], the users can estimate the channel gain of ANs within their coverage and determine the vector UV_t^u. Moreover, using message passing between ANs through the backhaul communication links [146], the loading status of ANs within the user's coverage can be obtained. Message passing incurs negligible communication overhead [146]. However, because any neural network-based architecture is trained with a fixed state dimension, users must maintain information about the achievable utility value and loading status of all ANs, even those out of their coverage. Therefore, the entries in UV_t^u and LF_t^u vectors corresponding to the ANs that are out of the user's reach are filled with dummy values chosen to be the worst possible values. In this way, the ANs that are reachable to the user will have higher Q-values than those out of the user's reach.

ii) Actions: To increase convergence speed, we limit the action set A^u of the agent u to consist of only ANs within the agent's coverage. Therefore, in each time step t, an agent u performs an action a_t^u that consists of choosing an AN $n_j \in A^u$ for the association.

iii) Reward: The reward function is designed to maximise the objective of the problem (5.7). Since the objective is to maximise static users' data rate while minimising mobile users' mobility-induced handoffs, the reward depends on whether the user/agent is static or mobile.

Reward function for a static user

Static users are associated with the appropriate ANs to maximise the network data rate. Consequently, the reward function of a static user u in time t is defined as

$$\begin{gathered} r_t^{u_\upsilon} = x_{t,n_j}^{u} \left(\delta\, \mathcal{C}_{n_j,u,w_j}\right) \quad - \quad \varphi_{u_\upsilon}(1 - x_{t,n_j}^{u}), \\ \forall\ u_{\mathcal{R}} \in \mathcal{U}_{\mathcal{R}}, \quad u_{\mathcal{E}} \in \mathcal{U}_{\mathcal{E}}, \quad \upsilon \in \{\mathcal{R}, \mathcal{E}\}, \end{gathered} \tag{5.16}$$

where $\delta\mathcal{C}_{n_j,u,w_j}$ is the normalised data rate achieved by user u over one BBU w_j of AN n_j. $x_{t,n_j}^{u} \in \{0,1\}$ denotes the association validity status of the user u associated with AN n_j during time t. $x_{t,n_j}^{u} = 1$, if the association of user u with the AN n_j is valid and 0 otherwise. The association of user u with the AN n_j is valid if the AN is capable of serving the user and has enough resources to meet the QoS requirements of the user, as mandated by C5 and C6 in **P4** for an feMBB/LDHMC or euRLLC user respectively. $\varphi_{u_\upsilon} \in [0,1]$ is the penalty cost incurred when a static user u_υ belonging to service group $\upsilon \in \{\mathcal{E}, \mathcal{R}\}$ is not served. The penalty φ_{u_υ} is varied depending on the service class υ of the user. The reward function of a mission-critical user is subjected to a higher value of φ_{u_υ} in order to prevent denial of service for this use-case.

Reward function for a mobile user

A mobile user u belonging to the $\mathcal{D}$ service group aims to minimise mobility-induced handoffs. Ultimately, using the handoff reduction ratio (R_{n_j}/R_{max}) defined in function

(5.6), the reward function of such a user is defined as

$$r_t^{u_{\mathcal{D}}} = x_{t,n_j}^u \ (R_{n_j}/R_{max}) \quad - \quad \varphi_{u_{\mathcal{D}}}(1 - x_{t,n_j}^u), \ \forall \ u_{\mathcal{D}} \in \mathcal{U}_{\mathcal{D}}, \tag{5.17}$$

where $\varphi_{u_{\mathcal{D}}}$ is a penalty for not serving a $u_{\mathcal{D}}$ user. $\varphi_{u_{\mathcal{D}}}$ is also used to prioritise the association of mobile users to ANs with the largest cell radius in order to minimise mobility-induced handoffs. Consequently, $\varphi_{u_{\mathcal{D}}}$ is high if a mobile user is associated with an AN with a small cell radius and yet resources are still available in the cell with large radius.

At each time step t, a user u as an agent observes the state s_t^u of the environment and accordingly takes action $a_t^u \in A^u$ according to a policy π, selecting an AN within its coverage, which is capable of meeting its QoS requirements.

5.4.2.2 The MA3DQN process

The user association and resource allocation problem **P4** in (5.7) is solved utilising the DDQN strategy with duelling architecture and experience replay as depicted in Fig. 5.3. Also, the approach used to solve this problem is based on centralised training and distributed execution, as was done by [148, 123]. Therefore, the MA3DQN process consists of two phases. The first is the offline training procedure, in which agents simultaneously take actions in a distributed manner, store their experiences in the replay memory, and a central node executes centralised training. In the second phase, each user performs the online distributed execution using the trained model to determine the best association decision.

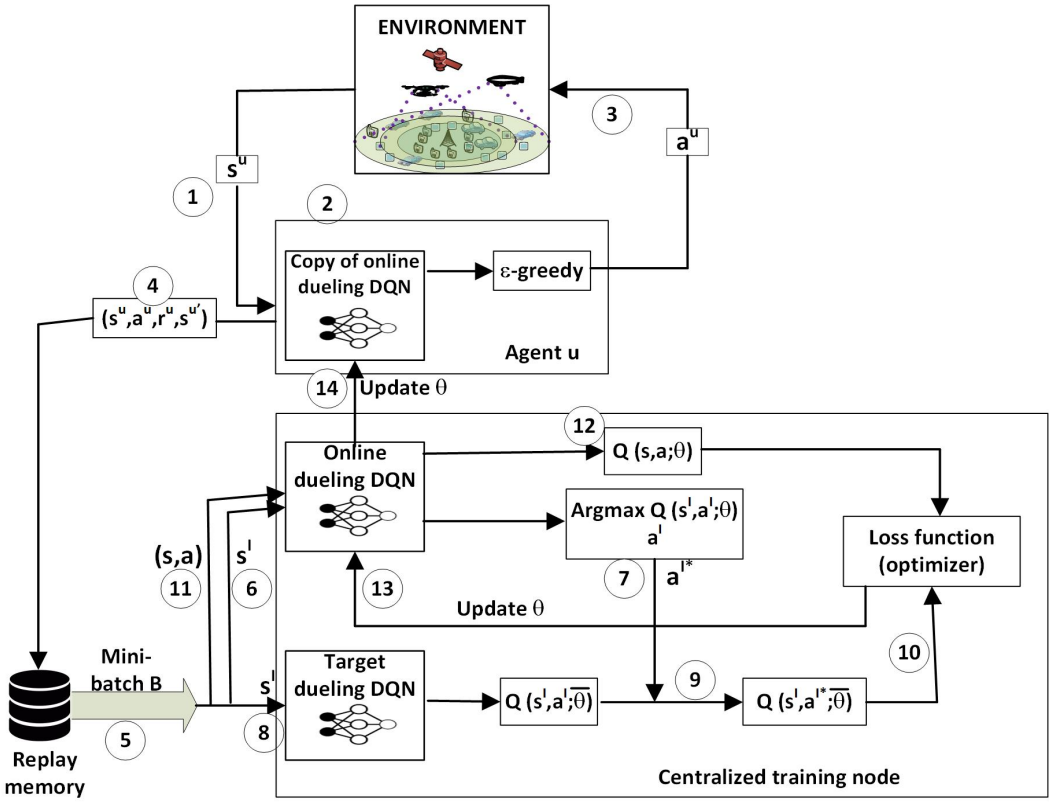

Figure 5.3: The training process utilising the DDQN architecture.

As depicted by Fig. 5.3, each agent u has the same copy of the online DQN, which it uses to select an action (AN to associate with). The online DQN is trained by a central node, using experiences gathered from all agents. The centralised training approach is similar to the parameter-sharing concept presented in [163]. Parameter sharing allows the agents to share parameters of a single policy, which is trained with the experiences of different agents simultaneously, thereby allowing the agents to learn together and thus achieve faster convergence and stability. Moreover, it significantly reduces the computation and storage resources required for the training phase, as only a single policy is trained. Besides, even if the agents share the same parameters, this approach still allows different behaviour between agents since each receives a different observation.

The offline training phase

In the following description, we drop the time index since the procedure happens within a single timestep. As illustrated by Fig. 5.3, an agent u observes the current state s^u of the environment (step 1). The agent then uses its copy of the online DQN and the ϵ-*greedy* decision policy in step 2 to determine the action a^u to take, i.e., the AN n_j to connect to and executes the action in step 3. If the chosen AN can serve the user and still has sufficient resources to meet the user's QoS requirements, the user receives a positive reward. Otherwise, it receives a negative reward as a penalty, as discussed in Section 5.4.2.1. All agents are synchronized to take their actions simultaneously. In step 4, the agent observes the reward r^{u_υ} $\forall \upsilon \in \{\mathcal{R}, \mathcal{D}, \mathcal{E}\}$ and the next state $s^{u'}$, and stores the experience $< s^u, a^u, r^{u_\upsilon}, s^{u'} >$ in the replay memory. Suppose the number of experiences stored in the replay memory exceeds the mini-batch size |B|. In that case, the central node randomly samples a mini-batch B having |B| experiences from the replay memory (step 5). For each sample $< s, a, r, s' >$ (index u is dropped since a sample in the mini-batch is not specific to any user) in the mini-batch, the next state s' is input in the online DQN of the central node in step 6. The corresponding action a'^* with maximum Q-value is determined in step 7. Using the same sample as in step 6, the next state s' is also input in the target DQN, also found at the central node (step 8), and the Q-value corresponding to the action a'^* determined in step 7 is derived as per step 9. Steps 6-9 execute the DDQN strategy described in Section 5.4.1.3. The Q-value is then fed to the optimiser in step 10 to yield the target y in (5.14). In step 11, the current state s of the same experience $< s, a, r, s' >$ used in step 6 is fed into the online network outputting the Q-value $Q(s, a)$ as depicted by step 12. The Q-value is fed into the optimiser, which

calculates the loss function between the target y and estimation of experience $< s, a, r, s' >$. The optimiser then minimises the loss function over the mini-batch B using

$$Loss^{\mathrm{B}}(\theta) = \sum_{<s,a,r,s'>\in \mathrm{B}} [y_{<s,a,r,s'>} - Q(s, a; \theta)]^2, \tag{5.18}$$

where $y_{<s,a,r,s'>} = r + \gamma\ \overline{Q}(s', \mathrm{argmax}_{a'}\ Q(s', a'; \theta); \overline{\theta})$. Finally, the optimiser updates the parameters θ of the online DQN in step 13, consequently training the network. At the end of each timestep, the new parameters θ are propagated from the central node to all agents to update their copy of the online DQN (step 14). The parameters $\overline{\theta}$ of the target DQN are updated to θ after a predefined number of steps τ. The pseudo-code for the MA3DQN training process is given in Algorithm 4.

The online distributed execution

Once the training is complete, the trained model can be used by the users in the ITNTN. After loading the trained online DQN parameters, each user must input its observed current state and determine the optimal AN to associate with. ϵ in the ϵ-*greedy* decision policy is set to 0, such that only greedy actions, i.e., those with maximum Q-value, are taken. Therefore, if the network is well-trained, users can take actions that yield near-optimal solutions without knowledge of other users' information in the network. Consequently, association decisions are made in real-time, and the computation cost of the online algorithm is less than that of traditional optimisation algorithms.

Algorithm 5 depicts the description of the online distributed execution. In this algorithm, a user uses the trained model to choose an action a^u and decide the AN to associate with.

Algorithm 4 MA3DQN-based service-aware user association and resource allocation training algorithm

Input: Learning rate α, mini-batch size |B|, replay memory capacity D, discount factor γ, the target DQN update frequency τ, List of allowed actions to be taken by the users, Number of episodes EP, Number of steps ST, Number of users $|\mathcal{U}|$, achievable data rate user statistics to the different ANs determined using (3.10)
Output: Online network weights

1: **procedure** MULTI-AGENT DRL TRAINING
2: Initialize the online duelling DQN (.,.;θ) with random weights θ
3: Initialize the target duelling DQN (.,.;$\overline{\theta}$) with weights $\overline{\theta} \leftarrow \theta$
4: **for** *episode* $= 1 : EP$ **do**
5: Initialise the network state $s = \{s^1, s^2, \ldots, s^{|\mathcal{U}|}\}$ as observed by the different agents
6: **for** *step* $= 1 : ST$ **do**
7: Each agent observes its current state s^u of the network
8: Each agent chooses an action a^u and executes the action
9: Each agent receives its reward R^{u_v}, and observes the next state $s^{u'}$
10: Each agent stores its experience $< s^u, a^u, R^{u_v}, s^{u'} >$ in the replay memory
11: If the experiences in the replay memory are more than the mini-batch size, the central node randomly samples |B| experiences
12: The central node performs a gradient descent using (5.18) and updates the weights θ
13: In every τ steps, the central node replaces the target parameters i.e., $\overline{\theta} \leftarrow \theta$
14: ϵ-*greedy* decision policy is updated and $s^u \leftarrow s^{u'}\ \forall u \in \mathcal{U}$
15: **end for**
16: **end for**
17: **end procedure**

The user then executes the action in line 5 by sending a request for service provisioning to the chosen AN. The ANs receive requests from the different users and execute Algorithm 6 to allocate the minimum number of BBUs determined by constraints C5 or C6 of problem **P4**, required by the users to meet their QoS requirements. As noted in Section 3.2.4, the channel gain at the ANs can be obtained as user feedback or determined through training data-based CSI estimation techniques for ANs at substantial altitudes. Algorithm 6 returns a list $Alloc^u_{n_j}$ containing the user u and the number $nb^{u_v}_{n_j}$ of BBUs allocated to the user. Each

user then receives its allocated BBUs and reward and observes the new state as depicted by line 6 of Algorithm 5.

Algorithm 5 Distributed execution algorithm using MA3DQN for service-aware user association and resource allocation

Input: User's observed current state s^u, online DQN network structure, Test steps TS
Output: Action a^u to take by the user u

1: **procedure** ONLINE EXECUTION OF THE TRAINED MODEL AT A USER u
2: Initialize: Load the online DQN trained weights θ
3: **for** $teststep = 1 : TS$ **do**
4: The user/agent selects the action a^u to take, based on its observed current state s^u
5: The user executes action a^u, thereby updating the environment. (At this point, ANs receive service provisioning requests from users and execute Algorithm 6 to allocate resources to the users)
6: The user receives its reward R^{u_v}, observes the next state $s^{u'}$, and receives the allocated BBUs determined from Algorithm 6
7: **end for**
8: **end procedure**

5.5 Computational complexity analysis of the MA3DQN algorithm

The computational complexity of the training phase depicted by Algorithm 4 and the execution/testing phase shown in Algorithm 5 are analysed in this sub-section using the big-O notation. The big-O representation gives a measure of an algorithm's worst-case execution time or required memory in tandem with the problem size.

Denote the number of layers characterised by θ in Fig. 5.2 by $\mathbb{Y}$, and let y represent a layer such that $y \in \{1, 2, \ldots, \mathbb{Y}\}$. Let $\mathbb{N}_y$ represent the number of neurons in layer y. The computational complexity of the layer y is then given by $\mathrm{O}(\mathbb{N}_{y-1}\mathbb{N}_y + \mathbb{N}_y\mathbb{N}_{y+1})$. Still referring

Algorithm 6 Resource allocation algorithm at AN n_j

Input: Set $\mathcal{U}_{n_j}$ of users requesting service provisioning from AN n_j, AN available number of BBUs $Num_{n_j}^{BBU}$, achievable data rate user statistics to the AN n_j determined using (3.10)
Output: Resource allocation set, $Alloc_{n_j}^{u}$

procedure RESOURCE ALLOCATION
AN n_j sorts received requests in $\mathcal{U}_{n_j}$ according to service group priority
Initialise: $Alloc_{n_j}^{u} = \emptyset$
    for User request $u \in$ sorted $\mathcal{U}_{n_j}$ **do**
        Determine validity status x_{t,n_j}^{u} of user u associating with AN n_j
        if $x_{t,n_j}^{u} == 1$ **then**
            Allocate $nb_{n_j}^{u_v}$ BBUs to user u according to C5 or C6 of **P4**
            Deduct $nb_{n_j}^{u_v}$ from $Num_{n_j}^{BBU}$
            Append $[u, nb_{n_j}^{u_v}]$ to $Alloc_{n_j}^{u}$
        else
            $nb_{n_j}^{u_v} = 0$
            Append $[u, nb_{n_j}^{u_v}]$ to $Alloc_{n_j}^{u}$
        end if
    end for
    Return $Alloc_{n_j}^{u}$
end procedure

to Fig. 5.2, the computational complexity of the layer characterised by the β parameters is given by $\mathrm{O}(\mathbb{N}_{\mathbb{Y}} + |\mathcal{N}|)$, where $|\mathcal{N}|$ is the number of ANs in the ITNTN. On the other hand, the computational complexity of the α-parameters layer is $\mathrm{O}(\mathbb{N}_{\mathbb{Y}}|\mathcal{N}| + |\mathcal{N}|^2)$, which is equivalent to $\mathrm{O}(|\mathcal{N}|(\mathbb{N}_{\mathbb{Y}} + |\mathcal{N}|))$. Therefore, the overall computational complexity of the duelling DQN is $\mathrm{O}(\sum_{y\in\{1,2,\ldots,\mathbb{Y}\}}(\mathbb{N}_{y-1}\mathbb{N}_y + \mathbb{N}_y\mathbb{N}_{y+1}) + (\mathbb{N}_{\mathbb{Y}} + |\mathcal{N}|) + |\mathcal{N}|(\mathbb{N}_{\mathbb{Y}} + |\mathcal{N}|))$, which can be reduced to $\mathrm{O}(\sum_{y\in\{1,2,\ldots,\mathbb{Y}\}}(\mathbb{N}_{y-1}\mathbb{N}_y + \mathbb{N}_y\mathbb{N}_{y+1}) + |\mathcal{N}|(\mathbb{N}_{\mathbb{Y}} + |\mathcal{N}|))$. Important to note is that for the term with the summation symbol, $\mathbb{N}_{y-1}$ for $y = 1$ represents the number of neurons in the input layer. In contrast, $\mathbb{N}_{y+1}$ for $y = \mathbb{Y}$ is the number of neurons in the next layer, which is either the layer characterised by β (in which case $\mathbb{N}_{y+1} = 1$) or the layer characterised by α (in which case $\mathbb{N}_{y+1} = |\mathcal{N}|$).

During the training phase, the online DQN extracts a mini-batch B of |B| experiences from the replay memory for backpropagation training. Therefore, the complexity of the training Algorithm 4 is $\mathrm{O}(|\mathcal{U}| \times ST \times EP \times |\mathrm{B}| \times \sum_{y\in\{1,2,\ldots,\mathbb{Y}\}}(\mathbb{N}_{y-1}\mathbb{N}_y + \mathbb{N}_y\mathbb{N}_{y+1}) + |\mathcal{N}|(\mathbb{N}_{\mathbb{Y}} + |\mathcal{N}|))$, where $|U|$ is the number of users, ST is the number of training steps of each episode and EP is the number of episodes.

In the testing phase (Algorithm 5), each agent has a copy of the trained model, which it uses to make an association decision. Thus, the computational complexity incurred by each agent is much reduced, given as $\mathrm{O}(TS \times \sum_{y\in\{1,2,\ldots,\mathbb{Y}\}}(\mathbb{N}_{y-1}\mathbb{N}_y + \mathbb{N}_y\mathbb{N}_{y+1}) + |\mathcal{N}|(\mathbb{N}_{\mathbb{Y}} + |\mathcal{N}|))$, where TS is the number of testing steps, which is usually small and thus negligible. Since the computational complexity in the execution phase is independent of the number of users in the ITNTN and using the intelligence attained during training, an agent can infer association decisions in real-time, as will be shown in Section 5.7.5.4.

5.6 Proposed benchmark solutions for problem P4

The performance of the MA3DQN solution is evaluated by comparing it to the GA, ILP, greedy, and RUA algorithms. The greedy scheme and its computational complexity were discussed in Chapter 3 while the GA, ILP, and RUA solutions were described in Chapter 4. Moreover, two additional benchmark solutions are considered: i) a heuristic approximation-based user association and resource allocation algorithm and ii) a MADQN solution.

5.6.1 The approximation-based solution

The problem defined in (5.7) is similar to the GAP [164]. The authors in [39] proposed a heuristic polynomial time approximation-based solution for GAP problems based on the criteria:

$$\min_{n_j{}' \neq n_j} \Delta_{u,n_j{}'} - \Delta_{u,n_j}$$

$$\textit{where} \tag{5.19}$$

$$n_j{}' = \underset{n_j}{\operatorname{argmax}} \ \Delta_{u,n_j}.$$

Δ_{u,n_j} in (5.19) is the desirability factor that measures the desirability of assigning user u to AN n_j. Therefore, each iteration in this solution consists of computing the difference between the highest desirability factor $\Delta_{u,n_j{}'}$ and the second highest factor for each unassociated user and then associating the user having the largest difference with the AN with the highest factor. Moreover, the solution is such that if an unassociated user has only one AN within its coverage, this user is prioritised. The algorithm for this solution can be found in [39], Algorithm 2. Considering problem (5.7), the desirability factor of a static user u_{υ} where $\upsilon \in \{\mathcal{R}, \mathcal{E}\}$ is the maximum data rate that can be achieved on a single BBU of a given AN, determined by (3.10). In contrast, the desirability factor of a mobile user, $u_{\mathcal{D}}$ is the handoff reduction ratio (R_{n_j}/R_{max}) in (3.22). The computation complexity of this algorithm is also described in [39] and given as $\mathrm{O}(|\mathcal{U}|^2 + |\mathcal{U}||\mathcal{N}| \log |\mathcal{N}|)$.

5.6.2 The multi-agent DQN (MADQN) algorithm

We validate the higher performance of the duelling double DQN architecture by comparing the proposed MA3DQN to the MADQN solution. The working of the MADQN algorithm is similar to the MA3DQN except that it does not use the duelling architecture and the double DQN technique described in sections 5.4.1.4 and 5.4.1.3 respectively. Accordingly, the computation complexity of the MADQN during the training phase is $\mathrm{O}(|\mathcal{U}| \times ST \times EP \times |\mathrm{B}| \times \sum_{y \in \{1,2,\ldots,\mathbb{Y}\}} (\mathbb{N}_{y-1}\mathbb{N}_y + \mathbb{N}_y\mathbb{N}_{y+1}))$, where $|U|$ is the number of users, ST is the number of training steps of each episode, and, EP is the number of episodes.

Similarly, the computation complexity incurred by each agent during the testing phase of the MADQN is $\mathrm{O}(TSX \sum_{y \in \{1,2,\ldots,\mathbb{Y}\}} (\mathbb{N}_{y-1}\mathbb{N}_y + \mathbb{N}_y\mathbb{N}_{y+1}))$, where TS is the number of testing steps. Note that the only difference between the MADQN and MA3DQN complexities in both the training and testing phases is the term $|\mathcal{N}|(\mathbb{N}_{\mathbb{Y}} + |\mathcal{N}|))$ that accounts for the duelling architecture complexity of the MA3DQN as described in Section 5.5.

5.7 Results and performance evaluation

This section provides the performance analysis of the proposed MA3DQN algorithm. First, the simulation parameters are discussed, and later, the MA3DQN solution is validated through comparison to the GA, the ILP solution to the problem (5.7) determined using the Gurobi solver via LP relaxation and branch and bound, the simulated MADQN solution, the approximation scheme [39], the greedy algorithm that associates static users based on maximum SINR and mobile users based on cell radius, and the RUA algorithm.

Table 5.2: Simulation parameters and values.

Parameter	Value
$\mathcal{T}_{w_{\mathcal{B}}}, \mathcal{T}_{w_{\mathcal{L}}}, \mathcal{T}_{w_{\mathcal{H}}}, \mathcal{T}_{w_{\mathcal{S}}}$	[0.18, 0.18, 1, 2] MHz
Number of BBUs for $[n_{\mathcal{B}}, n_{\mathcal{L}}, n_{\mathcal{H}}, n_{\mathcal{S}}]$	[10, 10, 20, 20]
$[P^{thres}_{n_{\mathcal{B}}}, P^{thres}_{n_{\mathcal{L}}}, P^{thres}_{n_{\mathcal{H}}}, P^{thres}_{n_{\mathcal{S}}}]$	[8, 5, 20, 25] Watts
Service group user ratio $[\lvert\mathcal{U}_{\mathcal{R}}\rvert : \lvert\mathcal{U}_{\mathcal{D}}\rvert : \lvert\mathcal{U}_{\mathcal{E}}\rvert]$	[0.3:0.1:0.6]
Noise spectral density	-174 dBm

5.7.1 Simulation setting

Similar to Chapter 4, we consider an urban circular region of 3 km radius under the coverage of a LEO satellite and a HAP AN. Within this region are several MBSs and 1 LAP, with the radius of 1 km and 2 km, respectively. The users within the considered area are randomly and uniformly distributed. Table 5.2 [19, 1, 111, 112] depicts the radio environment parameters used in the simulation. Similar to [35], the data packet arrival rate $\lambda_{u_v} \forall v \in \{\mathcal{R}, \mathcal{E}, \mathcal{D}\}$ is set to 20 packets/s, the packet size for the euRLLC service group is set to 500 bits while that for the feMBB and LDHMC to 9000 bits. The delay bound $\mathrm{D}_{\max}$ in all simulations except those in Section 5.7.5.3 is set to 1 ms while the delay bound violation probability threshold ϵ is fixed at 0.001.

Since the convergence of deep learning algorithms depends on hyper-parameters such as the learning rate, mini-batch size, and optimisation algorithm used [146], it is impossible to know the optimal configuration of hyper-parameters for a specific problem in advance. As a solution, trial-and-error procedure [146, 96, 165] is encouraged. To determine the appropriate configuration of hyper-parameters and consequently train the network, we consider the ITNTN to consist of 5 ANs, i.e., 2 MBSs, 1 LAP, 1 HAP, and 1 SatComs AN, serving 50 users.

5.7.2 DQN hyper-parameter setting

The simulated duelling DQN structure consists of four parts, as depicted by Fig. 5.4. The first part is the input layer with $1 + 3|\mathcal{N}|$ neurons corresponding to the environment state as defined in Section 5.4.2.1. The second part consists of two hidden layers, each having 256 neurons. Next are the two duelling architecture sub-layers: the value sub-layer with one neuron through which the state value function stream flows and the advantage comprising $|\mathcal{N}|$ neurons to output the advantage function stream as discussed in Section 5.4.1.4. The output layer consists of $|\mathcal{N}|$ neurons corresponding to the number of different ANs in the ITNTN. The activation function used is the ReLU function. At the same time, ϵ in the ϵ-*greedy* decision policy decays linearly as $\epsilon(t) = \max\{0.1, (MES - t)/MES\}$, where MES is a predefined number of time steps beyond which ϵ remains fixed at 0.1 (t, in this case, starts from zero, and incremented by one for each training step across all episodes). Furthermore, the discount factor $\gamma = 0.95$ while the replay memory follows the first-in-first-out service rule and its capacity is set to 10^6.

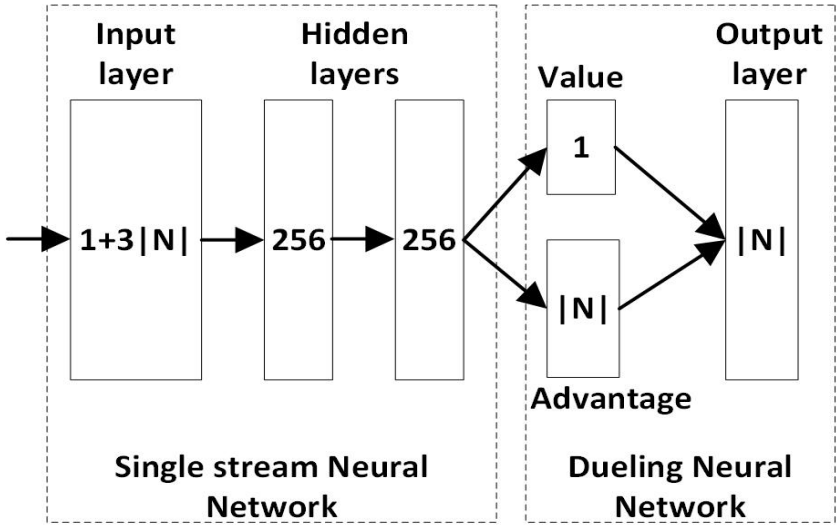

Figure 5.4: The duelling DQN structure used in the proposed MA3DQN.

In Fig. 5.5, we plot the smoothed average reward accumulated over an episode for different learning rates α. The mini-batch size |B| is set to 256 while the Adam optimisation strategy is used. The figure shows that the accumulated average reward for $\alpha = 0.1$ keeps decreasing as the training progresses, clearly showing that the model can not learn with this value of α. However, as α decreases, the accumulated average reward keeps increasing and eventually converges at about the 320th episode. The accumulated average reward for $\alpha = 0.01$ is relatively lower than that achieved by $\alpha = 0.001$ and $\alpha = 0.0001$, implying that $\alpha = 0.01$ leads to a sub-optimal solution. Since the performance of $\alpha = 0.001$ and $\alpha = 0.0001$ is almost similar, we choose $\alpha = 0.001$ because generally, a smaller learning rate leads to slower training and the possibility of becoming permanently stuck with a high training error is high [166].

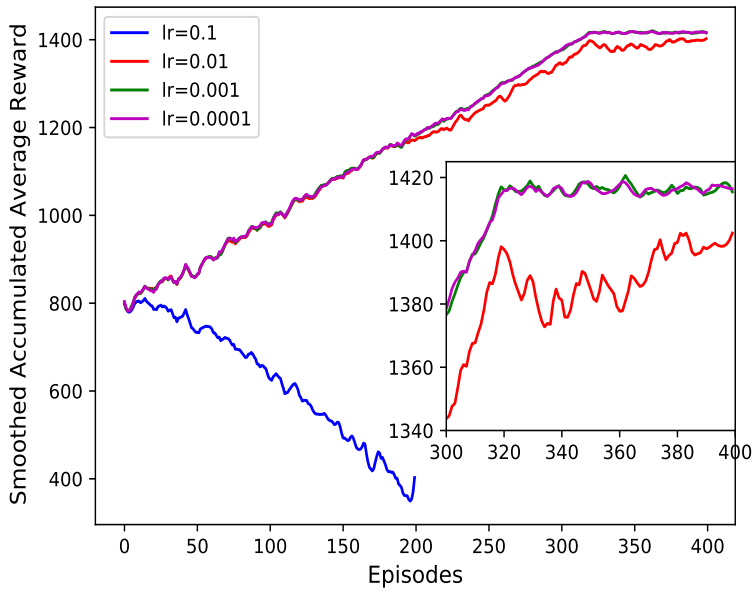

Figure 5.5: Effect of learning rate on convergence of the proposed MA3DQN.

Next, the effect of the mini-batch size on the convergence of the proposed MA3DQN algorithm is analysed. The learning rate is set to 0.001, and the Adam optimisation algorithm is still used. According to Fig. 5.6, the considered mini-batch sizes have a negligible effect on the algorithm's convergence. All mini-batch sizes converge at approximately the same episode, though 256 and 512 perform slightly better than 64 with regard to accumulated average reward. The mini-batch size chosen for this work is 256 since a bigger value generally results in a higher computational time.

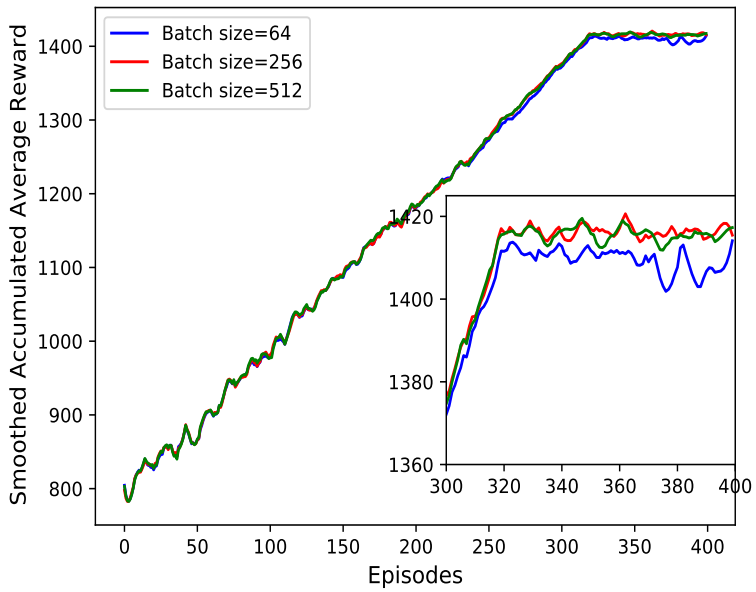

Figure 5.6: Effect of mini-batch size on convergence of the proposed MA3DQN.

Finally, the effect of different optimisation strategies on convergence is analysed in Fig. 5.7, with the learning rate and mini-batch size set to 0.001 and 256, respectively. All strategies converge, with the RMSProp optimiser showing the worst performance characterised by higher instability at convergence. The Adam optimiser has a slightly higher accumulated average reward, hence choosing it as the optimisation algorithm appropriate

for the MA3DQN. While the number of hidden layers, discount factor γ, and target DQN update frequency τ are also hyper-parameters that can affect the performance of the proposed algorithm, their values are kept as earlier described since the convergence of the algorithm has already been achieved as depicted by Figs. 5.5, 5.6 and 5.7. Therefore, the parameters used in the MA3DQN are summarized in Table 5.3.

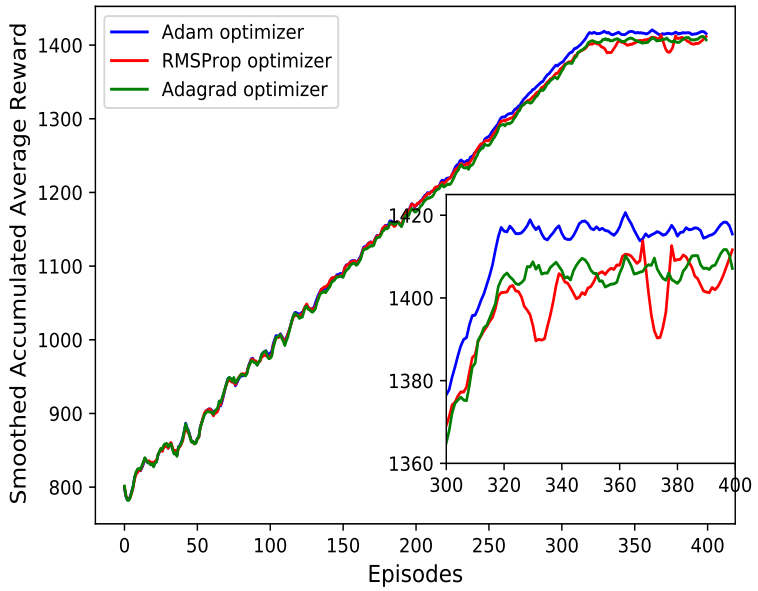

Figure 5.7: Effect of optimisation algorithm on convergence of the proposed MA3DQN.

Table 5.3: MA3DQN parameters.

Parameter	Value
Discount factor γ	0.95
Mini-batch size	256
Learning rate α	0.001
Optimiser	Adam
Activation function	ReLU
Replay memory capacity D	10^6
The target DQN update frequency τ	4500
[minimum ϵ, maximum ϵ]	[0.1, 1]
Number of episodes EP	400
Number of steps ST	2500

5.7.3 Performance metrics

The performance analysis of the proposed MA3DQN solution is based on a number of performance metrics explained below:

- The user AR: In this work, the user AR is defined as the ratio of served users to the total number of users in the network. This metric gives a measure of how effective the proposed MA3DQN algorithm is at sharing resources among the different users in the network.
- The total network data rate as defined by (3.19).
- The handoff probability: The handoff probability is defined as the ratio of the number of users that experience a handoff from one AN to another to the total number of mobile users in the ITNTN during a given transmission time interval.
- Algorithm runtime: This will give the time in seconds for each algorithm to return its best solution.

5.7.4 Performance analysis during training

Fig. 5.8 depicts the performance of the MA3DQN algorithm during training. In Fig. 5.8(a), it can be observed that the AR of the euRLLC users increases with training. At the beginning of the training process, the euRLLC AR is relatively low at about 0.6 because some users are dropped when associated with ANs that can not meet their QoS requirements, like the satellite AN. However, as the training progresses, the NN learns to associate the mission-critical users with the appropriate ANs, consequently increasing their AR. Also, from Fig.

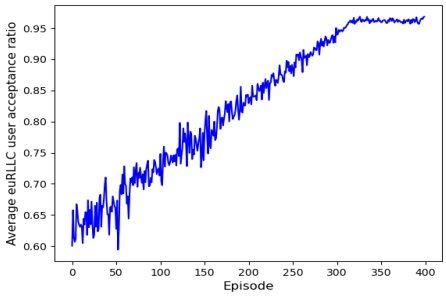

(a) Average euRLLC acceptance ratio.

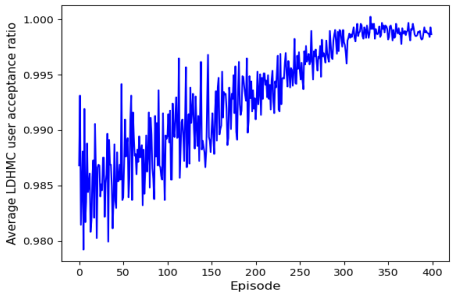

(b) Average LDHMC acceptance ratio.

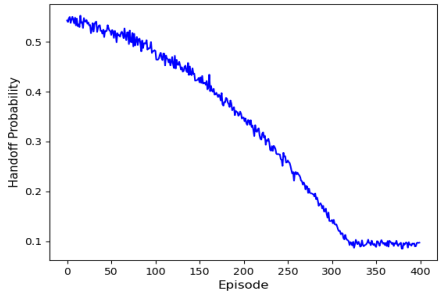

(c) Handoff probability.

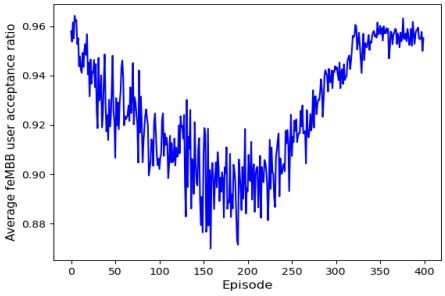

(d) Average feMBB acceptance ratio.

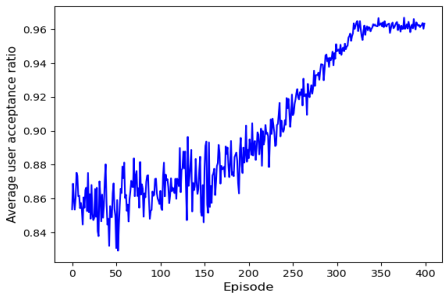

(e) Average user acceptance ratio.

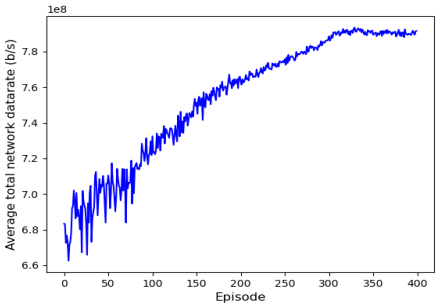

(f) Average total network data rate.

Figure 5.8: Performance evaluation of the MA3DQN during training.

5.8(b), the AR performance of the LDHMC users improves and becomes more stable with training, as the NN learns to associate these users to available ANs having large cell radius, thereby reducing the handoff probability as observed in Fig. 5.8(c).

On the other hand, as observed from Fig. 5.8(d), the AR of feMMB users is high at the beginning of the training process, then decreases up to about the 200th episode, after which it increases until convergence. The reason for such behaviour is that at the beginning of the training, the feMMB users are utilising resources later allocated to the euRLLC users, whose punishment for denial of service is much greater. As the NN learns to allocate these resources to the euRLLC service group, the AR for the feMMB drops. However, with increased training, the NN later learns the ANs with available resources to serve the feMMB users; hence, their AR increases.

Fig. 5.8(e) shows the performance of user AR with training. As observed, by the end of the training process, the NN admits almost all users in the network, with an AR of about 0.96. Important to remember is that the minimum value of ϵ was set to 0.1, allowing some possibility of exploration even at the end of the training. Hence, the AR can not reach one because of the random behaviour that may ensue. Finally, Fig. 5.8(f) depicts the behaviour of network data rate as training progresses. The NN learns to associate users with the appropriate ANs having sufficient resources to meet the user QoS requirements leading to an increase in total network data rate as training progresses.

5.7.5 Results and discussions

Once the training stage is completed, the performance of the trained model is validated through comparison to the GA, the ILP, the approximation, the greedy, the RUA, and the MADQN algorithms already discussed in Section 5.6.

5.7.5.1 Impact of user density

In Fig. 5.9, the AR performance of the different algorithms is depicted. The AR for a lower number of users, specifically below 50, is 1 for all algorithms since the available resources can support all users in the network. However, as users increase beyond 50, the resources become insufficient to meet their QoS requirements. Hence, some users are dropped, thereby decreasing the AR. On average, the AR of the MA3DQN, GA, ILP, MADQN, approximation, greedy, and RUA algorithms is 0.914, 0.917, 0.909, 0.897, 0.88, 0.879, and 0.888, respectively. Therefore, the GA achieves better AR than the MA3DQN algorithm by 0.3% on average.

On the other hand, the MA3DQN algorithm outperforms the ILP, MADQN, approximation, greedy, and RUA algorithms by 0.5%, 2.2%, 3.6%, 3.8%, and 2.8%, on average, respectively. The GA's good AR performance is because the algorithm's fitness function increases with the number of users admitted in the network, hence achieving a high AR. Similarly, the RL algorithms MA3DQN and MADQN utilise centralised learning that allows users to learn together, hence an equally high AR for the MA3DQN algorithm. The duelling architecture and double DQN framework enable the MA3DQN algorithm to make better actions that result in serving more users than the MADQN algorithm, hence the better AR performance. On the other hand, the ILP, greedy, RUA, and approximation algorithms are all based on functions whose optimisation does not focus on having a higher number of served users, hence the reduced performance when compared to the GA and MA3DQN algorithms.

Fig. 5.10 depicts the total network data rate achieved by the different algorithms. The figure shows that the GA, ILP, MA3DQN, MADQN, and approximation algorithms attain a

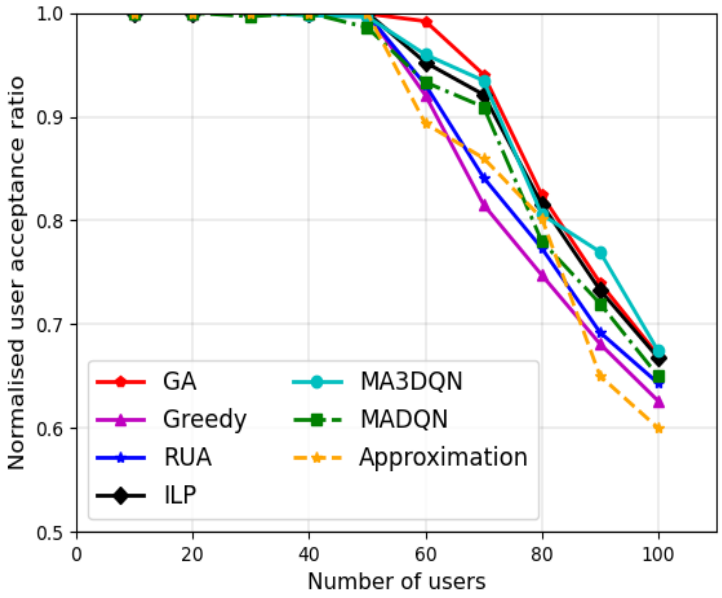

Figure 5.9: User acceptance ratio with varying number of users.

higher data rate than the greedy and RUA schemes for a low number of users. This behaviour is because these algorithms are optimised to associate users with ANs that result in a high data rate. On the other hand, the greedy algorithm associates users based on maximum SINR, yet the RANs in the ITNTN have differently sized BBUs. Thus, a RAN with the highest SINR may not necessarily have the highest data rate. Also, the RUA algorithm randomly associates users to any available capable RAN without regard to the achieved data rate. All algorithms achieve convergence at 50 users and above when the limit on the number of users the network can support is reached, and thus any increase in demand does not boost the total network data rate. The GA and ILP solutions perform better than the MA3DQN algorithm by 0.48% and 0.42% on average, respectively. However, the MA3DQN algorithm performs better than the MADQN, approximation, greedy, and RUA algorithms by 0.3%, 0.4%, 7%, and 7.2% on average, respectively.

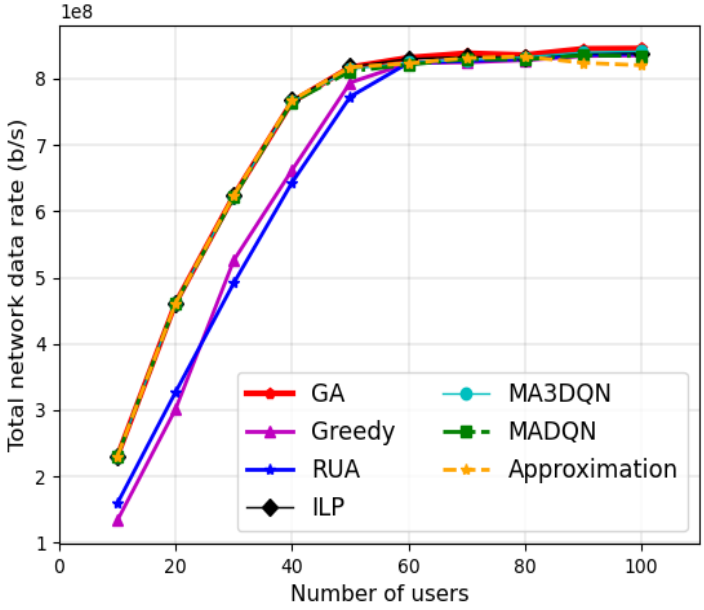

Figure 5.10: Total network data rate with varying number of users.

In Figs. 5.11, 5.12, and 5.13, we analyse the AR of the different service groups. In all algorithms, service provisioning of the mission-critical euRLLC service group is prioritised. As observed in Fig. 5.11, all algorithms achieve an AR of 1 for this service group until about 70 users, when the AR decreases slightly. The decrease is because of increased euRLLC users beyond what the available capable ANs can support. In Fig. 5.12, all algorithms achieve an AR of 1 as the LDHMC users increase in the network. This is because the ANs with the largest cell radius were prioritised in all algorithms to serve LDHMC users; hence, resources are available to meet their demands. In contrast, a steep decline in AR at about 50 users and above is observed for the feMMB users in Fig. 5.13. Since the feMBB users are not prioritised, increased demand beyond what the network can support implies a surge in the number of dropped feMBB users due to limited resources to meet their needs.

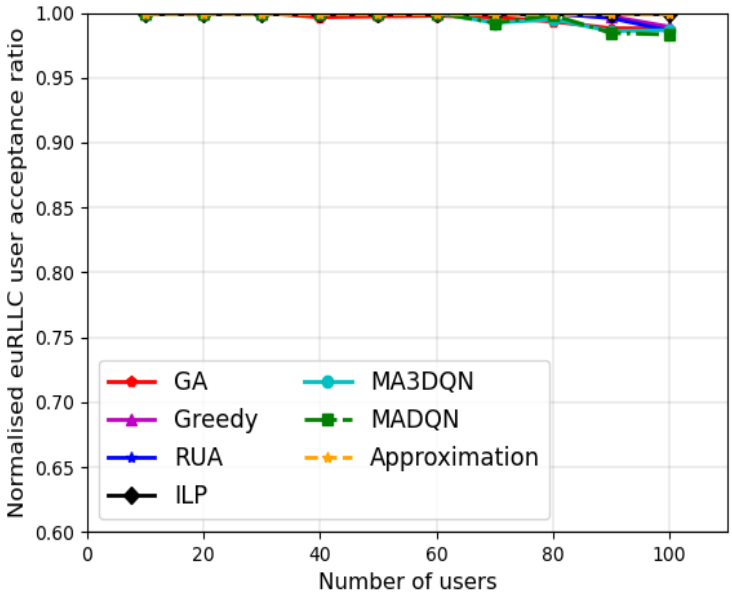

Figure 5.11: euRLLC acceptance ratio with varying number of users.

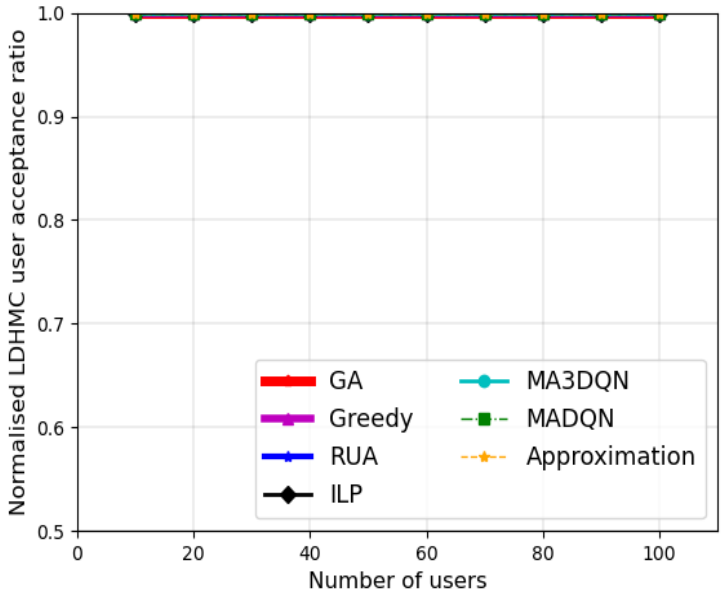

Figure 5.12: LDHMC acceptance ratio with varying number of users.

Fig. 5.14 portrays the mobility-induced handoff performance of all algorithms. The GA, ILP, greedy, MA3DQN, and MADQN algorithms maintain a handoff probability of 0

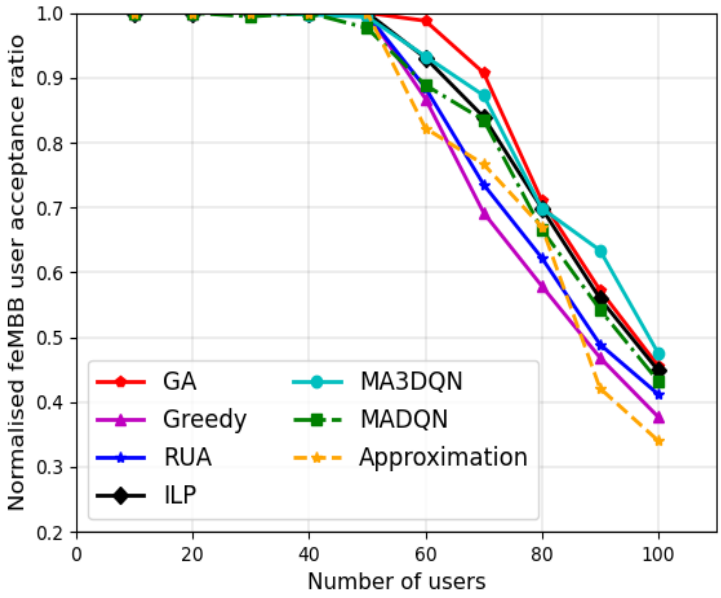

Figure 5.13: feMBB acceptance ratio with varying number of users.

for all numbers of users in the ITNTN. In the GA and RL algorithms, the cost or reward function ensures that the mobile users are associated with an available capable AN with the largest cell radius; hence, no handoff of users from one AN to another occurs during all transmission intervals. The greedy heuristic algorithm is also formulated to ensure the mobile users attach to the cell with the largest cell radius. Similarly, for the ILP solution, the Gurobi solver optimises the objective function by ensuring that the handoff reduction function in **P1** is maximised.

Conversely, the RUA algorithm associates mobile users randomly with any available NTN, achieving the highest handoff probability. As the number of users increases, the handoff probability performance of the RUA improves since resources of ANs with small radii get used up, forcing the mobile users to associate with the large cell radius ANs. On the other hand, the poor performance of the approximation algorithm is attributed to the

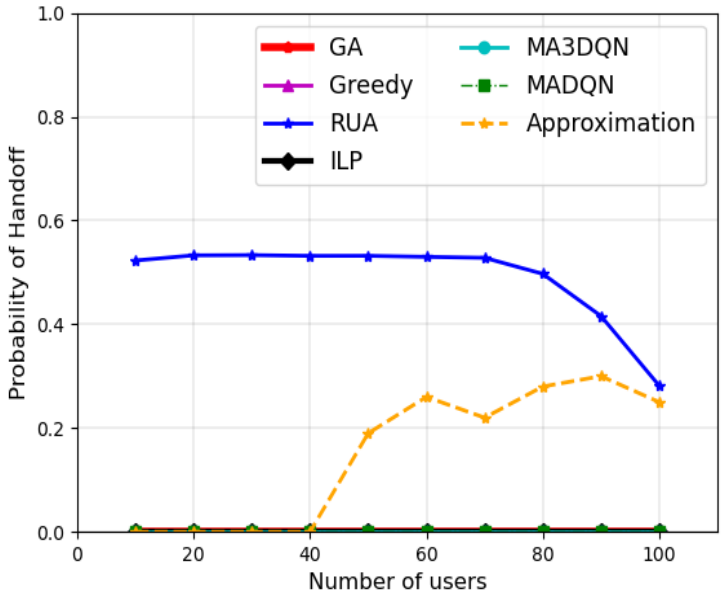

Figure 5.14: Probability of handoff with varying number of users.

fact that users with only one available AN are served first. When the number of users is small, particularly below 50, the algorithm performs well since the cell with the largest radius has enough resources for both the mobile users it is prioritised to serve and other users from the feMBB group that have access to only this AN. As the number of users increases, these users use up resources prioritised for the mobile service group, consequently increasing the number of handoffs.

5.7.5.2 Impact of access nodes density

In this subsection, we analyse the different algorithms' performance with varying access node densities in the network. The user distribution radius is increased to 4 km to allow deployment of more MBSs. This region is still within the coverage of 1 satellite and 1 HAP.

We also deploy 1 LAP and vary the MBSs from 2 to 10 while maintaining the number of users at 80.

Fig. 5.15 depicts that the GA achieves the best AR, with an average of 0.88, followed by the MA3DQN algorithm, which has an average AR performance of 0.833. The ILP, MADQN, approximation, greedy, and RUA algorithms attain an average AR of 0.831, 0.8, 0.75, 0.77, and 0.816, respectively. Unlike the AR performance depicted in Fig. 5.9, in which the MA3DQN solution was within the GA's performance by 0.3%, the MA3DQN algorithm's AR now falls by 5.67% on average, below that attained by the GA. The decline in performance is attributed to the expanding state space and action space as the number of ANs in the network increases, thereby reducing accuracy for the same hyper-parameters. Nonetheless, the difference in performance is slight, given the benefits of MA3DQN solution in terms of time taken to yield a solution, as will be discussed in Section 5.7.5.4. Besides, this performance can be improved during the training phase by changing the hyper-parameters; for example, the decaying rate of ϵ can be reduced to allow for more exploration during the training. Regardless of the reduction in AR performance, the MA3DQN algorithm still outperforms the ILP, MADQN, approximation, greedy, and RUA schemes by 0.08%, 3.4%, 10.4%, 7.2%, and 1.9%, respectively.

Fig. 5.16 compares the achieved data rate as the number of access nodes varies. The GA and ILP schemes attain higher average total network data rates than the proposed MA3DQN algorithm by 0.9% and 0.48%, respectively. On the other hand, the MA3DQN algorithm performs better than the MADQN, approximation, greedy, and RUA algorithms on average by 0.3%, 0.3%, 0.6%, and 0.4%, respectively. Fig. 5.17 shows the handoff performance of all

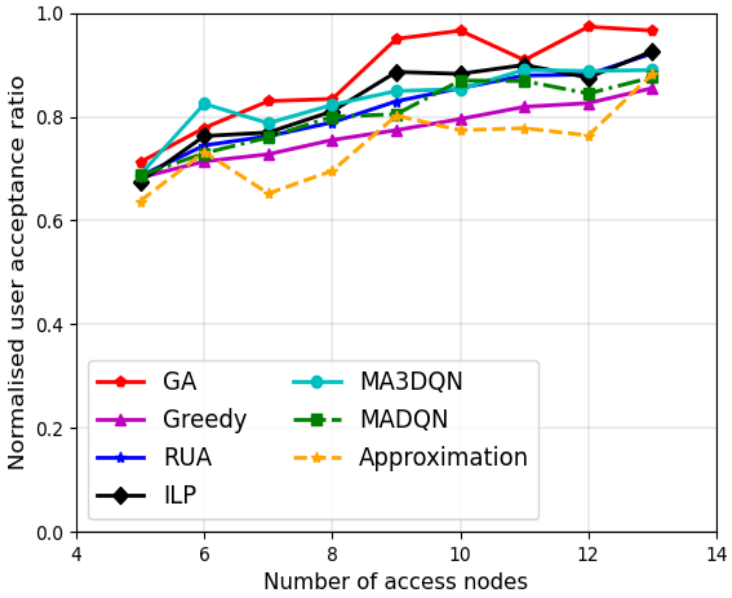

Figure 5.15: User acceptance ratio with varying number of access nodes.

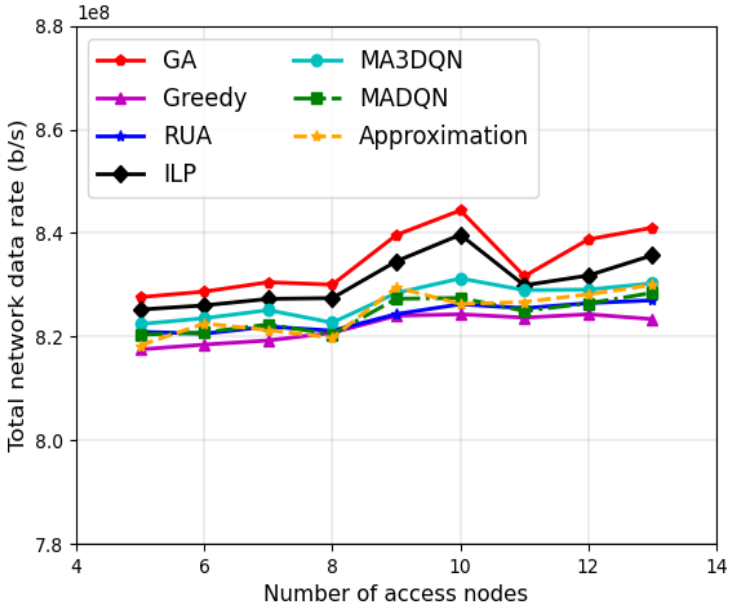

Figure 5.16: Total network data rate with varying number of access nodes.

the algorithms as the number of access nodes in the network increases. The GA, ILP, greedy, MA3DQN, and MADQN algorithms maintain a handoff probability of 0, outperforming the

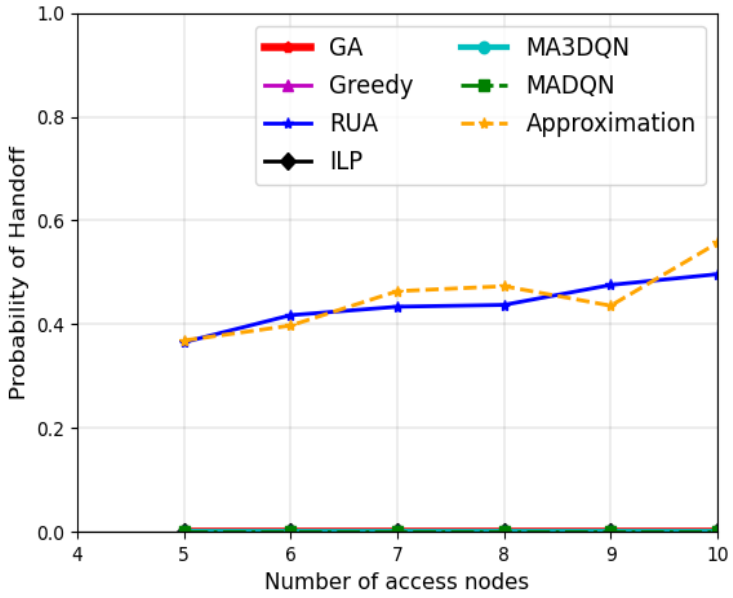

Figure 5.17: Probability of handoff with varying number of access nodes.

approximation, and RUA algorithms by 47%, and 50%. This illustrates the strength of the GA, ILP, greedy and RL algorithms in associating mobile users with an AN having the largest cell radius, thereby maintaining handoff probability at 0. On the contrary, the RUA framework still maintain poor data rate and handoff probability performance as it is not optimised to associate users with ANs that yield the highest data rate or the lowest handoff probability. On the other hand, the approximation technique lacks the intelligence to balance between serving users having one AN within their coverage and the mobile users, hence achieving high handoff probability. Moreover, the difference mechanism explained in Section 5.6.1 is subjected to two different functions, the maximum achieved data rate on a BBU and the handoff reduction value, that may present varying differences between the best and second best value, thereby not favouring some users, hence the poor performance observed for this algorithm.

5.7.5.3 Impact of the delay bound

This subsection analyses the impact of the delay bound on the user AR and achieved total network data rate. The number of users in the network is maintained at 40, while 5 ANs are used, that is, 1 satellite, 1 HAP, 1 LAP, and 2 MBSs. The area of user distribution used is a circular radius of 3 km. We start by first showing in Fig. 5.18 the effect of the delay bound on the minimum data rate $\mathcal{C}_{u_{\mathcal{R}}}^{min}$ that a served euRLLC user must receive to guarantee delay QoS requirements. The figure shows that for low values of delay bound, the expected minimum data rate is high, but an increase in delay bound results in a reduced required minimum data rate, which is in agreement with (5.5). This result implies that an euRLLC user requires a higher data rate to meet a more stringent delay-bound requirement.

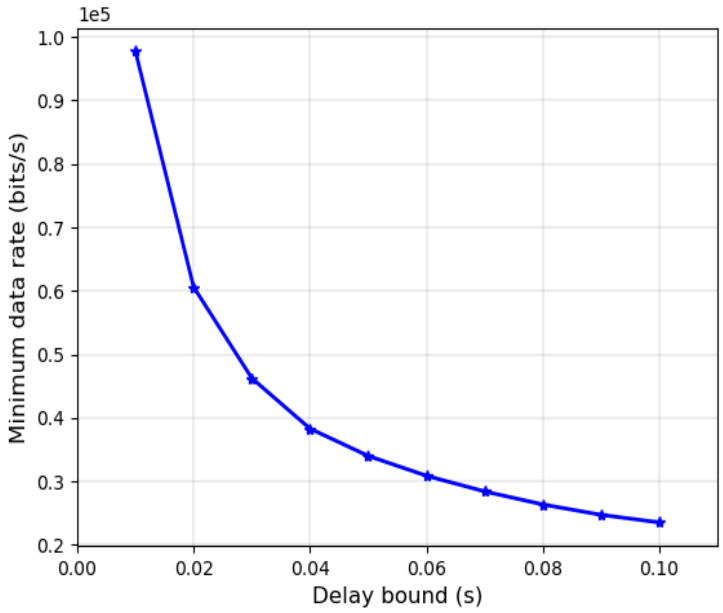

Figure 5.18: Effect of the delay bound on the minimum required data rate.

Tables 5.4, 5.5, and 5.6 give the performance of the different algorithms for delay bound D_{max} of 1 ms, 0.1 ms, and 0.01 ms respectively. It can be observed that for a higher delay bound, that is, D_{max} = 1 ms or 0.1 ms, the resource blocks are enough to support the minimum QoS requirements of all users. Therefore, the user AR is 1 for all algorithms. However, as the delay bound is reduced further to 0.01 ms, a served user in the euRLLC service group uses up more BBUs to meet the stringent delay bound, consequently increasing the total network data rate, as observed for all algorithms. Therefore, an euRLLC user requires more BBUs, consequently reducing the total resources available for all users in the network, thereby leading to a decline in AR for the euRLLC and feMBB service groups. The AR for the LDHMC remains one since, in this work, the NTN with the largest cell radius is prioritised to serve this service group to minimise the probability of mobility-induced handoff.

Table 5.4: Performance when $D_{max} = 1$ ms.

Method	user AR	euRLLC AR	LDHMC AR	feMBB AR	Network Data rate
GA	1	1	1	1	7.658×10^8
ILP	1	1	1	1	7.673×10^8
MA3DQN	1	1	1	1	7.653×10^8
MADQN	1	1	1	1	7.652×10^8
Approximation	1	1	1	1	7.659×10^8
Greedy	1	1	1	1	6.61×10^8
RUA	1	1	1	1	6.442×10^8

5.7.5.4 Execution time analysis

This section analyses the runtime of the different algorithms required to return the best solution as presented in sections 5.7.5.1 and 5.7.5.2. Since the ILP solution presents an

Table 5.5: Performance when $D_{max} = 0.1$ ms.

Method	user AR	euRLLC AR	LDHMC AR	feMBB AR	Network Data rate
GA	1	1	1	1	7.66×10^8
ILP	1	1	1	1	7.673×10^8
MA3DQN	1	1	1	1	7.653×10^8
MADQN	1	1	1	1	7.652×10^8
Approximation	1	1	1	1	7.657×10^8
Greedy	1	1	1	1	6.632×10^8
RUA	1	1	1	1	6.489×10^8

Table 5.6: Performance when $D_{max} = 0.01$ ms.

Method	user AR	euRLLC AR	LDHMC AR	feMBB AR	Network Data rate
GA	0.967	0.92	1	0.985	8.307×10^8
ILP	0.96	0.92	1	0.973	8.286×10^8
MA3DQN	0.955	0.917	1	0.964	8.198×10^8
MADQN	0.953	0.917	1	0.962	8.193×10^8
Approximation	0.952	0.917	1	0.961	8.189×10^8
Greedy	0.907	0.917	1	0.888	8.156×10^8
RUA	0.924	0.916	1	0.915	8.174×10^8

exponential worst-case time complexity as analysed in Section 4.4, its running time will not be analysed. Important to note is that the runtime analysed in this work is not inclusive of the time required by the controllers (in the GA, approximation, greedy, and RUA algorithms) or the users (in the MA3DQN and MADQN schemes) to obtain information such as ANs loading capacity or the SINR between users and the ANs. Therefore, it is assumed that such information is already known, and the task is then for each algorithm to determine its best solution.

Fig. 5.19 depicts the runtime of the different algorithms as the number of users in the network increases. The number of ANs is maintained at 6 for this simulation. The RL algorithms present the shortest running time of 0.00053 and 0.00054 seconds on average for

the MA3DQN and MADQN algorithms, respectively. On the other hand, the GA has the highest runtime of 1.7 seconds on average, and the runtime increases with the number of users in the network. The greedy, RUA, and approximation solutions require an average runtime of 0.0017, 0.0016, and 0.05 seconds, respectively. The runtime performance of the MA3DQN and MADQN algorithms outperform the GA, greedy, RUA, and approximation algorithms by 99.9%, 68%, 66%, and 98.9%, respectively, and is independent of the number of users in the network. Such a performance is achieved from the intelligence obtained during the learning process and the fact that each user has a copy of the trained model, enabling it to make association decisions on the fly. Also, it further shows that GA's excellent performance in the previous sections is obtained at the expense of an increased number of generations G and chromosomes M as discussed in Section 4.3.2.4, thereby increasing its running time and hence time complexity significantly. Such a high time complexity is not suitable for service provisioning of delay-intolerant mission-critical users expected in B5G networks.

In Fig. 5.20, the number of users in the network is fixed at 100. According to this figure, as the number of ANs in the network increases, the MA3DQN and MADQN algorithms still have the lowest runtime, independent of the number of ANs in the network. The greedy and RUA algorithms also have a low runtime that increases slightly with the number of ANs. The approximation algorithm presents a running time that is 99.6% worse than the RL algorithms, while the GA has the worst running time, which is within 99.99% that of the RL algorithms.

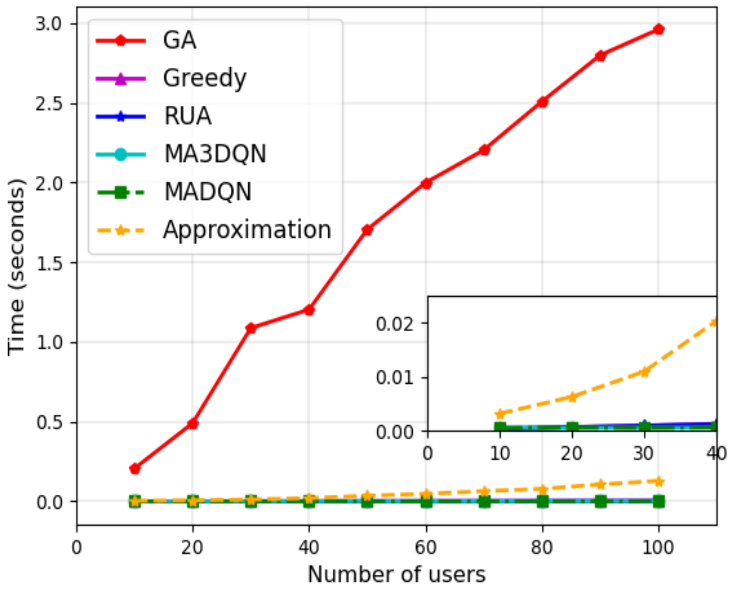

Figure 5.19: Runtime versus number of users.

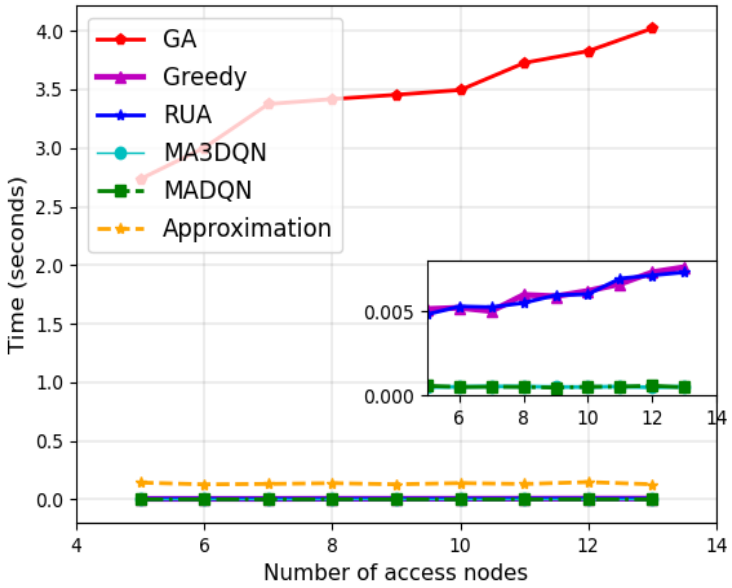

Figure 5.20: Runtime versus number of access nodes.

These results depict the strength of the proposed MA3DQN algorithm over the other algorithms. The results demonstrate that the MA3DQN algorithm can achieve a near-optimal data rate performance, that is within 0.48%, and 0.9% of the best solutions obtained

by the GA in Sections 5.7.5.1 and 5.7.5.2 respectively. This result is obtained in real-time, unlike the GA solution, characterised by a high time complexity that is 99.99% worse than the MA3DQN solution. Moreover, unlike the approximation and RUA algorithms that portrayed a high handoff probability, the MA3DQN algorithm maintained a zero probability of handoff. Therefore, the proposed MA3DQN algorithm is highly suitable for future scenarios characterised by mission-critical applications for which a high runtime implies increased delays and ultimately reduced user QoS. In addition, the algorithm is suitable for highly mobile applications for which increased handoff probability implies increased communication overhead, delays, probability of dropped calls, and consequently, reduced user QoS for these applications. While the MADQN algorithm equally performed well in terms of runtime and handoff probability, the MA3DQN algorithm presented a margin of 3.4% and 0.3% in user AR and total network data rate, respectively, as the number of ANs increased in the network. Also, as the number of users in the network increased, a difference in the performance of 2.2% and 0.3% in terms of AR and achieved total network data rate was observed in favour of MA3DQN solution.

5.7.5.5 Cumulative Distribution Function (CDF) of the total network data rate

Similar to Chapter 4, this section utilises the CDF to provide an insight on the performance bounds of the proposed MA3DQN algorithm. 1000 simulations are carried out to analyse data rate performance for 80 users in a network consisting of 2 MBSs, 1 LAP, 1 HAP, and 1 satellite AN. Fig. 5.21 shows a steep rise in CDF from 0 to 1, implying a small range within which all simulation data rate results fall. Considering the graph for 5 ANs, about 1% of

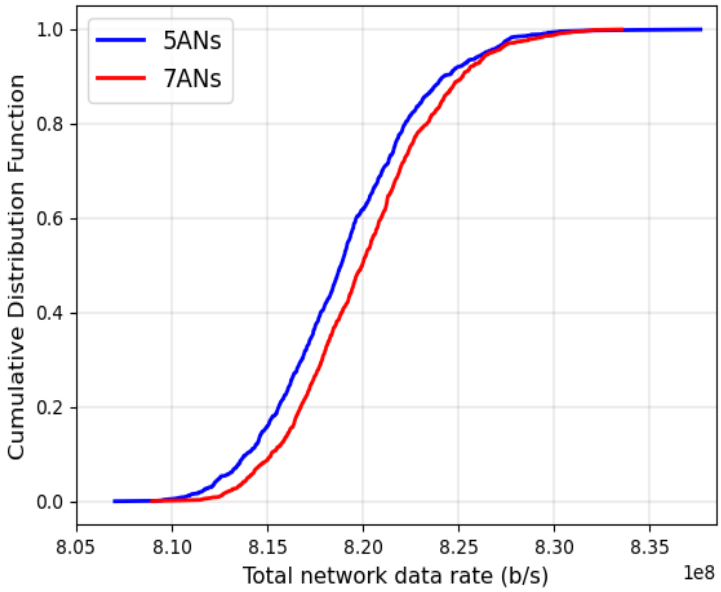

Figure 5.21: The CDF of the total network data rate using the MA3DQN.

simulations return a data rate that is less than 8.1×10^8 b/s while about 99.6% return data rates less than 8.3×10^8 b/s. In Chapter 4, Section 4.6.3.5, an upper bound for the GA was found to be about 8.35×10^8 b/s, giving a gain of about 3% and 0.6% from the lower bound and upper bound of the MA3DQN algorithm, respectively.

5.8 Chapter summary

This chapter presented a decentralised real-time RL solution to the user association and resource allocation problem **P1** described in Chapter 3. Moreover, **P1** was reformulated to account for the delay QoS requirement. The RL solution was based on the centralised training and distributively executed MA3DQN algorithm. The solution defined each user's state, action, and reward function that enabled the association of users to the appropriate

access nodes to maximise the total network data rate and minimise the handoff probability. Simulation results revealed that as the number of ANs increased, the MA3DQN algorithm achieved a total network data rate that was within 0.9% and 0.48% of the GA and ILP solutions, respectively, and outperformed the MADQN, approximation, greedy, and RUA algorithms on average by 0.3%, 0.3%, 0.6%, and 0.4%, respectively. Also, the total network data rate achieved by the MA3DQN algorithm was within 0.48% and 0.42% of the GA and ILP schemes, respectively, as the number of users in the network increased. Notably, the MA3DQN algorithm presented a 99.9% gain over the polynomial-time GA in terms of execution time. Moreover, it outperformed the approximation and RUA algorithms regarding handoff probability. Also, it outperformed the MADQN, approximation, greedy, and RUA algorithms in terms of acceptance ratio and total network data rate.

Chapter 6

Energy-Efficient User Association and Resource Allocation in the ITNTN

The preceding chapters have focused on maximising the achieved data rate and, hence, the spectrum efficiency of the ITNTN. However, the coexistence of the TN with the NTNs to provide radio access to multi-mode user equipment implies an increase in the number of wireless access nodes. It thus raises a justifiable concern over the drastic increase in energy consumption and carbon emission expected to ensue. Moreover, an increase in energy consumption may lead to high operational expenditure (OPEX) and thus threaten the profitability of ITNTNs. Therefore, this chapter addresses the energy efficiency (EE) problem in the ITNTN.

6.1 Introduction

The coexistence of the TN with the NTNs to provide radio access implies an increase in the number of ubiquitous wireless nodes, consequently escalating the total energy consumption and associated OPEX and carbon emissions [31]. Therefore, the role of EE in the ITNTN is significant and urgent. Since EE is the ratio of the total network data rate to total power consumption, it is a critical performance metric that provides an optimal trade-off between the network sum rate and the total power consumption. Several techniques have been used in literature to achieve EE in wireless networks, such as adaptive BS sleep control [167], beamforming [168], and energy-efficient UARA [169]. Similar to [169], this chapter focuses on improving the EE in the ITNTN through energy-efficient resource allocation.

As the RANs in the ITNTN have different capabilities and limitations in meeting the heterogeneous user demands envisaged in B5G, achieving an energy-efficient UARA strategy is challenging. Satellite communication is characterised by long delays and, as such, is not appropriate for radio access by mission-critical users. Similarly, the TN BSs have a smaller cell radius than the NTN ANs. Therefore, the TN is not a suitable RAN for high-speed and long-distance users. Its usage would increase the number of handoffs, consequently increasing the handoff signalling overhead, delays, and the probability of call drops due to handoff failures. The question that arises then is how to optimally map users with diverse needs to RANs faced with different challenges in meeting these requirements and simultaneously maximise the network's energy efficiency.

In the literature, some works have addressed energy-efficient UARA in the ITNTN. In [169], the authors integrate the LEO satellite with terrestrial D2D mode and formulate an

optimisation problem that maximises capacity and admitted users while allocating optimum power to the associated users. The authors in [170] investigate energy-efficient power allocation for cognitive satellite-terrestrial networks subjected to delay QoS constraints. In [171], the authors maximise the system EE of a space-air-sea network, simultaneously optimising user association, power control, and UAV deployment. In [20], the authors maximise the EE of an integrated terrestrial-satellite RAN in which both RANs provide content distribution and retrieval services. The authors in [172] propose an algorithm that maximises the EE of a hybrid satellite-aerial-terrestrial cooperative network subjected to power, QoS requirements, and backhaul capacity constraints.

The idea of B5G is to have the TN, space (satellite), and aerial (HAPs and LAPs) concurrently provide radio access to users. However, all the proposals in [169, 170, 171, 20] do not consider energy-efficient UARA in a network consisting of all the four RANs. Moreover, the different RAN characteristics are not optimised to meet the QoS requirements of divergent service groups efficiently. To this end, this chapter proposes an energy-efficient UARA framework for the ITNTN consisting of all four RANs. Similar to the preceding chapters, three service groups [3]: the feMBB, the euRLLC, and the LDHMC are considered.

A weighted sum SOOP is formulated to jointly maximise the global EE and minimise the number of mobility-induced handoffs experienced by the LDHMC use case. Handoffs are reduced by prioritising using NTNs characterised by large cell radii for LDHMC users. Moreover, as the euRLLC use case consists of mission-critical users for which denial of service is undesirable, the chapter still prioritises service provisioning of this use case and further limits its access to the satellite. The formulated SOOP problem is a non-convex and mixed

integer non-linear programming (MINLP) with no direct feasible solution. The problem's complexity is reduced by decomposing it into two sub-problems: i) the UARA problem and ii) the power allocation (PA) problem.

In the UARA phase, the BBU power is fixed, transforming the problem into a SOOP that maximises the network data rate and minimises the handoff probability. The solution to this problem was discussed in Section 3.4 and involved decomposing it into the user association sub-problem **P1** and the resource distribution sub-problem **P2**. Solutions to **P1** and **P2** have been discussed in the preceding Chapters 3 - 5. The PA problem is a non-linear fractional programming problem and is transformed into a weighted sum SOOP for better tractability and solved using the particle swarm optimisation (PSO) algorithm. PSO is a population-based search method characterised by high efficiency, simple implementation, and fast convergence [173]. Moreover, it can operate in a continuous number space directly, and as such, it is suitable for determining the optimal power values that satisfy the PA problem. The proposed particle swarm optimisation power allocation (PSOPA) algorithm is compared to the equal power allocation (EPA) scheme to validate its performance. The notations used in this chapter are in Table 6.1.

6.2 Problem formulation

The system model used in formulating the energy-efficient problem is similar to that presented in Section 3.2. In contrast, the delay QoS model adopted is as discussed in Section 5.2.1. The service-aware energy-efficient UARA problem is then formulated as a SOOP that maximises the EE while concurrently minimising the handoff probability. Mathematically,

Table 6.1: Notations defined in Chapter 6.

Symbol	Description
b, l, h, s	MBS, LAP, HAP, satellite AN
$\mathcal{B}, \mathcal{L}, \mathcal{H}, \mathcal{S}$	Set of ANs in the MBS, LAP, HAP, satellite RAN
$j, n_j, \mathcal{U}$	A RAN, AN in the j-th RAN, the set of users in the ITNTN
$\upsilon, \mathcal{E}, \mathcal{R}, \mathcal{D}$	A service group, feMBB, euRLLC, LDHMC service group
$\mathcal{U}_{\mathcal{E}}, \mathcal{U}_{\mathcal{R}}, \mathcal{U}_{\mathcal{D}}$	Set of users demanding $\mathcal{E}, \mathcal{R}, \mathcal{D}$
$u, u_{\mathcal{E}}, u_{\mathcal{R}}, u_{\mathcal{D}}, u_{\upsilon}$	User, an feMBB, euRLLC, LDHMC user, user belonging to service group υ
$\mathcal{W}_j, w_j, R_{n_j}$	A set of BBUs owned by RAN j, a BBU owned by RAN j, n_j cell radius
$\mathcal{T}_{w_j}, \Phi_{n_j}, \mathcal{N}$	Bandwidth of the BBU w_j, AN n_j bandwidth, set of all ANs in the ITNTN
$\mathcal{C}_{n_j,u,w_j}, \rho_{u_\upsilon}$	Data rate of a user u using BBU w_j of AN n_j, user priority factor
$\mu_{n_j,u}, \omega_{n_j,u,w_j}, \pi^u_{n_j}$	User association variable, resource allocation variable, coverage index
$\delta_1, \delta_2, \alpha_1, \alpha_2$	Normalisation factors
λ_{u_υ}, $\mathrm{L}_{u_\upsilon}, \mathcal{C}^{min}_{u_{\mathcal{R}}}$	Average packet arrival rate, packet size, delay bound, minimum delay bound rate
$nb^{u\upsilon}_{n_j}, P^{thres}_{n_j}$	Minimum number of BBUs allocated to user u belonging to service group υ by AN n_j, maximum available power at n_j
λ, ζ	Objective function trade-off factors
R_{max}	The largest possible cell radius in the ITNTN
$P_{n_j,u,w_j}, P_{cct_{n_j}}$	Transmit power of a user u using BBU w_j of AN n_j, constant circuit power that n_j consumes to process a call
$\mathcal{U}^{served}_{\mathcal{E}}, \mathcal{U}^{served}_{\mathcal{D}}$	Set of served users for the $\mathcal{E}, \mathcal{D}$ service groups
$\mathcal{U}^{served}_{\mathcal{R}_{n_j}}$	Set of served users for $\mathcal{R}$ service group
$\lvert\mathcal{U}^{n_j}_{as}\rvert$	Number of users associated with the AN n_j by the solution to problem **P5**.
$\mathcal{Y}, Y, y, Z$	Population set, population size, a particle/member of $\mathcal{Y}$, number of iterations
$\vec{x}_y, \vec{v}_y$	Particle position vector, particle velocity vector
$\vec{p}_y, \vec{g}$	Particle y's personal best position, the global best position of the group
$N_{\mathcal{B}}$	Number of MBSs

the global EE η_{EE} (in bits/Joule) of the ITNTN is the ratio of the entire network's sum rate

(in bits/s) to total power consumption (in Watts) [170], and is given as

$$\eta_{EE} = \frac{\sum_{n_j \in \mathcal{N}} \sum_{u \in \mathcal{U}} \sum_{w_j \in \mathcal{W}_j} \rho_{u_v} \ \mu_{n_j,u} \ \omega_{n_j,u,w_j} \ \mathcal{C}_{n_j,u,w_j}}{\sum_{n_j \in \mathcal{N}} \left(\sum_{u \in \mathcal{U}} \sum_{w_j \in \mathcal{W}_j} \rho_{u_v} \ \mu_{n_j,u} \ \omega_{n_j,u,w_j} \ P_{n_j,u,w_j} + P_{cct_{n_j}} \right)}, \tag{6.1}$$

where $\mu_{n_j,u} \in \{0,1\}$, $\omega_{n_j,u,w_j} \in \{0,1\}$, and $\rho_{u_v} \in [0,1]$ in (6.1) maintain their definitions given in Sections 3.2.5 and 3.2.6, as the user association variable, the resource allocation variable, and the priority factor respectively. $\mathcal{C}_{n_j,u,w_j}$ is the maximum data rate that can be achieved by user u on the BBU w_j of AN n_j, whose closed-form expression is given by (3.10). P_{n_j,u,n_j} denotes the transmit power from an AN n_j to a user u using BBU w_j while $P_{cct_{n_j}}$ is a constant circuit power that an AN belonging to the j-th RAN consumes to process a call.

On the other hand, the handoff reduction function was defined in Section 3.2.7 as

$$\Lambda = \sum_{n_j \in \mathcal{N}} \sum_{u \in \mathcal{U}} \sum_{w_j \in \mathcal{W}_j} \rho_{u_v} \ \mu_{n_j,u} \ \omega_{n_j,u,w_j} \ \frac{R_{n_j}}{R_{max}}. \tag{6.2}$$

Note that the bigger the user's handoff value R_{n_j}/R_{max}, the lower the number of handoffs since this user will be associated with an AN having a large cell radius. Therefore, the mobility-induced handoff probability is minimised by maximising the network handoff function Λ. The total system utility is the weighted summation of the entire network EE

and the handoff reduction function and is given by

$$\begin{aligned}\Gamma &= \lambda\ \delta_1\ \eta_{EE} + (1-\lambda)\ \delta_2\ \Lambda \\ &= \lambda\ \delta_1\ \frac{\sum\limits_{n_j\in\mathcal{N}}\sum\limits_{u\in\mathcal{U}}\sum\limits_{w_j\in\mathcal{W}_j}\rho_{u_v}\ \mu_{n_j,u}\ \omega_{n_j,u,w_j}\ \mathcal{C}_{n_j,u,w_j}}{\sum\limits_{n_j\in\mathcal{N}}\left(\sum\limits_{u\in\mathcal{U}}\sum\limits_{w_j\in\mathcal{W}_j}\rho_{u_v}\ \mu_{n_j,u}\ \omega_{n_j,u,w_j}\ P_{n_j,u,w_j} + P_{cct_{n_j}}\right)} \ + \\ &\quad (1-\lambda)\ \delta_2\ \sum_{n_j\in\mathcal{N}}\sum_{u\in\mathcal{U}}\sum_{w_j\in\mathcal{W}_j}\rho_{u_v}\ \mu_{n_j,u}\ \omega_{n_j,u,w_j}\ \frac{R_{n_j}}{R_{max}}.\end{aligned} \tag{6.3}$$

Given that an AN that maximises the EE does not necessarily maximise the handoff value, the weighting factor λ provides a trade-off between the two functions. In this chapter, the value of λ depends on the use case, such that $\lambda = 1$ for the static users demanding use cases $\mathcal{E}$ and $\mathcal{R}$, while it is zero for the mobile users requesting use-case $\mathcal{D}$. Hence, the priority of the static users is to maximise the EE, while the mobile users aim to reduce the number of mobility-induced handoffs. δ_1 and δ_2 are normalisation factors that enable the addition of the two functions having different units.

The energy-efficient UARA problem is then formulated as the maximisation of the weighted sum of the two functions η_{EE} and Λ in (6.3), subjected to minimum user QoS requirements and limited AN power and bandwidth resource budgets. Consequently, the optimisation problem is formulated as follows:

$$\max_{\mu_{n_j,u},\ \omega_{n_j,u,w_j},\ P_{n_j,u,w_j}} \quad \Gamma \tag{6.4}$$

s.t.

$$\text{C1: } \mu_{n_j,u} \leq \pi_{n_j,u}, \quad \forall\ n_j \in \mathcal{N}, \quad \forall\ u \in \mathcal{U} \tag{6.4a}$$

$$\text{C2:} \sum_{n_j \in \{\mathcal{B} \cup \mathcal{L} \cup \mathcal{H}\}} \pi_{n_j,u}\ \mu_{n_j,u}\ \omega_{n_j,u,w_j} \ \leqslant\ 1, \quad \forall\ u_{\mathcal{R}} \in \mathcal{U}_{\mathcal{R}} \tag{6.4b}$$

$$\text{C3:} \sum_{n_j \in \{\mathcal{S}\}} \pi_{n_j,u}\ \mu_{n_j,u}\ \omega_{n_j,u,w_j} \ =\ 0, \quad \forall\ u_{\mathcal{R}} \in \mathcal{U}_{\mathcal{R}} \tag{6.4c}$$

$$\text{C4:} \sum_{n_j \in \mathcal{N}} \pi_{n_j,u}\ \mu_{n_j,u}\ \omega_{n_j,u,w_j} \ \leqslant\ 1, \ \forall\ u_{\mathcal{E}} \in \mathcal{U}_{\mathcal{E}}, \ \forall\ u_{\mathcal{D}} \in \mathcal{U}_{\mathcal{D}} \tag{6.4d}$$

$$\text{C5:} \sum_{n_j \in \mathcal{N}} \sum_{w_j \in \mathcal{W}_j} \pi_{n_j,u}\ \mu_{n_j,u}\ \omega_{n_j,u,w_j}\ \mathcal{C}_{n_j,u,w_j} \geqslant \lambda_{u_\upsilon}\ \mathrm{L}_{u_\upsilon},$$

$$\forall\ \upsilon \in \{\mathcal{E}, \mathcal{D}\}, \ \ u_{\mathcal{E}} \in \mathcal{U}_{\mathcal{E}}^{served}, \ \ u_{\mathcal{D}} \in \mathcal{U}_{\mathcal{D}}^{served} \tag{6.4e}$$

$$\text{C6:} \sum_{n_j \in \mathcal{N}} \sum_{w_j \in \mathcal{W}_j} \pi_{n_j,u}\ \mu_{n_j,u}\ \omega_{n_j,u,w_j}\ \mathcal{C}_{n_j,u,w_j} \geqslant \mathcal{C}_{u_{\mathcal{R}}}^{min}, \ \ \forall\ u_{\mathcal{R}} \in \mathcal{U}_{\mathcal{R}}^{served}, \tag{6.4f}$$

$$\text{C7:} \sum_{u \in \mathcal{U}} \sum_{w_j \in \mathcal{W}_j} \pi_{n_j,u}\ \mu_{n_j,u}\ \omega_{n_j,u,w_j} \mathcal{T}_{w_j} \leq \Phi_{n_j}, \quad \forall\ n_j \in \mathcal{N} \tag{6.4g}$$

$$\text{C8:}\ P_{n_j,u,w_j} \geqslant 0, \quad \forall\ w_j \in \mathcal{W}_j \tag{6.4h}$$

$$\text{C9:} \sum_{u \in \mathcal{U}} \sum_{w_j \in \mathcal{W}_j} \pi_{n_j,u}\ \mu_{n_j,u}\ \omega_{n_j,u,w_j}\ P_{n_j,u,w_j} \leq P_{n_j}^{thres}, \quad \forall\ n_j \in \mathcal{N} \tag{6.4i}$$

$$\text{C10:} \sum_{u \in \mathcal{U}} \pi_{n_j,u}\ \mu_{n_j,u}\ \omega_{n_j,u,w_j} \leqslant 1, \ \ \forall\ n_j \in \mathcal{N}, \ \ \forall w_j \in \mathcal{W}_j \tag{6.4j}$$

$$\text{C11:}\ \mu_{n_j,u} = \{0,1\},\ \omega_{n_j,u,w_j} = \{0,1\}, \ \ \forall\ j \in \{\mathcal{B}, \mathcal{H}, \mathcal{L}, \mathcal{S}\}, \ \ \forall\ n_j \in \mathcal{N}, \ \ \forall\ w_j \in \mathcal{W}_j, \ \ \forall\ u \in \mathcal{U} \tag{6.4k}$$

$\pi_{n_j,u} \in \{0,1\}$ is a binary factor that is 1 when the user u is within the cell radius of AN n_j, and is 0 otherwise. Therefore, constraint C1 limits the association of users only to ANs in whose coverage the users lie. In constraints C2 and C3, a user belonging to $\mathcal{U}_{\mathcal{R}}$ may connect to only one AN $n_j \in \{\mathcal{B} \cup \mathcal{L} \cup \mathcal{H}\}$ at a time. C4 ensures that users belonging to $\mathcal{U}_{\mathcal{E}}$ or $\mathcal{U}_{\mathcal{D}}$ can connect to only one of the available ANs. Similar to Chapter 5, the traffic arriving at the transmission queue of an AN is modeled as a Poisson process with an average arrival

rate of λ_{u_υ} packets/s, each packet having a size L_{u_υ} bits $\forall\ \upsilon \in \{\mathcal{E}, \mathcal{D}, \mathcal{R}\}$. Thus, a user $u_\mathcal{E} \in \mathcal{U}_\mathcal{E}^{served}$ or $u_\mathcal{D} \in \mathcal{U}_\mathcal{D}^{served}$ is guaranteed its minimum QoS requirements in constraint C5. $\mathcal{U}_\mathcal{E}^{served}$ and $\mathcal{U}_\mathcal{D}^{served}$ represent sets of served users for the respective service groups. Similarly, a mission-critical user is guaranteed its minimum delay bound rate in C6, where $\mathcal{C}_{u_\mathcal{R}}^{min}$ is given by (5.5). C7 considers the capacity limitations of each AN. In C8, the transmit power on the BBU w_j of AN n_j can not be negative, while C9 ensures that the total consumed power at the AN can not exceed its maximum available power $P_{n_j}^{thres}$. A BBU can be used by at most one user as depicted by C10, while C11 ensures that the decision variables $\mu_{n_j,u}$ and ω_{n_j,u,w_j} are binary.

6.3 Proposed solution

The optimisation problem in (6.4) is a non-convex and MINLP problem with no direct feasible solution. Similar to [143] and in a bid to reduce complexity, the problem is subdivided into two sub-problems. The first sub-problem **P5** deals with UARA by fixing the BBU transmit power such that $P_{n_j,u,w_j} = P_{n_j}^{thres}/|\mathcal{W}_j|$, where $|\mathcal{W}_j|$ is the total number of BBUs available at the AN n_j belonging to the RAN j. **P5** is formulated as:

P5

$$\max_{\mu_{n_j,u},\ \omega_{n_j,u,w_j}} \quad \Bigg(\lambda\ \delta_1 \sum_{n_j \in \mathcal{N}} \sum_{u \in \mathcal{U}} \sum_{w_j \in \mathcal{W}_j} \rho_{u_\upsilon} \mu_{n_j,u}\ \omega_{n_j,u,w_j} \mathcal{C}_{n_j,u,w_j}$$

$$+ \quad (1-\lambda)\ \delta_2 \sum_{n_j \in \mathcal{N}} \sum_{u \in \mathcal{U}} \sum_{w_j \in \mathcal{W}_j} \rho_{u_\upsilon}\ \mu_{n_j,u}\ \omega_{n_j,u,w_j}\ \frac{R_{n_j}}{R_{max}} \Bigg) \tag{6.5}$$

$$\text{s.t.} \quad (6.4a), (6.4b), (6.4c), (6.4d), (6.4e), (6.4f), (6.4g), (6.4j), (6.4k).$$

The problem **P5** is similar to the SOOP defined in (3.24), which was a weighted sum of the total network data rate given in (3.19) and the network handoff minimisation function defined by (3.22). Hence, **P5** can be solved by decomposing it into two problems: **P1** and **P2** defined in (3.29) and (3.31), respectively. **P1** associated users to the appropriate ANs and allocated the minimum number of BBUs required to meet the user QoS. The GA described in Chapter 4 or the RL technique discussed in Chapter 5 can be used to solve this problem. On the other hand, for any AN that had users associated with it, **P2** allocated the excess unallocated BBUs after the association phase. **P2** was solved using the water-filling approach, as described in Section 3.4.2.

Having solved the UARA variables, the second sub-problem **P6** of the problem (6.4) allocates power to the allocated BBUs to maximise the global energy efficiency of the ITNTN. Thus, **P6** is formulated as follows:

$$\textbf{P6}:$$

$$\max_{P_{n_j,u,w_j}} \quad \frac{\sum_{n_j\in\mathcal{N}}\sum_{u\in\mathcal{U}} nb^{u}_{n_j}\ \mathcal{C}_{n_j,u,w_j}(P_{n_j,u,w_j})}{\sum_{n_j\in\mathcal{N}}\left(\sum_{u\in\mathcal{U}} nb^{u}_{n_j}\ P_{n_j,u,w_j} + P_{cct_{n_j}}\right)}, \tag{6.6}$$

s.t.

$$\text{C1:}\ \sum_{n_j\in\mathcal{N}} nb^{u}_{n_j}\ \mathcal{C}_{n_j,u,w_j}(P_{n_j,u,w_j}) \geqslant \lambda_{u_\upsilon}\ \mathrm{L}_{u_\upsilon},$$

$$\forall\ \upsilon\in\{\mathcal{E},\mathcal{D}\},\quad u_{\mathcal{E}}\in\mathcal{U}^{served}_{\mathcal{E}},\quad u_{\mathcal{D}}\in\mathcal{U}^{served}_{\mathcal{D}} \tag{6.6a}$$

$$\text{C2:}\ \sum_{n_j\in\mathcal{N}} nb^{u}_{n_j}\ \mathcal{C}_{n_j,u,w_j}(P_{n_j,u,w_j}) \geqslant \mathcal{C}^{min}_{u_{\mathcal{R}}},\quad \forall\ u_{\mathcal{R}}\in\mathcal{U}^{served}_{\mathcal{R}}, \tag{6.6b}$$

$$\text{C3: } P_{n_j,u,w_j} \geqslant 0, \quad \forall\ w_j \in \mathcal{W}_j \tag{6.6c}$$

$$\text{C4:} \sum_{u \in \mathcal{U}} nb^{u}_{n_j}\ P_{n_j,u,w_j} \leq P^{thres}_{n_j}, \quad \forall\ n_j \in \mathcal{N}, \tag{6.6d}$$

where $nb^{u}_{n_j} \in \{0, 1, 2, \ldots, |\mathcal{W}_j|\}$ is the number of BBUs of AN n_j that have been allocated to user u in the UARA phase. Note that the data rate $\mathcal{C}_{n_j,u,w_j}$ achieved by a user over a BBU depends on the allocated power P_{n_j,u,w_j} in **P6**.

While the original problem in (6.4) prioritised the EE maximisation for the $\mathcal{U}_{\mathcal{E}}$ and $\mathcal{U}_{\mathcal{R}}$ users, and handoff minimisation for the $\mathcal{U}_{\mathcal{D}}$ users, it is important to note that subdividing the problem into **P5** and **P6** enables maximisation of EE for the $\mathcal{U}_{\mathcal{D}}$ users as well. **P5** ensures that these users are served by the large coverage ANs, and **P6** then allocates power to the users' BBUs to maximise the global EE. **P6** is a non-linear fractional programming problem that maximises the total network data while minimising power consumption concurrently, and as such, can be represented as a MOOP [143]. Let $\mathcal{U}^{n_j}_{as}$ define the set of users associated by **P5** to the AN n_j. For each AN n_j, two functions are defined such that:

$$\begin{aligned} f1(P_{n_j,u,w_j}) &= -\sum_{u \in \mathcal{U}^{n_j}_{as}} nb^{u}_{n_j}\ \mathcal{C}_{n_j,u,w_j}(P_{n_j,u,w_j}), \\ f2(P_{n_j,u,w_j}) &= \sum_{u \in \mathcal{U}^{n_j}_{as}} nb^{u}_{n_j}\ P_{n_j,u,w_j} + P_{cct_{n_j}}. \end{aligned} \tag{6.7}$$

$f1$ is negative since this function will be minimised as elaborated in (6.8). Owing to its simplicity and low computational complexity, the weighted sum SOOP is used to reformulate

P6 for each AN as

P7:

$$\min_{P_{n_j,u,w_j}} \quad (\alpha_1\ \zeta\ f1(P_{n_j,u,w_j}) + \alpha_2\ (1-\zeta)\ f2(P_{n_j,u,w_j})), \tag{6.8}$$

s.t.

C1: $nb^{u}_{n_j}\ \mathcal{C}_{n_j,u,w_j}(P_{n_j,u,w_j}) \geqslant \lambda_{u_\upsilon}\ \mathrm{L}_{u_\upsilon}$,

$$\forall\ \upsilon \in \{\mathcal{E},\mathcal{D}\},\quad u_{\mathcal{E}} \in \mathcal{U}^{served}_{\mathcal{E}},\quad u_{\mathcal{D}} \in \mathcal{U}^{served}_{\mathcal{D}} \tag{6.8a}$$

C2: $nb^{u}_{n_j}\ \mathcal{C}_{n_j,u,w_j}(P_{n_j,u,w_j}) \geqslant \mathcal{C}^{min}_{u_{\mathcal{R}}},\quad \forall\ u_{\mathcal{R}} \in \mathcal{U}^{served}_{\mathcal{R}},$ (6.8b)

C3: $P_{n_j,u,w_j} \geqslant 0,\quad \forall\ w_j \in \mathcal{W}_j$ (6.8c)

C4: $\sum_{u\in\mathcal{U}} nb^{u}_{n_j}\ P_{n_j,u,w_j} \leq P^{thres}_{n_j},\quad \forall\ n_j \in \mathcal{N}.$ (6.8d)

In the first function ($f1(P_{n_j,u,w_j})$), the negative of the total accumulated data rate at the AN is minimised, translating into maximising the achieved data rate. The second function ($f2(P_{n_j,u,w_j})$) minimises the power consumption at the AN. Maximising the total achieved data rate while simultaneously minimising the power consumption at the AN are two contradictory requirements since minimising power consumption degrades the total data rate. Therefore, the weight $\zeta \in [0,1]$ defines the importance of the two objective functions, and the operator sets this weight. A complete Pareto optimal solution set for the MOOP of the two functions in (6.7) can be obtained by changing the weight ζ in (6.8) over the range [0,1] [174]. α_1 and α_2 represent normalisation factors that enable the addition of the two

functions $f1(P_{n_j,u,w_j})$ and $f2(P_{n_j,u,w_j})$ having different units. The SOOP **P7** (6.8) is solved using the PSO algorithm.

6.4 The PSO power allocation (PSOPA) solution

In this section, the PSO framework is first described, then the PSO algorithm used to solve problem **P7** is given.

6.4.1 A review of the PSO

The PSO is a population-based, self-adaptive, stochastic search optimisation algorithm introduced in 1995 to solve non-linear problems [175]. It belongs to a class of algorithms called metaheuristics. It is based on the paradigm of swarm intelligence, in which particles move around the search space, influenced by improvements discovered by other particles. PSO can operate in a continuous real number space directly, so it is suitable for determining the optimal power values for the problem **P7**. Moreover, it is characterised by high efficiency, simple implementation, and fast convergence [173].

The PSO algorithm generally begins by creating an initial population set $\mathcal{Y}$ consisting of Y particles. Each particle $y \in \mathcal{Y}$ is a potential solution to the optimisation problem and is defined by its coordinates in the search space. Moreover, each particle must be characterised by a movement that enables it to find the optimal solution. Consequently, at the beginning of the PSO algorithm, each particle $y \in \mathcal{Y}$ is initialized with random position and velocity vectors. Consider an m-dimensional search space: the position, and velocity of the particle

Table 6.2: PSO parameter definitions.

Parameter	Description
m	Total number of variables
Y	Number of particles
k	Iteration count
v_{yu}^{k+1}	Velocity of the u-th variable of the y-th particle in the $(k+1)$-th iteration.
x_{yu}^{k}	Position of the u-th variable of the y-th particle in the k-th iteration.
w	Inertia weight
$C_1,\ C_2$	Cognitive and social acceleration coefficients
p_{yu}^{k}	Personal best position of the u-th variable of the y-th particle in the k-th iteration.
g_{u}^{k}	Global best position of the u-th variable in the k-th iteration
$r_1,\ r_2$	Random variables uniformly generated in the range [0,1]

$y \in \mathcal{Y}$ are represented by vectors $\vec{x}_y = (x_{y1}, x_{y2}, \ldots, x_{ym})$ and $\vec{v}_y = (v_{y1}, v_{y2}, \ldots, v_{ym})$, respectively. Let $\vec{p}_y$ and $\vec{g}$ represent particle y's personal best position and the global best position of the group, respectively. The particle's velocity can be modified as

$$v_{yu}^{k+1} = w\ v_{yu}^{k} + C_1 r_1 (p_{yu}^{k} - x_{yu}^{k}) + C_2 r_2 (g_{u}^{k} - x_{yu}^{k})\ \ \forall u \in \{1, 2, \ldots, m\}\ \forall y \in \{1, 2, \ldots, Y\}, \quad (6.9)$$

where all the variables used in (6.9) are defined in Table 6.2.

According to (6.9), each particle's velocity is influenced by three primary parameters: the inertia weight w, the cognitive acceleration coefficient C_1, and the social acceleration coefficients C_2. These three weights are used to control the levels of exploitation and exploration. Exploitation enables the particle to target the best solution achieved so far. At the same time, exploration allows the particles to randomly search for better solutions, if any, that have not been identified yet. The inertia weight w defines the particles' ability to change their direction. The lower the value of w, the stronger the convergence; lower values

of w facilitate exploitation, while higher values lead to exploration. Therefore, the inertia w balances local exploitation and global exploration and thus keeps the algorithm from getting stuck in local optima.

On the other hand, the weights C_1 and C_2 define the magnitude of influence on the particle's velocity, either in the directional towards the particle's best position and hence the local optima, or towards the global best, which results in the global optima. If C_1 is much higher than C_2, convergence is not achieved since each particle is individualistic, focusing on only its personal best. On the other hand, a much larger value of C_2 when compared to C_1 favours exploitation to the group's global best value at the expense of exploration. Therefore, these two acceleration coefficients are complementary, and combining them increases exploitation and exploration. The weights r_1 and r_2 are used to stochastically adjust the cognitive acceleration and social acceleration coefficients, respectively, and thus enable an appropriate balance between exploration and exploitation.

After determining each particle's new velocity using (6.9), the new position is then updated using

$$x_{yu}^{k+1} = x_{yu}^{k} + v_{yu}^{k+1} \quad \forall u \in \{1, 2, \ldots, m\} \; \forall y \in \{1, 2, \ldots, Y\}. \tag{6.10}$$

Consequently, each iteration of the PSO algorithm involves determining each particle's velocity, which allows it to modify its position over the iterations to find the global optimal solution.

6.4.2 The proposed PSOPA algorithm

A population set $\mathcal{Y}$ consisting of Y particles is defined. For each particle $y \in \mathcal{Y}$, both the position and velocity vectors are defined as $|\mathcal{U}_{as}^{n_j}|$ dimensional vectors, where $|\mathcal{U}_{as}^{n_j}|$ represents the number of users associated with the AN n_j by the solution to problem **P5**. Therefore, each particle's position vector is defined as $\vec{x}_y = (x_{y1}, x_{y2}, \ldots, x_{y|\mathcal{U}_{as}^{n_j}|}) \in \mathbb{R}^{|\mathcal{U}_{as}^{n_j}|}$. On the other hand, the velocity vector is represented as $\vec{v}_y = (v_{y1}, v_{y2}, \ldots, v_{y|\mathcal{U}_{as}^{n_j}|}) \in \mathbb{R}^{|\mathcal{U}_{as}^{n_j}|}$. The element $x_{yu} \in [0, P_{n_j}^{thres}/|\mathcal{W}_j|]$ in $\vec{x}_y$ represents the power allocated to a user $u \in \{1, 2, \ldots, |\mathcal{U}_{as}^{n_j}|\}$ over one BBU. Thus, the purpose of the PSO algorithm is to determine the optimal solution $\vec{g}$, consisting of optimal power values x_{y^*u} $\forall u \in \{1, 2, \ldots, |\mathcal{U}_{as}^{n_j}|\}$ that satisfy the optimisation problem **P7** in (6.8).

Algorithm 7 depicts the proposed PSO power allocation algorithm. The population set $\mathcal{Y}$ is generated in line 2, and line 3 randomly generates the initial position $\vec{x_y}$ and velocity $\vec{v_y}$ of each particle $y \in \mathcal{Y}$. In line 4, each particle's initial position $\vec{x_y}$ is initialized as the particle's best value $\vec{p_y}$. Using the position vector $\vec{x_y}$, each particle's fitness value is evaluated using the optimisation problem **P7** in line 5. In line 6, the position vector with the highest fitness value is initialized as the global best value $\vec{g}$. Lines 7 - 17 iteratively run the PSO algorithm by updating the particles' velocity and position vectors in each iteration utilising equations (6.9) and (6.10), respectively, and consequently updating each particle's personal best value $\vec{p_y}$ and the global best value $\vec{g}$. As the position vectors are updated, the values obtained might fall out of the accepted range $[0, P_{n_j}^{thres}/|\mathcal{W}_j|]$. Therefore, line 12 ensures that these values fall within the problem's search space. Fig. 6.1 depicts the PSO process for a minimisation problem such as **P7** (6.8).

Algorithm 7 PSOPA at an access node

Input: Population size Y, inertia coefficient w, personal acceleration coefficient C_1, social acceleration coefficient C_2, Number of iterations Z, channel gain statistics determined using (3.8) between the AN n_j and the different associated users, the number of BBUs allocated to the different users as determined by problem **P5**

Output: Power allocation vector

1: **procedure** POWER ALLOCATION
2: Generate the initial population set $\mathcal{Y}$ containing Y particles
3: Randomly generate each particle's initial position $\vec{x}_y$ and velocity $\vec{v}_y$
4: Initialize each particle's best value as $\vec{p}_y \leftarrow \vec{x}_y$
5: Evaluate each particle's fitness value using **P7**
6: Initialize the global best value $\vec{g}$
7: **for** iteration $= 1 : Z$ **do**
8: **for** each particle $y \in \mathcal{Y}$ **do**
9: Pick two random numbers $r_1, r_2 \sim \mathrm{U}(0,1)$
10: Update particle's velocity $\vec{v}_y$ as follows:
$\vec{v}_y \leftarrow w\vec{v}_y + C_1 r_1(\vec{p}_y - \vec{x}_y) + C_2 r_2(\vec{g} - \vec{x}_y)$
11: Update particles new position using:
$\vec{x}_y \leftarrow \vec{x}_y + \vec{v}_y$
12: Bound the updated position to fall within the search space
13: Evaluate the fitness value **P7**$(\vec{x}_y)$ of $\vec{x}_y$
14: **If P7**$(\vec{x}_y) <$ **P7**$(\vec{p}_y)$, **then** $\vec{p}_y \leftarrow \vec{x}_y$
15: **If P7**$(\vec{x}_y) <$ **P7**$(\vec{g})$, **then** $\vec{g} \leftarrow \vec{x}_y$
16: **end for**
17: **end for**
18: Return the power allocation solution $\vec{g}$
19: **end procedure**

6.4.3 The computational complexity of the PSO power allocation algorithm

Similar to the previous chapters, the time complexity of the PSOPA algorithm is analysed using the big-O notation. Algorithm 7 starts with generating the particles' initial position and velocity vectors. The time complexity for generating random numbers is O(1), which is independent of the number of random numbers to be generated. Therefore, this complexity is negligible. Lines 7-17 of Algorithm 7 involve evaluating the objective function of each particle. This computation involves determining the data rate achieved for each power

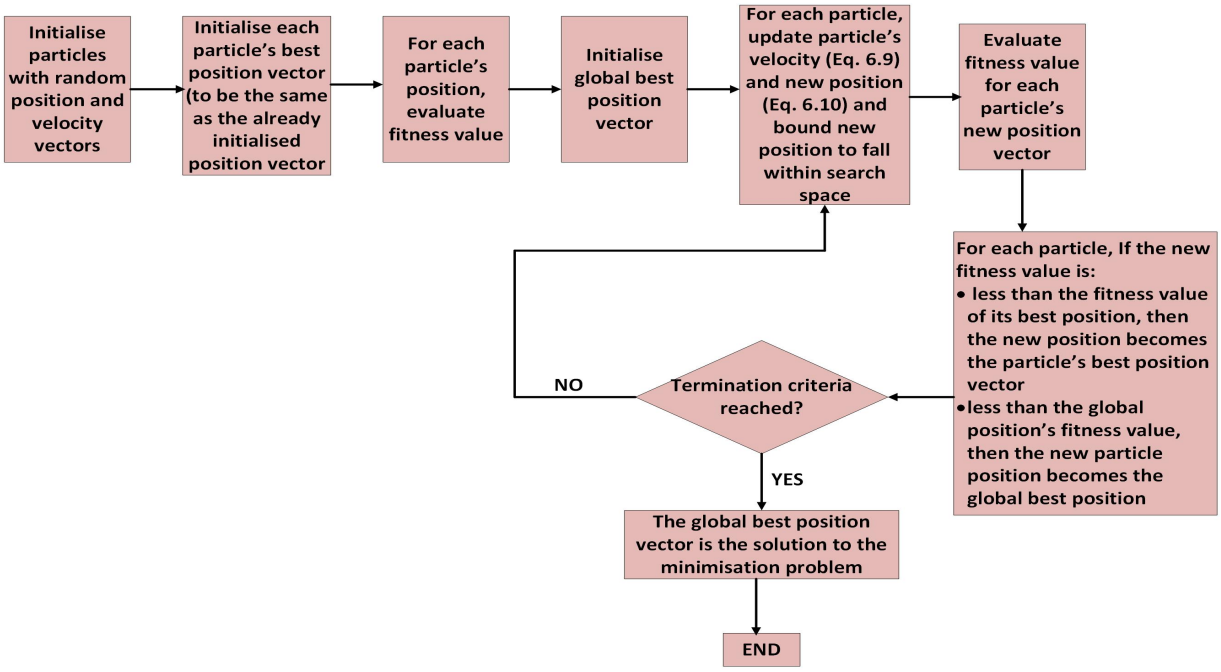

Figure 6.1: The PSO algorithm process.

value x_{yu} in $\vec{x_y}$ while ensuring the constraints are satisfied. The time complexity for this computation is $\mathrm{O}(|\mathcal{U}_{as}^{n_j}|)$, where $|\mathcal{U}_{as}^{n_j}|$ is the number of users associated and served by the AN n_j, according to problem **P5**. Also, updating the velocity of each variable v_{yu} in $\vec{v_y}$ requires a complexity of $\mathrm{O}(|\mathcal{U}_{as}^{n_j}|)$. In the same manner, the position vector of each variable x_{yu} in $\vec{x_y}$ has to be updated in each iteration, requiring a time complexity of $\mathrm{O}(|\mathcal{U}_{as}^{n_j}|)$ as well. Given that the above computations have to be done for all particles and in Z iterations, the overall time complexity of the PSO power allocation algorithm is then given by $\mathrm{O}(Z \times Y \times (|\mathcal{U}_{as}^{n_j}| + |\mathcal{U}_{as}^{n_j}| + |\mathcal{U}_{as}^{n_j}|))$, which can be reduced to $\mathrm{O}(Z \times Y \times |\mathcal{U}_{as}^{n_j}|)$. Consequently, the proposed power allocation algorithm is characterised by a polynomial time complexity that depends on the number of iterations Z, the population size Y and the number of users $|\mathcal{U}_{as}^{n_j}|$ associated to the AN n_j.

6.5 The equal power allocation scheme

The performance of the proposed PSOPA algorithm is validated through comparison to the EPA scheme, as utilised in [176, 177]. The EPA algorithm allocates the same power to all AN's BBUs as was done in solving problem **P5**. Therefore, the power allocated to any AN's BBU in the EPA is given by

$$P_{n_j,u,w_j} = \frac{P_{n_j}^{thres}}{|\mathcal{W}^{n_j}|}, \tag{6.11}$$

where $P_{n_j}^{thres}$ is the maximum power available at AN n_j and $|\mathcal{W}^{n_j}|$ is the number of BBUs available at that AN. Since the PSOPA algorithm allocates a power in the range $[0, P_{n_j}^{thres}/|\mathcal{W}_j|]$ to a BBU allocated to a user associated to AN n_j, it is clear that the EPA algorithm gives the upper bound of an AN's BBU allocated power.

6.6 Results and performance evaluation

To evaluate the performance of the proposed PSOPA algorithm, we consider a scenario in which users are randomly and uniformly distributed in an urban circular region of 3 km radius. This region is within the coverage of 1 LEO satellite and 1 HAP and consists of several MBSs and 1 LAP. The radius of an MBS is assumed to be 1 km, while that of the LAP is 2 km. The parameters used in the simulation are given in Table 6.3 [19, 1, 111, 112]. Similar to Chapter 5, the data packet arrival rate $\lambda_{u_v} \forall v \in \{\mathcal{R}, \mathcal{E}, \mathcal{D}\}$ is set to 20 packets/s, the packet size for the euRLLC service group is set to 500 bits while that for the feMBB and LDHMC to 9000 bits. The delay bound D_{max} and delay bound violation probability

Table 6.3: Simulation parameters and values.

Parameter	Value
$\mathcal{T}_{w_{\mathcal{B}}}, \mathcal{T}_{w_{\mathcal{L}}}, \mathcal{T}_{w_{\mathcal{H}}}, \mathcal{T}_{w_{\mathcal{S}}}$	[0.18, 0.18, 1, 2] MHz
Number of BBUs for $[n_{\mathcal{B}}, n_{\mathcal{L}}, n_{\mathcal{H}}, n_{\mathcal{S}}]$	[10, 10, 20, 20]
$[P_{n_{\mathcal{B}}}^{thres}, P_{n_{\mathcal{L}}}^{thres}, P_{n_{\mathcal{H}}}^{thres}, P_{n_{\mathcal{S}}}^{thres}]$	[8, 5, 20, 25] Watts
Service group user ratio $[\lvert\mathcal{U}_{\mathcal{R}}\rvert : \lvert\mathcal{U}_{\mathcal{D}}\rvert : \lvert\mathcal{U}_{\mathcal{E}}\rvert]$	[0.3:0.1:0.6]
Noise spectral density	-174 dBm

threshold ϵ used to obtain the minimum rate $\mathcal{C}_{u_{\mathcal{R}}}^{min}$ for the delay-sensitive users as described in Section 5.2.1 are set to 1 ms and 0.001 respectively.

As the PSO's performance depends on the inertia weight w, the acceleration coefficients C_1 and C_2, and the population size Y, the simulation started with determining the appropriate values to use, considering a case of 100 users in the network.

6.6.1 PSO parameter setting

The appropriate parameters used in the proposed PSOPA solution are identified in this subsection. Fig. 6.2 depicts the effect of the inertia weight w on the PSO convergence. The values of C_1, C_2, and the population size are fixed at 1, 2, and 200, respectively. The figure shows that $w = -0.2$ achieves the lowest fitness value at convergence. As w decreases below -0.2, the performance of the PSO worsens since we observe an increase in the fitness value at convergence. Such performance is because the rate of exploitation increases further, thereby increasing the chances of the algorithm getting stuck in a local optimum. Similarly, increasing w from 0.2 to 1 increases the fitness value achieved at convergence and does not provide the required minimum fitness value. As w increases, the rate of exploration increases, thereby influencing the particles' direction to their personal best and not the group's global

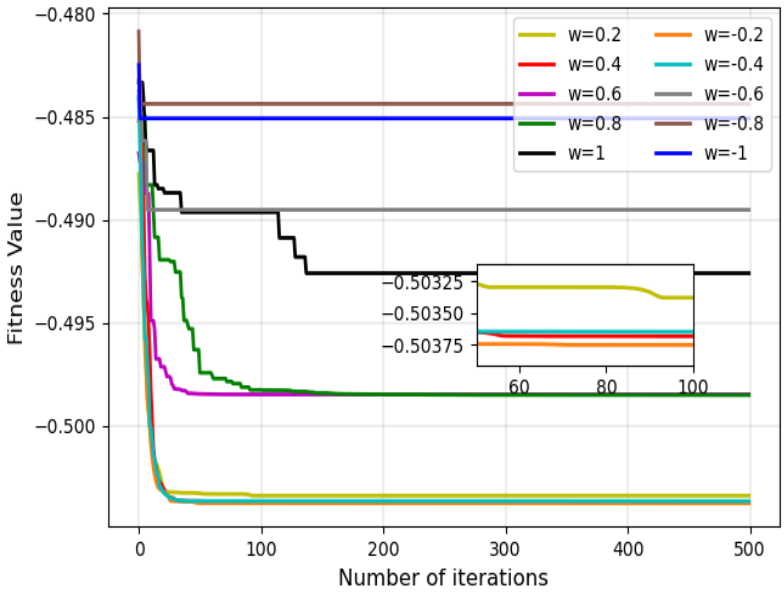

Figure 6.2: Effect of inertia w on convergence of the PSO.

best. This leads to the observed reduction in performance at convergence. Since $w = -0.2$ yields the best performance, this value is chosen for this work.

Fig. 6.3 depicts the effect of C_1 on the fitness value achieved at convergence. All values of C_1 yield almost the same fitness value at convergence, with $C_1 = 2$ slightly outperforming all other values of C_1. Consequently, $C_1 = 2$ is chosen for this work.

Fig. 6.4 shows the effect of C_2 on the convergence of the PSOPA algorithm. In this figure, $C_2 = 2$, $C_2 = 2.5$, and $C_2 = 3$ achieve almost the same fitness value at convergence. The value chosen for this work is $C_2 = 2$ since the higher values will increase exploitation which is already favoured by the lower inertia value. The population size's effect on the PSO convergence is shown in Fig. 6.5. It is observed that the performance of the PSO improves slightly as the population size Y increases. However, the higher the values of Y and iteration size Z are, the more the computational complexity of the PSO. Therefore,

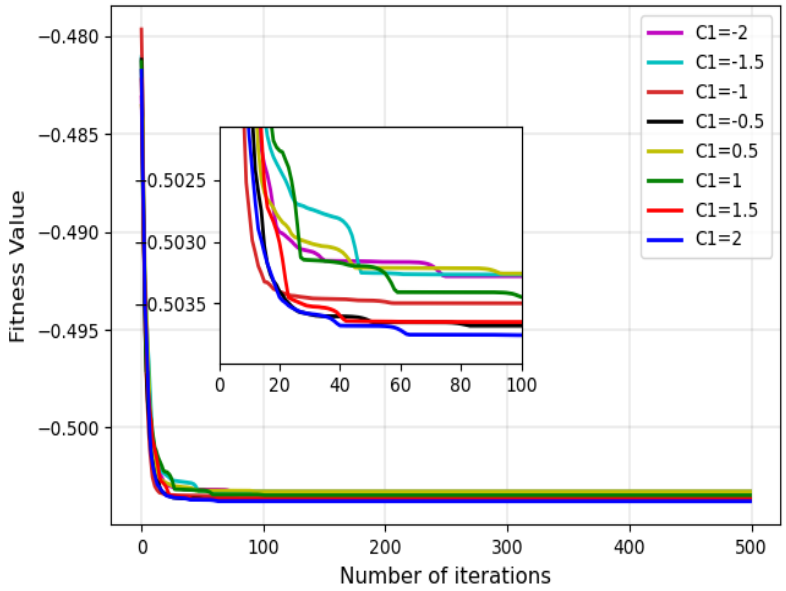

Figure 6.3: Effect of cognitive acceleration coefficient C_1 on convergence of the PSO.

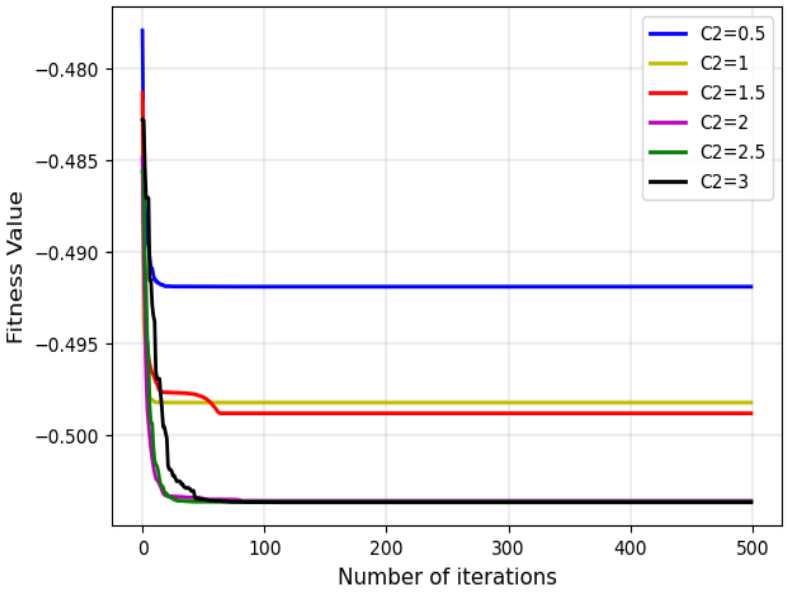

Figure 6.4: Effect of social acceleration coefficient C_2 on convergence of the PSO.

$Y = 300$ and iteration size $Z = 200$ were chosen to validate the proposed PSOPA algorithm.

Table 6.4 gives the parameters used for the PSO algorithm.

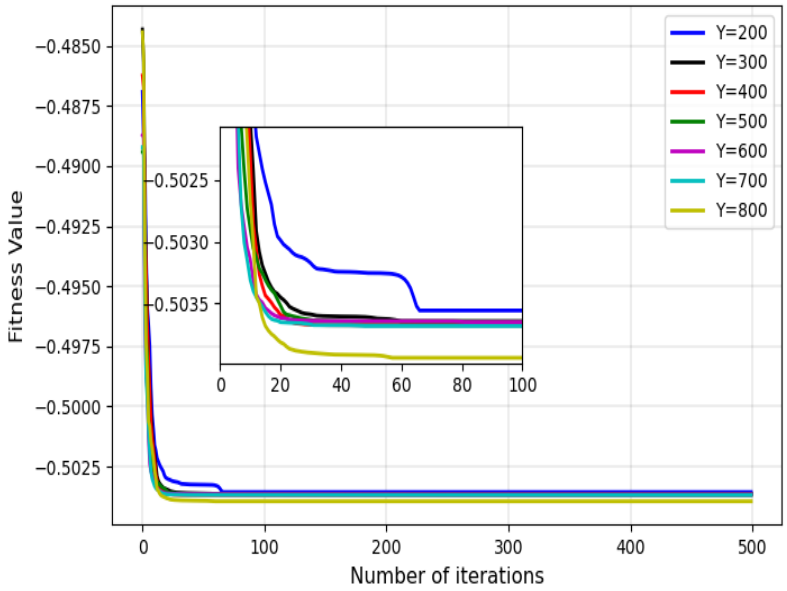

Figure 6.5: Effect of population size Y on convergence of the PSO.

Table 6.4: PSO parameters.

Parameter	Value
Inertia weight w	-0.2
Cognitive acceleration coefficient C_1	2
Social acceleration coefficient C_2	2
Particle size Y	300
Number of iterations Z	200

6.6.2 Simulation results

The performance of the PSOPA algorithm is analysed by comparing it to the EPA scheme. The performance evaluation is based on three metrics: i) the achieved data rate in bits/s, ii) the consumed power in Watts, and iii) the global energy efficiency defined as the ratio of the total network data rate to the total network power consumption as defined by (6.1).

6.6.2.1 Impact of the trade-off factor ζ

First, considering a scenario of 70 users in the network and power allocation to the users associated with the HAP AN, Fig. 6.6 shows that in solving **P6** as a weighted sum SOOP (6.8), a set of Pareto-optimal solutions exists. The figure is obtained using Algorithm 7 and varying the weighting factor ζ from 0 to 1 with an increment size of approximately 0.0526. The figure shows the functional relationship between the two functions $f1$ and $f2$ in (6.8). To maximise the data rate, the fitness value of objective function $f1$ (function 1 in Fig. 6.6) has to be minimised, which increases the power consumption in the network represented by objective function 2 in the figure. Therefore, there is a need for a trade-off between the two functions to achieve an energy-efficient network, with the optimal energy-efficient solution falling inside the circular region in Fig. 6.6.

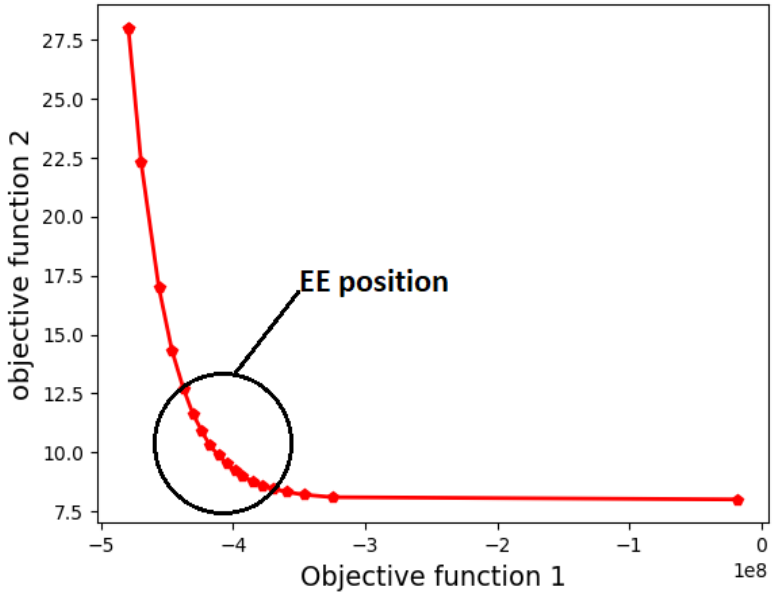

Figure 6.6: Pareto-optimal front of weighted sum SOOP in (6.8).

The contradiction of the two objective functions $f1$ and $f2$ in (6.8) is further illustrated by Fig. 6.7. This figure depicts the behaviour of the total achieved network data rate and the total power consumption as the weighting factor ζ varies. When ζ is low, objective function $f2$ is prioritised. Consequently, the total power consumed in the network is minimised but at the expense of a reduced network data rate. As ζ increases, the priority shifts to data rate maximisation, hence the observed increase in the achieved total network data rate. However, such a rise implies an upsurge in power consumption, as depicted by the figure, thereby further illustrating the importance of the trade-off factor ζ in achieving a balance between the two objective functions.

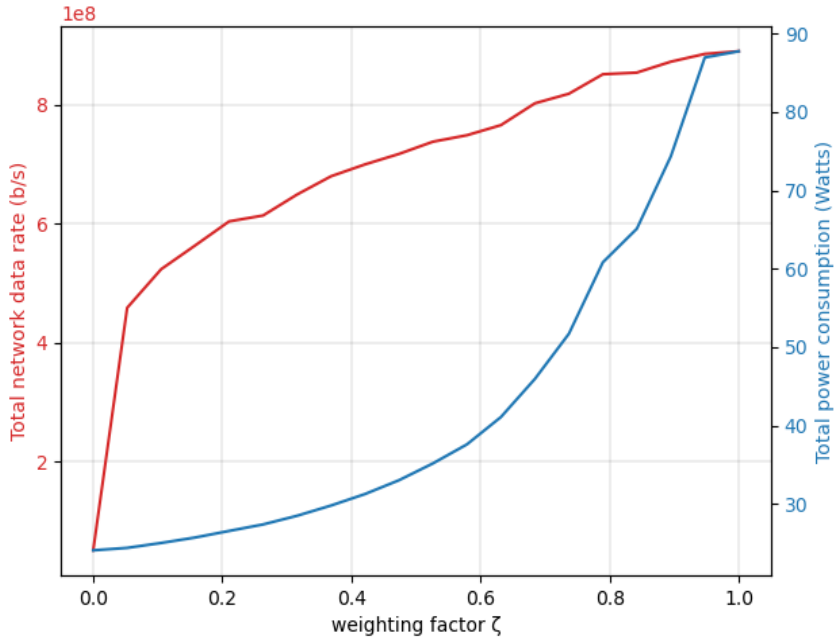

Figure 6.7: Effect of ζ on total network data rate and total power consumption.

6.6.2.2 Impact of user and access nodes densities

In this subsection, the PSOPA algorithm's performance is evaluated for a varying number of users in the network. Since the NTNs are characterised by a large coverage area, their ANs are maintained at 1 LAP, 1 HAP, and 1 LEO satellite. However, the effect of user density is analysed for varying MBS densities (i.e., $N_{\mathcal{B}} = 2, 4, 6$, and 8 MBSs, where $N_{\mathcal{B}}$ represents the number of MBSs.) The weighting factor ζ is set to 0.7 in these simulations.

Fig. 6.8 depicts the effect of user density on the total network power consumption for different numbers of deployed MBSs. As can be observed in the figure, an increase in the number of users in the network generally increases the total network power consumption. However, as the number of users exceeds what the network can serve, the power consumption saturates and thus remains almost constant for both algorithms. This is because the available resources have been depleted, and as such, the network serves a fixed number of users, which results in consuming almost constant power. Also, as expected, more power is consumed as the number of ANs increases in the network. An increase in the number of ANs allows a significant number of users that were initially dropped due to limited resources to be served, leading to an upsurge in power consumption for a large number of users in the network. As observed in the figure, as the number of users in the network increases, the PSOPA algorithm performs better than the EPA algorithm in terms of power consumption for all different AN densities. The power consumed by the PSOPA and EPA algorithms, on average, for the different AN densities is depicted in Table 6.5.

According to Table 6.5, the average power consumption for the PSOPA and EPA algorithms is 43.478 and 70.521 Watts, respectively, translating into a 38.3% performance

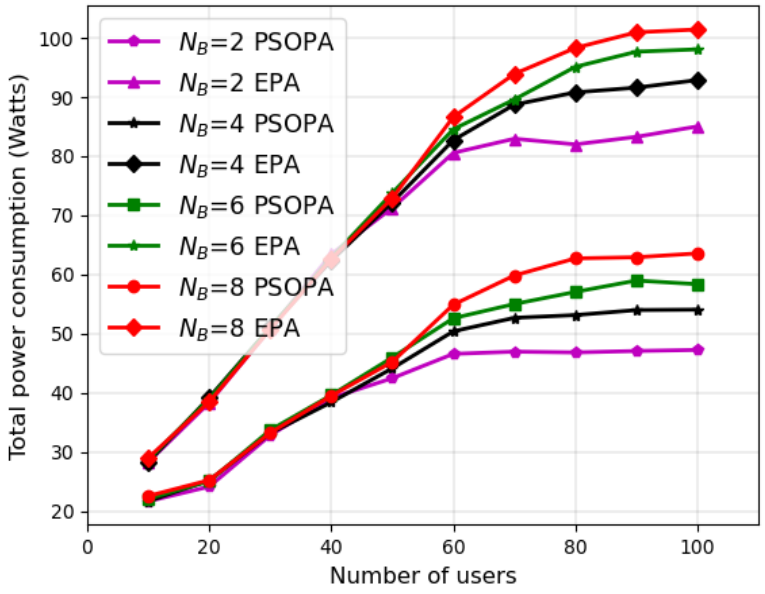

Figure 6.8: Effect of user density on the total network power consumption for varying number of MBSs $N_{\mathcal{B}}$.

Table 6.5: Average network power consumption for varying number of MBSs.

MBS density	Average power consumption by the PSOPA algorithm (Watts)	Average power consumption by the EPA algorithm (Watts)
2	39.46813324	66.589
4	42.66481536	69.975
6	44.82932332	72.024
8	46.95056691	73.498
Average power consumption (Watts)	**43.47820971**	**70.5215**

gain of the PSOPA algorithm over the EPA scheme. The PSOPA algorithm consumes less power than the EPA algorithm because it is formulated in a manner that enables it to reduce the power consumed by a BBU while still maintaining a data rate that satisfies the demands of the served users. Such a reduction in power consumption enables the PSOPA algorithm to achieve a better EE performance than the EPA algorithm, as shown in Fig. 6.9. The PSOPA

algorithm achieves an average EE of 5.125×10^7 bits/Joule, which is higher than 4.06×10^7 bits/Joule achieved by the EPA algorithm, as elaborated by Table 6.6. Such performance translates into a 20.7% performance gain of the PSOPA algorithm over the EPA algorithm in terms of EE.

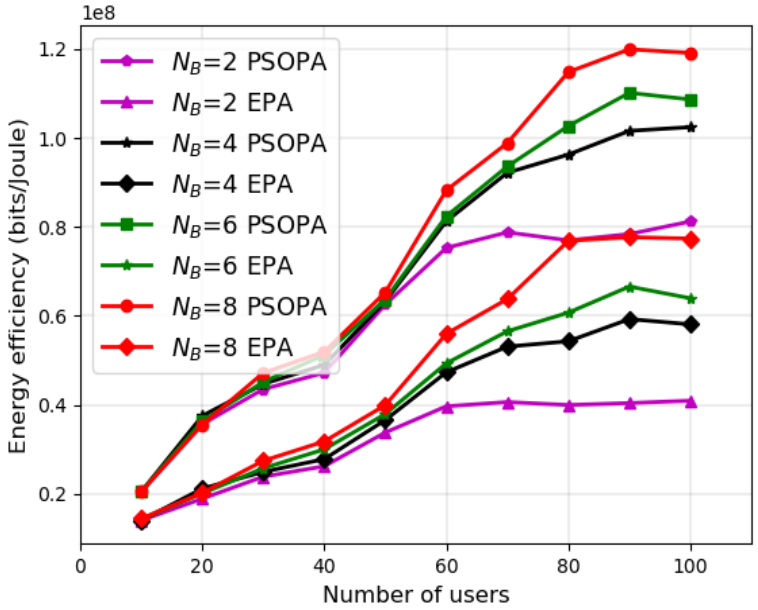

Figure 6.9: Effect of user density on the global energy efficiency for varying number of MBSs $N_{\mathcal{B}}$.

Table 6.6: Average global energy efficiency for varying number of MBSs.

MBS density	Average energy efficiency by the PSOPA algorithm (bits/Joule)	Average energy efficiency by the EPA algorithm (bits/Joule)
2	5.9998×10^7	3.1817×10^7
4	6.8866×10^7	3.9646×10^7
6	7.1450×10^7	4.2509×10^7
8	7.6144×10^7	4.8541×10^7
Average energy efficiency (bits/Joule)	5.1252×10^7	4.0628×10^7

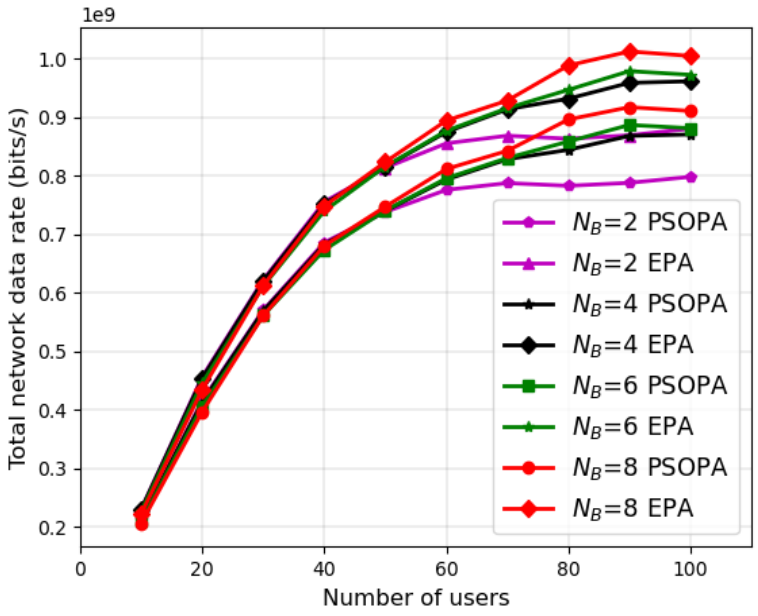

Figure 6.10: Effect of user density on the total network data rate for varying number of MBSs $N_{\mathcal{B}}$.

However, the PSOPA algorithm achieves a higher EE than the EPA algorithm at the expense of the achieved total network data rate. Fig. 6.10 shows that as the number of users increases in the network and for the different MBS densities, the EPA scheme achieves a higher data rate than the PSOPA algorithm. The exact average values achieved by both algorithms for the different MBS densities are presented in Table 6.7, with the EPA algorithm achieving an overall average data rate of 7.481×10^8 bits/s compared to 6.798×10^8 bits/s achieved by the PSOPA algorithm. Thus, the EPA algorithm outperforms the PSOPA algorithm by 9% in terms of achieved total network data rate. The reason for such a performance is that in the EPA scheme, each allocated BBU is allocated the maximum available power $P_{n_j,u,w_j} = P_{n_j}^{thres}/|\mathcal{W}_j|$, resulting in maximum possible data rate at each AN. This does not necessarily mean that maximum power is required to meet the

QoS requirements of the users. Hence, the PSOPA scheme efficiently allocates the required power according to ζ to meet the user QoS requirements and consequently achieve lower power consumption and a higher EE.

Table 6.7: Average network data rate for varying number of MBSs.

MBS density	Average network data rate by PSOPA algorithm (bits/s)	Average network data rate by EPA algorithm (bits/s)
2	6.555×10^8	7.214×10^8
4	6.823×10^8	7.511×10^8
6	7.145×10^8	4.251×10^8
8	6.843×10^8	7.530×10^8
Average network data rate (bits/s)	6.798×10^8	7.481×10^8

Figs. 6.11 and 6.12 further elaborate that depending on the operator's priority, ζ in (6.8) can be set to either maximise the achieved data rate or the energy efficiency. In Fig. 6.11, as ζ increases, the priority of the PSOPA algorithm shifts to maximising the achieved total network data rate. As such, the total network data rate achieved by the PSOPA algorithm approaches the upper bound set by the EPA scheme. However, Fig. 6.12 shows that increasing ζ reduces the energy efficiency achieved by the PSOPA algorithm, narrowing the gain in EE achieved over the EPA algorithm since a high ζ implies increased power consumption. On the other hand, lower values of ζ allow the PSOPA algorithm to prioritise minimisation of power consumption, resulting in higher performance in EE as depicted by Fig. 6.12. Consequently, ζ can be used in the PSOPA algorithm to either maximise the data rate, thereby maximising the ITNTN SE, or maximise the EE depending on the operator's needs. Also, it is worth noticing that in Fig. 6.12, the EE gain over the EPA algorithm is

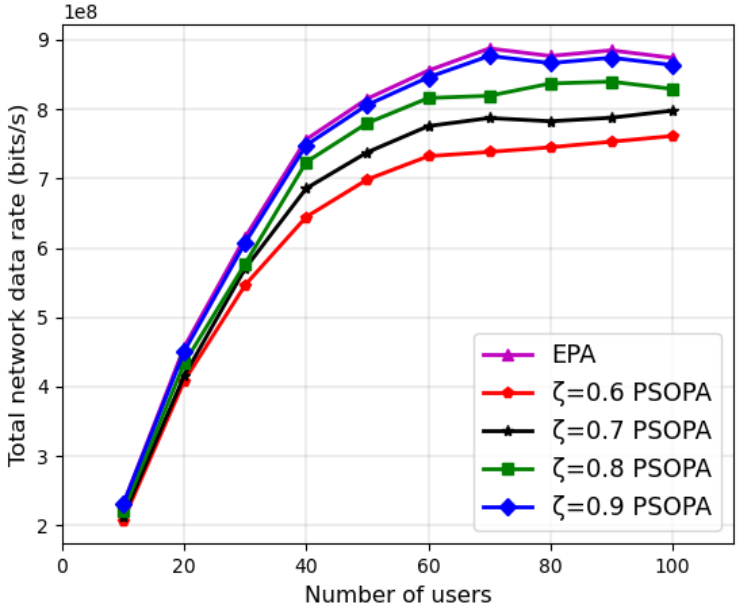

Figure 6.11: Effect of user density on the total network data rate for varying ζ.

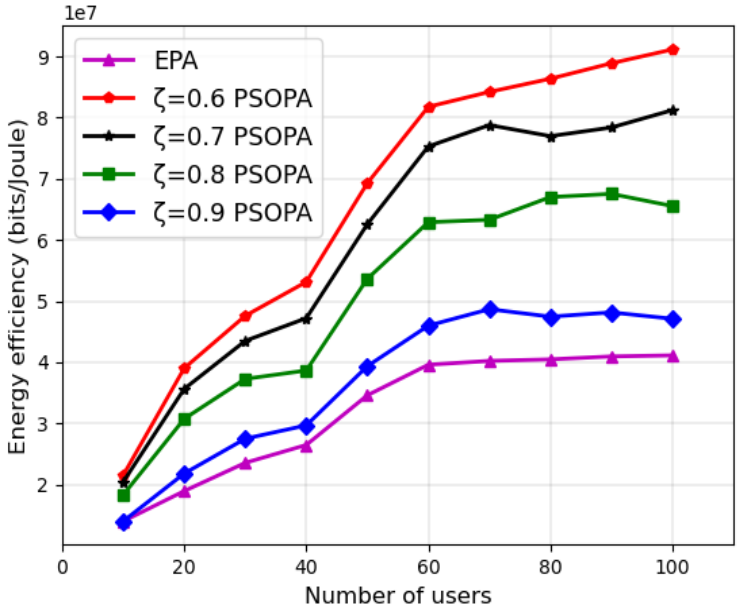

Figure 6.12: Effect of user density on the global energy efficiency for varying ζ.

more significant as the number of users in the network increases, further emphasizing the need for an energy-efficient algorithm, especially for many users in the network.

While this chapter formulated the optimisation problem (6.4) that maximised the global EE and minimised the mobility-induced handoffs in the ITNTN, it is essential to note that the effect on mobility-induced handoff has not been analysed in this chapter. The decomposition of the problem (6.4) into the UARA problem **P5** and the PA problem **P6** enabled the handoff effect to be evaluated in the solutions for problem **P5** presented in Chapters 3 to 5.

6.7 Chapter summary

This chapter addressed the EE problem in the ITNTN. A weighted sum SOOP that maximised the EE in the ITNTN while minimising the number of mobility-induced handoffs was proposed. The complexity of the SOOP was reduced by decomposing it into two sub-problems: the UARA and the PA problems. In the UARA sub-problem, the BBU power was fixed, ultimately transforming the problem into a SOOP that maximised the total network data rate while minimising the mobility-induced handoffs. The UARA SOOP was observed to be the same problem presented in Chapter 3, and as such, could be solved by any of the solutions discussed in Chapters 3 to 5.

On the other hand, the PA sub-problem was a non-linear fractional programming problem whose complexity was reduced by transforming it into a weighted sum SOOP that maximised the AN achieved data rate and minimised the BS total consumed power. The PSO algorithm was utilised to solve the SOOP PA sub-problem. The PSOPA scheme was validated through comparison with the EPA algorithm. Simulation results revealed that for different values of the weight ζ in the PA SOOP (6.8), the PSOPA algorithm could either maximise the EE of

the ITNTN and thus outperforms the EPA algorithm or maximise the achieved data rate, thereby approaching the data rate upper bound performance set by the EPA algorithm.

Chapter 7

Conclusion and Future Work

This thesis proposed efficient RRM schemes for the ITNTN. In particular, the research addressed the problem of efficient UARA in the ITNTN by developing algorithms that maximised the total network data rate (and hence SE) and the total network EE. Moreover, the UARA problem was formulated to allow differentiated service provisioning, ultimately enabling priority-based resource allocation. The users were differentiated based on their use cases, optimally and dynamically associating them with the appropriate RANs depending on the network capabilities, access nodes' resources, and power budgets. Furthermore, the work prioritised using RANs with the largest cell radius for service provisioning mobile users to minimise mobility-induced handoffs. The formulated UARA problems were non-linear and combinatorial, making them NP-hard. In order to reduce the complexity of these problems, they were decomposed into sub-problems and subsequently solved using algorithms that returned polynomial-time solutions. Moreover, the thesis investigated the use of RL to achieve intelligent UARA for the ITNTN, considering the heterogeneity in user QoS

requirements. The proposed algorithms were implemented using the Python programming language, and significant conclusions were drawn. Sections 7.1, 7.2, and 7.3 summarise the significant contributions, future work, and concluding remarks, respectively.

7.1 Summary of contributions

In addressing the UARA problem, this thesis considered a usage scenario in which many users exist, necessitating the deployment of NTN RANs to support the TN in meeting the exponential user demands. The RANs in the considered ITNTN have different capabilities and limitations in supporting users with contrasting demands. Therefore, this thesis focussed on providing effective radio resource management schemes that efficiently mapped users with diverse QoS requirements to the appropriate RAN of the ITNTN. The schemes focussed on maximising the total network data rate while minimising mobility-induced handoffs. Moreover, latency requirements, energy-efficient and priority-based resource allocation were also considered. The contributions of this thesis can be summarized as follows:

- Chapter 1 presented the thesis' research background, motivation, problem, and objectives. Chapter 2 detailed the ITNTN architecture, RRM frameworks, and a comprehensive literature review on RRM in the ITNTN. Moreover, some research gaps in the state-of-the-art literature regarding UARA in the ITNTN were identified and discussed.

- Chapter 3 presented the proposed service-aware UARA system model and problem formulation. The problem was formulated as a MOOP, maximising the total

network data rate while minimising the probability of mobility-induced handoffs. The complexity of the MOOP was then reduced by adopting the weighted sum method, which transformed the MOOP into a SOOP. The complexity of the equivalent NP-Hard SOOP problem was reduced by decomposing it into two sub-problems: the user association sub-problem and the optional resource distribution sub-problem. A service-aware greedy heuristic algorithm was proposed to solve the user association sub-problem, and simulations were carried out to validate the relevance of differentiated service provisioning in the ITNTN. Simulation results showed that the service-aware greedy algorithm outperformed the service-unaware scheme in terms of spectrum efficiency, user acceptance ratio, and handoff probability by 12%, 9.8%, and 78% on average, respectively. Moreover, the resource distribution problem was reformulated as a water-filling problem and solved using CVXPY, consequently analysing the effect of distributing the unallocated BBUs to the associated users.

- Since the greedy heuristic solution to the user association sub-problem does not ordinarily produce an optimal solution, Chapter 4 presented a polynomial-time solution based on the GA to solve the user association sub-problem presented in Chapter 3. The problem was encoded into a sequence of chromosomes with genes representing the user association solutions. Service group-dependent fitness functions were formulated to determine the near-optimal UARA solution. Moreover, to validate the performance of the GA solution, the Gurobi solver was utilised to determine the ILP solution to the user association. In addition, the GA was compared with two other solutions, the heuristic greedy algorithm described in Chapter 3 and the RUA algorithm. Simulation

results showed that as the number of ANs increased in the ITNTN, the GA's SE performance outperformed the ILP, greedy and RUA algorithms by 0.2%, 1.04% and 1.1%, respectively. Moreover, the GA outperformed the RUA algorithms in handoff probability by 51.8% on average. Furthermore, the GA showed a user AR performance that outperformed the ILP, greedy, and RUA solutions by 3.7%, 6.2% and 8.3%, respectively.

- Chapter 5 investigated the use of RL in solving the user association sub-problem defined in Chapter 3 to achieve an intelligent solution that makes resource allocation decisions for the ITNTN in real time. Consequently, a MA3DQN solution based on the centralised training but distributed execution approach was proposed. Besides, the chapter adopted the effective capacity theorem to guarantee the delay QoS requirements for mission-critical users. The performance of the MA3DQN algorithm was compared to the GA, the ILP solution, the greedy algorithm, the RUA algorithm, an approximation-based heuristic algorithm, and a simulated MADQN algorithm. Simulation results revealed that as the number of users in the network increased, the acquired data rate of the MA3DQN algorithm was within 0.48% and 0.42% of that achieved by the GA and ILP solutions, respectively, and outperformed all other algorithms. Moreover, for an increasing number of access nodes in the network, the MA3DQN algorithm achieved a total network data rate that was within 0.9% and 0.48% of the GA and ILP solutions, respectively. On average, it outperformed the MADQN, approximation, greedy, and RUA algorithms by 0.3%, 0.3%, 0.6%, and 0.4%, respectively. Notably, the proposed MA3DQN algorithm presented the

best running time, attaining a gain of 99.9% over the GA, which performed the poorest among the algorithms characterised by polynomial worst-case time complexity. Besides, the MA3DQN approach maintained a handoff probability of zero, unlike the approximation-based, and RUA solutions.

- In Chapter 6, a weighted sum SOOP that maximised the EE of the ITNTN while minimising the number of mobility-induced handoffs was proposed. The complexity of the SOOP was reduced through decomposition into two sub-problems: the UARA problem and the PA problem. The UARA problem was similar to the user association sub-problem described in Chapter 3, which maximised the total network data rate and minimised the mobility-induced handoffs and was subsequently solved in Chapters 3 to 5. On the other hand, the PA problem was a fractional programming problem whose complexity was reduced by transforming it into a weighted sum SOOP that maximised the AN achieved data rate and minimised the BS total consumed power. The PSO approach was used to solve the SOOP PA sub-problem. The PSOPA scheme was validated through comparison with the EPA algorithm. Simulation results revealed that for different values of the weight in the PA SOOP, the PSOPA algorithm could either maximise the EE of the ITNTN and thus outperform the EPA algorithm in terms of EE or maximise the achieved data rate, thereby approaching the achieved data rate upper bound performance set by the EPA algorithm.

7.2 Future work

Some research issues and avenues require further investigation to improve this work. Some of the possible future work related to this thesis are outlined below:

1. Future work can investigate the possibility of extending this work to the physical layer of the wireless network and thus investigate concepts such as spatial multiplexing, Intelligent reflecting surface, and reconfigurable intelligent surface in the ITNTN. Such an optimisation problem will consider a scenario in which the ANs and/or users are equipped with multiple antennas and thus will involve optimising the different beamforming vectors from the ANs to the users.

2. This work considers using multi-mode UE that can only connect to a single RAN for a particular call/session at a time. Future work can consider using multi-homed devices that allow simultaneous data transmission from multiple access nodes to any given UE. Such a scenario will provide macrodiversity against shadowing, path loss, and blockage. Macrodiversity allows the communication of the same signal over multiple paths, thereby exploiting the variations in large-scale fading of the different paths in the ITNTN and thus enhancing reliability, especially for the mission-critical use case. However, the joint transmission of the same signal from multiple nodes to a UE reduces resource utilisation, and hence, a trade-off between reliability and resource utilisation must be investigated.

3. This work considered a usage scenario in which the UAVs are quasi-stationary, deployed to serve a large group of users, say in an urban area, during a carnival event. Future

work can investigate UARA in the ITNTN for a scenario where the UAVs are moving. If users are moving (say in a scenario such as a pilgrimage), the UAVs must move along with them, as traffic keeps changing spatially. This usage scenario will necessitate tracking the movements of both users and the nodes to avoid multiple connections and disconnections that may result when an already connected user moves out of range of its access node, which is also moving.

4. Future work should also investigate the use of advanced RL algorithms, such as federated RL and transfer learning, to improve the performance of RL for service-aware UARA in the ITNTN.

5. In future work, the RRM schemes for the ITNTN described in this work can be implemented on light and cost-effective test beds.

7.3 Concluding remarks

This thesis proposed efficient radio resource management algorithms for the ITNTN consisting of the terrestrial, LAPs, HAPs, and satellite RANs. The solutions considered the different capabilities and limitations of the RANs and the heterogeneous user QoS requirements. Therefore, the thesis has contributed to ongoing research on combining TNs with NTNs to provide efficient radio access to users with contrasting demands.

References

[1] 3GPP, "Technical Specification Group Radio Access Network; Study on New Radio (NR) to support non-terrestrial networks (Release 15) ," 3rd Generation Partnership Project (3GPP), Technical Specification (TS) 38.811, 09 2019, version 15.2.0. xxiii, 2, 3, 5, 6, 26, 27, 28, 34, 36, 37, 38, 72, 73, 91, 116, 172, 215

[2] R. Li, "Network 2030 a blueprint of technology, applications and market drivers towards the year 2030 and beyond," *in Proc. 1st International Telecommunication Union Workshop on Network 2030*, 07 2019. 1, 7, 26

[3] Z. Zhang, Y. Xiao, Z. Ma, M. Xiao, Z. Ding, X. Lei, G. K. Karagiannidis, and P. Fan, "6G wireless networks: Vision, requirements, architecture, and key technologies," *IEEE Vehicular Technology Magazine*, vol. 14, no. 3, pp. 28–41, 2019. 1, 2, 8, 25, 26, 63, 199

[4] W. Saad, M. Bennis, and M. Chen, "A vision of 6G wireless systems: Applications, trends, technologies, and open research problems," *IEEE network*, vol. 34, no. 3, pp. 134–142, 2019. 1, 2, 25

[5] E. C. Strinati, S. Barbarossa, J. L. Gonzalez-Jimenez, D. Ktenas, N. Cassiau, L. Maret, and C. Dehos, "6G: The next frontier: From holographic messaging to artificial intelligence using subterahertz and visible light communication," *IEEE Vehicular Technology Magazine*, vol. 14, no. 3, pp. 42–50, 2019. 1, 2, 25

[6] B. Zong, C. Fan, X. Wang, X. Duan, B. Wang, and J. Wang, "6G technologies: Key drivers, core requirements, system architectures, and enabling technologies," *IEEE Vehicular Technology Magazine*, vol. 14, no. 3, pp. 18–27, 2019. 2, 25

[7] K. B. Letaief, W. Chen, Y. Shi, J. Zhang, and Y.-J. A. Zhang, "The roadmap to 6G: AI empowered wireless networks," *IEEE Communications Magazine*, vol. 57, no. 8, pp. 84–90, 2019. 2, 25

[8] M. Mozaffari, W. Saad, M. Bennis, Y.-H. Nam, and M. Debbah, "A tutorial on UAVs for wireless networks: Applications, challenges, and open problems," *IEEE Communications Surveys & Tutorials*, vol. 21, no. 3, pp. 2334–2360, 2019. 2, 4, 6

[9] G. Giambene, *Resource Management in Satellite Networks: Optimization and Cross-Layer Design*, 01 2007. 2, 28, 29, 42

[10] O. Kodheli, E. Lagunas, N. Maturo, S. K. Sharma, B. Shankar, J. F. M. Montoya, J. C. M. Duncan, D. Spano, S. Chatzinotas, S. Kisseleff *et al.*, "Satellite communications in the new space era: A survey and future challenges," *IEEE Communications Surveys & Tutorials*, vol. 23, no. 1, pp. 70–109, 2020. 2, 25, 27, 38

[11] J. Liu, Y. Shi, Z. M. Fadlullah, and N. Kato, "Space-air-ground integrated network: A survey," *IEEE Communications Surveys & Tutorials*, vol. 20, no. 4, pp. 2714–2741, 2018. 2, 7, 26, 28

[12] M. Giordani and M. Zorzi, "Non-terrestrial networks in the 6G era: Challenges and opportunities," *IEEE Network*, vol. 35, no. 2, pp. 244–251, 2020. 3, 5

[13] D. Wang, M. Giordani, M.-S. Alouini, and M. Zorzi, "The potential of multi-layered hierarchical non-terrestrial networks for 6G," *arXiv preprint arXiv:2011.08608*, 2020. 3

[14] Y. Hu, M. Chen, and W. Saad, "Joint access and backhaul resource management in satellite-drone networks: A competitive market approach," *IEEE Transactions on Wireless Communications*, vol. 19, no. 6, pp. 3908–3923, 2020. 3, 5, 44, 53, 63

[15] B. Deng, C. Jiang, J. Yan, N. Ge, S. Guo, and S. Zhao, "Joint multigroup precoding and resource allocation in integrated terrestrial-satellite networks," *IEEE Transactions on Vehicular Technology*, vol. 68, no. 8, pp. 8075–8090, 2019. 3, 44, 54, 63

[16] M. A. Habibi, M. Nasimi, B. Han, and H. D. Schotten, "A comprehensive survey of RAN architectures toward 5G mobile communication system," *IEEE Access*, vol. 7, pp. 70 371–70 421, 2019. 4

[17] W. Abderrahim, O. Amin, M.-S. Alouini, and B. Shihada, "Latency-aware offloading in integrated satellite terrestrial networks," *IEEE Open Journal of the Communications Society*, vol. 1, pp. 490–500, 2020. 5, 55

[18] B. Di, H. Zhang, L. Song, Y. Li, and G. Y. Li, "Ultra-dense LEO: integrating terrestrial-satellite networks into 5G and beyond for data offloading," *IEEE Transactions on Wireless Communications*, vol. 18, no. 1, pp. 47–62, 2018. 5, 69

[19] A. Alsharoa and M.-S. Alouini, "Improvement of the global connectivity using integrated satellite-airborne-terrestrial networks with resource optimization," *IEEE Transactions on Wireless Communications*, vol. 19, no. 8, pp. 5088–5100, 2020. 5, 44, 54, 68, 74, 91, 116, 172, 215

[20] J. Li, K. Xue, D. S. Wei, J. Liu, and Y. Zhang, "Energy efficiency and traffic offloading optimization in integrated satellite/terrestrial radio access networks," *IEEE Transactions on Wireless Communications*, vol. 19, no. 4, pp. 2367–2381, 2020. 5, 44, 54, 69, 199

[21] Y. Li, N. Deng, and W. Zhou, "A hierarchical approach to resource allocation in extensible multi-layer LEO-MSS," *IEEE Access*, vol. 8, pp. 18 522–18 537, 2020. 5, 55

[22] N. Saeed, A. Elzanaty, H. Almorad, H. Dahrouj, T. Y. Al-Naffouri, and M.-S. Alouini, "Cubesat communications: Recent advances and future challenges," *IEEE Communications Surveys & Tutorials*, vol. 22, no. 3, pp. 1839–1862, 2020. 6

[23] Y. Zeng, R. Zhang, and T. J. Lim, "Wireless communications with unmanned aerial vehicles: Opportunities and challenges," *IEEE Communications Magazine*, vol. 54, no. 5, pp. 36–42, 2016. 6, 32, 33, 67

[24] Airbus, *"Zephyr; Pionering the Stratosphere"*, Accessed: May 31, 2021. [Online]. Available: https://www.airbus.com/defence/uav/zephyr.html 6, 25, 30

[25] Google, *"Google LOON project"*, Accessed: May 31, 2021. [Online]. Available: https://loon.com/ 6, 25, 30

[26] J.-H. Lee, J. Park, M. Bennis, and Y.-C. Ko, "Integrating LEO satellite and UAV relaying via reinforcement learning for non-terrestrial networks," in *GLOBECOM 2020-2020 IEEE Global Communications Conference*. IEEE, 2020, pp. 1–6. 6

[27] 3GPP, "Technical Specification Group Radio Access Network Solutions for NR to support non-terrestrial networks (NTN) (Release 16)," 3rd Generation Partnership Project (3GPP), Technical Specification (TS) 38.821, 12 2019, version 16.0.0. 6, 26

[28] M. W. Akhtar, S. A. Hassan, R. Ghaffar, H. Jung, S. Garg, and M. S. Hossain, "The shift to 6G communications: vision and requirements," *Human-centric Computing and Information Sciences*, vol. 10, no. 1, pp. 1–27, 2020. 7

[29] F. Rinaldi, S. Pizzi, A. Molinaro, A. Iera, and G. Araniti, "Cooperative resource allocation in integrated terrestrial/non-terrestrial 5G and beyond networks," in *GLOBECOM 2020-2020 IEEE Global Communications Conference*. IEEE, 2020, pp. 1–6. 7

[30] C. Niephaus, M. Kretschmer, and G. Ghinea, "QoS provisioning in converged satellite and terrestrial networks: A survey of the state-of-the-art," *IEEE Communications Surveys & Tutorials*, vol. 18, no. 4, pp. 2415–2441, 2016. 8

[31] Y. Zhao, G. Yu, and H. Xu, "6G mobile communication network: vision, challenges and key technologies," *arXiv preprint arXiv:1905.04983*, 2019. 9, 198

[32] F. Rothlauf, *Design of modern heuristics: principles and application.* Springer, 2011, vol. 8, no. 9. 12

[33] Y. Bengio, A. Lodi, and A. Prouvost, "Machine learning for combinatorial optimization: a methodological tour d'horizon," *European Journal of Operational Research*, vol. 290, no. 2, pp. 405–421, 2021. 14

[34] S. He, H. Tian, X. Lyu, G. Nie, and S. Fan, "Distributed cache placement and user association in multicast-aided heterogeneous networks," *IEEE Access*, vol. 5, pp. 25 365–25 376, 2017. 14

[35] S. O. Oladejo and O. E. Falowo, "Latency-aware dynamic resource allocation scheme for multi-tier 5G network: A network slicing-multitenancy scenario," *IEEE Access*, vol. 8, pp. 74 834–74 852, 2020. 14, 74, 146, 172

[36] N. Mazyavkina, S. Sviridov, S. Ivanov, and E. Burnaev, "Reinforcement learning for combinatorial optimization: A survey," *Computers & Operations Research*, p. 105400, 2021. 14

[37] D. J. Birabwa, D. Ramotsoela, and N. Ventura, "Slice-aware user association and resource allocation in integrated terrestrial and non-terrestrial networks," in *Proc. Southern Africa Telecommunication Networks and Applications Conference (SATNAC)*, 2021, pp. 43–48. 17

[38] D. J. Birabwa, D. Ramotsoela, and N. Ventura, "Service-aware user association and resource allocation in integrated terrestrial and non-terrestrial networks: A genetic algorithm approach," *IEEE Access*, vol. 10, pp. 104 337–104 357, 2022. 17

[39] M. Zalghout, A. Khalil, M. Crussiere, S. Abdul-Nabi, and J.-F. Helard, "Context-aware and priority-based user association and resource allocation in heterogeneous wireless networks," *Computer Networks*, vol. 149, pp. 76–92, 2019. 18, 82, 144, 170, 171

[40] D. J. Birabwa, D. Ramotsoela, and N. Ventura, "Multi-agent deep reinforcement learning for user association and resource allocation in integrated terrestrial and non-terrestrial networks," *Computer Networks*, p. 109827, 2023. 18

[41] D. J. Birabwa, D. Ramotsoela, and N. Ventura, "Energy-efficient user association and resource allocation in integrated terrestrial and non-terrestrial networks," in *Proc. Southern Africa Telecommunication Networks and Applications Conference (SATNAC)*, 2022, pp. 249–254. 19

[42] M. Setayesh, S. Bahrami, and V. W. Wong, "Joint PRB and power allocation for slicing eMBB and URLLC services in 5G C-RAN," in *GLOBECOM 2020-2020 IEEE Global Communications Conference*. IEEE, 2020, pp. 1–6. 21, 68

[43] A. Guidotti, A. Vanelli-Coralli, M. Conti, S. Andrenacci, S. Chatzinotas, N. Maturo, B. Evans, A. Awoseyila, A. Ugolini, T. Foggi *et al.*, "Architectures and key technical challenges for 5G systems incorporating satellites," *IEEE Transactions on Vehicular Technology*, vol. 68, no. 3, pp. 2624–2639, 2019. 27, 38

[44] K. Liolis, A. Geurtz, R. Sperber, D. Schulz, S. Watts, G. Poziopoulou, B. Evans, N. Wang, O. Vidal, B. Tiomela Jou *et al.*, "Use cases and scenarios of 5G integrated satellite-terrestrial networks for enhanced mobile broadband: The SaT5G approach," *International Journal of Satellite Communications and Networking*, vol. 37, no. 2, pp. 91–112, 2019. 28, 39

[45] G. Maral, M. Bousquet, and Z. Sun, *Satellite communications systems: systems, techniques and technology.* John Wiley & Sons, 2020. 28

[46] X. Cao, P. Yang, M. Alzenad, X. Xi, D. Wu, and H. Yanikomeroglu, "Airborne communication networks: A survey," *IEEE Journal on Selected Areas in Communications*, vol. 36, no. 9, pp. 1907–1926, 2018. 29, 30, 31, 32, 33

[47] A. Mohammed, A. Mehmood, F.-N. Pavlidou, and M. Mohorcic, "The role of high-altitude platforms (HAPs) in the global wireless connectivity," *Proceedings of the IEEE*, vol. 99, no. 11, pp. 1939–1953, 2011. 29, 30, 31, 67

[48] Facebook Engineering, *"Aquila project"*, Accessed: May 31, 2021. [Online]. Available: https://engineering.fb.com/connectivity/flying-aquila-early-lessons-from-the-first-full-scale-test-flight-and-the-path-ahead/ 30

[49] Air Force Technology, *"Stratobus Autonomous Stratospheric Airship"*, Accessed: May 31, 2020. [Online]. Available: https://www.airforce-technology.com/projects/stratobus/ 30

[50] J. Qiu, D. Grace, G. Ding, M. D. Zakaria, and Q. Wu, "Air-ground heterogeneous networks for 5G and beyond via integrating high and low altitude platforms," *IEEE Wireless Communications*, vol. 26, no. 6, pp. 140–148, 2019. 31, 32, 45

[51] D. S. Lakew, A. Masood, and S. Cho, "3D UAV placement and trajectory optimization in UAV assisted wireless networks," in *2020 International Conference on Information Networking (ICOIN)*. IEEE, 2020, pp. 80–82. 32

[52] K. Gomez, T. Rasheed, L. Reynaud, and I. Bucaille, "Realistic deployments of LTE-based hybrid aerial-terrestrial networks for public safety," in *2013 IEEE 18th International Workshop on Computer Aided Modeling and Design of Communication Links and Networks (CAMAD)*. IEEE, 2013, pp. 233–237. 33

[53] 3GPP, "Technical Specification Group Radio Access Network; Study on new radio access technology: Radio access architecture and interfaces (Release 14)," 3rd Generation Partnership Project (3GPP), Technical Specification (TS) 38.801, 03 2017, version 14.0.0. 36, 43

[54] M. Bacco, F. Davoli, G. Giambene, A. Gotta, M. Luglio, M. Marchese, F. Patrone, and C. Roseti, "Networking challenges for non-terrestrial networks exploitation in 5G," in *2019 IEEE 2nd 5G World Forum (5GWF)*. IEEE, pp. 623–628. 38

[55] EU-H2020 Research Project, *"SAT5G Integrating SatCom into 5G"*, Accessed: May 11, 2020. [Online]. Available: https://www.sat5g-project.eu/ 39

[56] H2020-ICT-2014-1 Project VITAL, *"System Architecture: Final Report"*, 06 2016, deliverable D2.3. 40

[57] ESA Research Project, *"SATis5 Demonstrator for Satellite-Terrestrial Integration in the 5G Context"*, Accessed: May 11, 2020. [Online]. Available: https://satis5.eurescom.eu/ 40

[58] F. Völk, K. Liolis, M. Corici, J. Cahill, R. T. Schwarz, T. Schlichter, E. Troudt, and A. Knopp, "Satellite integration into 5G: Accent on first over-the-air tests of an edge node concept with integrated satellite backhaul," *Future Internet*, vol. 11, no. 9, p. 193, 2019. 40

[59] EU-H2020 Research Project, *"Shared Access Terrestrial-Satellite Backhaul Network enabled by Smart Antennas"*, Accessed: May 29, 2020. [Online]. Available: https://sansa-h2020.eu/ 40

[60] H2020-ICT-2014-1 Project SANSA, *"Definition of reference scenarios, overall system architectures, research challenges, requirements and KPIs"*, 02 2016, deliverable D2.3. [Online]. Available: https://sansa-h2020.eu/deliverables 40

[61] T. Tozer, G. Olmo, and D. Grace, "The european helinet project," in *Airship Convention*, 2000. 41

[62] F. Dovis, L. L. Presti, E. Magli, G. Olmo, and F. Sellone, "HeliNet: a network of UAV-HAVE stratospheric platforms- system concepts and applications to environmental surveillance," *DASIA 2000- Data systems in aerospace*, pp. 551–556, 2000. 41

[63] D. Grace, M. Mohorcic, M. Oodo, J. Horwath, M. Capstick, M. B. Pallavicini, and M. Lalovic, "An overview of the European CAPANINA project-broadband for all from high altitude platforms," in *Proc. 5th Stratospheric Platforms Syst. Workshop*, 2005, pp. 1–8. 41

[64] M. H. Ahmed, "Call admission control in wireless networks: a comprehensive survey," *IEEE Communications Surveys & Tutorials*, vol. 7, no. 1, pp. 49–68, 2005. 42

[65] F. Rinaldi, A. Raschella, and S. Pizzi, "5g nr system design: A concise survey of key features and capabilities," *Wireless Networks*, vol. 27, pp. 5173–5188, 2021. 43

[66] O. E. Falowo and H. A. Chan, "Joint call admission control algorithm for fair radio resource allocation in heterogeneous wireless networks supporting heterogeneous mobile terminals," in *2010 7th IEEE Consumer Communications and Networking Conference*. IEEE, 2010, pp. 1–5. 43, 68

[67] S. Kandukuri and S. Boyd, "Optimal power control in interference-limited fading wireless channels with outage-probability specifications," *IEEE Transactions on Wireless Communications*, vol. 1, no. 1, pp. 46–55, 2002. 43

[68] U. Madhow and M. L. Honig, "MMSE interference suppression for direct-sequence spread-spectrum CDMA," *IEEE Transactions on Communications*, vol. 42, no. 12, pp. 3178–3188, 1994. 43

[69] Y. Hu, M. Chen, and W. Saad, "Competitive market for joint access and backhaul resource allocation in satellite-drone networks," in *2019 10th IFIP International*

Conference on New Technologies, Mobility and Security (NTMS). IEEE, 2019, pp. 1–5. 44, 53

[70] S. M. Shahid, Y. T. Seyoum, S. H. Won, and S. Kwon, "Load balancing for 5G integrated satellite-terrestrial networks," *IEEE Access*, vol. 8, pp. 132 144–132 156, 2020. 44, 53

[71] C. Qiu, Z. Wei, Z. Feng, and P. Zhang, "Joint resource allocation, placement and user association of multiple UAV-mounted base stations with in-band wireless backhaul," *IEEE Wireless Communications Letters*, vol. 8, no. 6, pp. 1575–1578, 2019. 44, 54, 72

[72] L. Wang and G.-S. G. Kuo, "Mathematical modeling for network selection in heterogeneous wireless networks—a tutorial," *IEEE Communications Surveys & Tutorials*, vol. 15, no. 1, pp. 271–292, 2012. 46

[73] A. Keshavarz-Haddad, E. Aryafar, M. Wang, and M. Chiang, "HetNets selection by clients: convergence, efficiency, and practicality," *IEEE/ACM Transactions on Networking*, vol. 25, no. 1, pp. 406–419, 2016. 47

[74] H. AlNashwan and A. Agarwal, "User-centric network selection in wireless heterogeneous networks," in *2017 IEEE 30th Canadian Conference on Electrical and Computer Engineering (CCECE)*. IEEE, 2017, pp. 1–6. 47

[75] M. Zhang, X. Yang, T. Xu, and M.-T. Zhou, "Congestion-aware user-centric cooperative base station selection in ultra-dense networks," in *2017 9th International*

Conference on Wireless Communications and Signal Processing (WCSP). IEEE, 2017, pp. 1–6. 47

[76] A. Awad, A. Mohamed, and C.-F. Chiasserini, "User-centric network selection in multi-RAT systems," in *2016 IEEE Wireless Communications and Networking Conference Workshops (WCNCW)*. IEEE, 2016, pp. 97–102. 47

[77] X. Wang, J. Li, L. Wang, C. Yang, and Z. Han, "Intelligent user-centric network selection: a model-driven reinforcement learning framework," *IEEE Access*, vol. 7, pp. 21 645–21 661, 2019. 47, 48

[78] J. Montoya, A. Sethi, and N. G. Gómez, "A load-based and fair radio access network selection strategy with traffic offloading in heterogeneous networks," in *2018 7th International Conference on Computers Communications and Control (ICCCC)*. IEEE, 2018, pp. 193–202. 47

[79] N. Zarin and A. Agarwal, "A hybrid network selection scheme for heterogeneous wireless access network," in *2017 IEEE 28th Annual International Symposium on Personal, Indoor, and Mobile Radio Communications (PIMRC)*. IEEE, 2017, pp. 1–6. 47

[80] C. Sengupta and Y. K. Lee, "System, method, and computer-readable medium for user equipment decision-making criteria for connectivity and handover," Dec. 30 2014, uS Patent 8,923,852. 47

[81] 3GPP, "Technical Specification Group Services and System Aspects; Architecture enhancements for non-3GPP accesses (Release 15)," 3rd Generation Partnership Project (3GPP), Technical Specification (TS) 23.402, 03 2018, version 15.3.0. 47

[82] S. Andreev, M. Gerasimenko, O. Galinina, Y. Koucheryavy, N. Himayat, S.-P. Yeh, and S. Talwar, "Intelligent access network selection in converged multi-radio heterogeneous networks," *IEEE Wireless Communications*, vol. 21, no. 6, pp. 86–96, 2014. 48, 49

[83] J. Sachs, M. Prytz, and J. Gebert, "Multi-access management in heterogeneous networks," *Wireless Personal Communications*, vol. 48, no. 1, pp. 7–32, 2009. 50

[84] R. Trestian, O. Ormond, and G.-M. Muntean, "Game theory-based network selection: Solutions and challenges," *IEEE Communications Surveys & Tutorials*, vol. 14, no. 4, pp. 1212–1231, 2012. 50

[85] O. E. Falowo, S. Zeadally, and H. A. Chan, "Dynamic pricing for load-balancing in user-centric joint call admission control of next-generation wireless networks," *International Journal of Communication Systems*, vol. 23, no. 3, pp. 335–368, 2010. 51

[86] X. Li, W. Feng, Y. Chen, C.-X. Wang, and N. Ge, "Maritime coverage enhancement using UAVs coordinated with hybrid satellite-terrestrial networks," *IEEE Transactions on Communications*, vol. 68, no. 4, pp. 2355–2369, 2020. 55, 74

[87] X. Xi, X. Cao, P. Yang, Z. Xiao, and D. Wu, "Efficient and fair network selection for integrated cellular and drone-cell networks," *IEEE Transactions on Vehicular Technology*, vol. 68, no. 1, pp. 923–937, 2018. 55

[88] X. Li and W. Shi, "Hybrid satellite-UAV-terrestrial maritime networks: Network selection for users on a vessel optimized with transmit power and UAV position," *China Communications*, vol. 19, no. 9, pp. 37–46, 2022. 55

[89] P. Qin, M. Wang, X. Zhao, and S. Geng, "Content service oriented resource allocation for space–air–ground integrated 6G networks: A three-sided cyclic matching approach," *IEEE Internet of Things Journal*, vol. 10, no. 1, pp. 828–839, 2022. 56

[90] S. Zhu, S. Wang, and J. Chen, "Application of machine learning in space–air–ground integrated network data link," in *Communications, Signal Processing, and Systems: Proceedings of the 9th International Conference on Communications, Signal Processing, and Systems*. Springer, 2021, pp. 1596–1600. 56

[91] N. Kato, Z. M. Fadlullah, F. Tang, B. Mao, S. Tani, A. Okamura, and J. Liu, "Optimizing space-air-ground integrated networks by artificial intelligence," *IEEE Wireless Communications*, vol. 26, no. 4, pp. 140–147, 2019. 56

[92] S. Liu, H. Dahrouj, and M.-S. Alouini, "Machine learning-based user scheduling in integrated satellite-haps-ground networks," *arXiv preprint arXiv:2205.13958*, 2022. 56, 58, 144

[93] A. H. Arani, P. Hu, and Y. Zhu, "Fairness-aware link optimization for space-terrestrial integrated networks: A reinforcement learning framework," *IEEE Access*, vol. 9, pp. 77 624–77 636, 2021. 56, 58, 144

[94] X. Li, H. Zhang, W. Li, and K. Long, "Multi-agent DRL for user association and power control in terrestrial-satellite network," in *2021 IEEE Global Communications Conference (GLOBECOM)*. IEEE, 2021, pp. 1–5. 57, 58, 144

[95] X. Li, H. Zhang, H. Zhou, N. Wang, K. Long, S. Al-Rubaye, and G. K. Karagiannidis, "Multi-agent DRL for resource allocation and cache design in terrestrial-satellite networks," *IEEE Transactions on Wireless Communications*, 2022. 57, 58, 144

[96] Y. Cao, S.-Y. Lien, and Y.-C. Liang, "Deep reinforcement learning for multi-user access control in non-terrestrial networks," *IEEE Transactions on Communications*, vol. 69, no. 3, pp. 1605–1619, 2020. 57, 58, 141, 144, 150, 172

[97] N. Waqar, S. A. Hassan, A. Mahmood, K. Dev, D.-T. Do, and M. Gidlund, "Computation offloading and resource allocation in MEC-enabled integrated aerial-terrestrial vehicular networks: A reinforcement learning approach," *IEEE Transactions on Intelligent Transportation Systems*, vol. 23, no. 11, pp. 21 478–21 491, 2022. 57, 58, 144

[98] Y. Cao, S.-Y. Lien, and Y.-C. Liang, "Multi-tier collaborative deep reinforcement learning for non-terrestrial network empowered vehicular connections," in *2021 IEEE 29th International Conference on Network Protocols (ICNP)*. IEEE, 2021, pp. 1–6. 57, 58, 144

[99] X. Guan, Y. Huang, C. Dong, and Q. Wu, "User association and power allocation for UAV-assisted networks: A distributed reinforcement learning approach," *China Communications*, vol. 17, no. 12, pp. 110–122, 2020. 57, 58, 144

[100] H. A. Shah, L. Zhao, and I.-M. Kim, "Joint network control and resource allocation for space-terrestrial integrated network through hierarchal deep actor-critic reinforcement learning," *IEEE Transactions on Vehicular Technology*, vol. 70, no. 5, pp. 4943–4954, 2021. 57, 58, 144

[101] Z. Cheng, M. Liwang, N. Chen, L. Huang, N. Guizani, and X. Du, "Learning-based user association and dynamic resource allocation in multi-connectivity enabled unmanned aerial vehicle networks," *Digital Communications and Networks*, 2022. [Online]. Available: https://www.sciencedirect.com/science/article/pii/S2352864822001195 57, 58, 144

[102] M. Series, "IMT vision–framework and overall objectives of the future development of IMT for 2020 and beyond," *Recommendation ITU*, pp. 2083–0, 2015. 58

[103] 3GPP, "Technical Specification Group Radio Access Network;Study on Scenarios and Requirements for Next Generation Access Technologies;(Release 14)," 3rd Generation Partnership Project (3GPP), Technical Specification (TS) 38.913, 06 2017, version 14.3.0. 58

[104] H. Boostanimehr and V. K. Bhargava, "Unified and distributed QoS-driven cell association algorithms in heterogeneous networks," *IEEE Transactions on Wireless Communications*, vol. 14, no. 3, pp. 1650–1662, 2014. 64, 82, 84, 86

[105] M. Mozaffari, W. Saad, M. Bennis, and M. Debbah, "Efficient deployment of multiple unmanned aerial vehicles for optimal wireless coverage," *IEEE Communications Letters*, vol. 20, no. 8, pp. 1647–1650, 2016. 65

[106] M. Mozaffari, W. Saad, M. Bennis, and M. Debbah, "Unmanned aerial vehicle with underlaid device-to-device communications: Performance and tradeoffs," *IEEE Transactions on Wireless Communications*, vol. 15, no. 6, pp. 3949–3963, 2016. 65

[107] R. I. Bor-Yaliniz, A. El-Keyi, and H. Yanikomeroglu, "Efficient 3-D placement of an aerial base station in next generation cellular networks," in *2016 IEEE International Conference on Communications (ICC)*. IEEE, 2016, pp. 1–5. 65

[108] J. Lyu, Y. Zeng, R. Zhang, and T. J. Lim, "Placement optimization of UAV-mounted mobile base stations," *IEEE Communications Letters*, vol. 21, no. 3, pp. 604–607, 2016. 65

[109] Space Exploration Holdings, *"Application for Fixed Satellite Service by Space Exploration Holdings, LLC"*, Accessed: July 11, 2022. [Online]. Available: https://fcc.report/IBFS/SAT-MOD-20181108-00083 69

[110] H. Tabassum, M. Salehi, and E. Hossain, "Fundamentals of mobility-aware performance characterization of cellular networks: A tutorial," *IEEE Communications Surveys & Tutorials*, vol. 21, no. 3, pp. 2288–2308, 2019. 69

[111] A. Moubayed, A. Shami, and H. Lutfiyya, "Wireless resource virtualization with device-to-device communication underlaying LTE network," *IEEE Transactions on Broadcasting*, vol. 61, no. 4, pp. 734–740, 2015. 71, 73, 74, 91, 116, 172, 215

[112] A. Al-Hourani, S. Kandeepan, and S. Lardner, "Optimal LAP altitude for maximum coverage," *IEEE Wireless Communications Letters*, vol. 3, no. 6, pp. 569–572, 2014. 71, 72, 91, 116, 172, 215

[113] T. L. Marzetta and B. M. Hochwald, "Fast transfer of channel state information in wireless systems," *IEEE Transactions on Signal Processing*, vol. 54, no. 4, pp. 1268–1278, 2006. 73

[114] Z. Liu, L. Zhang, and Z. Ding, "Exploiting bi-directional channel reciprocity in deep learning for low rate massive MIMO CSI feedback," *IEEE Wireless Communications Letters*, vol. 8, no. 3, pp. 889–892, 2019. 73, 74

[115] J. Guo, C.-K. Wen, and S. Jin, "Deep learning-based CSI feedback for beamforming in single-and multi-cell massive MIMO systems," *IEEE Journal on Selected Areas in Communications*, vol. 39, no. 7, pp. 1872–1884, 2020. 74

[116] Y.-C. Liang, J. Tan, H. Jia, J. Zhang, and L. Zhao, "Realizing intelligent spectrum management for integrated satellite and terrestrial networks," *Journal of Communications and Information Networks*, vol. 6, no. 1, pp. 32–43, 2021. 74

[117] M. Arti, "Channel estimation and detection in hybrid satellite–terrestrial communication systems," *IEEE Transactions on Vehicular Technology*, vol. 65, no. 7, pp. 5764–5771, 2015. 74

[118] H. Chaouech and R. Bouallegue, "Channel estimation and detection for multibeam satellite communications," in *2010 IEEE Asia Pacific Conference on Circuits and Systems*. IEEE, 2010, pp. 366–369. 74

[119] M. Arti, "Imperfect CSI based AF relaying in hybrid satellite-terrestrial cooperative communication systems," in *2015 IEEE International Conference on Communication Workshop (ICCW)*. IEEE, 2015, pp. 1681–1686. 74

[120] Y. Sun, G. Feng, S. Qin, and S. Sun, "Cell association with user behavior awareness in heterogeneous cellular networks," *IEEE Transactions on Vehicular Technology*, vol. 67, no. 5, pp. 4589–4601, 2018. 74

[121] L. Liang, J. Kim, S. C. Jha, K. Sivanesan, and G. Y. Li, "Spectrum and power allocation for vehicular communications with delayed CSI feedback," *IEEE Wireless Communications Letters*, vol. 6, no. 4, pp. 458–461, 2017. 74

[122] C. Chaieb, Z. Mlika, F. Abdelkefi, and W. Ajib, "On the optimization of user association and resource allocation in hetnets with mm-wave base stations," *IEEE Systems Journal*, vol. 14, no. 3, pp. 3957–3967, 2020. 74

[123] J. V. Saraiva, I. M. Braga Jr, V. F. Monteiro, F. R. M. Lima, T. F. Maciel, W. C. Freitas Jr, and F. R. P. Cavalcanti, "Deep reinforcement learning for QoS-constrained resource allocation in multiservice networks," *arXiv preprint arXiv:2003.02643*, 2020. 75, 143, 150, 155, 158, 162

[124] D. A. Sousa, V. F. Monteiro, T. F. Maciel, F. R. M. Lima, and F. R. P. Cavalcanti, "Resource management for rate maximization with QoE provisioning in wireless networks," *Journal of Communication and Information Systems*, vol. 31, no. 1, 2016. 75

[125] F. R. M. Lima, T. F. Maciel, W. C. Freitas, and F. R. P. Cavalcanti, "Resource assignment for rate maximization with QoS guarantees in multiservice wireless systems," *IEEE Transactions on Vehicular Technology*, vol. 61, no. 3, pp. 1318–1332, 2012. 75

[126] M. Emmerich and A. Deutz, "Multicriteria optimization and decision making," *LIACS. Leiden University, NL*, 2006. 80

[127] H. Pervaiz, L. Musavian, Q. Ni, and Z. Ding, "Energy and spectrum efficient transmission techniques under QoS constraints toward green heterogeneous networks," *IEEE Access*, vol. 3, pp. 1655–1671, 2015. 81

[128] J. Tang, D. K. So, E. Alsusa, and K. A. Hamdi, "Resource efficiency: A new paradigm on energy efficiency and spectral efficiency tradeoff," *IEEE Transactions on Wireless Communications*, vol. 13, no. 8, pp. 4656–4669, 2014. 81

[129] L. Xu, G. Yu, and Y. Jiang, "Energy-efficient resource allocation in single-cell OFDMA systems: Multi-objective approach," *IEEE Transactions on Wireless Communications*, vol. 14, no. 10, pp. 5848–5858, 2015. 81

[130] C. A. C. Coello, G. B. Lamont, D. A. Van Veldhuizen *et al.*, *Evolutionary algorithms for solving multi-objective problems*. Springer, 2007, vol. 5. 82

[131] H. Boostanimehr and V. K. Bhargava, "Joint downlink and uplink aware cell association in hetnets with QoS provisioning," *IEEE Transactions on Wireless Communications*, vol. 14, no. 10, pp. 5388–5401, 2015. 82, 160

[132] R. M. Karp, "Reducibility among combinatorial problems." Springer Berlin Heidelberg, 2010, pp. 219–241. 85

[133] S. P. Boyd and L. Vandenberghe, *Convex optimization*. Cambridge University Press, 2004. 86

[134] D. Fooladivanda and C. Rosenberg, "Joint user association and resource allocation in heterogeneous cellular networks: Comparison of two modeling approaches," in *2019 31st International Teletraffic Congress (ITC 31)*. IEEE, 2019, pp. 66–74. 88

[135] D. E. Knuth, "Big omicron and big omega and big theta," *ACM Sigact News*, vol. 8, no. 2, pp. 18–24, 1976. 89

[136] P. E. Black, "big-O notation, dictionary of algorithms and data structures," *US National Institute of Standards and Technology*, 2008. 89

[137] M. Adedoyin and O. Falowo, "Joint optimization of energy efficiency and spectrum efficiency in 5G ultra-dense networks," in *2017 European Conference on Networks and Communications (EuCNC)*. IEEE, 2017, pp. 1–6. 92, 120

[138] C. Blum, A. Roli, and M. Sampels, *Hybrid metaheuristics: an emerging approach to optimization*. Springer, 2008, vol. 114. 102, 103

[139] J. Elhachmi and Z. Guennoun, "Cognitive radio spectrum allocation using genetic algorithm," *EURASIP Journal on Wireless Communications and Networking*, vol. 2016, no. 1, pp. 1–11, 2016. 103

[140] A. Hassanat, K. Almohammadi, E. Alkafaween, E. Abunawas, A. Hammouri, and V. Prasath, "Choosing mutation and crossover ratios for genetic algorithms—a review with a new dynamic approach," *Information*, vol. 10, no. 12, p. 390, 2019. 107, 111

[141] A. Lipowski and D. Lipowska, "Roulette-wheel selection via stochastic acceptance," *Physica A: Statistical Mechanics and its Applications*, vol. 391, no. 6, pp. 2193–2196, 2012. 112

[142] Gurobi Optimization, LLC, "Mixed Integer Programming Basics," 2022. 114

[143] X. Qi, S. Khattak, A. Zaib, and I. Khan, "Energy efficient resource allocation for 5G heterogeneous networks using genetic algorithm," *IEEE Access*, vol. 9, pp. 160 510–160 520, 2021. 141, 205, 207

[144] M. K. Hasan, T. C. Chuah, A. A. El-Saleh, M. Shafiq, S. A. Shaikh, S. Islam, and M. Krichen, "Constriction factor particle swarm optimization based load balancing and cell association for 5G heterogeneous networks," *Computer Communications*, vol. 180, pp. 328–337, 2021. 141

[145] S. Yan, M. Peng, and X. Cao, "A game theory approach for joint access selection and resource allocation in UAV assisted IoT communication networks," *IEEE Internet of Things Journal*, vol. 6, no. 2, pp. 1663–1674, 2018. 141

[146] N. Zhao, Y.-C. Liang, D. Niyato, Y. Pei, M. Wu, and Y. Jiang, "Deep reinforcement learning for user association and resource allocation in heterogeneous cellular networks," *IEEE Transactions on Wireless Communications*, vol. 18, no. 11, pp. 5141–5152, 2019. 142, 160, 172

[147] J. Tian, Q. Liu, H. Zhang, and D. Wu, "Multiagent deep-reinforcement-learning-based resource allocation for heterogeneous QoS guarantees for vehicular networks," *IEEE Internet of Things Journal*, vol. 9, no. 3, pp. 1683–1695, 2021. 142, 143

[148] Y. S. Nasir and D. Guo, "Multi-agent deep reinforcement learning for dynamic power allocation in wireless networks," *IEEE Journal on Selected Areas in Communications*, vol. 37, no. 10, pp. 2239–2250, 2019. 142, 143, 158, 162

[149] F.-L. Luo, *Machine learning for future wireless communications*. Hoboken, NJ, USA: John Wiley & Sons, 2020. 142, 154

[150] P. Dayan and C. Watkins, "Q-learning," *Machine Learning*, vol. 8, no. 3, pp. 279–292, 1992. 142

[151] H. Van Hasselt, A. Guez, and D. Silver, "Deep reinforcement learning with double q-learning," in *Proceedings of the AAAI Conference on Artificial Intelligence*, vol. 30, no. 1, 2016. 142, 143, 156

[152] Z. Wang, T. Schaul, M. Hessel, H. Hasselt, M. Lanctot, and N. Freitas, "Dueling network architectures for deep reinforcement learning," in *International Conference on Machine Learning*. PMLR, 2016, pp. 1995–2003. 143, 157

[153] A. Feriani and E. Hossain, "Single and multi-agent deep reinforcement learning for AI-enabled wireless networks: A tutorial," *IEEE Communications Surveys & Tutorials*, 2021. 143, 155

[154] D. Wu and R. Negi, "Effective capacity: a wireless link model for support of quality of service," *IEEE Transactions on Wireless Communications*, vol. 2, no. 4, pp. 630–643, 2003. 144, 146, 147

[155] Q. Ye, W. Zhuang, S. Zhang, A.-L. Jin, X. Shen, and X. Li, "Dynamic radio resource slicing for a two-tier heterogeneous wireless network," *IEEE Transactions on Vehicular Technology*, vol. 67, no. 10, pp. 9896–9910, 2018. 144

[156] P. M. Rabinovitch, "Statistical estimation of effective bandwidth." Ph.D. dissertation, Carleton University, 2000. 146

[157] A. Abdrabou and W. Zhuang, "Stochastic delay guarantees and statistical call admission control for IEEE 802.11 single-hop adhoc networks," *IEEE Transactions on Wireless Communications*, vol. 7, no. 10, pp. 3972–3981, 2008. 146

[158] R. S. Sutton and A. G. Barto, *Reinforcement learning: An introduction*. MIT press, 2018. 151, 152, 153, 156

[159] V. Mnih, K. Kavukcuoglu, D. Silver, A. A. Rusu, J. Veness, M. G. Bellemare, A. Graves, M. Riedmiller, A. K. Fidjeland, G. Ostrovski *et al.*, "Human-level control through deep reinforcement learning," *Nature*, vol. 518, no. 7540, pp. 529–533, 2015. 154, 155

[160] J. Fan, Z. Wang, Y. Xie, and Z. Yang, "A theoretical analysis of deep q-learning," in *Learning for Dynamics and Control*. PMLR, 2020, pp. 486–489. 155, 156

[161] V. François-Lavet, P. Henderson, R. Islam, M. G. Bellemare, J. Pineau *et al.*, "An introduction to deep reinforcement learning," *Foundations and Trends® in Machine Learning*, vol. 11, no. 3-4, pp. 219–354, 2018. 155

[162] M. L. Littman, "Markov games as a framework for multi-agent reinforcement learning," in *Machine Learning Proceedings 1994*. Elsevier, 1994, pp. 157–163. 158

[163] J. K. Gupta, M. Egorov, and M. Kochenderfer, "Cooperative multi-agent control using deep reinforcement learning," in *Autonomous Agents and Multiagent Systems: AAMAS 2017 Workshops, Best Papers, São Paulo, Brazil, May 8-12, 2017, Revised Selected Papers 16*. Springer, 2017, pp. 66–83. 163

[164] S. Martello, "An algorithm for the generalized assignment problem," *Operational Research*, pp. 589–603, 1981. 170

[165] B. Priya and J. Malhotra, "Qaas: Qos provisioned artificial intelligence framework for ap selection in next-generation wireless networks," *Telecommunication Systems*, vol. 76, no. 2, pp. 233–249, 2021. 172

[166] I. Goodfellow, Y. Bengio, and A. Courville, "Deep learning (adaptive computation and machine learning series)," *Cambridge Massachusetts*, pp. 321–359, 2017. 174

[167] F. Salahdine, J. Opadere, Q. Liu, T. Han, N. Zhang, and S. Wu, "A survey on sleep mode techniques for ultra-dense networks in 5G and beyond," *Computer Networks*, vol. 201, p. 108567, 2021. 198

[168] Q. Huang, M. Lin, J.-B. Wang, T. A. Tsiftsis, and J. Wang, "Energy efficient beamforming schemes for satellite-aerial-terrestrial networks," *IEEE Transactions on Communications*, vol. 68, no. 6, pp. 3863–3875, 2020. 198

[169] A. Awan, Z. Qi, and H. Shan, "Co-operative admission control and optimum power allocation underlying 5G-IoT networks aided D2D-satellite communication," in *2020 International Wireless Communications and Mobile Computing (IWCMC)*. IEEE, 2020, pp. 1025–1030. 198, 199

[170] Y. Ruan, Y. Li, C.-X. Wang, R. Zhang, and H. Zhang, "Energy efficient power allocation for delay constrained cognitive satellite terrestrial networks under interference constraints," *IEEE Transactions on Wireless Communications*, vol. 18, no. 10, pp. 4957–4969, 2019. 199, 202

[171] S. S. Hassan, D. H. Kim, Y. K. Tun, N. H. Tran, W. Saad, and C. S. Hong, "Seamless and energy efficient maritime coverage in coordinated 6G space-air-sea non-terrestrial networks," *arXiv preprint arXiv:2201.08605*, 2022. 199

[172] Y. Xu, Y. Wang, R. Sun, and Y. Zhang, "Joint relay selection and power allocation for maximum energy efficiency in hybrid satellite-aerial-terrestrial systems," in *2016 IEEE 27th Annual International Symposium on Personal, Indoor, and Mobile Radio Communications (PIMRC)*. IEEE, 2016, pp. 1–6. 199

[173] Y.-J. Gong, J. Zhang, H. S.-H. Chung, W.-N. Chen, Z.-H. Zhan, Y. Li, and Y.-H. Shi, "An efficient resource allocation scheme using particle swarm optimization," *IEEE Transactions on Evolutionary Computation*, vol. 16, no. 6, pp. 801–816, 2012. 200, 209

[174] R. T. Marler and J. S. Arora, "Survey of multi-objective optimization methods for engineering," *Structural and Multidisciplinary Optimization*, vol. 26, no. 6, pp. 369–395, 2004. 208

[175] N. Jain, U. Nangia, and J. Jain, "A review of particle swarm optimization," *Journal of The Institution of Engineers (India): Series B*, vol. 99, pp. 407–411, 2018. 209

[176] X. Zhang, H. V. Poor, and M. Chiang, "Optimal power allocation for distributed detection over mimo channels in wireless sensor networks," *IEEE Transactions on Signal Processing*, vol. 56, no. 9, pp. 4124–4140, 2008. 215

[177] S. O. Oladejo, "Efficient radio resource management for the fifth generation slice networks," Ph.D. dissertation, University of Cape Town, 2021. 215

Appendix

A Appendix 1

Equating (5.4) to (5.2) yields

$$-\frac{\log_e \varepsilon}{\vartheta_{u_{\mathcal{R}}} \mathrm{D}_{\max}} = \frac{\lambda_{u_{\mathcal{R}}} (e^{\vartheta_{u_{\mathcal{R}}}} - 1)}{\vartheta_{u_{\mathcal{R}}}}. \tag{1}$$

Making $e^{\vartheta_{u_{\mathcal{R}}}}$ in (1) the subject gives

$$e^{\vartheta_{u_{\mathcal{R}}}} = 1 - \frac{\log_e \varepsilon}{\lambda_{u_{\mathcal{R}}} \mathrm{D}_{\max}}. \tag{2}$$

Applying logarithms to the left and the right hand side of (2) yields

$$\vartheta_{u_{\mathcal{R}}} = \log_e \left(1 - \frac{\log_e \varepsilon}{\lambda_{u_{\mathcal{R}}} \mathrm{D}_{\max}} \right). \tag{3}$$

Substituting for $\vartheta_{u_{\mathcal{R}}}$ in (5.4) using (3) gives

$$\lambda_{u_{\mathcal{R}}}^{min} = -\frac{\log_e \varepsilon}{\mathrm{D}_{\max} \log_e \left(1 - \frac{\log_e \varepsilon}{\lambda_{u_{\mathcal{R}}} \mathrm{D}_{\max}} \right)}. \tag{4}$$

But $\lambda_{u_{\mathcal{R}}}^{min}$ in (4) is in packets/s. Multiplying it by the packet size $\mathrm{L}_{u_{\mathcal{R}}}$ yields the minimum rate $\mathcal{C}_{u_{\mathcal{R}}}^{min}$ in bits/s that guarantees the bound on the delay violation probability.

$$\mathcal{C}_{u_{\mathcal{R}}}^{min} = -\frac{\mathrm{L}_{u_{\mathcal{R}}} \log_e \varepsilon}{\mathrm{D}_{\max} \log_e \left(1 - \frac{\log_e \varepsilon}{\lambda_{u_{\mathcal{R}}} \mathrm{D}_{\max}} \right)}. \tag{5}$$